This electronic thesis or dissertation has been downloaded from the King's Research Portal at https://kclpure.kcl.ac.uk/portal/

EXPLORING THE ROLE OF L-SELECTIN SHEDDING IN REGULATING NEUTROPHIL POLARITY AND CHEMOTAXIS

Davies, Jessica Ellen

Awarding institution:
King's College London

The copyright of this thesis rests with the author and no quotation from it or information derived from it may be published without proper acknowledgement.

END USER LICENCE AGREEMENT

Unless another licence is stated on the immediately following page this work is licensed

under a Creative Commons Attribution-NonCommercial-NoDerivatives 4.0 International

licence. https://creativecommons.org/licenses/by-nc-nd/4.0/

You are free to copy, distribute and transmit the work

Under the following conditions:

- Attribution: You must attribute the work in the manner specified by the author (but not in any way that suggests that they endorse you or your use of the work).
- Non Commercial: You may not use this work for commercial purposes.
- No Derivative Works - You may not alter, transform, or build upon this work.

Any of these conditions can be waived if you receive permission from the author. Your fair dealings and other rights are in no way affected by the above.

Take down policy

If you believe that this document breaches copyright please contact librarypure@kcl.ac.uk providing details, and we will remove access to the work immediately and investigate your claim.

Download date: 05. May. 2023

EXPLORING THE ROLE OF L-SELECTIN SHEDDING IN REGULATING NEUTROPHIL POLARITY AND CHEMOTAXIS

Jessica Davies

This thesis is submitted for the degree of

Doctorate of Philosophy
(PhD)

King's College London, School of Medicine, University of London

Submitted September 2016

King's College London,
School of Medicine,
Cardiovascular division,
Denmark Hill Campus,
London, U.K.

Primary supervisor: Dr Aleksandar Ivetic
Secondary supervisor: Dr Guillaume Charras

Abstract

Inflammation is a biological response to injury – a fundamental part of which involves the influx of leukocytes to the affected area. Circulating neutrophils are typically the first responders to an inflammatory insult. Orchestrated interactions between neutrophils and the underlying endothelium and occurs in a process termed the "multi-step leukocyte adhesion cascade". L-selectin, a cell adhesion molecule, expressed on all circulating neutrophils, and facilitates the initial tethering and rolling events. Previously, L-selectin on CD14-positive ("inflammatory") monocytes was shown to undergo ectodomain "shedding", exclusively during transendothelial migration (TEM) and not before. The consequence of this was to establish monocyte polarity within the subendothelial space. The primary aim of this project was to determine if L-selectin shedding during TEM was exclusive to monocytes or extended to neutrophils. Perfusion of primary human neutrophils over activated endothelial monolayers revealed that L-selectin shedding was also activated specifically during TEM. Ectopic expression of L-selectin tagged to green fluorescent protein (GFP) in HL-60 cells (a neutrophil-like cell line that does not express endogenous L-selectin) significantly increased their invasive potential across activated endothelial cells under flow. Blocking L-selectin shedding (either pharmacologically in primary neutrophils or genetically in HL60 cells) promoted cell elongation in fully transmigrated cells, which significantly impacted cell polarity and directional persistence in 2D and 3D collagen scaffolds. Additionally, manufacturing bespoke microfluidic flow chamber devices revealed that blocking L-selectin shedding impacted the neutrophil chemotaxis towards classic "end-stage chemoattractants", such as fMLP. Taken together, L-selectin shedding ensures that fully transmigrated neutrophils can establish front-back polarity so that they can home optimally to their inflamed targets. As fMLP is secreted during sterile injury, the potential therapeutic targeting of L-selectin shedding in the setting of myocardial infarction is discussed.

Acknowledgments

Firstly, I would like to thank my supervisor Dr Aleksandar Ivetic whose vast knowledge and enthusiasm for the project has been a continual support and encouragement throughout the entirety of the PhD. He is a passionate teacher and the long hours of guidance have been very much appreciated. I would also like to thank my second supervisor Dr Guillaume Charras, who gave me the freedom to trial ideas, and was a good "sounding board" when it came to problems associated with fabrication and optimisation of the microfluidic devices.

My thanks also go to lab members past and present in both the Charras and Ivetic labs; Thomas, Nargess, Anna, Amina, Malti, Majid, Izaj, Hannah and Angela. All these people have provided me with scientific help, encouragement and support. I extend my sincerest gratitude, to these people without them life in the lab would not have nearly been as enjoyable. I also can't not mention Richard Thorogate whose patience with me was endless, without you I don't believe this PhD would have reached completion-Thank you.

I owe my deepest gratitude to my wonderful parents, who have continually supported me and made me believe in myself. My special thanks goes to my mum, Sue Davies, who proof read this thesis.

Finally, I would like to thank my boyfriend Ed, who firstly taught me time management and made coming home on a day when everything went wrong better.

Thank you all.

Declaration of independent work

I, the author of this thesis, declare that the work presented within this thesis was conducted by me, except where indicated in the text.

……

Jessica Davies

Abbreviations

2D	Two dimensional
3D	Three dimensional
A	Alanine
ADAM	A disintegrin and metalloprotease
aa	Amino acid
Arp 2/3	Actin-related protein 2/3
Akt	Protein kinase b
AJs	Adherens junctions
apoE	Apolipopreotein E
ATCC	American tissue culture collection
ATP	Adenosine triphosphate
BCR	B-cell receptor
BM	Basement membrane
BSA	Bovine serum albumin
CaM	Calmodulin
CAM	Cell adhesion molecule
CCD	Charge coupled device
CCL2	c-c motif chemokine 2
CCL7	c-c motif chemokine 7
Cdc42	Cell division control protein 42 homolog
CCR2	c-c motif chemokine receptor 2
CCR7	c-c motif chemokine receptor 7
CD "X"	Cluster of differentiation, X= number
Cdc42	Cell division cycle 42
CS	Chondroitin sulfate
C- terminal	Carboxy-terminal
CalA	Calyculin A
CVD	Cardiovascular disease
CXCR4	C-X-C motif chemokine receptor type 4
D	Aspartate
DCs	Dendritic cells
DMSO	Dimethyl-sulfoxide
DAMPS	Damage associated molecule patterns
DNA	Deoxyribonucleic acid
DAG	Diacylglycerol
DS	Dermatan sulphate
DRM	Detergent resistant membrane
ddH_20	Double-distilled water
DS	Dermatan sulfate
EAPs	Endothelial adhesion platforms
EC	Endothelial cell
ECM	Extracellular matrix
EDTA	Ethylene diamine- tetracetic acid
EEA1	Early endosomal antigen 1
EGF	Epidermal growth factor

ERK	Extracellular signal-regulated kinase
ERM	Ezrin/radixin/moesin
ESAM	Endothelial cell selective adhesion molecule
ECM	Extracellular matrix
ESL-1	E selectin ligand
FA	Focal adhesion
FACS	Fluorescence activated cell sorting
FCS	Foetal calf serum
F-actin	Filamentous actin
FERM	Band 4.1 ezrin/radixin/moesin
FITC	Fluorescein isothiocyanate
fMLP	Formyl-methionine-leucine-phenylalnine
FOXO-1	Forkhead box O1
FPR	N-formyl peptide receptor
FRET	Fluorescence resonance energy transfer
GAG	Glycosaminoglycan
Gro- α	CXCL1
G-CSF	Granulocyte colony stimulating factor
GDI	GDP dissociation inhibitor
GAP	Guanine activating protein
GDP	Guanosine diphosphate
GEF	Guanine nucleotide exchange factor
GPK	G-protein receptor kinase
GFP	Green fluorescent protein
GlyCAM-1	Glycosylation-dependent cell adhesion molecule-1
GPCR	G-protein coupled receptor
GTP	Guanosine triphosphate
HBSS	Hanks buffered saline solution
HEK 293T	Human embryonic kidney 232 cell line
HEPES	4-(2-hydroxyethyl)-1-piperazineethanesulfonic acid
HL-60	Human promyelocytic leukemia cells
HSPG	Heperan sulphate proteoglycan
HEV	High endothelial venules
HUVEC	Human umbical cord endothelial cells
ICAM-1	Inter-cellular adhesion molecule1
Ig	Immunoglobulin
IgA	Immunoglobulin with A class heavy chains
IgE	Immunoglobulin with E class heavy chains
IgG	Immunoglobulin with G class heavy chains
ITAM	Immunoreceptor tyrosine based activation motif
IL	Interleukin
IL-8	Interleukin -8
JAM	Junctional adhesion molecule
JNK	c-Jun N terminal kinase
KC	Keratinocyte chemoattractant
Klf2	Kruppel-like factor 2
K	Lysine

LAD	Leukocyte adhesion deficiency
LAM	Leukocyte adhesion molecule
LBRC	Lateral border recycling compartment
LSP-1	Leukocyte specific protein-1
LER	Low expression regions
LDL	Low density lipoprotein
LECAM-1	Lectin adhesion molecule-1
LFA-1	Lymphocyte function-associated antigen 1
LPS	Lipopolysaccharide
LTB_4	Leukotriene B4.
mAb	Monoclonal antibody
MAC-1	Macrophage 1 antigen
MadCAM-1	Mucosal addressin cell adhesion molecule 1
MAPK	Mitogen activated protein kinase
mCherry	Monomeric cherry fluorescent protein
MCP-1	Monocyte chemoattractant protein
M-CSF-1	Macrophage colony stimulating factor-1
MIP-2	Interleukin 32
MES	2-morpholinoethanesulfonic acid, monohydrate
MLC	Myosin light chain
MFI	Mean fluorescence intensity
MPO	Myeloperoxidase
MIF	Migration inhibitory factor
MI	Myocardial infarction
MLN	Mesenteric lymph node
MOI	Multiplicity of infection
mRNA	Messenger RNA
MW	Molecular weight
N	Asparagine
NEB	New England Biolabs
NK	Natural killer
NP-40	Nonident P-40 substitute
Nod like receptor	Nucleotide binding oligomerisation domain like receptor
NSAID	Non-steroid anti-inflammatory drugs
N-terminal	Amino-terminal
NETs	Neutrophil extracellular traps
NE	Neutrophil elastase
NADPH	Nicotinamide adenine dinucleotide phosphate
oxLDL	Oxidised LDL
PAF	Platelet activating factor
PAGE	Polyacrylamide gel electrophoresis
PBL	Peripheral blood lymphocyte
PBMC	Peripheral blood mononuclear cell
PMN	Polymorphonuclear cells
PBS	Phosphate buffered saline
PCR	Polymerase chain reaction
PLB	Protein loading buffer

PLC	Phospholipase c
PLL	Poly-L-lysine
PLN	Peripheral lymph node
PMA	Phorbol-12'-myristate-13'acetate
PNAd	Peripheral lymph node addressins
PFA	Paraformaldehyde
PG	Proteoglycan
PI3K	Phosphoinositide 3-kinase
Phospho-	Phosphorylated
PIP_2	Phosphatidylinositol (4,5) bisphosphate
PIP_3	Phosphatidylinositol (3,4,5) trisphosphate
PKC	Protein kinase C
PAMP	Pathogen associated molecule patterns
PPR	Pattern recognition receptor
PECAM-1	Platelet endothelial cell adhesion molecule
PSGL-1	P-selectin glycoprotein ligand-1
PDMS	Polydimethylsiloxane
Rac	Ras-related C3 botulinium toxin substrate
RFP	Red fluorescent protein
Rho	Ras homologue
R	Arginine
RNA	Ribonucleic acid
ROCK	Rho-associated coiled coil-containing protein kinase
ROS	Reactive oxygen species
rTEM	Reverse transmigration
PE	Phycoeyrthrin
rpm	Revolutions per minute
RPMI-1640	Roswell Park memorial Institure -1640
S	Serine
S.E.M	Standard error of the mean
SCR	Short consensus repeat
SDF-1	Stromal cell derived factor-1
SDS	Sodium dodecyl sulphate
SEM	Scanning electron microscopy
SFK	Src family kinases
SLC	Secondary lymphoid tissue chemokine
sLe^x	Sialyl Lewis X
Syk	Spleen tyrosine kinase
sL-selectin	Soluble L-selectin
TACE	TNF-α converting enzyme
TAE	Tris-acetate-EDTA
TBS	Tris-buffered saline
TCR	T cell receptor
TEM	Transendothelial migration
TF	Transcription factor
TJs	Tight junctions
TMD	Transmembrane domain

TNF-α	Tumour necrosis factor α
TAPI-0	Tnf-alpha protease inhibitor -0
TRITC	Tetra-methyl-rhodamine-5-(and-6)-isothiocyanate
VCAM-1	Vascular cell adhesion molecule 1
VLA-4	Very late antigen 4
VE-Cadherin	Vascular endothelial –cadherin
VVO	Vesiculo-vacuolar organelle
WT	Wild type
α	Alpha
β	Beta
Δ	Delta

Deleted: Theta

Contents

Abstract 2

Acknowledgments 3

Declaration of independent work 4

Abbreviations 5

Contents 10

Figures 14

Tables 17

1.Introduction 18

1.1 Inflammation 18

1.1.1 Acute inflammation *18*

1.1.2 Chronic inflammation *19*

1.2 The multi-step leukocyte adhesion cascade 20

1.2.1 Leukocyte initial capture and tethering *21*

1.2.2 Leukocyte rolling *23*

1.2.3 Leukocyte arrest *25*

1.2.4 Intraluminal crawling *28*

1.2.5 Endothelial docking structures *28*

1.2.6 Transendothelial migration (TEM) *29*

1.2.6.1 Paracellular transmigration 30

1.2.6.2. Transcellular transmigration 32

1.2.6.3 Reverse transmigration 33

1.2.7 Leukocyte migration beyond TEM *34*

1.3 Leukocyte migration in 3D environments 35

1.4 Leukocyte chemotaxis 39

1.4.1 Chemoattractant signalling and hierarchy *40*

1.4.2 The extracellular matrix and neutrophil migration *42*

1.5 Neutrophil effector functions 43

1.5.1 Phagocytosis *43*

1.5.2 Degranulation *44*

1.5.3 NETosis *44*

1.5.4 The role of neutrophils in chronic inflammation *45*

1.6 The selectin molecules 47

1.6.1 Structure of the selectins *48*

1.7 Binding partners of the L-selectin cytoplasmic tail 52

1.7.1 α-actinin *52*

1.7.2 The ezrin-radixin-moesin (ERM) proteins *53*

1.7.3 Calmodulin and its regulation of binding to the L-selectin tail *54*

1.7.4 Calmodulin and ERM as signalling adaptors during ligand-induced clustering of L-selectin *55*

1.7.5 PKC isoforms *55*

1.8 L-selectin ligands 56

1.9 Regulation of L-selectin expression 57

1.9.1 Transcriptional and post-translational control 57

1.9.2 Proteolytic cleavage of L-selectin *58*

1.10 Functional roles for L-selectin 59

1.10.1 The role of L-selectin within the vessel lumen *60*

1.10.2 The role of L-selectin beneath the endothelial monolayer and beyond *60*

1.11 The role of L-selectin as a signalling receptor 61
1.11.1 Integrin activation by L-selectin *62*
1.11.2 Regulation of chemokine receptors and chemotaxis *62*
1.12 The role of L-selectin in regulating TEM and polarity in monocytes 63
1.13 The role of L-selectin in neutrophil effector functions 65
1.14 The role of L-selectin in disease 66
1.15 Current methods to study L-selectin 68
1.16 Original hypothesis 69
1.17 Aims of the project 69

2. Materials and methods 70

2.1 Cell culture medium, buffers, reagents and chemical formulations 70
2.2 Antibodies 77
2.3 Cells and cell culture 79
2.3.1 HL-60 cells (Human promyelocytic leukaemia cells) *79*
2.3.2 HEK 293T cells (Human embryonic kidney cells) *79*
2.3.3 HUVEC cells (Human umbilical vein endothelial cells) *80*
2.3.4 Cryopreservation of cells *80*
2.3.5 Isolation of Primary Neutrophils *81*
2.4 Flow cytometry 82
2.4.1 Instrument and Instrument parameter settings *82*
2.4.2 Antibody labelling *83*
2.4.3 Flow Jo analysis *83*
2.5 Parallel plate flow chamber 84
2.5.1 Cell perfusion assays for binding dynamics *86*
2.5.2 Cell tracking of fully transmigrated neutrophils *87*
2.5.3 Cell perfusion of the 3D device *87*
2.6 Protein Biochemistry 89
2.6.1 Polyacrylamide gel electrophoresis of HL-60 cell lysates, using the Novex NuPAGE SDS-PAGE pre-cast gel system *89*
2.6.2 Western blotting *89*
2.6.3 Densitometry analysis *90*
2.7 Lentiviral transduction and generation of stable cell lines 90
2.7.1 Lentiviral production *90*
2.7.2 Estimating lentiviral titres *91*
2.7.3 Lentiviral infection of HL-60 cells *92*
2.7.4 FACS sorting *93*
2.8 Confocal microscopy 93
2.8.1 Equipment *93*
2.8.2 Cell fixation and labelling procedures *93*
2.8.4 Analysis of GFP and LAM1-14 positive "spots" *94*
2.8.5 Morphology analysis *94*
2.8.6 Subcellular localisation of L-selectin *95*
2.9 L-selectin shedding assays 95
2.9.1 Monitoring L-selectin shedding from cell suspensions *95*
2.9.2 Monitoring L-selectin shedding in neutrophil/HUVEC co-cultures *96*
2.10 Micropipette chemotaxis assays 96
2.11 Microfluidic 2D device 97
2.11.1 Gradient generation *97*
2.11.2 Cell seeding *98*
2.12 Microfluidic 3D device 98
2.12.1 Collagen imaging *98*
2.12.2 HUVEC seeding *99*
2.12.3 Optimisation procedure for gradient formation in the 3D device *99*

2.12.4 Static transmigration assays using 3D devices *100*
2.12.5 Measuring leukocyte invasion post-transmigration *100*
2.13 Statistical analysis 101

3. Establishing a cellular model to understand the importance of L-selectin shedding in regulating neutrophil migratory behaviour 102
3.1 Biological rationale 102
3.2 Results 103
3.2.1 Primary human neutrophils undergo L-selectin shedding during transendothelial migration (TEM) *103*
3.2.2 Behavioural analysis of primary neutrophils perfused over TNF-α activated HUVEC. *108*
3.2.3 Speed of neutrophil transmigration across TNF-activated HUVEC and within the sub endothelial space *111*
3.2.4 Monitoring the impact of blocking L-selectin shedding on neutrophil morphology within the sub endothelial space *112*
3.2.5 Monitoring the sub-cellular distribution of L-selectin in fTEM primary neutrophils *114*
3.2.6 Generation of an HL-60 cell line to study the contribution of L-selectin shedding in regulating neutrophil migratory behavior *116*
3.2.7 Differentiation of HL-60 cells with DMSO *117*
3.2.8 Blocking L-selectin shedding reduces fMLP chemotaxis *119*
3.2.9 CXCR2 is essential for HL-60 TEM *125*
3.2.10 Expression of CXCR2 does not prevent chemotaxis towards fMLP *129*
3.2.11 Engineering WT L-selectin and mutants into HL-60 cells expressing functional CXCR2. ..... *133*
3.2.12 L-selectin-GFP is deposited from the uropod as HL-60 cells complete TEM *138*
3.2.13 Understanding the role of the L-selectin cytoplasmic tail in contributing to the phenotypic changes observed in ΔMN cells *140*
3.2.14 Chemoattractant stimulated shedding of L-selectin in primary neutrophils *146*
3.2.15 fMLP induces phosphorylation of p38 MAPK in primary neutrophils *148*
3.2.16 PMA stimulates L-selectin shedding in WT but not ΔMN cell lines *150*
3.2.17 Activation of the p38 MAPK-dependent pathway in WT cells *151*
3.2.18 Monitoring L-selectin shedding in WT HL-60 cells undergoing TEM *153*
3.2.19 fMLP does not promote L-selectin shedding in HL-60 cells *154*
3.2.20 Regulation of FPR1/2 receptor expression in WT and ΔMN HL-60 cells *158*
3.3 Discussion 161
3.3.1 L-selectin shedding during TEM and beyond: similarities and differences in monocytes and neutrophils *161*
3.3.1.1 The role of p38 MAPK and L-selectin shedding during TEM 161
3.3.1.2 Blocking L-selectin shedding and its impact on chemotaxis and cell polarity 162
3.3.1.3 The contribution of S364 and S367 in driving phenotypic differences in WT and ΔMN cells 163
3.3.2 L-selectin enrichment at the cell rear *163*
3.3.3 L-selectin clustering in fTEM primary neutrophils *164*
3.3.4 Final thoughts *165*

4. Generating microfluidic devices to monitor neutrophil migration in complex environments 167
4.1. Generation of a 2D device to monitor leukocyte behaviour when responding to conflicting gradients of chemoattractants 167
4.1.1. Biological rationale behind the design of the 2D device *167*
4.1.2 Designing and generating the 2D device *167*
4.1.3 Quality control testing of a chemoattractant gradient *173*

4.1.4 Cell seeding within the 2D device ... *179*
4.2 Generation of a 3D device to monitor the entire leukocyte adhesion cascade from capture to chemotaxis ... 180
4.2.1 Biological rationale behind the design of the 3D device ... *180*
4.2.2 Design and fabrication of the 3D device ... *181*
4.2.3 Optimising extracellular components to support a HUVEC monolayer ... *186*
4.2.4 Factors contributing to collagen pore size ... *188*
4.2.5 HL-60 migration through a collagen matrix ... *191*
4.2.6 Optimising the collagen depths with the 3D device ... *192*
4.2.7 Generating a chemoattractant gradient within the 3D device ... *194*
4.2.8 Optimising neutrophil recruitment under flow conditions ... *198*
4.3 Discussion ... 199
4.3.1 The 2D device ... *199*
4.3.2 The 3D device ... *200*
4.3.3 Final thoughts ... *201*

Chapter 5. Understanding the role of L-selectin shedding in regulating neutrophil chemotaxis through 3D scaffolds. ... 202
5.1 Biological rationale ... 202
5.2 Results ... 203
5.2.1. Blocking L-selectin shedding alters directional migration of HL-60 cells within collagen matrices. ... *203*
5.2.2 Blocking L-selectin shedding impairs invasion into collagen matrices under static conditions ... *205*
5.2.3 Understanding the effect of L-selectin shedding in regulating chemoattractant-driven invasion in primary neutrophils ... *209*
5.2.4. Understanding the effect of L-selectin shedding in chemotaxis of HL-60 cells through collagen matrices. ... *214*
5.2.5 Understanding the contribution of the L-selectin tail in regulating HL-60 cell chemotaxis through collagen scaffolds. ... *218*
5.3 Discussion: ... 221
5.3.1 Comparing cell invasion ... *222*
5.3.1.1 Cell invasions in response to the intermediary chemoattractants IL-8 and Gro-α are L-selectin shedding independent ... 223
5.3.1.2 Cell invasions in response to the end-target chemoattractant fMLP are L-selectin shedding dependent ... 224
5.3.2 Final thoughts ... *224*

6. General Discussion ... 225
6.1 L-selectin shedding during TEM and chemotaxis ... 226
6.2 Putative mechanisms underpinning L-selectin regulation during TEM and interstitial chemotaxis ... 227
6.3 Putative mechanism underpinning L-selectin shedding and chemotaxis towards fMLP ... 231
6.5 Blocking L-selectin shedding – a possible therapy for myocardial infarction? ... 237
6.6 Concluding remark ... 240

References ... 241

Deleted: Abstract . 2¶
Acknowledgments . 3¶
Declaration of independent work 4¶
Abbreviations . 5¶
Contents 10¶
Figures . 14¶
Tables 17¶
1.Introduction . 18¶
1.1 Inflammation 18¶
1.1.1 Acute inflammation . 18¶
1.1.2 Chronic inflammation 19¶
1.2 The multi-step leukocyte adhesion cascade . 20¶
1.2.1 Leukocyte initial capture and tethering 21¶
1.2.2 Leukocyte rolling . 23¶
1.2.3 Leukocyte arrest 25¶
1.2.4 Intraluminal crawling . 27¶
1.2.5 Endothelial docking structures 27¶
1.2.6 Transendothelial migration (TEM) . 28¶
1.2.6.1 Paracellular transmigration 29¶
1.2.6.2. Transcellular transmigration . 31¶
1.2.6.3 Reverse transmigration 32¶
1.2.7 Leukocyte migration beyond TEM . 34¶
1.3 Leukocyte migration in 3D environments 34¶
1.4 Leukocyte chemotaxis . 38¶
1.4.1 Chemoattractant signalling and hierarchy 39¶
1.4.2 The extracellular matrix and neutrophil migration . 41¶
1.5 Neutrophil effector functions 42¶
1.5.1 Phagocytosis . 42¶
1.5.2 Degranulation 43¶
1.5.3 NETosis . 43¶
1.5.4 The role of neutrophils in chronic inflammation 44¶
1.6 The selectin molecules . 46¶
1.6.1 Structure of the selectins 47¶
1.7 Binding partners of the L-selectin cytoplasmic tail . 51¶
1.7.1 α-actinin 51¶
1.7.2 The ezrin-radixin-moesin (ERM) . 52¶
1.7.3 Calmodulin and its regulation of binding to the L-selectin tail 53¶
1.7.4 Calmodulin and ERM as signalling adaptors during ligand-induced clustering of L-selectin . 54¶
1.7.5 PKC isoforms 54¶
1.8 L-selectin ligands . 55¶
1.9 Regulation of L-selectin expression 56¶
1.9.1 Transcriptional and post-translational control . 56¶
1.9.2 Proteolytic cleavage of L-selectin 57¶
1.10 Functional roles for L-selectin . 58¶
1.10.1 The role of L-selectin within the vessel lumen 59¶
1.10.2 The role of L-selectin beneath the endothelial monolayer and beyond . 59¶
1.11 The role of L-selectin as a signalling receptor 61¶
1.11.1 Integrin activation by L-selectin . 61¶
1.11.2 Regulation of chemokine receptors and chemotaxis 61¶
1.12 The role of L-selectin in regulating TEM and polarity in monocytes . 62¶
1.13 The role of L-selectin in neutrophil effector functions 64¶
1.14 The role of L-selectin in disease . 65¶
1.15 Current methods to study L-selectin 67¶
1.16 Original hypothesis . 68¶
1.17 Aims of the project 68¶
2. Materials and methods . 69¶
2.1 Cell culture medium, buffers, reagents and chemical formulations 69¶

Figures

Figure 1.1: The leukocyte adhesion cascade 20
Figure 1.2: The cell adhesion molecules on EC and leukocytes responsible for tethering, rolling and arrest 23
Figure 1.3: Integrin bent-extended conformation change 26
Figure 1.4: Leukocyte transmigration 30
Figure 1.5: Leukocyte reverse transmigration 34
Figure 1.6: The differences between mesenchymal and amoeboid migration 36
Figure 1.7: A polarised leukocyte 37
Figure 1.8: The neutrophil effector functions 43
Figure 1.9 Neutrophil responses to early phase myocardial infarction 47
Figure 1.10: The domain structure of the selectin family of cell adhesion molecules 49
Figure 1.11: The binding partners of the cytoplasmic tail of L-selectin 52
Figure 1.12: Schematic model representing a novel function for L-selectin in regulating pseudopod number in the THP-1 cell line 65
Figure 2.1: Schematic demonstrating the procedure used to isolate neutrophils from human blood 82
Figure 2.2: Schematic depicting the parallel plate flow chamber set up 85
Figure 2.3: The micropipette set-up 97
Figure 3.1: L-selectin shedding occurs during transendothelial migration 104
Figure 3.2: Quantifying L-selectin shedding in transmigrated neutrophils 106
Figure 3.3: L-selectin shedding is initiated in pseudopods entering the sub endothelial space 107
Figure 3.4: Phase contrast image series of neutrophils accumulating into "clusters" within the sub endothelial space 109
Figure 3.5: Addressing the impact of blocking L-selectin shedding on neutrophil TEM behaviour 110
Figure 3.6: Blocking L-selectin shedding negatively impacts cell speed and directionality in fTEM neutrophils 112
Figure 3.7: Impact of blocking L-selectin shedding on the cross-sectional area and circularity ratio fTEM neutrophils 114
Figure 3.8: Organisation of L-selectin "spots" in fTEM neutrophils is not affected by TAPI-0. 115
Figure 3.9: Fluorescence intensity measurements of GFP in HL-60 cell lines 117
Figure 3.10: GFP levels in the HL-60 cell lines 118
Figure 3.11: The impact of DMSO treatment on L-selectin-GFP expression in HL60 cells 119
Figure 3.12: Micropipette assay 121
Figure 3.13: Blocking shedding of L-selectin inhibits chemotaxis towards fMLP 122
Figure 3.14: Blocking shedding of L-selectin inhibits chemotaxis towards fMLP 123
Figure 3.15. L-selectin subcellular localisation during chemotaxis 124

125
Figure 3.16 L-selectin is localised at the uropod 125
Figure 3.17: Relative expression levels of CXCR2 in the different HL-60 cell lines 127
Figure 3.18: Stills from a time-lapse movie showing HL-60 cells crawling along the apical aspect of TNF-activated HUVEC. 128
Figure 3.19: The importance of CXCR2 expression on HL-60 TEM behaviour. 129
Figure 3.20: Chemotaxis towards IL-8 131
Figure 3.21: Chemotaxis towards fMLP 132
Figure 3.22: Comparison of WT and mutant L-selectin-GFP fluorescence intensity values in HL-60 cells stably over expressing CXCR2 134
Figure 3.23: Monitoring HL-60 TEM behaviour and the contribution of L-selectin shedding to this mechanism 135
Figure 3.24: HL-60 dynamics beneath the endothelium 136
Figure 3.25: Characterisation of HL-60 circularity and cross-sectional area of fTEM HL-60 cells 138
Figure 3.26: Deposition of uropod spots during TEM 139
Figure 3.27: Frequency of uropod spots formed in HL-60 cell lines. 140
Figure 3.28: Defining the contribution of S364 and S367 in regulating TEM behaviour in HL-60 cells expressing ΔMN L-selectin-GFP 142
Figure 3.29: Monitoring migratory behaviour of fTEM HL-60 cells within the sub endothelial space 144
Figure 3.30: Assessment of cell morphology in fTEM HL-60 cells within the sub endothelial space 145
Figure 3.31 Frequency of uropod spots deposited by fTEM HL-60 cells 145
Figure 3.32: fMLP induces L-selectin shedding in primary neutrophils 148
Figure 3.33: Stimulation of primary human neutrophils with fMLP activates p38 MAPK 149
Figure 3.34: PMA stimulation of HL-60 cells expressing WT and ΔMN L-selectin 150
Figure 3.35: Time course of PMA-induced shedding of L-selectin by Western blotting 151
. 152
Figure 3.36: WT L-selectin-GFP is shed in response to stimulation with cantharidin or calyculin A 152
Figure 3.37: Monitoring L-selectin shedding in WT cells subjected to static TEM assays 154
Figure 3.38: L-selectin-GFP is not shed from HL-60 cells stimulated with fMLP 156
Figure 3.39: Stimulation of HL-60 cells with fMLP induces p38 MAPK phosphorylation 157
Figure 3.40: Formyl-peptide receptors surface expression is increased in WT HL-60 cells 159
Figure 3.41: Total protein levels of FPR1 and 2 are not altered between WT, ΔMN and GFP cells 160
Figure 4.1: Schematical representation of the 2D device. 168
Figure 4.2: Black emulsion masks for the 2D device 169

Figure 4.3: Schematic representing the 12 stages of the photolithography process for the 2D device fabrication 171
Figure 4.4: Schematic representing the soft lithography and 2D device assembly process. 173
Figure 4.5: Schematic of chemoattractant competition experiment 174
Figure 4.6: Diffusion within the 2D device 177
Figure 4.7: Fluorescence intensity line profile through the main 179
Figure 4.8: Alternative cell seeding approaches in the 2D device 180
Figure 4.9: Schematic of 3D device design. 183
Figure 4.10: Black emulsion mask for the 3D device 184
Figure 4.11: Schematic representing the 7 stages of the photolithography process for the 3D device fabrication 185
Figure 4.12: Schematic representing the soft lithography and 3D device assembly process. 186
Figure 4.13: HUVEC growth on different ECM components 188
Figure 4.14: Image analysis for estimating collagen pore size 190
Figure 4.15: Graph demonstrating the effect of change in collagen concentration and polymerisation temperature on gel pore size. 190
Figure 4.16: HL-60 migration through collagen gel 192
Figure 4.17: Optimising collagen depths within a trough 194
Figure 4.18: A line scan in XZ demonstrating FITC-dextran diffusion 195
Figure 4.19: Fluorescence intensity line profiles demonstrating the establishment of a concentration gradient along the z axis. 196
Figure 4.20: Gradient observation during flow assays 197
Figure 4.21: Leukocytes flowing across an activated HUVEC in the 3D device 198
Figure 5.1: Expression of WT L-selectin augments directional migration of HL-60 cells within 3D collagen scaffolds 204
Figure 5.2: Cell invasion assay 206
Figure 5.3: Blocking L-selectin shedding in primary neutrophils reduces invasion 207
Figure 5.4: WT L-selectin increases invasiveness of HL-60 cells through collagen. 208
Figure 5.5: Blocking L-selectin shedding reduces invasiveness towards gradients of fMLP and Gro-α, but not IL-8. 211
Figure 5.6. Side-by-side comparison of neutrophil invasiveness towards different chemoattractant gradients 212
Figure 5.7: Primary neutrophil chemotaxis through collagen matrices is concentration-dependent. 214
Figure 5.8: Investigating the contribution of L-selectin shedding in HL-60 cell chemotaxis through collagen matrices 217
Figure 5.9. Side-by-side assessment of invasiveness in GFP, WT and ΔM-N HL-60 cell lines responding to different chemoattractants within the 3D device. 218
Figure 5.10: Understanding the contribution of the L-selectin tail in regulating chemotaxis through collagen matrices 220
Figure 5.11: Side-by-side assessment of invasiveness in ΔMN, ΔMN SSAA and ΔMN SSDD HL-60 cell lines responding to different chemoattractants within the 3D device. 221

Figure 6.1: Schematic model representing the effects of L-selectin shedding on neutrophil polarity 228
Figure 6.2: Schematic model representing the effects of L-selectin phosphorylation 230
Figure 6.3: Schematic model representing L-selectin dependent FPR1 regulation 232
Figure 6.4: Schematic model representing L-selectin dependent FPR1 regulation 234
Figure 6.5: A possible therapy for myocardial infarction 239

Tables

Table 1.1: L-selectin ligands 57
Table 2.1: A tabulated list of chemicals, buffer formulations and cell culture resources used within this PhD project. 76
Table 2.2: Table of Primary Antibodies used within this thesis. 78
Table 2.3: A Tabulated list of the secondary antibodies used within this thesis. 78
Table 2.4: Virus titres and MOI used for cell line generation 92
Table 4:1: The specifications and justifications for the design of the 3D device. 182

Deleted: Figure 1.1: The leukocyte adhesion cascade 20¶
Figure 1.2: The cell adhesion molecules on EC and leukocytes responsible for tethering, rolling and arrest. 23¶
Figure 1.3: Integrin bent-extended conformation change 26¶
Figure 1.4: Leukocyte transmigration 29¶
Figure 1.5: Leukocyte reverse transmigration 33¶
Figure 1.6: The differences between mesenchymal and amoeboid migration 35¶
Figure 1.7: A polarised leukocyte 36¶
Figure 1.8: The neutrophil effector functions 42¶
Figure 1.9 Neutrophil responses to early phase myocardial infarction 46¶
Figure 1.10: The domain structure of the selectin family of cell adhesion molecules 48¶
Figure 1.11: The binding partners of the cytoplasmic tail of L-selectin 51¶
Figure 1.12: Schematic model representing a novel function for L-selectin in regulating pseudopod number in the THP-1 cell line 64¶
Figure 2.1: Schematic demonstrating the procedure used to isolate neutrophils from human blood. 81¶
Figure 2.2: Schematic depicting the parallel plate flow chamber set up. 84¶
Figure 2.3: The micropipette set-up 95¶
Figure 3.1: L-selectin shedding occurs during transendothelial migration 102¶
Figure 3.2: Quantifying L-selectin shedding in transmigrated neutrophils 104¶
Figure 3.3: L-selectin shedding is initiated in pseudopods entering the sub endothelial space 105¶
Figure 3.4: Phase contrast image series of neutrophils accumulating into "clusters" within the sub endothelial space. 107¶
Figure 3.5: Addressing the impact of blocking L-selectin shedding on neutrophil TEM behaviour 108¶
Figure 3.6: Blocking L-selectin shedding negatively impacts cell speed and directionality in fTEM neutrophils 110¶
Figure 3.7: Impact of blocking L-selectin shedding on the cross-sectional area and circularity ratio fTEM neutrophils. 112¶
...
Formatted: Font: Bold
Deleted: Table 1.1: L-selectin ligands 56¶
Table 2.1: A tabulated list of chemicals, buffer formulations and cell culture resources used within this PhD project. 75¶
Table 2.2: Table of Primary Antibodies used within this thesis. 77¶
Table 2.3: A Tabulated list of the secondary antibodies used within this thesis. 77¶
Table 2.4: Virus titres and MOI used for cell line generation 90¶
Table 4:1: The specifications and justifications for the design of the 3D device. 180¶
Table 5.1: The chemotactic scores 221¶
Deleted: ¶
¶
¶
¶
¶

1.Introduction

1.1 Inflammation

Inflammation is defined as a biological response to injury, which culminates in healing of the afflicted site. The Romans originally termed inflammation as "inflammare", which literally means "on fire". The physician and medical writer Aulus Cornelius Celsus was the first to characterise inflammation, and defined it as having four cardinal signs; rubor et tumor cum calore et dolore (redness and swelling with heat and pain)(1). Approximately 100 years later, the physician Aelius Galenus added a fifth cardinal sign: "loss of function". Typically, any organ or tissue afflicted with inflammation will be suffixed with "itis", for example: ilitis, pancreatitis, rhinitis. Although the cardinal signs of inflammation have been observed for approximately twenty centuries, the underlying cellular and molecular mechanisms that govern this process are only beginning to be appreciated in the past 70 years. Inflammation can be defined as acute or chronic, which are elaborated on within the sections below.

1.1.1 Acute inflammation

Acute inflammation is a short-lived response that typically lasts for days to weeks. Acute inflammation is initiated by infectious (bacteria, fungal, parasitic, viral) or non-infectious (chemical/physical, trauma, foreign bodies) agents, causing localised tissue damage. The response is often initiated by tissue-resident mast cells and/or macrophages, releasing vasoactive components (histamine and serotonin), which mediate vasodilation and increased permeability of the local microvasculature. Secretion of cytokines, such as TNF-α, by stromal cells (e.g. fibroblasts), tissue-resident macrophages and mast cells stimulate endothelial cells within local microvessels to up regulate cell adhesion molecules and chemokines, which collectively direct leukocytes from the circulation towards the site of damage (2). Increased vascular permeability leads to the delivery of blood plasma components into the affected area, which contains a multitude of anti-microbial weaponry, such as complement and antibodies. Increased microvascular permeability also results in the slowing down of blood, allowing leukocytes to "marginate" close to the vessel wall. Contact between leukocytes (such as neutrophils and monocytes) and activated endothelial cells will drive

neutrophil diapedesis and extravasation into the affected area. The invading monocytes and neutrophils migrate towards the site of damage by virtue of their surface pattern recognition receptors (PRRs), which can recognise a multitude of structures. Broadly speaking, PRRs can recognise "non-self" or intracellular "self" components. The non-self components include pathogen associated molecular patterns (PAMPs). In the case of "sterile injury", where intracellular self-components are recognised, neutrophils will respond rapidly to these structures, as they are released by necrotic cells (i.e. cells that have undergone uncontrolled death). The intracellular self structures are called damage associated molecular patterns (DAMPs) (3). Resolution of inflammation is determined when the noxious stimulus is no longer present and production of pro-inflammatory mediators (leukotrienes) are exchanged to anti-inflammatory molecules (lipoxins) leading to subsequent tissue healing (4)(5). Failure to resolve an acute inflammatory insult can lead to chronic inflammation.

1.1.2 Chronic inflammation

The pathway that determines the transition from acute to chronic inflammation is unclear and can be unique to any given pathology. What is clear is that the "cellularity of inflammation", which describes the timely influx and efflux of immune cells, is disturbed. Persistent inflammation leads to continued necrosis and severe tissue remodelling, and the deposition of tough fibrous scar tissue, which over time may result in permanent organ dysfunction. Literature and current studies have linked chronic inflammation to cancers, diabetes and autoimmune and cardiovascular diseases (6)(7)(8)(9)(10). The impact of neutrophils as the cellular driver for chronic inflammation will be highlighted in ***section 1.5.4***.

1.2 The multi-step leukocyte adhesion cascade

The migration of leukocytes from the circulation towards an extravascular site of damage requires a series of highly organised events, collectively termed the "multi-step leukocyte adhesion cascade" (11). The classical leukocyte adhesion cascade is depicted in (***figure 1.1***). Discreet stages of the pathway will be discussed at greater lengths in the following sections.

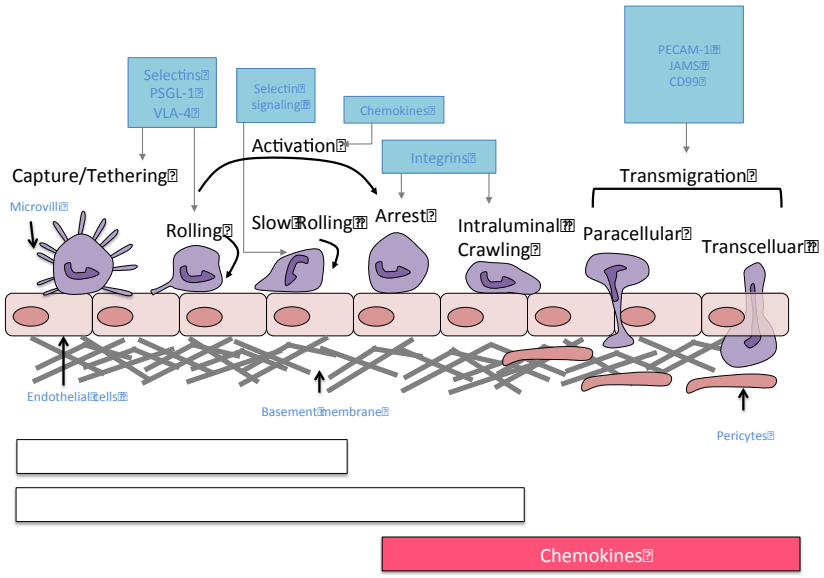

Figure 1.1: The leukocyte adhesion cascade
The recruitment of leukocytes to sites of inflammation requires interaction between the endothelium and the leukocyte. Initially, leukocytes are captured from blood flow and form transient tethers through the interaction of selectins and PSGL-1. Selectin/ligand interactions are also involved in leukocyte rolling. Chemokine mediated inside-out activation of integrins and subsequent inside-out integrin signalling results in the leukocyte arrest. Leukocyte survey the endothelium for permissive transmigration routes, this step is ICAM-1/MAC-1 dependent. Transmigration through the endothelium can occur either between endothelial cell junctions (paracellular route) or directly through the body of an endothelial cell (transcellular route). Both routes are dependent on the PECAM-1, JAMs and CD99. For abbreviations see ***Abbreviations section***. Image modified from Ley et al., Nat Rev Immunol, 2007 (11).

1.2.1 Leukocyte initial capture and tethering

Activation of the endothelium is the decisive first step in establishing a weak interaction between the leukocyte and endothelium. Upon tissue damage/infection resident macrophage release cytokines (IL-1β and TNF-α) to stimulate the expression of cell adhesion molecules (CAMs) on the luminal surface of the endothelium(2). Mast cells release histamine, among other mediators of acute inflammation, which stimulate the delivery of secretory granules to the plasma membrane. These secretory granules include Weibel-Palade bodies, which contain presynthesised P-selectin (12). The decrease in bloodline velocity (as a consequence of increased permeability) concentrates the leukocyte number locally in the microvasculature, together these biophysical processes dramatically increase the likelihood of a leukocyte–endothelium interaction (13)(14). The initial contacts between the two cell types are transient and collectively termed "tethers", thin elastic cell membrane protrusions, which effectively reduce the leukocyte's velocity. It is suggested that tethers are nucleated from actin rich "microvilli" structures, which elongate in length upon exertion of hydrodynamic force (15). It has been proposed that microvilli are crucial in penetrating the thick glycocalyx (~0.5-1.2μm), but this still remains a point of controversy (16). Characterisation of the microvillus tip by Immunogold labelling and electron microscopy techniques revealed the presence of dense populations of CAMs. One such CAM is L-selectin, 78% of which is localised to microvilli (17). The selectin family, a group of three cell adhesion molecules, L-selectin, P-selectin and E-selectin, mediate tethering of the leukocyte, Both E-selectin and P-selectin and found on the endothelium, while L-selectin is found on virtually all leukocytes. Collectively, the selectin/ ligand interactions actively recruit leukocytes to sites of inflammation. P-selectin glycoprotein ligand-1 (PSGL-1) plays a dominant role as the archetypal ligand for all selectins, (***figure 1.2***) (18). L-selectin was originally shown to be primarily responsible for homing of naïve lymphocytes to the peripheral lymph node (PLN) (19), but has since been shown to play an important role in regulating leukocyte recruitment to sites of inflammation(20). L-selectin was discovered as a primary contact to endothelial cells through the use of function-blocking antibodies(19). Treatment with such antibodies impaired L-selectin-dependent tethering of lymphocytes, neutrophils and monocytes

Deleted: e, L-selectin, P-selectin and E-selectin

Deleted: playing

endothelial monolayers under flow conditions (21)(22). Initial contact of L-selectin with the endothelium is perhaps facilitated due to its anchorage within the microvilli, poised at the most distal aspect of the cell body. The integrin very late antigen α4 (VLA-4) also potentiates tethering, demonstrating this process is not solely driven by selectins (***figure 1.2***)(23). Interestingly, tethering is mitigated completely in vessels smaller than 20 μm, implying that in this situation leukocyte close contact with the endothelium would be enough for initial capture (24). Bystander leukocytes (that are in blood flow) can also tether to endothelial-bound leukocytes via L-selectin/PSGL-1 interaction. This phenomenon is known as "secondary tethering", which occurs when the endothelium supports an overwhelming number of adherent leukocytes that the endothelial-derived ligand becomes inaccessible to the bystander leukocyte(24). As such, the L-selectin and PSGL-1 on static and flowing leukocytes become the appropriate ligand/receptor interactions. This interaction will continue until the tethering leukocyte reaches a stretch of endothelium that it can adhere to (25). Secondary capture can account for up to 70% of total leukocyte accumulation given the right hydrodynamic and vessel conditions(25)(26). This mechanism of leukocyte capture has been observed to form "long strings" in the murine cremaster (27)(28). However in another *in vivo* study secondary capture does not play an important role in leukocyte capture. Here, Kunkel et al. observed that leukocyte-leukocyte interactions accounted for only 1.2% of total recruited leukocytes in an TNF-α stimulated vessel (29). It is however likely that secondary capture is employed in a vessel dependent manner, in a vessel where the diameter is of comparative size to the leukocyte diameter leukocytes will be forced to deform and involuntarily contact the vessel wall. In this scenario the use of the secondary capture is redundant. Eriksson et al., have demonstrated that secondary capture events in small venules, with low wall shear rate, was infrequent, yet, a higher secondary capture frequency was observed in larger vessels with higher shear forces (27)(25). It is possible that secondary capture is important for high leukocyte densities during inflammation, as inflammation prompts vasodilation, enlarging vessel diameter.

Deleted: also potentiates

Deleted: as the diameter is of a similar magnitude to the leukocytes it would

Deleted: importance is more questionable,

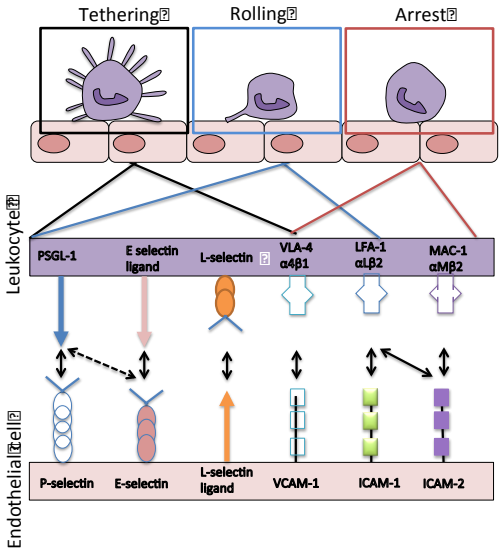

Figure 1.2: The cell adhesion molecules on EC and leukocytes responsible for tethering, rolling and arrest.
The schematic illustrates the cell adhesion molecules (CAMs) found on both the endothelium and leukocyte in the three stages of the adhesion cascade, tethering, rolling and arrest. Full names of CAMs can be found in the ***Abbreviations section***.

1.2.2 Leukocyte rolling

For tethering to progress to rolling there needs to be sufficient available ligand presented by the endothelium. Leukocyte rolling is a vital biological process as it provides sustained intimate contact between the leukocyte and endothelium, providing the first opportunity for information to be exchanged between the inflamed endothelium and the sensing leukocyte(11). Rolling is a continuous movement, heavily dependent on the fast on/off rate of the selectin/ligand interactions(11). The selectin family are the major mediators of rolling, a triple L/E/P-selectin knock-out mouse revealed a dramatic decrease in rolling flux (30)(31). All three selectin molecules are involved in rolling; however, they regulate different rolling velocities (32)(33). Deletion of the last 11 amino acids at the C terminus of L-selectin completely abolishes lymphocyte rolling on glycosylation-dependent cell adhesion molecule-1 (GlyCAM-1) *in vitro* (34). In rat mesenteric venules, introduced human neutrophils, pre-treated with a function-blocking antibody for L-selectin reduces rolling flux by more than 70% (35). P-

Deleted: binding

Deleted: s

selectin is the first selectin molecule to be expressed on the surface of the endothelial cell (EC), this occurs within a minutes of stimulation(12). EC activation stimulates P-selectin release from pre-stored granules called Weibel-Palade bodies, the molecule then becomes expressed at the plasma membrane through membrane fusion of intracellular stores(12). P-selectin involvement in rolling has been demonstrated both *in vivo* and *in vitro*. Exteriorised cremaster vessels from a P-selectin knockout mouse showed leukocytes lack the ability to roll (37)(38). *In vitro*, treating neutrophils and monocytes with neutralising antibodies for PSGL-1 completely blocked rolling when perfused over recombinant purified P-selectin, suggesting PSGL-1 is the only ligand for P-selectin that is expressed on leukocytes (36)(37). Together, these experiments conclude the vital role P-selectin and L-selectin play in rolling. E-selectin requires de-novo synthesis, delaying its expression at the plasma membrane to around four hours post cytokine stimulation (38). Unlike P-selectin, blocking E-selectin function *in vitro* and *in vivo* does not completely reduce rolling (37)(36). This is likely due to the complementary roles of P-selectin and E-selectin. In fact leukocytes in an E-selectin knockout mice increased rolling velocity compared to their WT counterparts; this led to E-selectin being identified as a mediator of slow rolling(39). Paradoxically, it was noted that P-selectin and L-selectin could not mediate rolling below a critical shear stress(40)(41). This can be explained using the "catch-slip" model of adhesion (39)(40). The selectin/ligand interaction transitions between two forms of bonding "Catch" or "Slip". The strength of bonding is increased with increasing shear stress (Catch), after the shear stress increases to a non-optimal value the bonds become weaker and break at a higher frequency (Slip). On a tethered leukocyte the hydrodynamic force exerted on the cell rear is high and non-optimal producing short-lived bond formation, conversely, at the cell front the bonds are longer lived. Together, this phenomenon encourages the leukocyte to roll in the direction of the blood flow. Of the three selectin molecules L-selectin mediates the fastest rolling velocity (~100μm/second), in comparison P-selectin mediates rolling at a velocity of ~50μm/second(32)(41). Rolling provides an appropriate ligand/receptor interaction lifetime for the leukocyte to survey the apical aspect of the

endothelium for chemokines, which are involved in activating another set of CAMs – the integrins(11).

Deleted: ’

1.2.3 Leukocyte arrest

Leukocyte arrest relies on the activation of integrins. Integrins are heterodimers composed of an α and β subunit, which are both type I transmembrane proteins(42). The three most studied integrins within the leukocyte adhesion cascade are: (i) lymphocyte function-associated antigen-1 (LFA-1), which is composed of αLβ2 and expressed on virtually all leukocytes; (ii) macrophage-1 antigen (MAC-1), is composed of αMβ2 subunits and expressed on neutrophils and monocytes; (iii) very late antigen-4 (VLA-4) is composed of α4β1 and expressed on monocytes and eosinophils and neutrophils under certain conditions (43)(44). Integrins bind to members of the immunoglobulin (Ig) superfamily expressed on the endothelium. Integrins can transition from “inactive” to “intermediate” to “active” states(42). The outcome of each integrin activation state is driven by different stimuli. During inflammation, endothelial cells distribute chemokines in a polarised manner, with abluminal chemokines being transported via transcytosis for presentation on glycosaminoglycans (GAGs) on the luminal surface. In the circulation, integrins decorate the leukocyte in low numbers and in a bent conformation. The bent conformation has a low affinity state for ligand binding (***figure 1.3***). Integrins can signal bidirectionally, referred to as inside-out and outside-in. Typically intracellular signalling initiates inside-out signalling, allowing the integrin to bind to its appropriate ligand, conversely, the interaction between integrin and ligand can induce outside-in signalling which allows the cell to response to its environment, for example induce cell spreading or migration. One common example of inside-out signalling occurs when a leukocyte becomes in contact with the chemokine decorated endothelial cells(11), G-protein coupled receptors (GPCRs) become engaged, activating downstream signalling to release endoplasmic reticulum (ER) stored calcium. In turn, the influx of calcium into the cytosol leads to activation of calcium dependent kinases and modulates talin and β2 (integrin subunit) interactions(45). Talin binding to the cytoplasmic tail of β2 induces a

Deleted: conditions

Deleted: ,

conformational shift forcing the β2 and α subunits of the integrin apart "pushing" the integrin into the active state (45). In this conformation integrins bind with high affinity to their endothelial ligands, vascular cell adhesion molecule 1 (VCAM-1) intracellular cell adhesion molecule–1 (ICAM-1), which allows for the leukocyte to firmly adhere to the endothelium (***figure 1.2***). Alternatively, integrins can be activated through the interaction of CAMs (***figure 1.3***). Leukocytes binding to either E-selectin or P-selectin or ligand binding to L-selectin have all been shown to activate integrins(46). For example E-selectin binding to PSGL-1 leads to activation of tyrosine kinases (MAPK, Syk), which shifts the conformation of LFA-1 from the bent to the extended (high affinity) state (46).

Deleted: Leukocyte binding to either E-selectin or P-selectin or ligand binding to L-selectin ha

Deleted: s

Outside-in signalling has been suggested to operate discreetly from inside-out signalling and be involved post leukocyte arrest(47). Removing the protein kinases hck and fgr (both required for mediating the outside-in signalling pathway) did not effect chemokine dependant integrin activation (inside-out signalling), yet neutrophil spreading over β2 ligand was severely reduced and neutrophils rapidly detached (47). Finally, ligand induced integrin clustering can form a signalling hub known as "signalosomes", delivering intracellular messages to regulate the cytoskeleton, priming the cell for invasion through the endothelial barrier (48).

Deleted: a

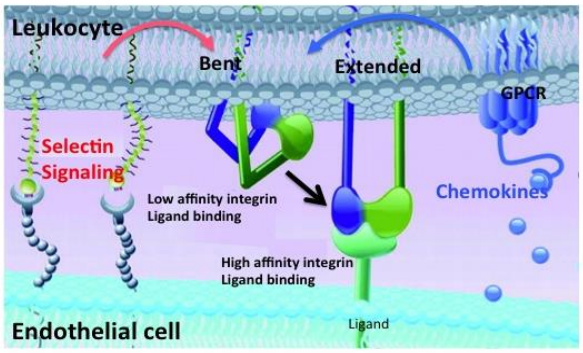

Figure 1.3: Integrin bent-extended conformation change

To initiate leukocyte firm arrest to the endothelium, integrins alter their conformation to result in high affinity ligand binding. Integrin activation is evoked through many signalling processes. Image adapted from Totani and Evangelista, Arterioscler Thromb Vasc Biol, 2010 (49).

The importance of selectins and integrins are acknowledged in human leukocyte adhesion deficiencies (LAD I, LAD II &LAD III), which occur due to defects in β2 integrin structure and also mutations in the major ligand for selectins Sialyl-Lewis (x). Here, patients present with severe immunodeficiencies due to insufficient integrin activation and leukocyte capture (50).

Deleted: ’

Deleted: , two being selectin or chemokine dependent

Deleted: y’s

1.2.4 Intraluminal crawling

Following firm adhesion and spreading, leukocytes often migrate away from their initial site of arrest in order to identify an appropriate exit point. Crawling has been observed in all different directions with respect to blood flow(51). Leukocytes adopt a cellular morphology that is similar to migration on 2D substrates, e.g. formation of a leading edge with a lamellipodium and a retracting rear (sometimes referred to as a "uropod"). MAC-1 was identified as a critical integrin involved in mediating intraluminal crawling, murine neutrophils lacking MAC-1 were seen to emigrate without any intraluminal crawling(52). The emigration of MAC-1-deficient neutrophils was sub-optimal, which manifested in prolonged transmigration times compared to neutrophils in WT littermate control mice (52)(53). In comparison, LFA-1-deficient neutrophils adhered poorly to inflamed venules, yet normal intraluminal crawling was observed in the population of neutrophils that could adhere to the endothelium, again highlighting a unique role for MAC-1 in intraluminal crawling(52). However, a study using a combination of function-blocking antibodies against LFA-1 and MAC-1, demonstrated that monocytes require both LFA-1 and MAC-1 to undergo intraluminal crawling and reach junctions (52). Together, this demonstrates the complexity of how integrins on the leukocyte are employed for the adhesion and crawling steps of the adhesion cascade. It also alludes to how different leukocyte subtypes, or even leukocytes from different species, may use integrins to mediate the steps prior to and during transmigration.

Deleted: will

Deleted: was

Deleted: identified as

1.2.5 Endothelial docking structures

The endothelium actively participates in transendothelial migration (TEM) through the formation of apical actin rich protrusive structures. These structures have been given a multitude of names: docking structures, endothelial adhesion platforms and transmigratory cups (54)(55)(56).These structures are enriched in ICAM-1, VCAM-1 and the tetraspanin proteins CD9 and CD15 (57)(58). Evidence has emerged that irrespective of which route of transmigration (paracellular or transcellular) the majority of diapedsis events *in vitro* are aided with the formation of these structures. Live cell imaging showed that greater than 70 % of neutrophils migrated across a HUVEC monolayer were supported by these

structures (59). Over the past decade ICAM-1 has emerged as a pivotal protein in the formation of these docking structures. Clustering of ICAM-1, which is driven by integrin binding (LFA-1 or MAC-1) promotes the assembly of F-actin driven docking structure formation(60). Additionally, the GTPase RhoG and its upstream regulator SH3-containing guanine nucleotide exchange factor (SGEF) have recently been implicated in the molecular pathway for docking structure formation;(60) this was prompted by a previous finding demonstrating that expressing SGEF in fibroblasts induced the formation of dorsal membrane ruffles and enhanced macropinocytosis (60). So far the pathway breaks down as follows; ICAM integrin engagement rapidly activates Rho G, and both RhoG and SGEF colocalise with clustered ICAM-1 (61). It has been suggested that these endothelial docking structures have a protective physiological function, shielding the leukocytes from shear stress (62). Interestingly, observations *in vivo* have shown docking structures mature to fully envelope the leukocyte, termed endothelial domes (63). Recently an F-actin binding protein, leukocyte-specific protein 1 (LSP1) was shown to be important for the formation of endothelial domes *in vivo* in response to the neutrophil chemokine called keratinocyte-derived chemokine (KC) (64)(65). LSP1 is actively recruited from the cytosolic and nuclear compartments to the cytoskeleton in response to endothelial activation. Studies in Lsp1-/- mice not only revealed a significant reduction in the number of endothelial domes formed in response to KC stimulation, but also increased vascular permeability (65). This permeability data may underpin the physiological role for endothelial domes and specifically the role of LSP1 in endothelial barrier integrity (65).

Deleted: .

Deleted: permeability

1.2.6 Transendothelial migration (TEM)

Leukocytes can undergo two distinct modes of diapedesis: paracellular (between adjacent endothelial cells) or transcellular (through the body of a single endothelial cell), (***figure 1.4***). Both modes have been observed *in vitro* and *in vivo,* although ~70-90 % of all studied TEM routes occur via the paracellular pathway (66)(67). There are however certain exceptions when the transcellular route is thought to be favoured – for example where adjoining endothelial junctions are extremely tight, as in the blood-brain barrier (68)(69)(70).

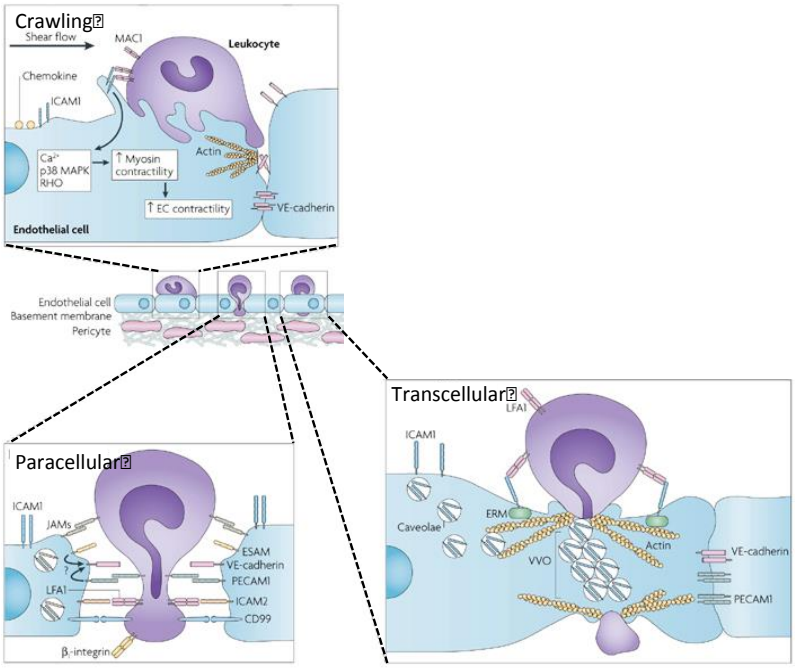

Figure 1.4: Leukocyte transmigration
Crawling: Leukocytes initiate transmigration through the extension of leukocyte membrane protrusions into the endothelial cell body or at EC junctions, triggering MAC-1/ICAM-1 interaction, clustering and subsequent increased intracellular Ca^{2+}, downstream activation of p38 MAPK and RHO. Collectively, these intracellular signalling events promote myosin contractility within endothelial cells, and separation of adjoining endothelial cells. *Paracellular pathway*: Homotypic VE-cadherin binding is disrupted, facilitated by the addition of new membrane from the LBRC (not shown discussed in the text). Leukocyte-endothelial cell interactions can now form using homotypic interactions between CD99 and PECAM-1. *Transcellular pathway*: ICAM-1 signalling fuses vesiculo-vacuolar organelles (VVOs) to form an intracellular channel. For abbreviations used, see ***Abbreviations section***. Image adapted from Ley et al. Nat, Rev, Immunology, 2007, (11).

1.2.6.1 Paracellular transmigration

Successful paracellular transmigration relies on the "unzippering" of junctional molecules joining two adjacent endothelial cells. The loosening of the junctions occurs through initial clustering/cross linking of luminally expressed ICAM-1 and VCAM-1, leading to transmissions of numerous signalling pathways (71). One such pathway involves transient increases in cytosolic calcium, which activates myosin light chain kinase to mediate cell contraction (72). This introduction of internally contractile forces encourages separation of adjoining endothelial cells.

Additionally, ICAM-1 clustering can promote phosphorylation of VE-cadheren and subsequent redistribution away from adherens junctions (73). *In vitro* culture assays demonstrated that ICAM-1 clustering mediates Src and Pyk2 kinases to phosphorylate VE-cadherin at regions that are necessary for p120 and β catenin binding (74). VE-cadherin relies on such binding partners for its localisation at adherens junctions. It has been hypothesised that phosphorylation of VE-cadherin prevents p120 binding(75)(76). Overexpression of p120 leads to VE-cadherin remaining at the junctions, again supporting the hypothetical view that p120 stabilises endothelial junctions (77).

Using electron microscopy, investigators observed endothelial-derived intracellular vesicles surrounding leukocytes at the point of TEM (78).These vesicles were defined as the "lateral border recycling component" (LBRC), considered to be a unique organelle composed of multiple vesicles. Each vesicles ~50nm in diameter contains many junctional molecules; PECAM-1, JAM-A, CD99, but notably not VE-cadherin (67)(78). Approximately one third of leukocyte PECAM-1 resides in the LBRC, PECAM-1 mutation studies have indicated that tyrosine 663 is responsible for maintaining PECAM-1 within the LBRC (79)(80). The LBRC is responsible for the continual turn over of plasma membrane at the cell borders. The function of this constitutive recycling of membrane is poorly understood, however it has been strongly linked to driving successful TEM. Blocking the transport of membrane from LBRC consequently blocks TEM (81). Given the high-energy expenditure required to break the large concentration of homophillic interactions at the EC-EC contact points, one theory suggests that LBRC inserts new membrane to dilute endothelial junctions with bound CAMs(82). This newly added membrane would contain unengaged PECAM-1, JAM-A and CD99 to form interactions in trans with the same molecules expressed on the transmigrating leukocyte and aid passage. Genetic ablation or antibody function blocking studies have delineated unique roles for PECAM-1 and CD99. Disrupting PECAM-1 function led to leukocyte arrest on the apical surface of the endothelium, whilst blocking CD99 interactions traps leukocytes mid-way through TEM (83)(84)(85). Taken together, these results imply that PECAM-1 works upstream of CD99. Although, there appears to be conflicting data from in

Deleted: it's

Formatted: Justified, Indent: Left: 0 cm, First line: 0 cm, Widow/Orphan control, Adjust space between Latin and Asian text, Adjust space between Asian text and numbers

Formatted: Font color: Auto

Formatted: Font color: Auto

Formatted: Font color: Auto

Formatted: Font color: Auto

Formatted: Font color: Auto

Formatted: Font color: Auto

Field Code Changed

Field Code Changed

Formatted: Font: Not Italic

Formatted: Font color: Auto

Formatted: Font color: Auto

Formatted: Font: Not Italic

vivo studies regarding the sequential order in which CAMs are involved in TEM. In the C57B1/6 mouse strain the site of arrest was examined in mice lacking either JAM-A or PECAM-1, here neutrophils arrested between the abluminal surface of the endothelium, partway through the junctions, or at the basement membrane, respectively (86). Additionally, the role of PECAM-1 in regulating neutrophil TEM in C57Bl/6 mice appears to be cytokine-specific. PECAM-1 knockout mice challenged with TNF-α mimicked the results found in WT littermate controls. In contrast, IL-1β stimulation led to a significant decrease in neutrophil recruitment(87). This would suggest PECAM-1 recruitment is dependent on the inflammatory stimuli; with PECAM-1 redundant for TNF-□ activation, but non-redundant for IL-1□□□activation (87). These studies highlight that the requirement of CAMs may change over the course of an inflammatory response. As these studies were conducted in the peritoneum and cremaster muscles, more work is required to determine what recruitment profiles are dependent and independent on other CAMs in disease models. Upon the leukocyte reaching the basaolateral surface of the endothelium, the endothelial junctions re-seal behind the transmigrating leukocyte to maintain endothelial barrier integrity and minimise oedema formation.

Deleted:
Formatted: Font color: Auto
Formatted: Font color: Auto
Formatted: Font color: Auto
Deleted: a
Deleted: appeared to
Deleted: c
Formatted: Font: Cambria
Formatted: Font: Cambria
Formatted: Font color: Auto
Formatted: Font color: Auto
Formatted: Font color: Auto
Deleted: O
Deleted: n
Deleted: aspect

1.2.6.2. Transcellular transmigration

In 1998 the Dvorak lab provided the first evidence that transcellular migration occurs *in vivo* (88). Electron microscopy revealed neutrophils indisputedly passing directly through a single endothelial cell. Transcellular migration has been suggested to be favourable in a number of circumstances, one example being neutrophils migrating through an endothelial cell at the thinnest region, presumably to coincide with the region of lowest resistance in that immediate environment (89). Additionally, this route may be adopted if leukocytes have impaired intraluminal crawling and cannot migrate towards a junction. Neutrophils lacking the integrin MAC-1 could adhere to the endothelium, but could not migrate towards endothelial cell junctions(52). Although the efficiency of TEM was low, those that could undergo TEM exited via the transcellular route (84)(53). Leukocytes are believed to commence transcellular migration by probing the endothelial monolayer with "invasive podosomes", presumably to

Deleted: un

"sense" for regions of low resistance (66). During transcellular migration ICAM-1 enriches at sites of diapedesis. Engagement of ICAM-1 by leukocytes leads to it's clustering, which in turn recruits caveolin-1 and filamentous actin (90). The LBRC and caveolin-1 containing vesiculo vacuolar organelles (VVOs) have both been described for the formation of the membrane fenestra observed. VVOs are small continuous links of internal vesicles rich in caveolin-1, it is hypothesised that these internal vesicles provide a transcellular channel permissive for leukocyte migration through a single endothelial cell. Depleting cellular levels of caveolin-1 by siRNA significantly decreased the transcellular pathway (91)(90), while overexpressing ICAM-1 lead to an increase in transcellular transmigration(90)(91). It is believed that ICAM-1 lines the internal channel through which the leukocytes can pass via integrin-based migration (90)(91). Interestingly, VVO's and LBRC share many of the same adhesion molecules found at junctions, for example PECAM-1 and JAM-A. Currently it remains unclear if these two organelles (VVOs and LBRC) work synergistically or independently of one another.

1.2.6.3 Reverse transmigration

The term TEM describes the movement of a leukocyte crossing the endothelial barrier via a luminal-to-abluminal direction. However, with the increasing advances in technologies supporting intravital microscopy, neutrophils have recently been observed to undergo abluminal to luminal TEM. This process, termed reverse transmigration (rTEM), has been observed *in vivo* and *in vitro*. Furthermore, most major leukocyte subsets have been observed to undergo rTEM: monocytes, neutrophils and T cells (92) (93) (93). Woodfin and colleagues revealed that rTEM is enhanced following pharmacological blockade or genetic deletion of the endothelial CAM called junctional adhesion molecule-C (JAM-C) (94)(95).The model for neutrophil rTEM outlined by Colom et al.,(95) will be described below (***figure 1.5***). In response to ischemia reperfusion injury, a type of sterile injury, leukotriene B_4 is synthesised and secreted from tissue resident leukocytes(95). Blood borne neutrophils react to this pro-inflammatory signal through their LTB_4 receptor BLTR, in turn this induces neutrophil elastase (NE) production and secretion. The interaction of MAC-1 with NE, allows NE to be

spatially regulated and brought close to JAM-C, as MAC-1 is a known ligand for JAM-C. NE proteolytically cleaves JAM-C, (***figure 1.5***) (96). So far, the physiological relevance for reverse transmigration is unclear. Potentially, rTEM might be linked to dampening the immune response; rTEM neutrophils may act as cellular sentinels(97)(98). Alternatively, the role may encourage systemic inflammation(95)(97). Leukocyte undergoing rTEM have a distinctive ICAM-1 ^{hi} phenotype, allowing these cells to be tracked. Studies which have following rTEM neutrophils, exiting either the cremaster muscle or the ear after ischemia reperfusion injury or LTB_4 administration, have detected these ICAM-1 ^{hi} neutrophils in the lung vasculature, and their presence is associated with lung inflammation and priming of reactive oxygen species (ROS) production (99). The work above highlights the ability for rTEM neutrophils to dramatically spread a local acute inflammatory response (99).

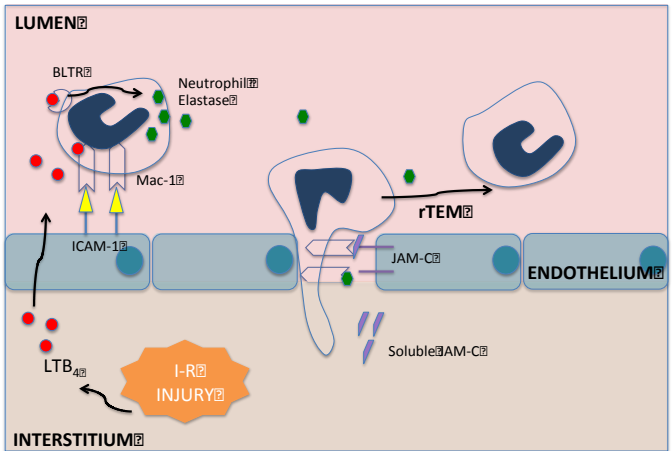

Figure 1.5: Leukocyte reverse transmigration
Following ischemia reperfusion injury (I-R) the lipid chemoattractant leukotriene B_4 (LTB_4) is produced and secreted by tissue resident macrophages. Relseased LTB_4 can now bind to the neutrophil receptor (BLTR) aiding neutrophil elastase (NE) stimulation. Binding of NE to MAC-1 supports JAM-C cleavage, producing soluble JAM-C. Cleavage of JAM-C resulted in reverse transmigration. Image adapted from Colom et al., Immunity, 2015 (95).

1.2.7 Leukocyte migration beyond TEM

After successful TEM, leukocytes are confronted with other physical obstacles. The first is the pericyte sheath, made up of pericytes - contractile cells that wrap around venules in a discontinuous manner(11). Previously, known as effectors of

Deleted: be more sombre

Deleted: were

Formatted: Superscript

Deleted: leukocytes

Deleted: ,

Deleted: which

Deleted: s

Deleted: its

angiogenesis, there is now a growing body of evidence highlighting pericytes as regulators of the inflammatory response (100) (101) (102). Pericytes provide an ICAM-1 dependent adhesive platform for the leukocytes to bind (103). Inflammatory signals also dictate the pericyte shape, which, if contracted, can create large gaps between adjacent pericytes to provide an exit portal for the leukocyte (104) . Emigration of leukocytes through a pericyte via a transcellular route have been observed in strongly activated tissues, indicating that in some cases the pericyte sheath may act as a true barrier (88). Like the endothelium, pericytes are responsible for secreting components that form the basement membrane (BM), a complex mesh work of fibrous proteins namely laminins and collagen IV which cross-link together through glycoproteins(105). Early electron microscopy noted that most leukocytes were captured between the endothelium and BM interface rather than in the process of passing between endothelial cells, suggesting that the BM offers more resistance (105). Immunofluorescence studies of inflamed cremasteric tissue revealed the presence of "low expression regions" (LER), where the BM is less densely packaged. Interestingly this LER coincided with areas of low pericyte coverage, suggesting that pericytes are involved in shaping permissive exit points for transmigrated leukocytes (106). Interestingly, leukocytes exiting the endothelium display protrusive pseudopods, suspected to be used to probe and identify the permissive LER (66)(107).

1.3 Leukocyte migration in 3D environments

Single cell migration can be broadly defined into two categories: amoeboid and mesenchymal. Mesenchymal migration describes a slow (less than 1 μm/min) locomotion, which is dependent on strong adhesive linkage to the ECM and metoproteinase remodelling of the ECM(112). The mesenchymal mode of migration is adopted by: cancer cells, fibroblasts, smooth muscle cells and endothelial cells. In contrast, immune cells use the amoeboid mode (108), which is fast moving (up to 30 μm/min) and independent of integrins and strong linkage to the ECM (109). ***Figure 1.6*** demonstrates the fundamental differences between mesenchymal and amoeboid styled migration. How a leukocyte polarises and is able to migrate in an amoeboid fashion will be discussed further below.

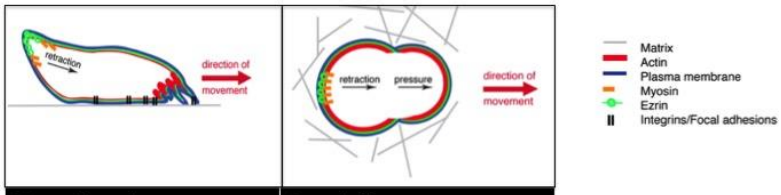

Mesenchymal	Amoeboid
Elongated morphology	Rounded morphology
Lamellipodia protrusion	Blebbing protrusion
Strong adhesion	Weak adhesion
MMP activity	Low MMP activity
Low cortical tension	High cortical tension
Low Rho/ROCK activity	High Rho/Rock activity

Figure 1.6: The differences between mesenchymal and amoeboid migration
Graphical representation and tabulation of differences observed from the two different migration modes. Figure adapted from (110).

The establishment of leukocyte front-back polarity is critical for migration to be achieved; this can be influenced through external cues for example cytokines, chemokines and extracellular matrix fragments (111) (112). Alternatively, when faced with a homogenous chemokine environment a leukocyte can spontaneously polarise (113)(114). ***Figure 1.7*** depicts a typical polarised leukocyte; the leading edge, mid-body and uropod, each of these sections of the cell will be discussed in detail below.

Deleted: .

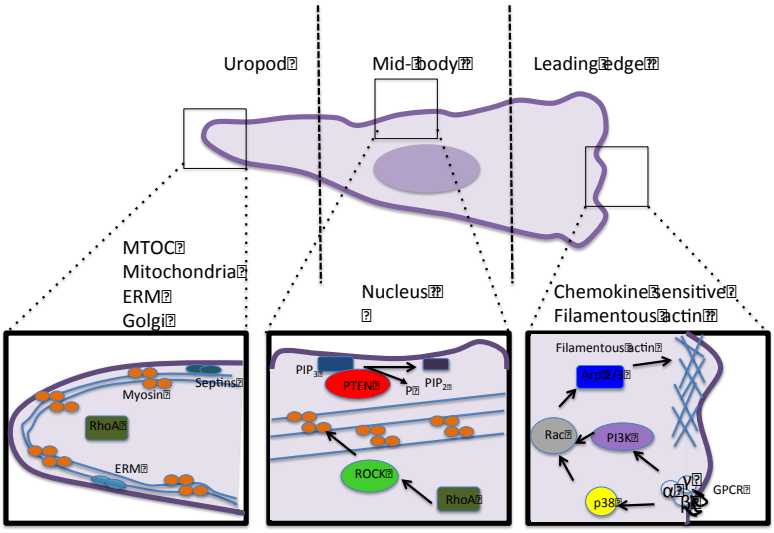

Figure 1.7: A polarised leukocyte
The cell has adopted a polarised leukocyte. At the leading edge, surface receptors, GPCRs, activate PI3K that phosphorylate PIP_2 to PIP_3. Rac is activated through both PI3K and p38 MAPK mediated pathways, to facilitate actin polymerisation and branching. The mid-body, contains actin fibres that are under control of Rho and ROCK. The uropod forms a highly contractile rear that contains ERMs and septins. For abbreviations used see ***Abbreviations section***. Image adapted from Friedl and Weidelin, Nature Immunology, 2008 (115).

Deleted:

Deleted: amoeboid shape

Leukocyte migration can be described through four stages; i) the leading edge protrudes, generating one or more short lived pseudopods or alternatively form blebs ii) the protruding membrane interacts with the substrate in a low adhesive manner iii) actomyosin mediated contractile forces occur at the mid-body and rear regions increasing the hydrostatic pressure at the front of the cell iv) the cell rear moves forward. These four stages are repeated in a cyclic manner to generate forward movement (115).

Deleted: Amoeboid

Deleted: forms adhesive contacts with the substrate

Deleted:

Deleted: iv

Deleted: releases from the substrate

Deleted: movement(

Cytoskeletal dynamics are regulated by the Rho GTPase family, in mammals the Rho family consists of 22 members, however the most commonly studied members contributing to leukocyte migration are the three proteins; Cdc42, Rho A and Rac(115). Rho GTPase proteins cycle between their inactive and active

Deleted: ranes

forms through binding guanine diphosphate (GDP) and guanine triphosphate (GTP) respectively. How Cdc42, Rac and Rho A contribute to leukocyte migration will be discussed below.

The leading edge

To initiate a leading edge there must be a breakage of cytoskeletal symmetry, which can be triggered by G-protein-coupled receptor (GPCR) signalling (115). In leukocytes most GPCRs transmit through the G protein subtype $G_i\alpha$ (115). Here, for example, chemoattractants such as N-formylmethionine-leucyl-phenylalanine (fMLP) bind to GPCRs and activate phosphoinositide 3-kinase (PI3K), which in turn converts phosphatidylinositol (4,5) bisphosphate (PIP_2) to phosphatidylinositol (3,4,5) trisphosphate (PIP_3). PIP_3 serves as a docking site for pleckstrin-homology domain containing proteins; one example being the kinase Akt which through its downstream effector the Rho GTPase Rac induces actin polymerisation leading to pseudopod protrusion (116)(117). PIP_3 is predominantly found at the leading edge. Alternatively, in neutrophils the formyl peptide receptor (FPR) can activate Rac through p38 MAPK (118). Activated Rac induces actin polymerisation through the WAVE complex and branched actin filaments are created by the actin nucleator protein Arp2/3. Actin growth pushes the plasma membrane outwards propelling the leading edge. Cdc42 shortens the stability of the leading edge (119). Together this work suggests different roles for the two GTPases found at the leading edge; Rac is involved in producing cell polarity, whilst Cdc42 maintains the stability of the leading edge.

The mid-body

In the mid-body there is a contractile ring of actin filaments, cross-linked through the motor protein myosin II. This contractile ring prevents lateral protrusions forming, further encouraging polarity, and additionally can distort the shape of the nucleus. Neutrophils have a segmented, "pearl chain nuclei", and making traversing small pores within the ECM more manageable. Deformation of the nucleus is dependent on myosin II, pharmacologically inhibiting myosin II activity rendered the nuclei of dendritic cells spherical and migration was severely reduced (120). At the uropod and mid-body, PIP_3 is dephosphorylated by PIP_3 phosphatases (PTEN & SHIP), which convert PIP_3 back to PIP_2 (121).The distribution of PIP_3 is crucial: Heit et al., demonstrated that PTEN-deficient

Deleted: these three proteins

Deleted: signalling(

neutrophils display random migration rather than directed migration in response to chemokine stimulation (122). Recently, work in fibroblasts has suggested that the nucleus can act as a piston, physically compartmentalising the rear and front of the cell to increase the hydrostatic pressure at the leading edge (123), this behaviour is yet to be characterised in leukocytes.

The uropod

The uropod contains the microtubule organising centre (MTOC), the Golgi complex and an abundance of mitochondria (115). The enrichment of mitochondria is presumably due to the high levels of ATP driven actomyosin contractility (115). RhoA is found most abundantly at the uropod and activates Rho-associated protein kinase (ROCK), which phosphorylates myosin light chain (MLC). Phosphorylation of MLC increases MLC ATPase activity, sliding adjoining actin filaments over one another to drive cell contraction; this in turn propels the cell forward via cytosolic hydrostatic pressure. A lack of RhoA leads to the formation of multiple lamellipodia in monocytes, whereas expression of its dominant negative form results in a non-protrusive cells (124)(125). Hence, it has been proposed that RhoA must be actively inhibited at the leading edge to allow lamellipodial protrusion formation, but must be active at the rear to confer "backness". The uropod is enriched in proteins to strengthen cortical integrity (ERMs and septins) ensuring that protrusion formation is not favoured at the rear of the cell (126)(127)(128).

1.4 Leukocyte chemotaxis

Chemotaxis describes the movement of a cell towards a chemical stimulus. In order for a leukocyte to chemotax, the cell must polarise and migrate towards the chemical cue. The most classically studied chemoattractants are formylated peptides (bacterial or mitochondrial derived peptides), C5a (a product of the complement cascade), LTB_4 (a product of phospholipid metabolism) and chemokines (secreted by numerous different cell types)(3). Upon a chemoattractant binding to its appropriate GPCR receptor, a series of symmetry breaking events occur, described in ***section 1.3***, to allow the cell to follow its chemotactic cue. The formylated tri-peptide fMLP is frequently used within this thesis; this potent chemoattractant can mimic sterile injury, as it is analogous

Deleted: increase the

Deleted: mitochondria(

Deleted: is presumably

Deleted: contractility(

Deleted: its

Deleted: contraction,

Deleted: S

Deleted: .

with eukaryotic mitochondrial derived N-formyl-methionine proteins. Upon sterile injury, necrotic tissue, specifically the rupture of mitochondria releases chemotactic formylated proteins (129).

Deleted: and release

Deleted: these

1.4.1 Chemoattractant signalling and hierarchy

Once within the perivascular space, the leukocyte is confronted with a multitude of conflicting chemotactic signals. Several studies have demonstrated that neutrophils prioritise their responses to chemoattractants in a hierarchical manner (130)(131)(132). Chemoattractants have been categorised as either end-target (a signal emanating from the site of infection or damage) or intermediary (a signal encountered on route)(118). Intermediary chemoattractants include: IL-8, Gro-α and LTB_4, while end-target chemoattractants include fMLP and C5a(118). Leukocytes place their highest priority response to end-target cues, irrespective of concentration (118).Seminal work by Heit et al. and colleagues demonstrated that neutrophils migrated towards end-target chemoattractants via p38 MAPK-dependent signalling, whilst migration towards intermediary signals was governed by PI3K/Akt signalling(118).Interestingly, each chemoattractant can activate different integrin sub-sets. Two-dimensional chemotaxis assays were conducted on a composition of integrin ligands (fibronectin, fibrinogen, ICAM-1 and VCAM-1) neutrophils responding to fMLP required MAC-1 integrins, while neutrophils migrating towards IL-8 required LFA-1 integrins (133). This data was reflected in neutrophil integrin surface expression, neutrophils stimulated with fMLP or IL-8 led to respective increases in MAC-1 and LFA-1 expression. The phosphatase PTEN (phosphatase and tensin homolog) is also thought to be responsible for "prioritising" chemoattractants. In opposing gradients PTEN distribution becomes uniform, moving from the rear of the cell. PTEN activity inhibits PI3K activity (***section1.3***), thus only permitting the p38 MAPK directed signals. Pten -/- neutrophils could not effectively clear bacterial infections *in vivo* due to becoming "distracted" by intermediary chemokines (122).

Deleted: r

Additionally, heterologous desensitisation (also known as cross-desensitisation) may explain leukocyte preference to migrate towards fMLP. Briefly, heterologous desensitisation occurs when a receptor looses it responsiveness following

phosphorylation by a secondary messenger, which has been activated through a different chemoattractant receptor signalling. A prominent messenger responsible for receptor desensitisation is protein kinase C (PKC). Under cross-desensitisation conditions, PKC has previously been shown to phosphorylate and down regulate CXCR1, C5aR and platelet-activating factor receptor PAFR, surprisingly FPR receptors remained unaffected (i.e. not phosphorylated) by PKC (134)(135). Therefore, when interstitial leukocytes are exposed to multiple chemotactic cues, the fact that FPR remains untargeted by PKC, allows downstream signalling to dominate from this receptor.

Chemoattractant receptors can also exhibit "homologous desensitisation" where the receptor decreases its response to the chemoattractant following prolonged exposure to a high concentration. The widely accepted model for homologous desensitisation describes a system where the chemoattractant receptor becomes phosphorylated by a G-protein coupled receptor kinase (GRK). This phosphorylated receptor now acts as a binding substrate for a group of proteins called the arrestins. β-arrestin knockout mice exhibited a dramatic prolonged response to the alengesic effect to morphine, consistent with impaired GPCR opioid receptor desensitisation (136). β-arrestin interaction with the GPCR sterically precludes binding to the G-protein. GPCR bound β-arrestin acts as a adaptor protein binding to components of the clathrin endocytosis machinery (137)(138). Once internalised, GPCR receptors display two behaviours dependent on the strength of binding between the specific β-arrestin and GPCR. Transient GPCR-β-arrestin complexes encourage rapid recycling of GPCR back to the plasma membrane; alternatively a stable GPCR-β-arrestin complex favours GPCR degradation. Eliminating GPCR-β-arrestin interaction stability through the receptor mutation R137H, re-establishes GPCR trafficking to the plasma membrane (139).

Deleted: secondary

Deleted: re

Deleted: lowing

Deleted: d

Deleted: s

1.4.2 The extracellular matrix and neutrophil migration

The extracellular matrix (ECM) describes the protein/glycoprotein scaffold within the perivascular space. It is produced through secretion by endothelial cells, pericytes and fibroblasts (140),(141).The ECM can include: (i) the basement membrane, which is composed mainly of laminins and collagen IV; (ii) the interstitial matrix, which is composed largely of collagens and elastins. Functionally, the ECM is not solely limited to the structural role of supporting blood vessels; it also contributes to numerous signalling roles. Collins et al., identified an ECM specific mechanosensitive signalling pathway and found that ECM composition has a profound effect on endothelial cell stiffness (142). Alongside this, the ECM can have a direct impact on leukocyte recruitment, either acting as a chemoattractant or coupling to chemoattractants. The best-known examples so far for the ECM acting as a chemoattractant, are the cleaved fragments of type I collagen, the acetylated tri-peptide Pro-Gly-Pro (acetyl PGP) (143). Using a lung inflammation model, this tri-peptide has been shown *in vivo* to mimic the chemotactic effect of IL-8 on neutrophils (144). Interestingly, a large proportion of all known chemokines interact with glycans that decorate the ECM, such as heparan sulphate (145). There is mounting evidence suggesting that binding to heperan sulphate renders the chemokine active (146). In addition, the glycans that decorate the ECM can be altered quite radically between states of health and disease. Such changes in ECM glycosylation will add to the complexity of how the ECM contributes to chemoattractant immobilisation and influences inflammatory cell recruitment during disease. In summary, the ECM plays a multitude of roles, crucially contributing to chemotactic properties governing leukocyte diapedesis.

1.5 Neutrophil effector functions

Once neutrophils have reached a site of damage, they will undergo a series of events that leads to the release of their "killing machinery" (***figure 1.8***).

Deleted: of

Deleted: its

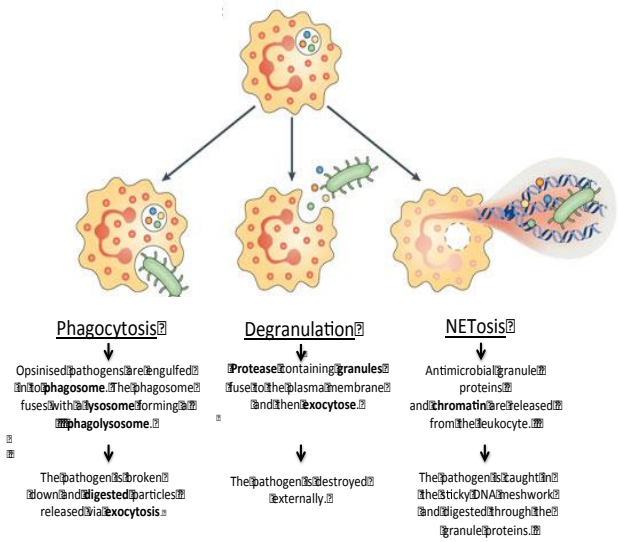

Figure 1.8: The neutrophil effector functions
After neutrophil chemotaxis to the foci of insult/injury the neutrophil initiates its assault, through one of the three effector functions, phagocytosis, degranulation and NETosis. Image adapted from Kolaczkowska and Kubes, Nat Rev Immunology. 2013 (147).

1.5.1 Phagocytosis

Phagocytosis is an active receptor-mediated response. Neutrophils express a large array of PPRs that recognise PAMPs and DAMPs, which include Toll-like receptors, Nod-like receptors and Fcγ class receptors(3). Of the three mentioned above the Fcγ receptors are the most studied, these receptors traditionally harbour the immunoreceptor tyrosine based activation motif (ITAM) within their cytosolic tails, from which signalling adaptors bind and transduce downstream signals (148). Briefly, ligand interaction leads to phosphorylation of tyrosine in the cytoplasmic ITAM motif, which leads to NADPH oxidase activation, actin polymerisation and granule secretion (149). Neutrophils are extremely efficient phagocytes and can internalise IgG-opsonised particles in seconds. Signals

downstream of the Fcγ receptor drive cytoskeleton remodelling, which contributes to the production of an engulfing membranous cup to internalise the targeted pathogen or pathogen-like substance. Once engulfed the pathogen remains in a "phagosome", where the internal environment is made toxic through two means; firstly, assembly of NADPH oxidase on the phagosomal membrane drives reactive oxygen species (ROS) production in the form of superoxide ions, and secondly fusion of the phagosome with serine protease-containing granules (150).

1.5.2 Degranulation

Degranulation is also a receptor-mediated response to a pathogen or pathogen-like substance, yet, in this circumstance, anti-microbial cytotoxic granules are actively transported and released via a microtubule-dependent process to the plasma membrane where they undergo excocytosis(3). There are at least four different types of granules within a neutrophil: (i) primary or azurophilic granules (containing elastase, myeloperoxidase and cathepsins); (ii) secondary granules or specific granules; (iii) tertiary granules (both secondary and tertiary granules containing matrix metalloprotease), and (iv) secretory granules (containing human serum albumin)(3).

1.5.3 NETosis

A final and more recently discovered neutrophil effector function is NETosis. This process is when neutrophils undergo cell death through the expulsion of nuclear chromatin into the extracellular environment. The act of nuclear extracellular traps (NETs) formation is often described as "NETosis". The obvious function for this sticky (negatively charged) meshwork of fibres is to trap pathogens, this has been confirmed in basophils, neutrophils, macrophages, and interestingly plant root tip cells, suggesting that NETosis is evolutionary conserved (151)(152). NETosis can be triggered by an array of different pathogens; Gram negative bacteria, Gram positive bacteria, HIV virus particles, and candida albicans (153) (154) (155) (156). NETosis has also been observed in non-infectious diseases such as cancers and atherosclerosis (157). A lot of attention has been given to understanding the mechanism underpinning NETosis, which is molecularly and morphologically distinct from apoptosis. Commitment of a neutrophil to undergo

Deleted: altruistic

Deleted: commit themselves to an act of suicide

Deleted: g

Deleted: g

NETosis leads to nuclear envelope disintegration and cell contraction. At the molecular level, NETosis is initiated through translocation of neutrophil elastase (NE) and myeloperoxidase (MPO) to the nucleus, which degrades the linker histone H1 and de-condenses chromatin respectively (158). Neutrophils isolated from NE-deficient mice or patients lacking MPO cannot be stimulated to undergo NETosis (158). Seminal work by Branzk and colleagues has demonstrated that neutrophils competitively chose between NET formation or phagocytosis, dependent on pathogen size (159). In response to large pathogens for example Candida albicans hyphae and bacterial aggregates NET formation was preferential over phagocytosis, in comparison unicellular yeast or single bacteria drove phagocytosis. Here, the decision to release one killing mechanism over the other was driven by NE. In phagocytosis NE is sequestered away from the nucleus preventing proteolytic cleavage of the histones and the ultimate driving of chromatin decondensation that is fundamental for NETosis.

1.5.4 The role of neutrophils in chronic inflammation

Neutrophils are typically described as the first cellular defence in acute inflammation. There is a wealth of data using clinical and experimental approaches examining neutrophils crucial role in infection clearance (160)(161)(162).However recently, the neutrophil function has been extended to highlight pathophysiological consequences. Below are two selected examples indicating how neutrophils aid chronic inflammatory disease progression.

Atherosclerosis

Atherosclerosis is a cardiovascular disease that is the underlying cause of 50% of all deaths in the western world (163). Briefly, it is the build-up of crystalized cholesterol within the intima of arteries, leading to a chronic inflammatory situation that persists and remains clinically silent for decades. Continued progression of inflammation ultimately leads to the formation of an atherosclerotic plaque that grows into the vessel lumen. This causes gradual constriction of the blood that supplies oxygen to vital organs such as the heart and brain. If left untreated this can lead to hypertension, thrombus formation (if the plaque is unstable), and stroke and/or myocardial infarction. Neutrophils have been implicated in promoting atherosclerosis (164)(165). Typically,

Deleted: atherosclerosis(

monocytes have been classically described as the driver of atherosclerotic plaque growth, but through more sensitive immunohistochemistry staining of aortic and coronary artery sections, neutrophils were detected in early human and mouse plaques (164)(165).Proteins found in neutrophil granules including azurocidin, and α-defensins has been found in human atherosclerotic lesions(166). Whilst in murine models, neutropenia induced through CXCR2 deficiency resulted in a reduction in plaque size (167). Recently, neutrophils NETs have been implicated in plaque development; NET deficient mice displayed reduced plaque growth (168). Additionally, cholesterol crystals trigger NET formation which in turn prime macrophages to release cytokines to amplify monocyte recruitment to the plaque and further progress plaque growth. These studies taken together build a strong case for the neutrophils role in this disease progression.

Acute Myocardial infarction

Myocardial infarction (MI) is commonly referred to as a heart attack. Occlusion of a coronary vessel can result in an anoxic low nutrient tissue environment also referred to as the infarct zone, within this area cardiomyocyte necrosis takes place, releasing mitochondrial DAMPs, which signal to activate tissue resident immune cells for example mast cells (***figure 1.9***) (169)(170). Mast cells release histamine, TNF and IL-1β to activate the endothelium to encourage neutrophil TEM(2). Additionally, neutrophils release the complement protein C5, amplifying neutrophil infiltration (***figure 1.9***). Once within the infarct zone, neutrophils produce numerous proteases that further tissue damage and release more inflammatory amplifying DAMP signals. Above, describes the biological activity during the acute phase (first 3 days of MI) and leading to an increase in infarct size, which ultimately lowers patient outlook. The true extent of neutrophil behaviour is demonstrated in a canine model. Here, induced neutropenia decreases infarct size and the extent of damage (171)(172).

Deleted: area cardiomyocyte

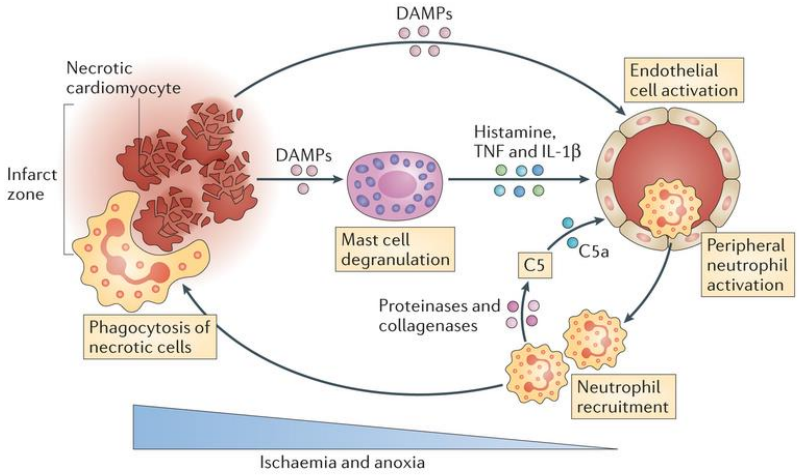

Figure 1.9 Neutrophil responses to early phase myocardial infarction
In the early stages, first 3 days post myocardial infarction necrotic cardiomyocyte within the infarct zone release DAMPs, which directly or indirectly activate the endothelium. Endothelial cell activation allows neutrophil TEM. Infiltrated neutrophils release proteinases and collagenases to negatively remodel the local tissue environment, ultimately increasing the infarct zone size. For abbreviations see **Abbreviations page.** Figure taken from Epelman et al, Nat Rev Immuno, 2015 (173).

Now that the mechanism by which leukocytes exit the vasculature, use chemoattractant signalling to gain access to the site of damage, and undergo neutrophil effector functions have been described, the final section of this introduction will focus on the contribution that L-selectin plays in regulating neutrophil effector function. Before its contribution to neutrophil effector function can be discussed, a series of sub-sections below will detail the structure and function of L-selectin.

Deleted: form

1.6 The selectin molecules

The selectins are a family of three cell adhesion molecules that mediate leukocyte adhesion to the vasculature. All the selectins bind to carbohydrate-based ligands. The three members L-selectin, P-selectin and E-selectin were discovered in the 1980s (174) (175)(176) with the selectin nomenclature describing how each selectin was first discovered. **L**-selectin (CD62L) is expressed on virtually all circulating leukocytes, but was initially identified on **l**ymphocytes. **P**-selectin and

E-selectin were first discovered on **p**latelets and **e**ndothelial cells, respectively. P–selectin (CD62P) is also expressed on endothelial cells and is stored in granules known as Weibel–Palade bodies (WPB). After activation by pro-inflammatory mediators, WPB fuse with the plasma membrane and mobilise P-selectin to the apical surface (177). E-selectin (CD62E) is not expressed under basal conditions, with the exception of the microvasculature of the bone marrow and skin(178) . E-selectin undergoes de novo transcription and translation in response to pro-inflammatory stimuli. Earlier work in cultured primary human endothelial cells and knock-out mice revealed that E-selectin expression peaks at a time when P-selectin expression begins to decline (179). Expression of E–selectin mRNA has been noted two hours post-stimulation and maximal protein expression peaks between 6-12 hours (180). In contrast to E-selectin and P-selectin, L-selectin is constitutively expressed at the plasma membrane and following stimulation it is proteolytically cleaved through a recognised mechanism known as "ecto-domain shedding" (***section 1.9.2***).

1.6.1 Structure of the selectins

The selectins are a family of single-pass type I transmembrane proteins. All the selectins share similar domain structures: (i) an N-terminal C type lectin domain, which binds to glycans in a calcium-dependent manner; (ii) a single epidermal growth factor (EGF)-like domain; (iii) two to nine short consensus repeat (SCR) domains, which share homology with complement proteins; (iv) a transmembrane domain and; (v) a C-terminal cytoplasmic tail (see ***figure 1.10***).

Deleted: -

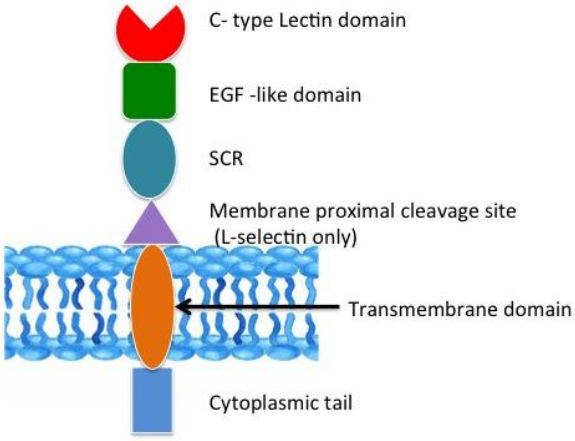

Figure 1.10: The domain structure of the selectin family of cell adhesion molecules
L/E/P-selectin are all composed of an N-terminal calcium-dependent (C-type lectin), which is responsible for the binding of carbohydrates. The epidermal growth factor (EGF)-like domain is followed by a series of short consensus repeats (SCR). The number of SCR is dependent on the selectin molecule. L-selectin possesses a unique membrane-proximal cleavage domain. Each selectin has a transmembrane domain, followed by a short cytoplasmic tail. There is very little homology between the cytoplasmic tails, suggesting that regulation at this site could be unique to the each selectin.

Deleted: Below this, is the

Deleted: ,

N-terminal C-type lectin domain

The lectin domain is a calcium-dependent glycan-binding domain responsible for binding the tetrasaccharide Sialy Lewis (x)(181). The lectin domain possesses two calcium-binding sites; occupancy of these sites induces a conformational change exposing the epitope responsible for ligand binding (181)(182). All selectins share ~52% homology for the lectin domain (37).

EGF domain

Amongst the selectin family members, the epidermal growth factor (EGF)-like domains carry approximately 47% homology at the amino acid level (37). Interestingly, there appears to be a higher evolutionary conservation of the EGF-like domain ~60% (between the same selectin molecule yet in different mammalian species)(37). The function of the EGF-like domain has been confirmed by X-ray crystallography (183)(184), where the EGF-like domains are required for optimal ligand binding. P-selectin and L-selectin EGF-like domains were captured in either a bent or extended conformation(185). The shift towards

Deleted: level(

Deleted: , which is ~60%

the extended conformation is achieved when the selectin is exposed to tensile forces. The linker region between the lectin domain and EGF-like domain acts as a hinge, allowing the selectins to interact with ligands via a "catch slip" mechanism; (see ***section 1.2.2***). The higher the "pulling force" the stronger the bond.This is confirmed by observations that non-optimal tethering of leukocytes was achieved when the hydrodynamic stressed was below a certain threshold(186).

Deleted: high pulling forces the bonds get stronger.

SCR domain

The short consensus repeats vary in number between the selectin family members. L-selectin in all species so far described have two SCR repeats, while E-selectin and P-selectin vary between four to nine repeats (37). In humans, E-selectin contains 6 SCR while P-selectin contains 9 SCR (187)(188). Domain swap experiments, where SCR domains were interchanged between the selectins showed very little change in function, suggesting that its main purpose is to act as a structural spacer between the lectin domain and the plasma membrane (189). In other words, the SCR domains act to extend the ligand-binding domain away from cell body. L-selectins relatively few SCR may be explained by its sub-cellular location, where it is typically anchored to the tips of microvilli(17). Unique to L-selectin is a membrane-proximal cleavage site, which is where the ectodomain of L-selectin is proteolytically removed from the rest of the molecule (***figure 1.10***). The regulation of L-selectin "shedding" will be discussed in more detail in ***section 1.9.2***.

The transmembrane domain

P-selectin has been shown to form homodimers within the plasma membrane, which is dictated by the presence of the GxxxG motif within the transmembrane domain (190)(191). Additionally, P-selectin purified from platelets forms oligomers and dimers in detergent solution (192). The functional significance of P-selectin dimerization has been suggested to contribute to rolling stability and cell rebinding during rolling events (193). In comparison, L-selectin is monomeric in the plasma membrane and it is the transmembrane domain has been implicated in microvilli positioning(17). Transmembrane domain-swap experiments between CD44 (a hydaluronan

Deleted: s

binding transmembrane protein) and L-selectin revealed that the transmembrane domain is responsible for L-selectin location at the microvilli (194).

The cytoplasmic tail of the selectin family members

The cytoplasmic tail is short for all family members, consisting of 35 amino acids (aa) for P-selectin, 32 aa for E-selectin and 17 aa for L-selectin (37). Interestingly, the cytoplasmic tail shares very little homology between selectin family members. E-selectin has been reported through biophysical and biochemical assays to interact with α-actinin, vinculin and filamin (195) (196). The cytoplasmic tail of E-selectin is phosphorylated at serine residues. However, in IL-1β activated HUVEC, where E-Selectin is constitutively expressed antibody or ligand induced cross-linking induces dephosphorylation of the cytoplasmic tail(197). *In vitro* studies reveal that phosphorylation of the cytoplasmic tail of P-selectin is required for trafficking into granules and internalisation from the plasma membrane(198). *In vivo* truncation of P-selectin, lacking the cytoplasmic domain, severely compromised the storage of P-selectin in endothelial cells (198). The cytoplasmic tail of L-selectin and its cytosolic binding partners will be discussed in greater detail in ***section 1.7.***

Deleted: has been shown to be

1.7 Binding partners of the L-selectin cytoplasmic tail

Despite its small size of 17 amino acids, the cytoplasmic tail of L-selectin is known to bind multiple partners (***figure 1.11***). The binding partners of L-selectin include α-actinin and the ERM proteins ezrin and moesin, (note that radixin is absent in leukocytes), calmodulin (CaM) and PKC isoforms. These interactions will be discussed briefly below.

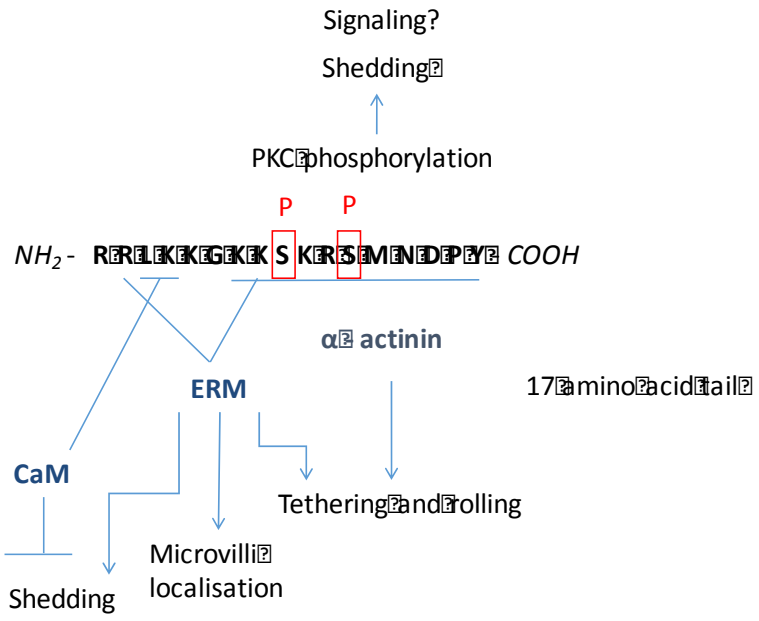

Figure 1.11: The binding partners of the cytoplasmic tail of L-selectin
The 17 amino acid tail of L-selectin interacts with CaM (L358 and K359), ERM (R357 and K362) and α-actinin (K363 to Y372). The two serines, S364 and S367 can become phosphorylated. The consequence of specific protein bindings and phosphorylation is highlighted (blue arrows). For abbreviations see ***Abbreviation section***. Image adapted from Ivetic and Ridley, Biochem. Soc.Trans,2004. (199)

1.7.1 α-actinin

The interaction between the actin binding protein, α-actinin, and L-selectin was identified through co-immunoprecipitation, and was shown to be mediated by the

last 11 amino acids of the L selectin tail (200). The L-selectin/α-actinin interaction has been implicated in leukocyte tethering and rolling as truncating the final 11 and 15 amino acids of L-selectin tail significantly reduced tethering efficiency and abrogated rolling, respectively (200). However, removal of these 11 aa residues did not alter microvilli positioning of L-selectin (***figure1.10***). L-selectin and α-actinin are thought to form a complex with talin and vinculin (200).

1.7.2 The ezrin-radixin-moesin (ERM) proteins

ERM proteins act as essential linker proteins between the plasma membrane and the cortical actin-based cytoskeleton. ERM remain inactive in the cytosol, where they adopt an auto-inhibited folded conformation (203)(202). In their inactive state, the N- and C-terminal domains of the same ERM bind to one another, which mask its ability to bind the tails of transmembrane proteins (such as L-selectin) and F-actin. Upon binding of the N-terminal domain to PIP_2, which is enriched specifically within the inner leaflet of the plasma membrane, ERM unfold to expose their binding sites for cytoplasmic tail interaction and F-actin(201). Phosphorylation at a conserved C-terminal threonine is involved in stabilising the unfolded molecule (202) (203). The threonine residue phosphorylated is T567 in ezrin, T564 in radixin and T 558 in moesin (204)(205)(206). The kinase responsible for phosphorylating the C-terminal threonine is cell-type and stimulus-specific. In addition to having a structural role in the cell, ERMs can also act as signalling adaptors. Numerous reports have shown ERM act both upstream and downstream of Rho GTPases (207)(208). Abrogating L-selectin/ERM interaction can be achieved through mutagenesis of the L-selectin tail: arginine at position 357 (R357) or lysine at position 362 (K362) (209) (210). Replacing either R357 or K362 with alanine (i.e. R357A and K362A) resulted in a significant reduction of L-selectin located on microvilli, which manifested in reduced cell tethering efficiency on immobilised recombinant PSGL-1 (210). Both R357A and K362A L-selectin failed to shed as efficiently as WT L-selectin when stimulated with the phorbol ester, phorbol 12–myristate acetate (PMA), implying ERM can act as pro-shedding factor (210)(209). PMA is a mimic of DAG, which is a potent PKC activator.

Deleted: s

Deleted: conformation(

Deleted: was

Deleted: M

Deleted: A

Deleted: an

Deleted: analogue

The functions of moesin and ezrin have often been thought as redundant to one other, however this appears to not be the case in relation to L-selectin interaction. An affinity column carrying a 17 aa synthetic peptide that corresponds to the tail of L-selectin selectively retained ezrin from resting lymphocyte cell lysates(199). Interestingly, the affinity column retained both ezrin and moesin only from lysates derived from lymphocytes pre-treated with PMA. These biochemical findings would suggest that ezrin binds constitutively to the L-selectin tail, whereas moesin binds to L-selectin in response to cell stimulation that drives shedding.

Deleted: .

Deleted: PMA .

1.7.3 Calmodulin and its regulation of binding to the L-selectin tail

Another binding partner is the ubiquitous calcium binding protein, calmodulin. Calmodulin is thought to associate constitutively with the cytoplasmic tail of L-selectin. This interaction imposes a conformational constraint on the cleavage site to an extent that renders it protected from proteolytic attack. Indeed, incubation of cells with the calmodulin antagonists, calmidazolium and W7, can promote rapid shedding of L-selectin (211). The amino acids contributing to calmodulin binding are leucine L358 and lysine K359. More recently, serine phosphorylation of the L-selectin tail at position 364 (S364) was shown to be important in abrogating binding of calmodulin from L-selectin (212). Interestingly, S364 is conserved in humans and mice, hinting at a preserved mechanism for calmodulin displacement. The exact mechanism by which calmodulin negatively regulates shedding is not fully understood. Biophysical studies suggest that calmodulin may actively pull the proximal cleavage site of L-selectin into, or closer to, the plasma membrane, restricting access of its protease ADAM-17 (see ***section 1.9.2***) from clipping L-selectin at the appropriate site (213). This hypothetical model suggests displacing a series of hydrophobic residues from the transmembrane domain into the cytosol, and hydrophilic residues from the ectodomain into the lipid bilayer of the plasma membrane. Collectively, this displacement of amino acids into conflicting microenvironments would be energetically unfavourable.

Deleted: 83

1.7.4 Calmodulin and ERM as signalling adaptors during ligand-induced clustering of L-selectin

Ligand induced L-selectin clustering results in multiple signalling pathways; promoting β1 and β2 integrin activation, and mobilisation of the chemokine receptor CXCR4, these will both be reviewed more closely in ***section 1.11.1*** and ***section 1.11.2*** respectively (214)(215). A detailed study by Killock et al., employed molecular modelling to better understand how such a short cytoplasmic tail can accommodate more than one binding partner. They demonstrated that L-selectin/ERM/Calmodulin form a 1:1:1 ternary complex (216). This data has recently been supported by two additional papers which predict that ERM binding is required to desorb the highly basic L-selectin tail from the inner leaflet of the plasma membrane, which then allows calmodulin to bind (217)(218). Upon L-selectin ligand induced clustering novel protein interactions may form as a consequence of L-selectin tails being brought together. Brenner and colleagues demonstrate that L-selectin clustering activated the GTPase Ras (219). Ras is activated upstream by the activator son of sevenless (SOS) (220). Biochemically calmodulin has been shown to interact with K-Ras (221). Molecular modelling revealed that CaM and ERM within the 1:1:1 ternary complex L-selectin/ERM/Calmodulin can bind to Ras and SOS respectively (216). Downstream, Ras activates both MEKK and PI3K pathways and is implicated in cancer progression, cell migration, adhesion, and differentiation (222)(223)(224)(225).

1.7.5 PKC isoforms

Kilian et al., showed that the PKC isozymes θ and ι interact with L-selectin and subsequently phosphorylate L-selectin at the serine residues S364 and S367(226). Once the L-selectin tail is phosphorylated it interacts with another member of the PKC family, PKCα. PKC and calmodulin have been shown to compete for overlapping binding sites (226), it is therefore not inconceivable that L-selectin shedding is regulated by PKC and calmodulin competition. It is possible that transient association of PKC θ with the L-selectin tail leads to S364 phosphorylation, forcing the dissociation of CaM and subsequent shedding.

Deleted: sites(

Although, it is currently unclear whether PKCα associates exclusively with phosphorylated S364.

1.8 L-selectin ligands

The selectin family recognise an array of simple and complex carbohydrate ligands. These ligands are modified through sulfation, fucosylation and sialylation(227). The most common ligand building block for all the selectins is the tetracasaccharide Sialyl-Lewis (x) also known as sLe^x. The covalent attachment of sLe^x can be mediated through either O or N type glycans (228)(229). O-linked glycans are sugar moieties linked to the protein via an oxygen molecule from either a serine or threonine side chain, while N-linked glycans are sugar moieties linked to a protein via a nitrogen molecule from a asparagine side chain. Selectins can identify and bind to different sugar moieties, for example E-selectin ligand binding does not require sulfation, however this is important for L-selectin and P-selectin ligand binding (230). There are a multitude of ligands that have been identified for L-selectin; the table below illustrates some of the ligands for L-selectin present within and beyond the vessel lumen.

Deleted:

Deleted: This glycan is often displayed on glycoproteins.

Deleted: s

Deleted: ,

Deleted: s

Deleted: .

Ligand	Expression	Role	Reference
P-selectin glycoprotein ligand (PSGL-1)	Leukocytes	Leukocyte – leukocyte interactions in secondary tethering	(231)
Nepmucin	HEV	Lymphocyte rolling and adhesion	(232)
GlyCAM-1	Secreted by endothelial cells	Soluble signalling molecule. Ligation of L-selectin via GlyCAM-1 enhances β_2 integrin function in naïve T cells	(215)
CD34	Mesenteric lymph nodes. HEV in tonsils. Peripheral lymph nodes.	Supports rolling in lymphocytes	(233)(234)(235)
Peripheral lymph node addressin (PNAd)	HEV within tonsils	Lymphocyte trafficking to the peripheral lymph node	(236)
Podocalyxin like protein	HEV	Tethering and rolling of lymphocytes *in vitro.*	(237)
MadCAM-1	Mesenteric lymph nodes	Rolling of lymphocytes	(238)
Versican	Extravasculature in the kidney	Potential role of leukocyte trafficking into the kidney under disease conditions	(239)(240)
Biglycan	Endometrium	Tethering and rolling of NK cells.	(241)
Collagen XVIII	ECM of rat kidney	Possible linking molecule binding both L-selectin on a leukocyte and the chemokine MCP-1.	(242)(243)
E –selectin	Endothelial cells	Supports leukocyte adhesion *in-vitro*	(244)

Table 1.1: L-selectin ligands
This is an in exhaustive list of L-selectin ligands, alongside the details of the location of the ligand. For the abbreviations used see ***Abbreviations section***.

1.9 Regulation of L-selectin expression

1.9.1 Transcriptional and post-translational control

Human L-selectin is encoded on chromosome 1 and its short gene name was originally termed: leukocyte adhesion molecule- 1, or LAM-1. The human L-selectin gene is formed of 10 exons, of which 9 are translated in to the L-selectin protein(245). Recently in 2015, a novel isoform was revealed in humans, a result of alternative splicing, excluding the 7th exon which encodes the transmembrane

region, rendering this variant of L-selectin soluble. The mRNA of this splice variant was isolated, alongside the conventional transcript, from lymphoid organs. The function of this soluble form of L-selectin is currently unknown, but human T cells markedly increased this splice variant mRNA upon activation(246).Transcriptional regulation has also been reported in pathological conditions, mice exposed to live scabies mites exhibited decreased L-selectin mRNA expression in the primary follicle and the marginal zone of the spleen (247)(248). Once translated L-selectin is post-translationally modified through glycosylation, glycosylation patterns appear to be cell type specific (245). Differences in glycosylation denote a change in weight of the protein, human soluble L-selectin has a MW of ~62kDa in lymphocytes and a MW of ~80 in neutrophils (249)(250).

Deleted: but human

1.9.2 Proteolytic cleavage of L-selectin

Cleavage of L-selectin, also termed shedding, occurs at the proximal cleavage site (K283-S284). Shedding splits L-selectin into two fragments, a 6 kDa transmembrane fragment and a 68 kDa soluble fraction (251). L-selectin has been reported to be cleaved by three A Disintegrin and metalloproteases; ADAM-8, ADAM-10 and ADAM-17 (also known as TNF-α converting factor–TACE) (252) (253) (254) (255). ADAM-17 is known as the predominant L-selectin cleavage enzyme, however there are exemptions when ADAM-8 and ADAM-10 are responsible for L-selectin shedding (253)(256). In neutrophils ADAM-8 is present on the cell surface and in granules. Upon inflammatory activation ADAM-8 translocates from intracellular granules to the plasma membrane, increased levels of ADAM-8 was also observed in synovial fluid of rheumatoid arthritis (RA) patients which directly corresponded to shedding of L-selectin (253). Co-transfection of ADAM-8 and L-selectin into HEK293 cells, showed an increase in the amount of soluble L-selectin in the supernatant (253). In an ADAM 17-/- background, ADAM-10 could shed L-selectin in primary B cells (256). However, ADAM-17 deficient neutrophils, monocyte and lymphocytes failed to shed L-selectin in response to PMA, as did neutrophil infiltrating the peritoneum under inflammatory conditions, suggesting that specific ADAM activation may be cell type specific or depend on the inflammatory stimulus(255).Shedding of L-selectin

Deleted: shedding(

can either be "prompted" through cell activation or can occur basally(255)(257). Soluble L-selectin is present within the circulation at ~1.6μg/ml in healthy humans (258)(259). This soluble form within the circulation remains activate able to bind ligand (260), leading to the hypothesis that soluble L-selectin acts to buffer the immune response, competitively binding endothelial ligands and preventing excess leukocyte adhesion to the vascular walls. Soluble levels of L-selectin increase in patients suffering from chronic inflammatory diseases; systematic lupus erythematosus, obesity and type 1 diabetes (261)(262)(263). Perhaps this increase in soluble L-selectin has a protective function, as described above, preventing excess leukocyte infiltration. Basal shedding occurs at the same cleavage site but a definite mechanism remains elusive. Stimulation of L-selectin shedding has been reported through numerous means; PMA, fMLP, TNF-α, LPS, C5a, IL-8 and hydrogen peroxide (264)(265)(266)(267)(209). The above is list of a few of the biological/biochemical triggers of shedding. However, biophysical conditions such as osmotic pressure and mechanical force have also been shown to induce shedding (268). Killock et al., clearly identified shedding as being either PKC or p38 MAPK dependent, this was achieved through selective activation of the kinases using PMA and cantharidin respectively (209). The PKC dependent pathway relies on the presence of ERM/L-selectin interaction, while the p38 MAPK pathway increases ADAM-17 activation and surface expression (209).

Deleted: an

Deleted: in -exhaustive

Deleted: respectively(

1.10 Functional roles for L-selectin

L-selectin is present on virtually all circulating leukocytes with the exception of activated B and T cells and effector memory T cells (269)(270)(271). Butcher and colleagues were the first the identify L-selectin as a CAM responsible for migration of lymphocytes from high endothelial venules into peripheral lymph nodes and Peyers patches (specific lymph nodes within the gut) (176). Since then, the role of L-selectin in leukocyte trafficking has been extended to recruitment in inflammation. L-selectin role in inflammation comes from early studies using L-selectin-deficient mice challenged with different inflammatory stimuli. For example, impaired leukocyte recruitment was observed when sheep's blood was injected into the footpad of L-selectin-deficient mice (272).

1.10.1 The role of L-selectin within the vessel lumen

L-selectin catch-slip bonding (see ***section 1.2.2***) produce tethers that will progress to rolling under high hydrodynamic shear force. L-selectin-dependent adhesion does not occur below 0.1 dynes/cm^2 (273)(40)(274).Additionally, genetic modification, where the C terminus of L-selectin was truncated, abolished binding of the cytoskeletal binding partner α-actinin, significantly reducing the duration of tethers(34).Of the three selectin molecules L-selectin mediates the fastest rolling velocity (~100μm/second), in comparison P-selectin mediates rolling at a velocity of ~50μm/second(32)(41)(32). L-selectin has been shown to mediate leukocyte rolling *in vivo* within the cremaster muscle and *in vitro* on cytokine activated endothelial cells (275)(276)(277)(35). Additionally, leukocytes are captured indirectly to the endothelium through secondary tethering (see ***section 1.2.1***). *In vitro,* secondary tethers were abolished when L-selectin deficient neutrophils were perfused across E-selectin, and addition of a function blocking L-selectin antibody led to an 80% decrease in secondary capture from whole blood (278). L-selectin deficient mice have a dramatic effect on lymphocyte rolling reducing accumulation on the PLN HEV (279).

Deleted: L-selectin has been shown to mediate leukocyte rolling *in vivo* within the cremaster muscle and *in vitro* on activated endothelial cells (271)(272)(273)(274).

1.10.2 The role of L-selectin beneath the endothelial monolayer and beyond

For a long time, L-selectin function has been characterised solely in tethering and rolling. However, it is now emerging that L-selectin may play a role in regulating TEM and subsequent chemotaxis(212). In mouse models leukocyte infiltration into the peritoneum was significantly reduced in L-selectin deficient mice, or through the administration of L-selectin neutralising antibodies or a soluble recombinant L-selectin IgG chimera (20)(280). Using MEL-14 a function blocking antibody against L-selectin, it was shown that CD8+ T cells rely on L-selectin to migrate into virus infected tissues (281) L-selectin is also responsible for aiding leukocyte migration into skin graft (272)(282). Alongside this T $_{reg}$ cells deficient in L-selectin showed a 90% decrease in the PLN (283). Above, illustrates a wealth data characterising L-selectin as a "pro invasive" molecule. L-selectin's role in chemotaxis has also been addressed, Hickey et al., saturated an agarose block with keratinocyte chemokine (KC) the block was positioned on the excised cremaster muscle, generating a diffusible gradient (284). The study demonstrated

Deleted: ice

Deleted: phs

Deleted: gradient(

that L-selectin lacking neutrophils had a profound decrease in neutrophil ability to migrate towards the agarose block (284).Similarly the path length in the L-selectin null neutrophils was 40-50 % decreased in comparison to WT neutrophils upon cremaster superfusion with platelet activating factor (PAF) and KC(284) . Finally, studies *in vivo* and *in vitro* have demonstrated the role of L-selectin shedding in migration and chemotaxis, discussed below. *In vitro,* genetically blocking L-selectin shedding in the monocyte cell line (THP-1), a cell line that cannot complete full transendothelial migration, led to dramatic increases in the number of transmigrated pseudopods formed, suggesting a polarity defect(212). Whilst *in vivo*, a mouse generated through replacement of the proximal cleavage domain with an analogous region of P-selectin and further crossed with an L-selectin null mouse, resulted in a "sheddase resistant" form of L-selectin, expressed only on T-cells (LΔP)(285). Upon engagement of the T cell receptor (TCR), WT cells shed their L-selectin, and lost their ability to re-enter the lymph node (LN), in LΔP mice however shedding did not occur and re-entry into the LN was possible (285).Here, it appears that the main function of L-selectin shedding is to prevent activated T-cells returning to the PLNs. The described studies above have identified a role for L-selectin in successful migration. Further to this, L-selectin's involvement in chemotaxis has also been observed. This was investigated using another L-selectin "sheddase resistant" mice strain (L (E) ^{same}), generated through exchanging the cleavage region of L-selectin with a sequence from E-selectin(264). In L (E) ^{same} mice, leukocytes travelled no further then 50 μm away from the cremaster microvessel after KC perfusion. In comparison, WT mice counterpart leukocytes travelled a distance three fold greater (264).Additionally *in vitro*, when THP-1 cells were subjected to monocyte chemoattractant protein-1 (MCP-1) blocking L-selectin shedding was coupled with the prevention of front-back polarity (212).In summary, when L-selectin is lacking and if L-selectin is in its non-cleavable form both have profound influences in inhibiting polarity and directed migration.

1.11 The role of L-selectin as a signalling receptor

The section below demonstrates L-selectin's ability to behave as a signalling molecule.

1.11.1 Integrin activation by L-selectin

As described in ***section 1.2.3***, integrins can be activated through chemokine and L-selectin signalling. In Jurkat T cells, L-selectin binding to the ligands GlyCAM-1 and fucoidin promoted β1 integrin activation, this was assessed through fibronectin binding (214). Additionally, L-selectin also contributes to β2 integrin activation, recently work in primary neutrophils started to pinpoint molecular players of this signalling cascade(286). Here, L-selectin's association with PSGL-1 induced phosphorylation of the kinase Fgr (286). FcR and DNAX-activating protein-12 (DAP-12) are phosphorylated by Fgr to recruit spleen tyrosine kinase (SyK), which subsequently phosphorylates Bruton's tyrosine kinase (Btk). Btk regulates p38 MAPK resulting in extension of LFA-1 (β2 integrin) into its high affinity binding form, to allow ICAM-1 binding (287). Along side this, mAb crosslinking of L-selectin encouraged β2 integrin/L-selectin co-localisation, additionally, L-selectin cross-linking induced leukocyte binding to albumin coated microspheres (used to test for MAC-1 driven adhesion) (288). The potentiation of leukocyte adhesion of MAC-1 and LFA-1 to ICAM-1 has been attributed to L-selectin cross-linking in the presence of IL-8 (289). Cross-linking of L-selectin has been directly associated with p38 MAPK activation(288). In fact, p38 MAPK phosphorylates after 1 minute post L-selectin cross-linking (288).

Deleted: e

1.11.2 Regulation of chemokine receptors and chemotaxis

Antibody-mediated cross-linking of L-selectin with LAM1-3 promoted an increase in surface expression of the chemokine receptor, CXCR4, on human peripheral blood lymphocytes (290). Lymphocyte incubated with the L-selectin ligands fucoidan and sulfatide, also significantly increased the levels of surface CXCR4 (291) and in both cases CXCR4 was mobilized to the surface from intracellular stores. Interestingly, this response appeared to be subtype specific as sulfatide ligation increased CXCR4 expression in CD4+ T cells but not CD8+ T cells or B cells. Coupled with aiding CXCR4 surface mobilization ligand bound L-selectin additionally prevented the CXCR4 from undergoing receptor internalization (see ***section 1.4.1***). Exposing these T cells to high levels (500ng/mL) of SDF-1 also known as CXCL12 (CXCR4 ligand) for 1 hour resulted in CXCR4 internalisation. This phenomenon could be reversed upon L-selectin ligand binding. The

functional consequences for the prolonged exposure to SDF-1 and retention of surface expression of CXCR4 were increased actin polymerization producing leukocyte firm adhesion. Suggesting that signalling derived from both SDF-1 /CXCR4 interaction and L-selectin cross-linking worked in a synergistic manner to increase migration(290)(291).Furthermore L-selectin's up regulation of chemokine receptor CXCR4 was considered to be unique, as expression of other chemokine receptors (CCR5 and CCR7) did not have the same outcome. On a molecular level L-selectin dependent CXCR4 up regulation was due to tyrosine phosphorylation, proven through pre-treating the cells with tyrosine phosphatase inhibitors. A further study demonstrated that ligand interaction with L-selectin resulted in enhanced chemotaxis of B cells (~70%) and T cells (~30%) towards secondary lymphoid tissue chemokine (SLC)(292). The mechanism behind this L-selectin mediated response to SLC remains unclear; it is unlikely due to the up-regulation of the corresponding receptor (CCR7) as no differences in surface level expression was observed before and after L-selectin ligand-induced clustering (292). However, L-selectin mediated chemotaxis towards SLC could be blocked using inhibitors for PKC, p38 MAPK and Syk kinases. This would suggest that L-selectin signalling acts synergistically with CCR7 to mediate chemotaxis. This data is in line with previous findings that L-selectin cross-linking, produces a downstream signalling cascade, which leads to an increase in MAPK activity(288). Taken together, these experiments clearly suggest L-selectin is not only a CAM but also a signalling molecule.

1.12 The role of L-selectin in regulating TEM and polarity in monocytes

Work by the Ivetic lab (myself included), used human primary monocytes to specifically identify L-selectin was shed during TEM(212). This study confirms L-selectin is regulated differently dependent on species, in mice L-selectin expression is retained post emigration(293). Introducing either C-terminally green fluorescent protein (GFP) tagged WT L-selectin (WT GFP) or sheddase resistant L-selectin (ΔMN GFP) molecules into the monocyte cell line THP-1 the subcellular distribution could be observed. Perfusion of the two cell lines across a TNF-α-activated HUVEC monolayer revealed that of the monocytes caught in mid transendothelial migration (mTEM) the ΔMN GFP cells displayed significantly

Deleted: Rzeniewicz and

Deleted: colleagues

higher numbers of transmigrated pseudopods per cell. L-selectin distribution in these transmigrated pseudopods was monitored, WT L-selectin were preferentially observed in clusters, these clusters were not apparent in ΔMN GFP cells (212). Clustering was attributed to L-selectin ligands based within the interstitium (verisan, biglycan and collagen XVIII) (240)(242). Additionally, the interaction of CaM and L-selectin was investigated in THP-1 cells caught in mTEM. FRET studies imply that once the serine residue S364 becomes phosphorylated (examined through the use of a serine mutant S364D) CaM is displaced. In evolution S364 is conserved in both mice and humans, which possibly reflects the importance of S364 phosphorylation. Beneath the endothelium, primary monocytes were tracked, pharmacologically blocking L-selectin shedding decreased the cells "straightness of migration" or directionality. Together, the work illustrated both spatially and temporally when L-selectin shedding occurred and eloquently demonstrated that blocking L-selectin shedding influences front/back polarity and directional migration persistence. The paper proposes that L-selectin ligand clustering is a prerequisite for L-selectin shedding, shed L-selectin can now display distinct signalling to limit or retract multiple protrusions (212).Below is a model illustrating the key findings identified within this paper (***figure 1.12***).

Deleted: displaced. The importance of S364 phosphorylation is reflected in

Deleted: body of work

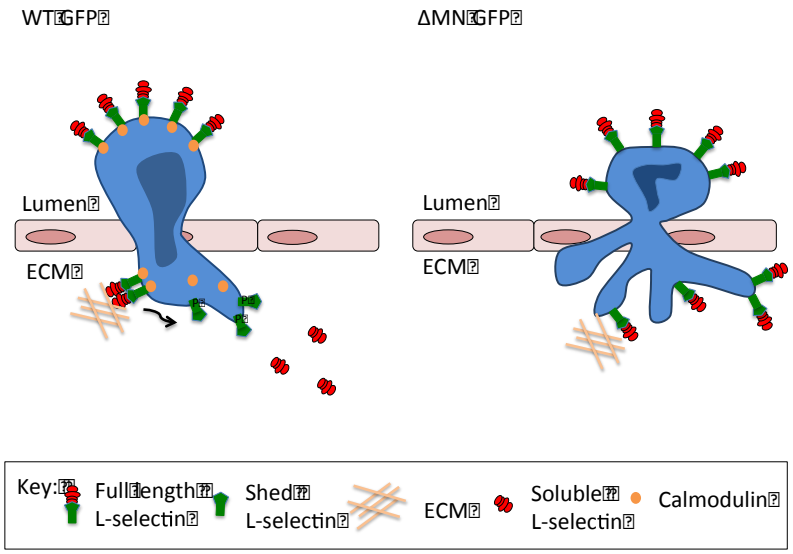

Figure 1.12: Schematic model representing a novel function for L-selectin in regulating pseudopod number in the THP-1 cell line

In the WT GFP cell line model: During TEM L-selectin in the transmigrated pseudopods becomes clustered via ECM ligand binding. Clustering leads to L-selectin phosphorylation at S364 and calmodulin displacement, which ultimately causes L-selectin shedding. Shed L-selectin displays unique signalling which limits/retracts multiple protrusions. The monocyte is now polarised. *In the ΔMN GFP cell line model*: During TEM ΔMN L-selectin in the transmigrated pseudopods doesn't become clustered via ECM ligand binding. Preventing L-selectin shedding leads to multiple protrusions. Calmodulin and ΔMN interaction was not actively investigated in this study so calmodulin is not represented in the model. Image created through key findings from (212).

Formatted: Font: +Body (Cambria)

1.13 The role of L-selectin in neutrophil effector functions

L-selectin has been acknowledged in the literature for indirect roles in NETosis and degranulation. Recently, neutrophils have be shown to undergo NETosis through signalling initiated by salival mucins decorated with Sialyl Lewis (x)the necessary binding partner for L-selectin (294). Pre-incubating neutrophils with anti-L-selectin antibodies before incubating the cells with mucin rich saliva prevented NET formation. This study confirms that the signalling mediated from the Sialyl Lewis (x) and L-selectin interaction is crucial for NET formation (294). In further work, P-selectin transduced in to murine neutrophils promoted NETosis though PSGL-1 binding (295). Neutrophils have also been shown to be

more sensitive to degranulation of secondary, tertiary and secretory vesicles after L-selectin cross-linking (288) (296). For a more detailed discussion exploring how L-selectin governs neutrophil effector function see ***section 6.4***.

1.14 The role of L-selectin in disease

L-selectin plays a major role in driving chronic inflammation progression. L-selectin monoclonal antibodies have been shown to reduce the number of infiltrating neutrophils in a mouse model of peritonitis, and protect against a hyper-inflammatory response in parasitic infections (272). In an endotoxaemic model of inflammation, where lipopolysaccharide (LPS) is injected systemically into mice, L-selectin deficient mice showed 9-fold higher survival rates than their wild type littermate controls (272). Using a mouse model of cutaneous inflammation, skin graft rejection was significantly delayed in L-selectin-deficient mice compared to that of WT mice (272). The findings above demonstrate that the absence of or functional inhibition of L-selectin provides a protective role in inflammation. The above studies have been carried out in various animal models, but how this work translates to human models remains elusive.

In humans, L-selectin has been implicated as a possible therapeutic target for atherosclerosis, although this is controversial. Two prominent studies carried out in the same lab produced conflicting roles for L-selectin in atherosclerosis progression. Eriksson et al., demonstrated using a murine model that L-selectin dependent secondary tethering accounted for 20-50 % of all leukocytes captured at atherosclerotic lesions(25). Imaging of advanced plaques identified a network of microvessels permeating the lesions, which appeared to serve as entry points for leukocytes to enter the lesion (25).Here, the role of L-selectin in leukocyte capture ultimately leads to plaque growth (297). Conflictingly, a double knockout mouse model (apoliopoprotein E (ApoE) -/- and L sel -/-) showed that when fed a high cholesterol diet for 6 weeks aortic lesions increased 2 fold, compared to a ApoE-/- control (298). Apo E is responsible for the catabolism of triglyceride rich lipo-proteins. Confusingly this result suggests that L-selectin plays a protective role in atherosclerosis. Taken together there is a clear link between L-selectin and atherosclerosis, however, there appears to be no one model to fits all answers.

The role of L-selectin could vary dependent on what vessel is being studied or the stage of atherosclerosis progression.

L-selectin and its ligands are continually being assessed as potential targets for anti-inflammatory therapies. Currently, to my knowledge there is no commercalised therapy that manipulates or blocks the function of L-selectin (299)(300). Clinical trails, using L-selectin as a target have so far been unsuccessful. Clinical trials blocking L-selectin failed to improve psoriatic lesions, while another presently in phase II, named Aselizumab, was associated with higher rates of infection and leukopenia compared to the control placebo group (301)(302). Together, these failures may be due to the redundancy within the selectin family; simply blocking one may not be enough. However there are other studies were the outcome does not look as bleak. The introduction of recombinant fusion protein, PSGL-1 linked to IgG-Fc, blocks leukocyte adhesion, the drug YSPSL is currently in trials to assess renal allograft rejection (303). Another exciting *in vivo* murine study transiently expresses L-selectin into a cardiomyocyte precursor cell (304). These cells home more effectively than non transfected cells to damaged tissue in the heart after myocardial infarction and initiate regeneration (304).

Formatted: Font: Italic

Deleted: that is currently being worked up in a mouse model,

Deleted: cell(

1.15 Current methods to study L-selectin

The molecular tools to study L-selectin

To date there has been a multitude of molecular technologies employed to study L-selectin. Genetic manipulation is conducted *in vivo* and *in vitro* to either visualise the cellular distribution of the molecule or to prevent a specific function/interaction or delete the molecule completely. Genetically rendering the L-selectin sheddase resistant has obvious advantages over mAb studies, where function-blocking antibodies may block L-selectin ligand binding, but also introduce L-selectin clustering which initiates downstream signalling. Additionally, L-selectin shedding can be blocked pharmacologically through the use of metalloproteinase inhibitors, but as discussed later in the text this poses caveats.

The experimental tools to study L-selectin

In vivo, L-selectin and other molecules involved in the adhesion cascade are studied using intravital microscopy of organs within the mouse. This technique has obvious advantages, allowing complete visualisation of the adhesion cascade. However, no detailed information of the subcellular location of L-selectin and its relative binding partners can be gained. *In vitro,* experimental methods include Transwell assays and parallel plate flow chambers. The Transwell assay functions by establishing a concentration difference between the upper and lower wells, which are separated by a microporous filter. Simply, cells that are added to the upper well "sense" the chemokine in the lower well and migrate through the porous membrane. This assay has no direct imaging window and cells push through an inert membrane. The parallel plate flow chamber relies on the perfusion of leukocytes over an EC monolayer at physiological shear stress through negative pressure generated by a syringe pump, however this assay does not look beyond transendothelial migration so 3D migration and chemotaxis information is not collected.

Deleted: to

Deleted:

Deleted: Genetic manipulation

Deleted: s

Deleted: t

Deleted: t

Deleted: gradient

1.16 Original hypothesis

The role of L-selectin shedding in human monocytes has been recently reported to occur during transendothelial migration (TEM) (212). It is therefore proposed that L-selectin shedding may occur in human neutrophils during TEM. It is also postulated that preventing L-selectin shedding may result in defects in polarity-dependent events for example during chemotaxis.

1.17 Aims of the project

In order to test the hypothesis several aims were established.

1. Use primary human neutrophils and generate HL-60 cell lines expressing WT and mutant forms of L-selectin-GFP to address the role of L-selectin shedding in TEM and chemotaxis.
2. Design and fabricate microfluidic devices to monitor chemotaxis in 2D and 3D scaffolds.
3. Determine a role for serine phosphorylation of the L-selectin tail (through generating cytoplasmic serine mutant cell lines) in regulating neutrophil behaviour that manifest in response to blocking L-selectin shedding.

Deleted: Based on recent findings in monocytes, the objective of this PhD thesis is to determine if L-selectin shedding in neutrophils occurs specifically during TEM to regulate cell polarity within the subendothelial space (205). It is believed that, when L-selectin shedding is blocked,

Deleted: will manifest - e.g.

Formatted: Normal

2. Materials and methods

2.1 Cell culture medium, buffers, reagents and chemical formulations

	Product	Source	Composition/stock	Storage condition
Buffer and solutions	MES (2-morpholinoethanesulfonic monohydrate)-SDS buffer (Running buffer)	Invitrogen®, U.K.	20x	RT
	20x Novex® NuPAGE® transfer buffer	Invitrogen®, U.K.	20x	RT
	4x Protein Loading buffer	Made in house	200mM Tris-HCL pH6.8, 8% SDS (v/v), 20% glycerol (v/v), 0.4% bromphenol-blue (w/v), 3.6% β-mercaptoethanol (v/v)	RT
	Dulbecco's Phosphate buffered saline modified (PBS), pH 7.4. Sterile filtered	Sigma - Aldrich®, Germany	0.8% sodium chloride (w/v), <0.1% potassium chloride (w/v), <0.2%monosodium phosphate (w/v), <0.1 potassium phosphate (w/v), 0.1%sodium azide (w/v).	RT
	HEPES (4-(2-hydroxyethyl)-1-piperazineethanesulfonic	Sigma - Aldrich®,	1M	+4°C

	acid)	Germany		
	Milk blocking buffer	Supermarket	5% dry milk powder (w,v), in TBS with 0.1% (v/v) NP-40.	RT
	Tris-buffered saline (TBS) solution	Made in house	150mM NaCL /15mM tris-HCL, pH 7.4 in ddH_20.	RT
Chemicals	4', 6 – Diamidino-2-phenylindole (DAPI)	Sigma - Aldrich®, Germany	N/A	-20°C
	Calyculin A	Sigma - Aldrich®, Germany	20µM in DMSO	-20°C
	Cantharadin	Sigma - Aldrich®, Germany	12.5mM in DMSO	-20°C
	Celltracker™ Green CMFDA (5-Chloromethylfluorescein Diacetate)	Life technologies	1mM in DMSO	-20°C
	Celltracker™ Orange CMTMR (5(and -6)-(((4-chloromethyl) benzoyl)amino) tetramethylrhodamine	Life technologies	1mM in DMSO	-20°C
	Celltracker™ Deep red	Life technologies	1mM in DMSO	-20°C
	Dimethylsulphoxide (DMSO; cell culture tested)	Sigma - Aldrich®, Germany	neat	RT

	Glutaraldehyde	GPR ™	N/A	4°C
	Glycerol	Sigma - Aldrich®, Germany	N/A	RT
	Isopropanol	Fisher Scientific, U.S.A.	N/A	RT
	Acetone	Fisher Scientific, U.S.A.	N/A	RT
	Methanol	Fisher Scientific, U.S.A.	N/A	RT
	Nonidet P-40 substitute (NP-40)	Fluka®, Sigma - Aldrich®, Germany	N/A	RT
	Novex® NuPAGE ® Bis-Tris 4-12% gradient gels, 10 well, thickness 1.0 or 1.5 mm	Invitrogen®, U.K.	Composition as stated by manufactures	RT
	PageRuler ™ Plus prestained protein ladder 10 – 250 kDa	Life technologies	N/A	4°C
	Paraformaldehyde (PFA)	BDH laboratory Supplies, U.K.	8% (w/v) in PBS	-20°C
	Poly-L-lysine (PLL)	Sigma - Aldrich®, Germany	0.1% (w/v) manufactures solution	4°C
	Tween-20	Sigma - Aldrich®, Germany	N/A	RT
	Tetra-methyl-rhodamin-5-	Sigma -	0.2mg/mL in methanol	-20°C

	(and-6)-isothiocyanate (TRITC)-conjugated phalloidin	Aldrich®, Germany		
	Phorbol 12- myristate 13-acetate	Sigma - Aldrich®, Germany	32.5 mM in DMSO	-20°C
	Recombinant Human Monocyte chemoattractant protein 1 (MCP-1)/CCL2	R&D systems	100 μg/mL	-20°C
	Recombinant Human Tumor Necrosis factor alpha (TNF-α)	R&D systems	100 μg/mL	-20°C
	Sodium Chloride (NaCl)	Sigma - Aldrich®, Germany	1M in ddH_20	RT
	Recombinant Human protein CXC motif chemokine ligand 8, CXCL8.	Sigma - Aldrich®, Germany	100 μg/mL	-20°C
	Recombinant Human protein CXC motif chemokine ligand 1, Gro α	R&D systems	100 μg/mL	-20°C
	N-formyl-Met-Leu-Phe	Sigma - Aldrich®, Germany	10 mM in DMSO	-20°C
	Retinoic acid	Sigma - Aldrich®, Germany	10 mM in DMSO	-20°C
	TNF-α protease inhibitor -0 (TAPI-0)	Santa Cruz Biotechnologies	2 mM in DMSO	-20°C

	SB 202190	Sigma - Aldrich®, Germany	3 mM in DMSO	-20°C
	Sylgard®184 Silicon elastomer kit, 2-part kit containing elastomer base and curing agent.	Dow corning	Use at a 10:1 (v/v) elastomer base: curing agent	RT, as separate components.
	Microposit ™ EC solvent II	DOW®	Used as prepared by manufacture's instruction.	RT
	Microchem Negative epoxy resist SU-8 2000 series, 2005, 2025 and 2050.	Microchem	N/A	4°C for long term storage, 24 hours prior to experimentation leave at RT.
	Fluorescence mounting media (DAKO)	DAKO, agilent pathologies solutions	N/A	4°C
	Zymosan A (s.cerevisiae) Bio particles ®, Alexa Fluor ®594.	Thermofisher	20 mg/mL in Human Serum Albumin, (HSA).	4°C
	Dextran, Alexa Fluor® 488, 10,000 mw	Life technologies	1 mg/mL in PBS	-20°C
	Dextran, Alexa Fluor® 647, 10,000 mw	Life Technologies	1 mg/mL in PBS	-20°C
	Dextran, Alexa Fluor® Rhodamine B 10,000 mw	Life Technologies	1mg/mL in PBS	-20°C

	Histopaque® – 1077	Sigma - Aldrich®, Germany	N/A	4°C
	Dextran 500 mw from leuconostoc.spp.	Sigma - Aldrich®, Germany	Prepared in HBSS	RT
	HBSS (Hank's buffered salt solution) without calcium and magnesium salts	Sigma - Aldrich®, Germany	Manufactures formulation	RT
	Sodium Citrate	Phoenix Pharma Ltd.	Used as prepared by manufactures	4°C
	FC receptor block	MACS Miltenyi Biotec	Use at 1/100	4°C
Cell culture	Fibronectin	Sigma - Aldrich®, Germany	1mg/mL in PBS	4°C
	Foetal calf/bovine serum	Gibco® Invitrogen, U.K.	N/A	-20°C
	Optimem®	Gibco® Invitrogen, U.K	Manufactures confidential formulation	4°C
	Penicillin/Streptomycin	Sigma - Aldrich®, Germany	10,000 Units penicillin and 10,000 μg/mL streptomycin	-20°C
	Matrigel®	Corning®	18-21mg/mL	4°C
	Puromycin	Sigma - Aldrich®, Germany	10 mg/mL in ddH_20	4°C
	G418 (Geneticin)	Sigma -	10 mg/mL in ddH_20	4°C

		Aldrich®, Germany		
	RPMI (Roswell Park Memorial Institute) 1640	Gibco® Invitrogen, U.K	Manufactures formulation	4°C
	Trypsin – EDTA solution	Sigma - Aldrich®, Germany	0.5g/l porcine trypsin and 0.2g/l EDTA.4Na in Hank's balanced salt solution with phenol red.	-20°C
	Rat tail collagen	Cell matrix, Nitta gelatin inc, Japan.	Preparations in v/v ratios 4:2:1:1 (collagen , 5xDMEM, reconstitution buffer, HL-60 media (RPMI with 10% v/v FCS and 1%v/v Pen/Strep))	4°C
	5X DMEM	PAA, Colbe, Germany	1mg in ddH_20	4°C
	Reconstitution buffer for rat tail collagen	Made in house	2.2g $NaHCO_3$ in 100mL of 0.05N NaOH and 200mM Hepes.	4°C
	EGM-2 Media Bulletkit	Lonza	Walkersville Endothellial growth medium supplemented with hEGF, Hydrocortisone, FBS (fetal bovine serum), GA-1000 (gentamicin, Amphotericin-B),VEGF, hFGF-B, R3-IGF-1, Ascorbic acid, Heparin.	4°C

Table 2.1: A tabulated list of chemicals, buffer formulations and cell culture resources used within this PhD project.

2.2 Antibodies

Antibody	Antigen	Origin	Mono(M)/ Poly(p) clonal	Isotope	Stock conc. (µg/mL)	Source	Dilution
Primary Antibodies							
Anti- GFP	GFP	Rat	M	IgG_{2a}	1000	Chromotek	WB 1:1000
Anti-actin	β-actin	Mouse	M	IgG_{2a}	2000	Sigma-Aldrich	WB 1:1200
Anti–VE cadherin	VE-cadherin	Rabbit	M	IgG	-	Cell signalling technology®	IF 1:400
Dreg-56	L-selectin	Mouse	M	IgG_1	200	ATCC – HB-300 hybridoma	FC 1:200
LAM1-14	L-selectin	Mouse	M	-	1000	Kind gift from Prof. T Tedder Duke University, USA	IF 1:400
DREG-56-PE	L-selectin	Mouse	M	IgG_1	200	Santa cruz biotechnology	FC 1:250
Anti- TACE	TACE/ ADAM-17	Goat	M	IgG_1	200	Santa cruz biotechnology	FACS 1:200
Anti-FPR1	FRP1	Rabbit	P	IgG	1000	Sigma life sciences	WB 1:500
Anti –FPR2	FPR2	Rabbit	P	-	100	Merck millipore	WB 1:500 FC 1:200
Anti – p-P38 MAPK	p-P38 MAPK	Rabbit	P	IgG	-	Cell signalling technologies	WB 1:1000
Anti-P38 MAPK	P38 MAPK	Rabbit	P	IgG	-	Cell signalling technologies	WB 1:1000
Anti -CXCR2	CD182	Mouse	M	$IgG_1κ$	200	Biolegend	FC 1:250
Anti-FRP1		Mouse	M				**FC 1:200**
Isotype controls							
IgG_1-647 AlexaFluor®	N/A	Mouse	M	$IgG_1κ$	100	Biolegend	**FC 1:200**
IgG_1	N/A	Mouse	M	IgG_1	200	Santa cruz biotechnology	**FC 1:200**
IgG_1- PE	N/A	Rat	M	$IgG_1κ$	**200**	Biolegend	**FC 1:250**

Table 2.2: Table of Primary Antibodies used within this thesis.

Antibody	Antigen	Origin	Source	Dilution
Goat anti-mouse AlexaFluor ®633	Mouse immunoglobulins	Goat	Molecular probes Invitrogen®	IF 1:400 FC 1:200
Goat anti-rabbit AlexaFluor®633	Rabbit immunoglobulins	Goat	Molecular probes Invitrogen®	IF 1:400 FC 1:200
Donkey anti-goat AlexaFluor®633	Goat immunoglobulins	Donkey	Molecular probes Invitrogen®	IF 1:400 FC 1:200
Goat anti-rabbit AlexaFluor®405	Rabbit immunoglobulins	Goat	Molecular probes Invitrogen®	IF 1:400
IRDye 680RD donkey anti-goat	Goat immunoglobulins	Donkey	LI-COR® Biosciences	WB 1:15000
IRDye 680RD donkey anti-rabbit	Rabbit immunoglobulins	Donkey	LI-COR® Biosciences	WB 1:15000
IRDye 680RD donkey anti-mouse	Mouse immunoglobulins	Donkey	LI-COR® Biosciences	WB 1:15000
IRDye 680RD goat anti-rat	Rat immunoglobulins	Goat	LI-COR® Biosciences	WB 1:15000
IRDye 800CW goat anti-mouse	Mouse immunoglobulins	Goat	LI-COR® Biosciences	WB 1:15000
IRDye 800CW donkey anti-goat	Goat immunoglobulins	Donkey	LI-COR® Biosciences	WB 1:15000
IRDye 800CW donkey anti-rabbit	Rabbit immunoglobulins	Donkey	LI-COR® Biosciences	WB 1:15000

Deleted: T

Deleted: T

Deleted: T

Deleted: T

Deleted: T

Deleted: T

Deleted: T

Table 2.3: A Tabulated list of the secondary antibodies used within this thesis.

WB = Western blot IF= immunofluorescence FC= flow cytometry

2.3 Cells and cell culture

All cells were cultured at 37°C, 5% carbon dioxide, under humidifying conditions and in compatible sterile plastic ware.

2.3.1 HL-60 cells (Human promyelocytic leukaemia cells)

HL-60 cells were purchased from American Type Culture Collection (ATCC). HL-60 cells stably overexpressing the chemokine membrane receptor CXCR2 were a generous gift from the Richmond Lab, Vanderbilt University, U.S.A. Cells were maintained in HL-60 media (RPMI-1640 (GIBCO®, Invitrogen) medium supplemented with 10% (v/v) FCS, 1% (v/v) antibiotics (penicillin/streptomycin). Cells were seeded at a density of $0.3x10^6$ cells/mL and split every 3-4 days upon reaching a density of $1x10^6$ cells/mL. The cell line largely resembles promyelocytes, a granulocyte precursor. HL-60 cells can be induced to differentiate to either a neutrophil-like or monocyte-like phenotype, depending on the reagent used. Compounds such as retinoic acid and DMSO cause neutrophil-like differentiation, whereas vitamin D and GM-CSF promote a monocyte-like differentiation(305). For all experimentation conducted within this thesis HL-60 cells were terminally differentiated using 1.3% (v/v) DMSO, producing neutrophil-like cells. Fresh HL-60 media was supplemented with 1.3% (v/v) DMSO and cell density was adjusted to $0.5x10^6$/mL. Cells were used for experimentation 4-5 days after incubation with DMSO. Cells proliferation dramatically slows upon differentiation and the cell typically decreases in size. All experimentation was carried out on differentiated HL-60 cells (4-5 days post DMSO treatment) unless stated otherwise.

2.3.2 HEK 293T cells (Human embryonic kidney cells)

HEK 293T cells were a kind gift from Dr Yolanda Calle (University of Roehampton, London, UK). Cells were maintained in HL-60 media. Every 2-3 days media was replenished and cells were passaged by trypsinisation and "split" 1:3. In order to split cells, 3 mL of warmed trypsin (serine protease, Sigma-Aldrich) was added per dish and left to incubate at 37 °C and 5 % CO_2 for approximately 5 minutes.

Deleted: .

Deleted: pithelial

Deleted: ipsinisation

2.3.3 HUVEC cells (Human umbilical vein endothelial cells)

HUVEC were purchased from Lonza as a cryovial containing 0.5 x 10^6 cells from pooled donors. HUVEC were cultivated in endothelial growth media (EGM™-2 Lonza) supplemented with growth factors and antibiotics (EGM™-2 Bullet kit, Lonza). Cells were expanded to a maximum of 6 passages. For expansion cells were grown on 14cm diameter dishes, pre-coated with 10µg/mL fibronectin. Media was aspirated from confluent dishes and washed twice with sterile PBS. When confluent HUVEC were "split" as described above (***section 2.3.2***). Complete cell detachment was verified by light microscopy using an x4 objective, 8 mL fresh pre-warmed endothelial growth media was then added to neutralise the action of the trypsin. After centrifugation the cell pellet was re-suspended to achieve a 1:3 dilution for further passage. Upon reaching the 6th passage, HUVEC were trypsinised, harvested and re-suspended in cryopreserving medium (**section 2.3.4**). Cells were kept in 1 mL aliquots so that they could be thawed for a once-only use. Typically, one cryovial could be used to coat 4x35mm diameter fibronectin coated coverslips (***section 2.5.1***).

Deleted: ,

Deleted: to ensure integrity of cellular characteristics.

Deleted: tyrpsinised

2.3.4 Cryopreservation of cells

Cells grown for cryopreservation were amplified in log phase, harvested at approximately 10 million cells for each Corning ® Cryogenic vial. The pellet was re-suspended in 10% DMSO and 90% FCS (v/v) making a total volume of 1 mL, this was placed in one pre-chilled Corning ® Cryogenic vial. The vial was transported on dry ice to an -80 freezer for 24 hours then transferred to liquid nitrogen for long-term storage. Vials were rapidly thawed through submerging them in 37°C water bath. The DMSO/cell suspension was then immediately diluted in 9 mL of pre-warmed culture media (to minimize the toxic effects of the DMSO) and the cells harvested by centrifugation. After centrifugation the pellet was re-suspended in fresh warm culture media and grown in a tissue culture flask.

2.3.5 Isolation of Primary Neutrophils

All primary neutrophils were isolated from healthy volunteers; a maximum of 50 mL of blood was taken from the brachial vein. Trained medical professionals, working within the Cardiovascular Division, carried out the phlebotomy. The work complied with the regulations stipulated in the Human tissue act of 2004. Blood was drawn into a syringe preloaded with sodium citrate (Phoenix Pharma Ltd.); citrate ions chelate the calcium ions in the blood, forming calcium-citrate complexes. Removal of calcium disrupts the coagulation process. Blood was carefully layered on top of Histopaque-1077 (Sigma- Aldrich) in a 50 mL falcon tube. This was then centrifuged for 30 minutes at 1450 rpm (with no brake on the centrifuge). The Histopaque-1077 solution composed of polysucrose and sodium diatrizoate, gives a density of 1.077g/mL. After centrifugation polysucrose stimulates erythrocytes aggregation and consequential sedimentation, granulocytes become hypertonic, the decrease in cell volume prompts sedimentation (***figure 2.1***). Monocytes and other mononuclear cells remain at the plasma/Histopaque – 1077 interface, in a narrow fraction known as the buffy coat (***figure 2.1***). Top layers were carefully removed with a Pasteur pipette, making sure not to disrupt the erythrocyte/granulocyte rich pellet. The pellet was then mixed at a 1:1 (v/v) ratio with HBSS (free from calcium and magnesium). The new total volume was then added to an equal amount of 2% (w/v) dextran solution (filter sterilised through 0.22 μm filter). To ensure thorough mixing the falcon tube was inverted several times, and left for 20-30 minutes at room temperature. Erythrocytes sediment through gravity, the opaque neutrophil rich layer was carefully removed. The aspirate was mixed in a 1:1 (v/v) of HBSS and spun for 5 minutes at 1150 rpm. The pellet was re-suspended with 3mL of deionised sterile water for 30 seconds to lyse any residual erythrocytes through osmotic shock. The falcon tube was then rapidly topped up with 50mL of HBSS and spun for a further 5 minutes at 1150rpm. The pellet was re-suspended at the desired neutrophil density in pre-warmed RMPI culture media. Experimentation with primary neutrophils was conducted on the same day as the isolation procedure.

Deleted: is

Deleted: is

Deleted: eak

Deleted: is

Deleted: is

Deleted: is

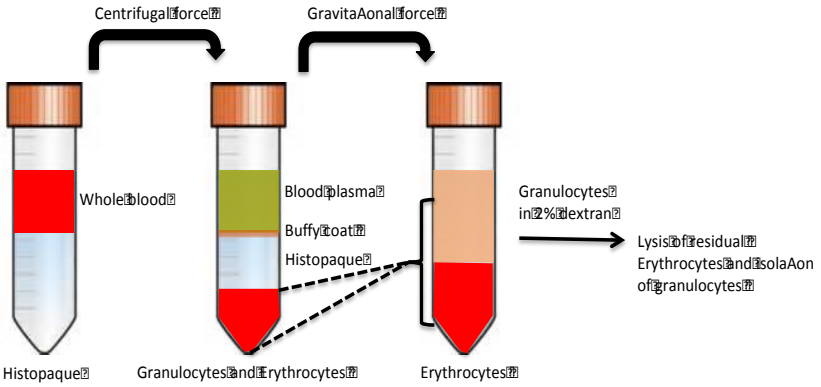

Figure 2.1: Schematic demonstrating the procedure used to isolate neutrophils from human blood.
Blood was collected from a brachial vein of healthy volunteers. To avoid coagulation blood was collected in sodium citrate (already present in the syringe). The neutrophil isolation process is a staged process. First whole blood is layered onto Histopaque-1077, providing a dense barrier through which mononuclear cells cannot penetrate, but erythrocytes and granulocytes can. After centrifugation, whole blood is separated into distinct layers. Further suspension of the pellet in 2% dextran allows erythrocytes to sediment and granulocytes to remain in suspension. The upper fraction containing granulocytes is finally harvested by centrifugation and any residual erythrocytes are lysed by osmotic shock.

Deleted: erythrocytes are

2.4 Flow cytometry

2.4.1 Instrument and Instrument parameter settings

Samples were analysed using a FACS BD ACCURI C6 (BD biosciences). FITC and GFP signals were excited at 488nm and detected at 530nm. Data was acquired with the acquisition software CellQuestTMPro version 4.0.2 (BD biosciences). In total a minimum of 20,000 events were collected per sample. All data was analysed using the FlowJo cytometry analysis software vX 0.7 (Tree Star,Inc). Initially live cell populations were gated using the forward (FSC-H) and side scatter (SSC-H) profiles to exclude dead cells and cellular debris. The gated population was then examined for the fluorescence intensity of antibody-labelled protein or GFP-tagged protein.

Deleted: ed

Deleted: /RFP

2.4.2 Antibody labelling

Indirect antibody labelling of surface protein levels was conducted, using a fluorescently tagged secondary antibody, which has specificity for the antibody species of both the isotype control and primary antibody being used. This indirect detection method has increased sensitivity due to signal amplification; multiple epitopes are available on the primary antibody. All cell labelling was conducted on ice in 1.5 mL Eppendorf tubes. Primary and secondary antibody incubations were performed on ice for 30 and 20 minutes, respectively. Neutrophils were labelled with the appropriate antibody in block solution containing 33% FCS (v/v) in PBS, to ensure blocking of non-specific interactions. Between primary and secondary antibody incubations, the cells were subjected to two PBS washes to remove excess antibody. Prior to FACS analysis, cells were re-suspended in 3% FCS (v/v) in PBS within a 1.5 mL Eppendorf. For actual antibody concentration used see ***table 2.2*** and ***table 2.3.*** Briefly, 200,000 cells were isolated per replicate per sample; analysis was conducted on gated populations to remove cell debris and dead cells. All FACS experimentation unless otherwise stated was conducted in triplicate-where three repeats on the same day represents N = 1, and an N = 3 completes the data set for any given FACS experiment.

Deleted: e

Deleted: e

2.4.3 Flow Jo analysis

As information on every single cell is acquired digitally, gating of cell populations could be performed post-acquisition using the Flow Jo vX 0.7 analysis software. Cell gating was performed to include singlet live cells but remove: cell aggregates, dead cells, bubbles and cellular debris. This gating could be achieved within histograms showing forward and side scatter profiles. Non-fluorescently labelled cells were used to measure auto-fluorescence, which could then be subtracted from the fluorescence intensity measurements. Antibody isotype-matched controls were used to measure fluorescence detected from non-specific binding arising from the Fc region of the conjugated secondary antibody. The fluorescence values from the above controls were used to threshold a positive signal. Median fluorescence intensity values were taken from each positively

gated sample. All experiments were performed in triplicate and data is represented as a mean +/- standard error of the mean (SEM).

2.5 Parallel plate flow chamber

Prior to perfusion assays, cells were re-suspended to an appropriate density in HL-60 media supplemented with 25mM 4-(2-hydroxyethyl)-1-piperazineethanesulfonic acid (HEPES). The imaging platform for the perfusion assays has no in-built CO_2 supply; therefore, Hepes acts to maintain the culture medium at physiological pH. Experimentation was performed at 37°C and visualised using an Olympus IX81 time-lapse inverted fluorescence microscope connected to a Hamamatsu C10600 ORCA-R2 digital video camera. A silicon gasket was vacuum-sealed to the activated endothelium, either seeded in the 3D device or on a coverslip. A Harvard syringe pump (Harvard Apparatus®, U.S.A) was used to draw leukocytes across activated HUVEC monolayers at a fixed flow rate (0.25mL/min). Typically, cells were perfused at 1.24 dynes/cm^2, which falls within a physiological shear stress of blood flow within post capillary venules. Volocity®, Imaging software Perkin Elmer, was used to control the acquisition rates, which was stored as digital data files. ***Figure 2.2*** outlines the main features of the parallel plate flow chamber.

Deleted: EPES

Deleted: a coverslip

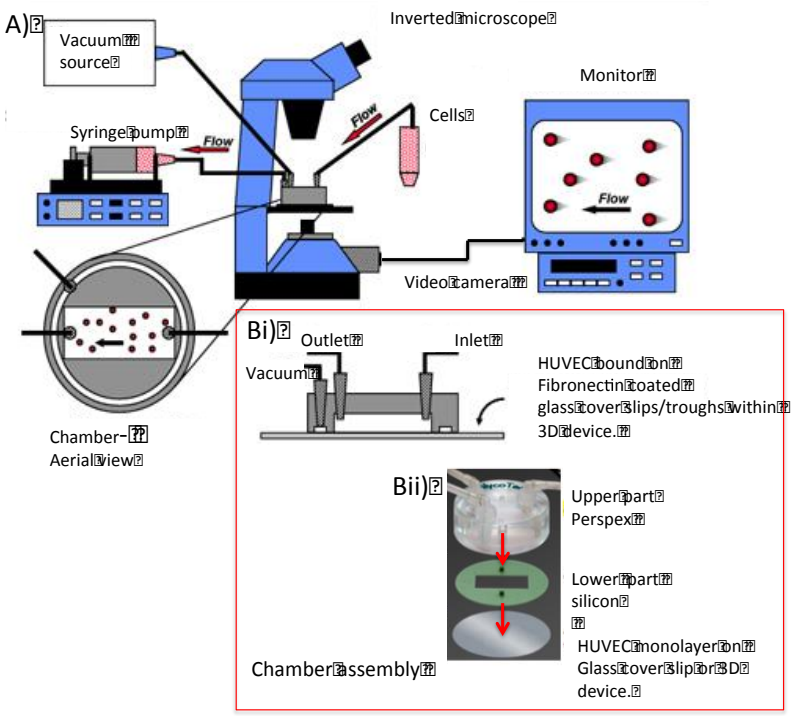

Figure 2.2: Schematic depicting the parallel plate flow chamber set up.
The images show the microscope set up, all assays were performed in plastic housing, (not shown), to maintain temperature control. A) The parallel plate flow chamber is attached via a vacuum seal to an endothelial monolayer; together this is placed onto an inverted fluorescence microscope. A syringe pump draws leukocytes via negative pressure from a receptacle across the activated HUVEC. Unbound leukocytes alongside media are collected into a syringe. Time-lapse videos were recorded through a CCD (charge coupled device) camera with a video recorder connected to the computer. Volocity software (Perkin Elmer, USA) acquired movies throughout the experiment. Bi) Schematic demonstrating connections found in the Perspex part of the parallel plate flow chamber-vacuum inlet and an inlet and outlet to allow the passage of leukocytes. Bii) An Image to demonstrate the assembly of the parallel plate flow chamber.

2.5.1 Cell perfusion assays for binding dynamics

Differentiated HL-60 cells or primary neutrophils were cultured at a density of $0.5x10^6$ cells/mL in HL-60 media (RMPI media, 10% (v/v) FCS, 1% penicillin/streptomycin) the night before the experiment. A total of 3mL of the cell suspension was delivered into the flow chamber, followed by media alone. The cells were perfused over TNF-α-activated HUVEC monolayer grown on fibronectin-coated 35 mm diameter sterile glass coverslips. In cases where L-selectin shedding was pharmacologically blocked, primary neutrophils were pre-treated with cell media supplemented with 10μM TAPI-0 twenty minutes prior to perfusion. Media supplemented with 10μM TAPI-0 was also used to condition the TNF-activated HUVEC monolayer for 5-10 min before each flow experiment. Image acquisition started from the moment the syringe pump was switched on. All recordings were performed using a 10x objective microscope. The dead volume of tubing from the cell suspension to the flow chamber was approximately 0.5 mL. Given that the flow rate was set to 0.25 mL/min, the cells would begin to enter the flow chamber by 2 min and cell binding would typically be seen a few minutes after that. To avoid bias in recording cell adhesion and transmigration events, a minimum of three fields of view was acquired for every flow assay conducted. Typically, for every phase contrast and GFP channel, each field of view was acquired every 30 seconds. To monitor the leukocyte's dynamic behaviour with activated endothelial monolayers, video stills at 6 minutes, 10 minutes and 30 minutes were scored for stages of the adhesion cascade; binding, intraluminal crawling, mid-transendothelial migration (mTEM – where cells are captured in mid-transmigration) and full transendothelial migration (fTEM – where the process is complete). The time taken for the entire adhesion cascade to be executed was also monitored and scored from the moment cells were captured to the activated HUVEC monolayer up until the cells entered the sub endothelial space. Conveniently, TEM is easy to observe by eye: leukocytes appear phase bright when above the endothelium and phase dark when within the sub

Deleted: the cell

endothelial space. Volocity software (PerkinElmer,U.S.A) was used to analyse leukocyte transmigration events.

Samples prepared for confocal analysis requires disassembly of the parallel plate flow chamber to retrieve of the 35 mm glass coverslip. The coverslip is then subsequently submerged into 4% PFA(W/V) made up in PBS. Retrieval of the coverslip is performed in less than a minute to avoid any radical changes in cell morphology. The coverslip is then permeabilised, blocked and stained for intracellular/extracellular markers. See ***section 2.8.2*** for more detailed description on immunostaining for microscopy. Shorter perfusions (15 minutes) were conducted to optimise visualisation of cells engaged in mid-transendothelial interaction, and address the subcellular distribution of L-selectin.

Deleted: would

Deleted: , which would

Deleted: be

Deleted: would be

Deleted: would be subsequently

2.5.2 Cell tracking of fully transmigrated neutrophils

To determine the speed and directionality, cells were manually tracked using the ImageJ (NIH) plugin, MTrackJ. The co-ordinates of the cell trajectories were input into a custom-made open source computer program-Diper. A more comprehensive documentation of the code can be found in the report by Gorelik et al (306).

Deleted: here

2.5.3 Cell perfusion of the 3D device

The 3D devices were prepared as described in ***section 2.12*** and subjected to activation for 12-16 hours with TNF-α. Perfusion was conducted in HL-60 media, supplemented with 25mM Hepes (pH 7.3). Where HL-60 cells were co-perfused over activated endothelial monolayers, each cell line was uniquely stained with 1μM cell tracker dye (Cell Tracker®). To stain, neutrophils were incubated in RPMI media only (no FCS) for 15 minutes at 37 °C, after; cells were washed and re-suspended in appropriate media. To avoid bias and prevent any adverse effects on cell behaviour, dyes were exchanged periodically between lines and experiments. Primary neutrophils were stained with 1μM Cell Tracker® Orange. In experiments where L-selectin shedding was pharmacologically inhibited, the neutrophils and HUVEC monolayer were pre-treated for 20 minutes with 10μM TAPI-0. Each flow assay was performed for 2 hours per device, after which the devices were fixed with 4%(w/v) PFA in PBS, permeabilised and stained for

Deleted: EPES

visualisation (see ***section 2.8.2***) on an inverted spinning disk (Yokagawa) confocal.

Formatted: Font: Bold, Italic

2.6 Protein Biochemistry

2.6.1 Polyacrylamide gel electrophoresis of HL-60 cell lysates, using the Novex NuPAGE SDS-PAGE pre-cast gel system

To generate whole cell lysates, 2 million HL-60 cells were pelleted for 5 minutes by centrifugation. The pellet was lysed in 200 μL 2x protein loading buffer (see ***table 2.1***), then transferred into a 1.5mL Eppendorf. To decrease the viscosity of the sample (generated by nuclear lysis) and ensure accurate gel loading, the preparation was sonicated for a few pulses. Samples were subsequently placed in a heat block at 95 °C for 5 minutes to complete protein denaturation. For static transmigration assays, HUVEC monolayers were grown to confluence in fibronectin coated 6 well plates and activated overnight in 10 ng/mL^{-1} TNF-α. The added neutrophils were left to transmigrate for 45 minutes at 37°C and 5% CO_2. For each well, 200 μL of 2x protein loading buffer was added and lysate harvested instantaneously using a cell scraper and then processed by sonication as described above. The denatured protein samples were resolved by polyacrylamide gel electrophoresis on pre-cast Novex® NuPAGE® 4-12% Bis-Tris gradient gels (Life Technologies, U.K.) in 1x MES buffer. To characterise the molecular weights of proteins, Novex® sharp pre-stained protein standard molecular weight markers (Life Technologies, U.K.) were used for all gels. Electrophoresis was performed at a voltage between 100-180 volts, and was stopped when the dye front reached the base of the gel casing.

Deleted: e

Deleted: o

Deleted: which

2.6.2 Western blotting

Protein was transferred from the polyacrylamide gels to Nitrocellulose (Millipore®, U.K.) membrane; the membrane was pre-wet in transfer buffer, (see ***table 2.1***). Transfer was carried out in a NuPAGE® transfer blot module (Invitrogen, U.K.) at 27 volts for 2 hours. The membrane was then blocked for 1 hour in 5% (w/v) milk (MARVEL) made up in TBS solution, known as blocking solution (see ***table 2.1***). The membrane probed with the appropriate primary antibody in blocking solution and left at 4°C on a rocker for overnight incubation.

Deleted: containing Tris buffered saline solution, known as blocking solution. The membrane was then

Formatted: Font: Bold, Italic

The following day the membranes were washed for 10 minutes with TBST (0.1% v/v tween-20) followed by three consecutive short 3 minute washes with TBS (see ***table 2.1***). The membrane was further blocked for 1 hour before addition of the secondary antibody at a dilution of 1:15,000 again for 1 hour. Both these incubations were conducted at room temperature. Membranes were washed as described above before imaging.

Deleted: then again

Deleted: on the LI-COR® system

2.6.3 Densitometry analysis

Deleted:

Nitrocellulose membranes labelled using LI-COR® compatible antibodies were scanned using the LI-COR® system; bands were analysed and quantified using Image Studio Software (Version 2.1, LI- COR® Biosciences, UK). Protein levels were determined based on their band intensities normalised to their respective loading control intensities, for example β-actin. In the case of L-selectin shedding, the intensity of the membrane-retained fragment, or "stump", was normalized against total L-selectin: bands corresponding to both full-length L-selectin and "stump". This normalisation is represented by "stump"/("stump"+Full length).

Deleted: PVDF

2.7 Lentiviral transduction and generation of stable cell lines

2.7.1 Lentiviral production

Lentivirus particles encoding L-selectin were produced using the packaging cell line HEK 293T. For the generation of lentiviral particles HEK 293T cells were transfected with three plasmids; psPAX2 (packaging), pMD2.G (envelope) and pHR'SIN (carrying the gene of interest). Prior to transfection HEK 293T cells were grown to ~80% confluence in a sterile T175 flask. On the day of transfection 30µg psPAX2, 40µg pHR'SIN and 10µg pMD2.G were mixed together with 4mL of OPTIMEM(GIBCO®, Invitrogen). In a separate tube another 4mL of OPTIMEM was mixed with 1µL of 10mM polyethylene imine (PEI). The contents of the two tubes were then combined and left to incubate at RT for 15 minutes. HEK 293T culture media was aspirated and replaced with 8mL of transfection media and incubated for 4 hours under normal culture conditions, after which the transfection media was then replaced with 14mL of warmed fresh HEK 293T culture media. HEK 293T cell media was carefully harvested at 48 and 72 hours post-infection. Note that after the first harvest, 14mL of fresh HEK 239T culture media was added

Deleted: envelope

Deleted: packaging

back to the flask. The supernatants from both harvests, containing the lentiviral particles, were pooled, filter sterilised (0.45µm) and stored at -80°C.

To concentrate the virus particles, the supernatants were thawed and ultracentrifuged (Sorvell® Discovery) for 2 hours (4°C , 19,990rpm). From each 13.2 mL polyallomer ultracentrifuge tube (Beckman Coulter) the supernatant was carefully discarded and the pellet re-suspended in 50µL of HL-60 culture media. All re-suspended pellets were pooled and incubated on ice for 50 minutes to ensure complete suspension of virus particles, after which the suspension was aliquoted into smaller volumes ~20 µL to prevent excessive freeze thaw cycles. Each aliquot was stored at -80 °C until further use.

Deleted: 19,900 rpm

2.7.2 Estimating lentiviral titres

In order to establish the viral titre (number of virus particles per mL), THP-1 cells were grown in a 24-well plate, at a density of $2x10^5$ cells/well at day 0. THP-1 cells were counted and transduced by adding increasing dilutions of the concentrated lentivirus, (10^{-5}– 10^{-1}) to a total volume of 200µl (per well) HL-60 cell culture media. On day 2 an additional 200µl HL-60 cell culture media was added to each well. On day 4, cells were collected and GFP expression levels monitored through FACSCalibur flow cytometer (BD Biosciences). The percentage of GFP positive cells was plotted against the lentiviral particle concentrate added. This was then used to determine a concentration of lentivirus that infected no more than 25% of the THP-1 population within the well. This low infection percentage would lower the risk of multiple insertions within the genome.

Deleted: y

Titres and MOI were calculated according to the following equations:

a) $T=((PXN)/(DXV))$

b) $MOI= VT/N$

Where: (a) *T = titre, P =number of GFP positive cells, D = dilution and V = volume*, (b) MOI = multiplicity of infection, *V = volume of lentivirus required, T= titre, N= number of transduced cells.*

Volume of concentrated virus used for the generation of a stable cell line was found on the basis of titre and desired multiplicity of infection (MOI).
Below is a table highlighting the titres used within this thesis to generate the HL-60 cell lines stably expressing L-selectin-GFP (***table 2.4***). These viruses, with the exception of ΔMN SSAA GFP, had been previously made, and titres quantified, by a previous PhD student in the Ivetic lab - Karolina Rzeniewicz. I generated the ΔMN SSAA GFP virus, as the viral stock had previously run out.

Cell line	Plasmid backbone	Titre $X10^8$ i.u/mL	MOI
WT L-selectin GFP	pHR'-SIN-SEW	2.128	10
GFP	pHR'-SIN-SEW	2.56	5
ΔMN L-selectin GFP	pHR'-SIN-SEW	2.84	10
ΔMN SSAA L-selectin GFP	pHR'-SIN-SEW	13.3	8
ΔMN SSDD L-selectin GFP	pHR'-SIN-SEW	3.56	9

Table 2.4: Virus titres and MOI used for cell line generation

2.7.3 Lentiviral infection of HL-60 cells

One day prior to transduction, HL-60 cells were passaged to a density of 0.5 x 10^6 cells/mL, to ensure cells were in log phasic growth. The following day cells were enumerated and 1 million cells re-suspended to 0.5x10^6 cells/mL in HL-60 culture media, lentiviral particles were added. The volume of lentiviral particles to add was calculated using viral titre and desired multiplicity of infection. Transduced

cells were stored at 37°C and 5% $C0_2$; cells were supplemented with fresh media 24 hours after transduction, and then passaged as normal (***section 2.3.1***).

Deleted: y

Formatted: Font: Not Bold

2.7.4 FACS sorting

All cells were sorted using a FACSAria II cell sorter housed within King's College London's Biomedical Research Centre. Cells were sorted to match the expression of their WT/control counterpart to ensure the tagged protein level remained similar for each cell line.

2.8 Confocal microscopy

2.8.1 Equipment

Unless stated otherwise confocal images were acquired using the Leica TCS SP5 confocal microscope (Leica Microsystems,Germany). GFP was excited at λ = 488 nm with an Argon laser, whereas TRITC-phalloidin and AlexaFluor®633 were excited with Helium Neon lasers at λ = 543/568 and 633 nm, respectively. AlexaFluor®405 and DAPI (4',6-diamidino-2- phenylindole) were excited at λ = 405 using a UV laser line. Images were acquired using LAS AF software (Leica Microsystems, Germany). Images were acquired at 1024 x 1024 pixels with a 16-bit resolution at a frequency of 400Hz and 32 line averages.

Deleted: M

2.8.2 Cell fixation and labelling procedures

For visualization of L-selectin in primary neutrophils or HL-60 cells, specimens were fixed in 4% PFA (w/v) in PBS for 20 minutes at RT and washed 3 times in PBS. It is important to note that washes were conducted with extreme care with respect to the troughs in the 3D devices, as the fixed specimen was highly susceptible to disintegrate through harsh pipette action. Coverslips or 3D devices were incubated with 0.1 % (v/v) ice cold Nonident P-40 (NP40) (FlukaBioChemika) in PBS for 3 minutes to permeabilise the leukocytes and HUVEC plasma membranes. Coverslips and 3D devices were then subjected to three short PBS washes, then blocked in 33%(v/v) FCS in PBS for 30 minutes at RT. The appropriate primary antibody/ies concentration/s can be found in ***table 2.2*** and ***table 2.3***. To visualise actin, either TRITC or FITC conjugated phalloidin was used at a dilution of 1:300 (***table 2.1***). Block solution (33%FCS in PBS) was supplemented with Fc receptor block (1:100 (v/v) dilution). Fc receptor block

ensures that the Fc region of an antibody does not react with Fc receptor on the neutrophil plasma membrane. Samples were stained overnight at 4 °C. The following day coverslips or 3D devices were washed 3 times in PBS and incubated in the above blocking solution with the appropriate fluorescently conjugated secondary antibody. Again, secondary antibodies (see ***table 2.3*** for correct concentration/s) were incubated in block solution containing 1:100 (v/v) Fc receptor block. Following an overnight incubation in the dark at 4°C, samples were washed three times in PBS. Coverslips were mounted onto a microscope slide using the mountant DAKO, which preserves the fluorescent signals from the immunostaining process. In order to prevent collagen dehydration a square glass cover slip was placed on top of the trough to act as a lid, fluorescent mountant was used the seal the PDMS and glass interface. Both coverslips and 3D devices were stored at 4°C prior to imaging, ensuring the stability/longevity of the samples.

Deleted: fluorescent

Deleted: (

Deleted:)

Deleted: .

2.8.4 Analysis of GFP and LAM1-14 positive "spots"

Neutrophils were perfused over TNF-α activated HUVEC as described in ***section 2.5.1.*** TRITC-phalloidin labelling enabled visualisation of HUVEC actin cables and VE-cadherin marked adjoining endothelial adherens junctions. Disruption of this junctional marker denotes a breach in the endothelial monolayer and signifies bona fide paracellular TEM, as opposed to transcellular TEM. Single z-plane images were acquired with a Leica TCS SP5 confocal microscope. Images were acquired using a 63X oil immersion objective. To ensure high quality images line averages of 32 and a line scan speed of 200Hz was used. L-selectin rich areas was defined through either the GFP signal or LAM1-14 antibody binding to L-selectin EGF domain. Analysis was performed using the Volocity (PerkinElmer), "find spots" tool. HL-60 cells transduced with GFP alone was used to threshold spot area in HL-60 cells stably expressing L-selectin-GFP.

2.8.5 Morphology analysis

Images of fully transmigrated neutrophils acquired by confocal microscopy and stored in Leica-based Liff files were imported into the open licence software Fiji. Using the freehand tool, individual cells were manually traced and the circularity

ratio obtained. Cells were traced using the outline of the cell cortex (established by phalloidin labelling).

$$\text{Circularity ratio: } 4\,\pi((\pi r^2)/(2\pi r)^2)$$

This ratio is set between 1 and 0, where 1 is "a perfect circle". As the value becomes closer to zero, the shape will increase disproportionally in one axis and result in irregular or elongated morphologies. For each cell line, fifteen cells were analysed for each experimental repeat, a total of three repeats were conducted for this analysis.

2.8.6 Subcellular localisation of L-selectin

HL-60 cells chemotaxing on fibronectin-coated 2D substrates were analysed for the subcellular distribution of WT or mutant forms of L-selectin-GFP. Images were captured using differential interference contrast (DIC) and 488nm excitation. A line 30-pixels wide was drawn through the front-back of a clearly polarised cell; using the line profiler in Fiji, DIC determined the front-back cellular extremities. Greyscale values along the line profile for the green channel (corresponding to the GFP signal) was obtained, and internally normalised for each cell. An in-house MATLAB® code was written to "stretch" each data set to account for differences in cell length, which allows all data to become superimposed and accurately averaged. All line profiles were "stretched" to 100 pixels in length, for example if a cell was 50 pixels in length through the front-back line the code "stretches" the data to form 100 pixels while still maintaining the original GFP intensity profile. The code uses interpolation as it creates new data points in between existing data points.

Deleted: from the front to rear

2.9 L-selectin shedding assays

2.9.1 Monitoring L-selectin shedding from cell suspensions

Primary Neutrophils and HL-60s were stimulated with PMA or various chemoattractants in 10% (v/v) FCS in Hanks buffered saline solution at 37°C. For each experiment, 200,000 cells were incubated in HL-60 culture media

Deleted: .

supplemented with one of the above stimuli, and left at 37°C and 5% CO_2 for 30minutes. Cells were then centrifuged, the supernatant aspirated and placed on ice. Cells were then prepared for FACs as described in ***section 2.4.2***. Experiments were conducted on three days, each day carried out in triplicate to ensure accuracy.

2.9.2 Monitoring L-selectin shedding in neutrophil/HUVEC co-cultures

Confluent HUVEC monolayers were grown in 6 well plates and activated with 10ng/ml TNF-α. Cells ($2x10^6$ million) were added to each plate and incubated for 45 minutes. Each plate was gently washed with pre-warmed cell media to remove any unbound leukocytes. Extracts were harvested and resolved on polyacrylamide gels for Western blot analysis (***section 2.6***).

2.10 Micropipette chemotaxis assays

Micropipette assays were employed to monitor chemotaxis and cellular behaviour of leukocytes challenged with a single gradient of chemoattractant (***figure 2.3***). Glass-bottomed dishes (5 cm in diameter) were coated with 5 μg/mL of fibronectin (diluted in PBS) and left to incubate for 1 hour at 37 °C. Excess fibronectin was removed through two rounds of aspiration and PBS washes. Before the addition of cells, dishes were further incubated in imaging media (PBS containing calcium and magnesium supplemented with 1% FBS, penicillin/ streptomycin, 1 mg/mL BSA) to block nonspecific binding of cells to the glass bottoms. Cells were seeded at a density of 1×10^6 cells/mL in warm imaging media and left to adhere for 30 min at 37 °C. Excess unbound cells were removed before imaging. All experiments were conducted at 37 °C and performed within 1 hour. Micropipettes were manufactured in-house. Borosilicate glass capillaries with an inner diameter of 0.5 mm were pulled using a P-97 Flaming/Brown micropipette puller (Sutter Instrument Company). Pipettes were pulled using the following parameters: heat = 500, pull = 500, velocity = 30, and time = 250. The micropipette was attached to a pressure system (Narishige IM300 microinjector (0.7 psi)). Avoiding air bubbles, the pipette tip was filled with the desired chemoattractant diluted in imaging media supplemented with a 10kDa TRITC-dextran tracer to observe gradient formation. Note that the average molecular weight a chemokine corresponded to 10kDa molecular weight.

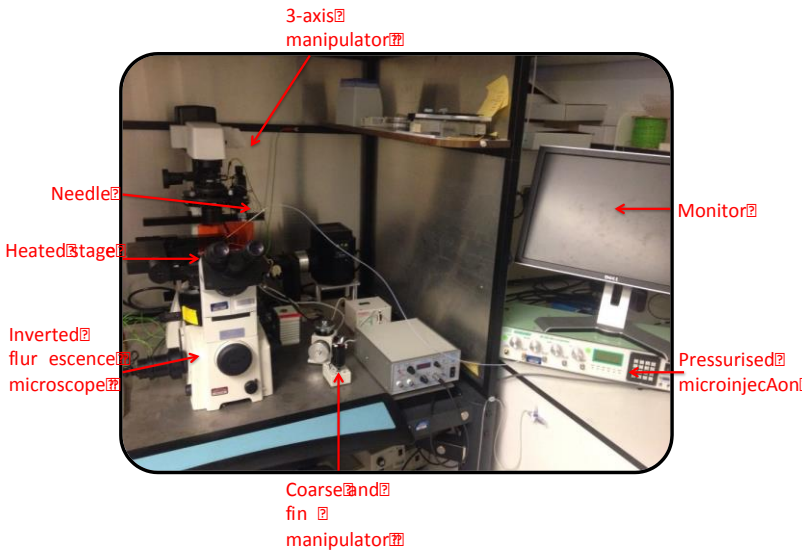

Figure 2.3: The micropipette set-up
The sample, in an open top glass dish is placed into a heated stage unit; a pressurised needle housing the glass capillary micropipette chemoattractant-filled tip is placed into the glass dish. The tip can be manipulated in X, Y and Z-axes with both coarse and fine movements. Cell migration behaviour is captured by the use of an inverted microscope objective lens.

2.11 Microfluidic 2D device

The design and fabrication (photolithography and soft lithography) are discussed in detailed in ***section 4.1.2***.

2.11.1 Gradient generation

Gradients were established using the Fluigent system (MFCS-8C). The microfluidic flow rate controller allows a stable and continuous free flow from 8 independently controlled outlets, which uses positive pressures ranging from 0 to 1000mbar. Fluigent allows control over multiples inlets simultaneously, a great advantage over the syringe pump. Gradients were visualised using fluorescently conjugated dextran (see ***section 4.1.3***) and analysed using the intensity profiler in Fiji.

Deleted: pulsatile

2.11.2 Cell seeding

The device was filled with 30μg/mL fibronectin for HL-60 cell seeding. The fibronectin in the device was incubated for 1 hour at 37°C. PBS was then flushed through to remove excess fibronectin. Particular attention was paid to remove all bubbles from the microchannels. Cells were seeded through the open inlet and unbound cells left through the opposite outlet; cells were left to adhere for 20 minutes at 37°C. During this time all inlets and outlets are sealed to prevent internal fluid movement. For information on cell streaming to correctly position cells in the middle of the main channel see ***section 4.1.4.***

Deleted: removing

2.12 Microfluidic 3D device

The design and fabrication (photolithography and soft lithography) are discussed in detailed in ***section 4.2.2***.

2.12.1 Collagen imaging

Rat tail type 1A collagen (Cellmatrix, Nitta gelatin Inc, Japan) was reconstituted on ice to prevent premature gel polymerisation in the following (v/v) proportions: 4 parts collagen; 2 parts 5X DMEM (PAA, Colbe, Germany); 1 part sterile reconstitution buffer made up to a total of 120mL (2.2g$NaHCO_3$ (0.2M) in 100mL of 0.05N NaOH and 200mM Hepes) and 1 part HL-60 culture media, this formulation would provide a protein concentration of 2.5 mg/mL. Culture media volume was adjusted in optimisation experiments when varying the total collagen concentration see ***section4.2.4***. The reconstituted collagen solution was deposited within the PDMS bespoke cut trough and left within a humidified sterile environment at 37°C to polymerise for 30 minutes. Successful collagen polymerisation was assessed through light microscopy through the presence of collagen fibres. To assess collagen fibre heterogeneity and collagen depth within the 3D device reflective confocal imaging was adopted, first reported by the lab of Voytik-Harbin (307). Briefly, the microscope parameter settings are readjusted so the emission spectrum is lowered to around the same wavelength range as its respective laser excitation spectra; this ensures that any light collected is reflected.

Deleted: Colbe ,

Deleted:

Deleted: i

Deleted: l

Deleted: epes

2.12.2 HUVEC seeding

Although PDMS has major advantages, e.g. similar reflective index to glass and biocompatibility, it does have some disadvantages; it is hydrophobic and has low adhesive properties for cell attachment. To overcome this the glass (bottom of the 3D device was pre-coated with poly-L-lysine (PLL) treatment for 20 minutes after which the polymer polydimethylsiloxane (PDMS) was subjected to oxygen plasma for 2 minutes. The troughs were then pre-chilled on ice, after which 30μL of reconstituted collagen (***section 2.12.1***) was carefully placed into the centre of the trough and a tilting motion was used to gently cover all the glass surface area. The device was then placed into a 14 cm dish, which was placed into a cell culture incubator for 45 minutes. To minimise a collagen meniscus being formed, a hydrophobic pen outlined the PDMS edges of trough prior to collagen addition. Once set, the collagen was inspected visually and devices with concave or convex menisci, or devices where the collagen had pulled away from the sides of the PDMS trough were discarded. Where successful collagen polymerisation was achieved, HUVEC were thawed and immediately seeded on to the collagen bed. Approximately half a million cells were added to each (2.3 cm x 0.5 cm) rectangular trough; a confluent monolayer was achieved 24 hours post-seeding. Prior to any flow assay, HUVEC were stimulated overnight with 10 ng/ml TNF-α.

2.12.3 Optimisation procedure for gradient formation in the 3D device

Gradients were generated using a 10,000 Da fluorescently labelled dextran. The movement of this polysaccharide through the microfluidic channels and the polymerised collagen scaffold mimics the diffusion of most chemokines, which are of comparable molecular weights (8-10kDa). Gradients were established using a Harvard syringe pump. To visualise the establishment of diffusion gradient across the collagen scaffold over time, a single Z line scan was taken every minute. The Z line scan was imaged using an inverted scanning confocal microscope (FV1000 confocal head-Olympus) with a 10x objective lens. Diffusion gradients were left to establish for 1 hour and imaging was acquired in a heated chamber set at 37 °C. Gradients were analysed using the line profiler plugin in the image analysis platform Fiji. Unless stated otherwise the width of the line profile was averaged

Deleted: k

Deleted: a diffusion

over 30 pixels. More information regarding gradient generation and analysis can be found in ***section 4.2.7***.

2.12.4 Static transmigration assays using 3D devices

Rectangular troughs were cut from cured PDMS, and plasma bonded to cleaned glass coverslips, 5 cm in diameter. For every trough, 50µL of Rat-tail collagen type 1A was dispensed and allowed to polymerise for 30 minutes at 37°C. Once set, the collagen acted as a solid support for the establishment of activated HUVEC monolayers. All leukocytes were labelled with 1µM CellTracker (Molecular Probes, Life Technologies) for 10 minutes at 37°C in RPMI containing no FCS only 25mM Hepes(pH 7.3). Labelled cells were harvested by centrifugation and re-suspended at 0.5 x10^6 cells/mL in culture medium. 0.5 x10^6 cells were added per trough and left for 1 or 4 hours, after which the assay was stopped, washed and preserved by fixation in 4% paraformaldehyde (made up in PBS). In TAPI-0-treated experiments, neutrophils were pre-incubated for 20 minutes with 10µM TAPI-0 prior to cell labelling. In these assays the HUVEC were also treated with 10µM TAPI-0 20 minutes prior to neutrophil addition. TAPI-0 also remained present within the culture medium at 10 µM for the duration of the experiment. When HL-60 cells were co-introduced on an activated endothelium, each cell line was uniquely stained with cell tracker dyes. To avoid bias and overcome any adverse effect of dye loading on cell behaviour, dyes were exchanged sequentially between lines and experiments.

Deleted: HEPES

Deleted: .

Deleted: hours

2.12.5 Measuring leukocyte invasion post-transmigration

In order to measure the extent of invasion post-transmigration, paraformaldehyde-fixed 3D devices (described in ***chapter 5***) were imaged using an inverted spinning disk confocal (Yokagawa). A 30x objective was used and fields of view were selected on the basis of an intact endothelial monolayer and proximity to the chemoattractant source. Laser excitement at 488nm, 543nm and 633nm was used to specifically discriminate between cell lines that were co-perfused. Multiple fields of view were imaged per trough (n=1). FITC-phalloidin staining was used to identify HUVEC monolayers, which possess characteristically large cable-like stress fibres. A total of 200 x 1 micron-thick Z-slices were taken downward into the collagen trough. The extent of leukocyte invasion through the

collagen trough was manually enumerated, using a 16-colour heat map (Fiji); leukocytes in focus become labelled with a representative "hotter" colour. Neutrophils were enumerated in 10μm steps, downward from the HUVEC monolayer. For a more detailed description of the post acquisition analysis see ***chapter 5***.

2.13 Statistical analysis

All quantified data was evaluated using the statistical analysis package GraphPad Prism®. Significance was determined using unpaired Student t-tests, Mann Whitney tests and one-way ANOVA followed by either Dunnett's or Tukey's post test. Data was deemed significant when $p<0.05$. Both the unpaired Student t test and one-way ANOVA are parametric tests; these statistical models assume that data follows a probability distribution with a fixed set of parameters. T tests were used to compare means from two samples, while the one-way ANOVA with appropriate post test was used to compare means from more than two samples. Unlike Student t-test the Mann Whitney test does not assume a normal distribution of data and is therefore a form of non-parametric testing.

3. Establishing a cellular model to understand the importance of L-selectin shedding in regulating neutrophil migratory behaviour.

3.1 Biological rationale

Recently, L-selectin shedding has been shown to occur specifically during TEM in primary human monocytes(212). Blocking L-selectin shedding induced dramatic effects on cell polarity and chemotaxis (see ***section1.12***). The primary aim of this chapter was to determine if L-selectin shedding occurred during primary human neutrophils TEM, and, if so, does blocking L-selectin shedding alter cell polarity and migration during either transendothelial migration or chemotaxis within the subendothelial space.

This study employed the use of primary neutrophils and HL-60 neutrophil-like cell lines. To investigate L-selectin shedding in primary neutrophils, cells were incubated with 10 μM TAPI-0 (which is: TNF-α protease inhibitor) a known inhibitor of ADAM17, previously shown to block L-selectin shedding in monocytes. The cell line chosen for this study is an immortalised cell line, HL-60, derived from human promyelocytic leukaemia cells. HL-60 cells are routinely used in leukocyte research, importantly in migration assays (308)(309). Crucially, DMSO differentiated HL-60 cells do not express any detectable levels of endogenous L-selectin. This fact allows direct comparisons between cell lines expressing WT and mutant forms of L-selectin. In order to mimic all stages of the leukocyte adhesion cascade it was paramount that the leukocyte underwent full transendothelial migration, this was achieved through overexpression of chemokine C-X-C receptor 2 (CXCR2) in the HL-60 cells. With primary neutrophils, L-selectin could not be engineered as a GFP fusion and so was visualised using the mAb LAM1-14. LAM1-14 detects L-selectin at the EGF-like domain a region that is above the cleavage site, meaning that only the full-length form can be detected.

Deleted: levels of

Deleted: to express

Deleted: GFP

Deleted: a

Four L-selectin constructs, (WT, ΔMN, ΔMNSSAA and ΔMNSSDD) were virally transduced into the HL-60 cells. All these L-selectin molecules were C-terminally tagged with GFP to allow real time visualisation of the molecule. Given the relative size of GFP (238 amino acids) compared to the shed form (cytoplasmic tail+transmembrane domain alone) of L-selectin (17 amino acids), previous studies were carried out to establish the tag exhibited no adverse effects on L-selectin expression form and function(212). These control experiments were conducted in THP1 cells by Karolina Rzeniewicz a past PhD student (212). The genetic "sheddase resistant" mutant of L-selectin was generated through an eight amino acid deletion, (ΔMIKEGDYN) below the proximal cleavage site, rendering the site unrecognisable to cleavage enzymes. This mutation shall be termed ΔMN for simplicity. To verify L-selectin's contribution towards any observed phenotypes, cells were transduced with GFP alone for direct comparison.

To dissect the molecular mechanisms governing the phenotypes observed from blocking L-selectin shedding, sheddase resistant cells (ΔMN) harbouring substitution mutations in both the serine residues of the cytoplasmic tail were generated. Here, the serines, (S364, S367), were converted to either alanines (A) or aspartates (D), to mimic serines in a permanently phospho-dead or phospho-active form, respectively.

Finally, L-selectin shedding was assessed in response to either end-stage or intermediary chemoattractants.

3.2 Results

3.2.1 Primary human neutrophils undergo L-selectin shedding during transendothelial migration (TEM)

Previous reports have stated that neutrophils undergo L-selectin shedding during the firm adhesion phase of the multi-step adhesion cascade. The Ivetic lab recently showed that L-selectin shedding in CD14-positive primary human monocytes underwent L-selectin shedding specifically during TEM and not before (212). To determine if this phenomenon also applies to primary human neutrophils, cells were isolated from healthy volunteers and perfused over TNF-

Deleted:

Deleted: ce

Deleted: historically

Deleted: would

α-activated HUVEC monolayers for 30 minutes. In parallel experiments where L-selectin shedding was blocked, neutrophils were pre-incubated with 10 μM TAPI-0. This inhibitor was supplemented in the perfusion media throughout the flow assay to ensure that its effect lasted during the entire perfusion experiment. After each flow assay, all specimens were fixed in 4% paraformaldehyde and analysed by laser scanning confocal microscopy. In experiments where the carrier, dimethyl sulfoxide (DMSO), was used, neutrophils that underwent full (or complete) TEM (fTEM) were virtually all L-selectin negative (***figure 3.1***). This observation was reversed when flow experiments were supplemented with TAPI-0 (***figure 3.1***). To ensure that the endothelial monolayer was intact in all experiments, junctional staining of F-actin and VE-cadherin was used to detect actin cables and endothelial junctions, respectively.

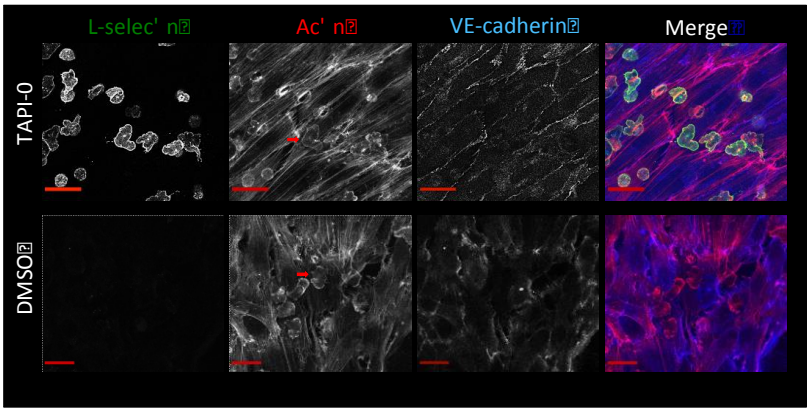

Figure 3.1: L-selectin shedding occurs during transendothelial migration
Primary human neutrophils were perfused over TNF-activated HUVEC for 30 min. Flow assays were supplemented with either 10 μM TAPI-0 (to block L-selectin shedding) or DMSO carrier alone. Specimens were fixed with 4% (w/v) PFA, permeabilised and stained with LAM1-14-488, TRITC-phalloidin and VE-Cadherin-633 to visualise L-selectin, F-actin and endothelial junctions, respectively. Instrument parameter settings remained unchanged during acquisitions. Confocal images were acquired with a 63x oil immersion lens. Scale bar = 24μm. Red arrows indicate cells that have undergone complete TEM, e.g. fTEM cells.

To quantify the fluorescent signal corresponding to L-selectin signal at the plasma membrane, a line profile was drawn along the longest axis of the cell, (***figure 3.2 A***). The phalloidin signal was used as a guide for the plasma membrane to accurately define the beginning and ending of the cell. This was particularly important in the situation where TAPI-0 was not used and the L-selectin signal

Deleted:

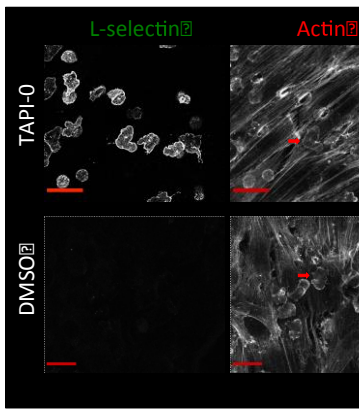

Deleted: front-rear

was minimal. Fluorescence intensities from the peripheral LAM1-14 signal were outputted as greyscale values (***figure 3.2 B***).

Greyscale is an image that represents black and white shades, producing a combination of levels, 0=black and 255=white, the range between is a continuous spectrum of grey shades. Thus the higher the greyscale value the higher the fluorescence signal intensity. To directly compare greyscale values between cells, imaging parameters and microscope setting remained constant. Greyscale values for the first three and last three pixels in the line profile for each cell were taken as the plasma membrane (PM) (***figure3.2 A&B***). Care was taken to only include cells, which had undergone complete transmigration; this was achieved through taking confocal z-slices 1μm above and below the endothelium. Fully transmigrated cells were only in focus below the endothelium.

A total of 80 cells were counted for each condition, TAPI-0 treated cells registered a mean greyscale value at the PM of 115.3 +/- 4.18, while DMSO control cells had a mean grey scale value of 14.22 +/- 0.90 (***figure 3.2 B***). The percentage of cells with a positive L-selectin signal at the PM in fTEM was enumerated: 10.03% +/- 3.303 and 95.31% +/-2.259 for DMSO treated and TAPI-0 treated cells, respectively (***figure 3.2 C***). Given that ~10% of the fTEM DMSO-treated neutrophils remained L-selectin positive suggests that the isolation was not 100% pure; basophil and eosinophil contaminations could explain the remaining DMSO treated L-selectin positive fTEM cell (***figure 3.2 C***).

To elucidate whether L-selectin is shed prior, during, or after TEM, primary neutrophils were continuously perfused over TNF-α activated HUVEC for 15 minutes, to capture a higher percentage of cells in mid-TEM (referred to as mTEM). Perfusion assays were performed as described in, (***section 2.5.1***) and samples were prepared for confocal microscopy as described in (***section 2.8.2***). Again, line profile analysis was conducted to quantify the signal corresponding to L-selectin, as described above. Line profiles were performed on non-transmigrated and transmigrated parts of the same DMSO treated cell caught in mTEM, these cells were compared against TAPI-0 treated fTEM cells (***figure 3.3***).

Deleted: in ,

Again, to allow direct comparisons of greyscale values microscope parameters and setting were kept constant.

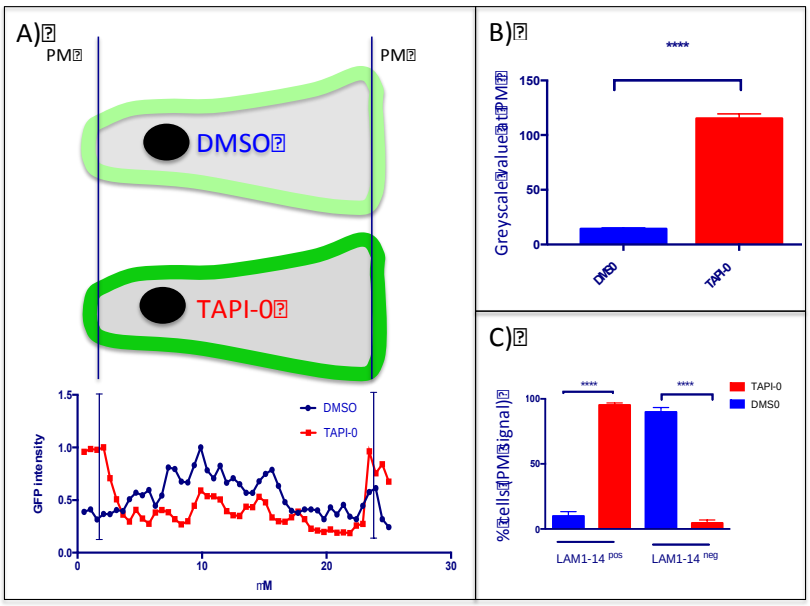

Figure 3.2: Quantifying L-selectin shedding in transmigrated neutrophils
A) A schematic to represent L-selectin signal distribution at the plasma membrane within a DMSO or TAPI-0 treated cell of the same dimensions. Line profiles where the L-selectin signal is internally normalised for each cell. A line profile is taken along the front-rear axis of the cell and the plasma membrane is defined as the intensity values for the first three and last three pixels of the line. B) Averaged greyscale value at the plasma membrane (PM), each value at the plasma membrane represents 3 pixels averaged. A total of 80 cells were analysed per condition. Error bars represent standard error of the mean, TAPI-0; 115 +/- 4.18, DMSO; 14.22 +/- 0.90. The statistical test conducted was a two-tailed unpaired t-test, **** p<0.0001. C) Percentage of transmigrated cell with L-selectin present at the PM. A total of 80 cells were analysed per condition. Error bars represent standard error of the mean. Student t test was conducted, **** p<0.0001. Three separate experiments conducted.

Mean greyscale values for the transmigrated ("Bottom"), 116.7 +/- 4.606, and non-transmigrated ("Top"), 84.31 +/- 4.36, parts of the neutrophil suggests that L-selectin shedding is triggered either: (i) upon neutrophil contact with receptors on the endothelial abluminal plasma membrane or (ii) ECM components (e.g. Biglycan) (***figure 3.3 Bii***). No significant difference in greyscale value was observed between the non-transmigrated parts of DMSO-treated neutrophils and TAPI-0-treated neutrophils that had undergone fTEM. This data strongly suggests

that little to no shedding occurs when neutrophils adhere to the apical aspect of the endothelium (***figure 3.3 C***). In other words, this data strongly supports the notion that L-selectin shedding occurs within the sub-endothelial space of transmigrating neutrophils.

Deleted: *<object>*

Formatted: Font: 10 pt

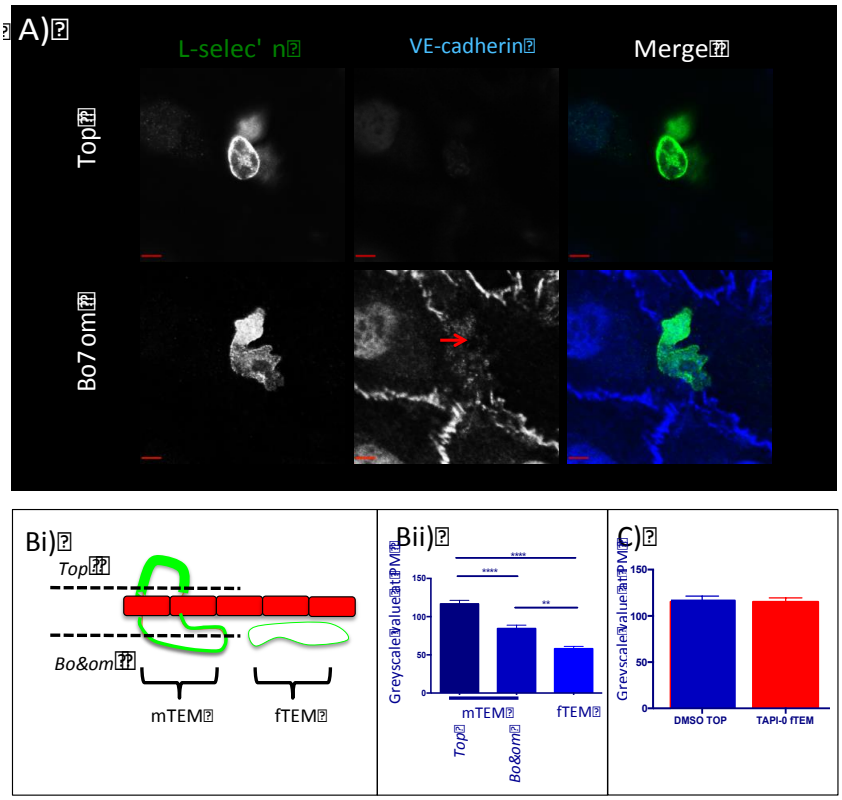

Figure 3.3: L-selectin shedding is initiated in pseudopods entering the sub endothelial space

Neutrophils were perfused over TNF-activated HUVEC for 15 min and subsequently fixed in 4% PFA to capture neutrophils in mTEM. A) Specimens were permeabilised and stained with LAM1-14-488, TRITC-phalloidin and VE-Cadherin-633 to visualise full-length L-selectin, F-actin and endothelial junctions, respectively. Red arrow denotes where the continuity of the VE-cadherin signal has been breached, and represents bonafide TEM. Scale bar is 3µm. Confocal images were acquired with a 63x oil immersion lens. Bi) Schematic represents neutrophils undergoing mTEM or fTEM. Line profiles (represented as black dotted lines) were drawn across the longest axis of the cross-sectional area of the cell. Bii) Quantification of greyscale values at the plasma membrane (PM) that correspond to the LAM1-14 L-selectin signal, where each value at the plasma membrane represents 3 averaged pixels. A total of 132, 112 and 96 cells were analysed for "top", "bottom" and "fTEM" respectively. Error bar represents SEM.Top; 116.7 +/- 4.60, Bottom; 84.31 +/- 4.36 and fTEM; 57.88 +/- 3.06. Statistical test; one-way ANOVA followed by Tukey's multiple comparison test, **** p<0.0001, ** p <0.01. C) Quantification of signals corresponding to L-selectin

were compared between non-transmigrated DMSO-treated neutrophils and TAPI-0-treated neutrophils that had undergone fTEM. Averaged greyscale values corresponding to L-selectin at the plasma membrane (PM). Each value at the plasma membrane represents 3 pixels averaged. A total of 132 and 80 cells were analysed for DMSO (Top) and TAPI-0 (fTEM), respectively. Error bars represent standard error of the mean, TAPI-0; 115 +/- 4.18. Top; 116.7 +/- 4.60. Student t–test was conducted, no statistical significance. Three separate experiments conducted on different days.

3.2.2 Behavioural analysis of primary neutrophils perfused over TNF-α activated HUVEC.

A previous study revealed that blocking L-selectin shedding with 30 μM of the sheddase inhibitor, Ro 31-9790 had no effect on neutrophil adhesion and TEM (310). To interrogate the dynamic behaviour of primary human neutrophils perfused over TNF-activated HUVEC, and to determine if blocking L-selectin shedding influenced changes in cell behaviour, cells were subjected to 30 minutes of flow using the parallel plate flow chamber (see ***section 2.5.1***). In short, a bolus (a single high density wave) of neutrophils was perfused over activated HUVEC for three minutes and perfusion with just media alone continued for a further 27 minutes. In each field of view the percentage of neutrophils bound or fully transmigrated (fTEM) was quantified from the total number of recruited cells (TRC). Assessment of binding, crawling, mTEM and fTEM was monitored over a series of time points: 6 minutes, 10 minutes and 30 minutes. Once captured from flow, neutrophils typically remained bound before embarking TEM. In other words, little "crawling" behaviour was observed. ***Figure 3.4,*** shows an image series of a neutrophil undergoing fTEM from capture. Fully transmigrated cells could be easily identified by their phase-dark appearance in the bright-field channel (***figure 3.4***). Interestingly, once neutrophils had undergone fTEM, they appeared to aggregate into "clusters". This did not appear to be because neutrophils would preferentially transmigrate through "hotspots". In support of this, as mentioned before, neutrophils would engage in very little crawling on top of the endothelial monolayer.

Among all the time points analysed TAPI-0 pre-treatment of neutrophils led to no significant difference in the percentage of TEM at all three time points. At ten and 30 minutes it appears that blocking L-selectin shedding marginally increases the

Deleted: ,

Deleted: a

Deleted: but modest increase

Deleted: TEM rates at the 10 minute time point: 34.04 %+/- 3.27 compared to the DMSO treated cells, 21.94% +/-2.01. Yet, no significance was found at 6 or 30 minutes (***figure 3.5***).

Deleted: This would indicate that

"invasive potential" of neutrophils across activated endothelial cells, perhaps due to inhibition of basal shedding of L-selectin (***figure 3.5***).

Deleted: .

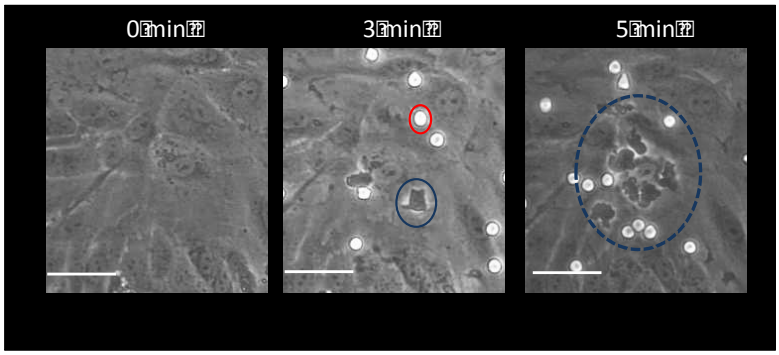

Figure 3.4: Phase contrast image series of neutrophils accumulating into "clusters" within the sub endothelial space.
Primary human neutrophils were perfused across a TNF-α-activated HUVEC. Phase contrast time-lapse microscopy reveals that neutrophils bound to the apical aspect of the endothelium appear "phase-bright" (red circle) and those that have undergone fTEM appear "phase-dark" (blue circle). Over time, it was noticed that fTEM neutrophils would aggregate into "clusters" (broken blue circle). Scale bar is 30μm.

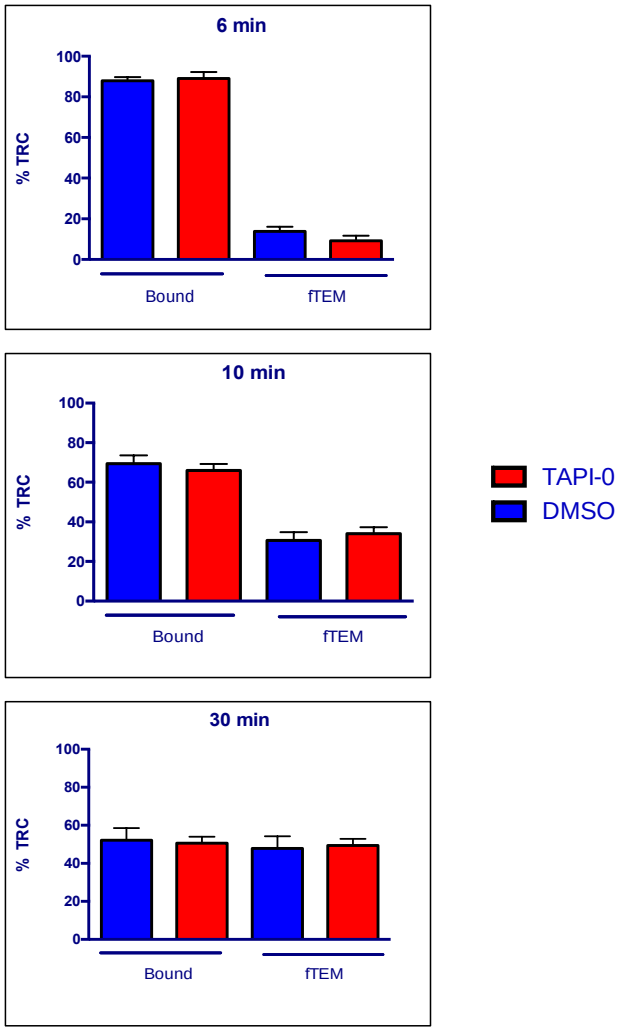

Figure 3.5: Addressing the impact of blocking L-selectin shedding on neutrophil TEM behaviour

Primary neutrophils were perfused over TNF-activated HUVEC as a bolus for 3 minutes, followed by 27 minutes of culture media alone. Neutrophils were pre-treated with 10μM TAPI-0 or DMSO carrier (control). Dynamics were recorded by time-lapse bright-field microscopy (10 x inverted objective lens) over the 30-minute period. Bound or fTEM neutrophils were scored at 6, 10 and 30 minute time points as a percentage of the total cells recruited (TRC) in any given field of view (FOV). Experiments were conducted in triplicate with 3 FOV per repeat. A total of 343 and 321 cells were scored for the TAPI-0 and DMSO condition, respectively. Error bars represent SEM and statistical significance was assessed through unpaired Student t-test, comparing different cell treatments with respect to the bound or fTEM. Three separate experiments conducted on different days.

Formatted: Font: 10 pt, Bold

Formatted: Font: 10 pt, Bold

Formatted: Tab stops: Not at 2.54 cm

Deleted: ¶
¶
¶
¶
¶
¶
¶
¶
¶
¶
¶
¶
¶
¶
¶
<object>¶
¶
¶
¶

Deleted: . **p<0.01

3.2.3 Speed of neutrophil transmigration across TNF-activated HUVEC and within the sub endothelial space

To address this aspect more closely, primary human neutrophils were monitored from the moment of capture up until fTEM. The average rate (in minutes) of TEM was astonishingly fast: 2.21 +/- 0.11 and 2.11+/- 0.10 in DMSO and TAPI-0 treated cells respectively, indicating that preventing L-selectin shedding does not regulate the actual TEM times (***figure 3.6 A***).

To determine if blocking L-selectin shedding impacts neutrophil locomotion beneath the endothelium, fTEM neutrophils were manually tracked so that their average speeds could be quantified. Directionality and speed was deciphered using a free access excel macro, DIPER (306). To ensure speed did not bias the directionality ratio, cells were all tracked for a fifteen minute time period. Directionality ratio or straightness ratio; is defined as the straight distance between the start and end point of a cell's journey, divided by the length of the actual journey. A cell with a high directional persistence of migration will have a directionality ratio close to 1, while an undirected cell will have a directionality ratio close to 0.

As mentioned before, fTEM neutrophils migrating within the sub endothelial space aggregated to form large clusters of cells, between 5-30 cells large, (***figure 3.4***). Within these clusters, TAPI-0 treated cells appeared disoriented, switching front–back polarity rapidly, which is reflected in the directionality scores. Although clusters of neutrophils have been observed *in vivo* (termed "neutrophil swarming") it is not clear what is driving the phenomenon in these flow chamber assays (311). TAPI-0 treatment affected cell speed; averaged cell speed was 1.57 µm/min +/- 0.02, compared to DMSO treated cell, 1.92µm/min +/- 0.03 (***figure 3.6 B***). Directionality was significantly impaired in TAPI-0 treated cells; with average directionality ratio for DMSO and TAPI-0 treated cells was 0.197 +/- 0.01 and 0.15+/- 0.01,respectively (***figure 3.6 C***).

Deleted: The data obtained in ***figure 3.5*** suggests that blocking the shedding of L-selectin could increase the speed at which the neutrophils are undergoing TEM.

Deleted: 1

Deleted: 09

Deleted: 109

Deleted: Instead, it is likely that the actual numbers are increased – again favouring the notion that blocking L-selectin shedding may increase the invasive potential of more cells.

Deleted: can

Deleted: with

Deleted: a

Deleted: 49

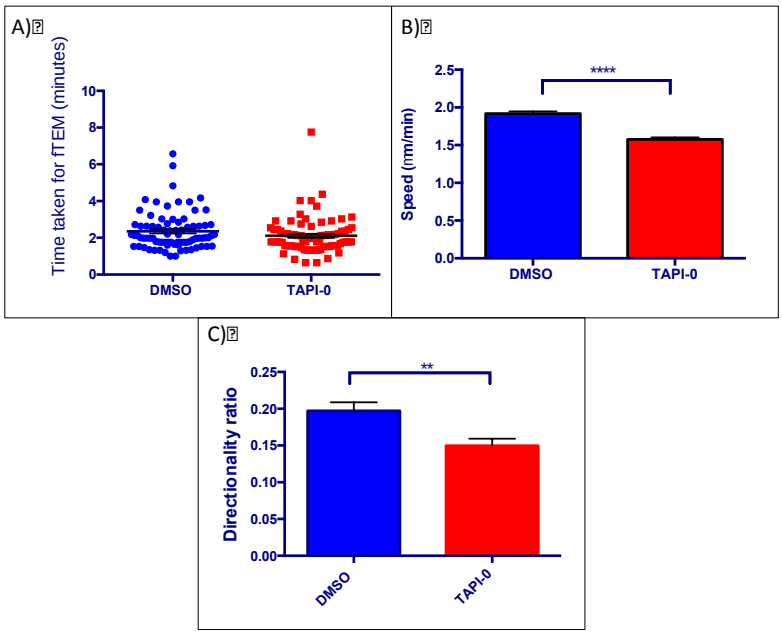

Figure 3.6: Blocking L-selectin shedding negatively impacts cell speed and directionality in fTEM neutrophils

A) Primary human neutrophils were perfused over a TNF-α-activated HUVEC and recorded using a 10x inverted objective lens. To avoid bias, three fields of view were selected before perfusion of neutrophils, which were conducted in triplicate on separate days. The rate of TEM was calculated as the time taken from initial capture to fTEM. At least 80 cells were scored for each condition. Student t-test carried out. B&C) Over 250 fTEM cells were tracked for 15 minutes for each condition over three separate experiments. B) Student t-test, **** p<0.0001 C): Mann- Whitney test, **p<0.01

Deleted: ..

Deleted: .

3.2.4 Monitoring the impact of blocking L-selectin shedding on neutrophil morphology within the sub endothelial space

Cell polarity is an essential prerequisite for neutrophil effector responses. In other words, if neutrophils cannot reach their target sites, they are unlikely to execute their effector functions such as: degranulation, phagocytosis and NETosis. As mentioned previously, directionality was dramatically hindered when cells were exposed to TAPI-0. These results match what is seen in primary human monocytes (212). To determine if blocking L-selectin shedding in neutrophils also impacted cell morphology, primary human neutrophils were perfused over TNF-activated HUVEC and allowed to undergo fTEM before fixing in 4% PFA.

Specimens were stained for phalloidin to stain the actin-based cytoskeleton. Thin (0.75 micron) optical z-sections were acquired by confocal microscopy and the perimeter of neutrophils was traced using a free-hand line tool from Fiji (freeware post-acquisition analysis tool), using the actin cortex as a marker for the cell periphery (***figure 3.7 A***). No differences in cell area were observed in DMSO and TAPI-0 treated cells with respective cell areas of: 198 μm^2 +/- 3.64 and 200 μm^2 +/- 3.77, suggesting blocking L-selectin does not effect cell spreading (***figure 3.7 B***). To compare cell polarisation, the circularity ratio was quantified (see ***section 2.8.5***). Note that the closer to 1 the circularity ratio is, the more circular the object. Typically, TAPI-0-treated neutrophils possessed "rougher" undulating cell edges, and were elongated in shape with no obvious "front" or "back" (see upper panel in (***figure 3.7 A***). Quantification of the circulatory ratio was significantly different between groups: 0.66 +/- 0.01 for TAPI-0-treated cells and 0.72 +/- 0.01 for DMSO-treated cells (***figure 3.7 C***). This data further confirms that blocking L-selectin shedding in neutrophils impacts their polarity once within the sub endothelial space.

Deleted: .3

Deleted: 4

Deleted: 67

Deleted: 2

Deleted: 4

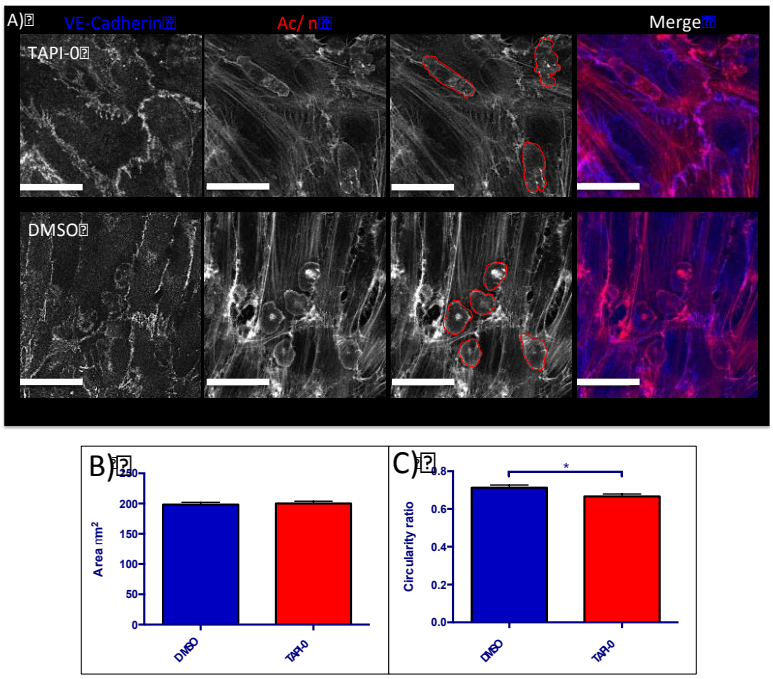

Figure 3.7: Impact of blocking L-selectin shedding on the cross-sectional area and circularity ratio fTEM neutrophils.
Primary neutrophils were perfused over a TNF-α-activated HUVEC for 30 minutes and subsequently fixed in 4% PFA treatment. The specimen was stained with phalloidin to visualise F-actin. Single z-plane images were acquired by confocal microscopy and cell size parameters measured by using the free hand drawing tool, Fiji. A) Cells were individually traced, using the phalloidin signal as a marker of its cellular boundary. B&C) 65 cells were scored for each condition. Error bars represent standard error of the mean. An unpaired Students t-test conducted. * $p < 0.05$. Scale bar is 24μm.

3.2.5 Monitoring the sub-cellular distribution of L-selectin in fTEM primary neutrophils

It is possible that the defects in neutrophil directionality and polarity that are impacted by TAPI-0 treatment could be due to altered sub-cellular distribution of L-selectin. Confocal microscopy was therefore used to monitor the subcellular distribution corresponding to LAM1-14 staining. It should be noted that LAM1-14 detects L-selectin at the EGF-like domain, meaning that only the full-length form is detected in this approach. PFA-fixed samples were processed as described in ***section 2.8.2*** and stained with LAM1-14-488 and TRITC phalloidin. L-selectin

Deleted:

Deleted: a region that is higher than the cleavage site

"spots" were seen in fTEM cells in both TAPI-0 and DMSO treated cells (***figure 3.8 A***). Spots were determined by using a size thresholding tool in Fiji, excluding spots smaller than 0.1µm; below this size differentiation between a spot and background noise could not be obtained. The number of spots per cell and spot area were enumerated. No statistical differences in spot number or size could be detected between the treatment groups (***figure 3.8 B&C***). The function of the spots could not be elucidated through this assay. L-selectin is known to have multiple ligands within the sub-endothelium, binding to which could promote L-selectin clustering and subsequent spot formation. Indeed, the heparan sulphate proteoglycan, biglycan, has been recently shown to be enriched in the basolateral aspect of the endothelium and drive L-selectin clustering in the pseudopods of transmigrating CD14-positive monocytes (212).

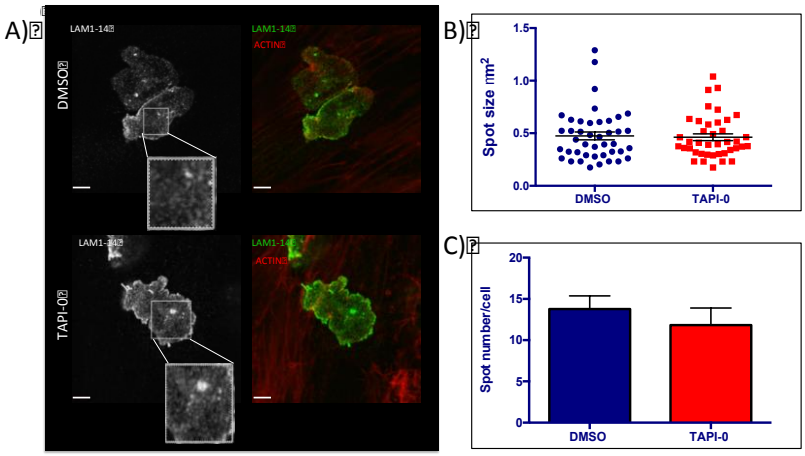

Figure 3.8: Organisation of L-selectin "spots" in fTEM neutrophils is not affected by TAPI-0. A) Primary neutrophils were perfused over a TNF-α activated HUVEC, for 30 minutes, fixed in 4% PFA. F-actin was stained with TRITC-phalloidin and LAM1-14-488. Single z-plane images were acquired by confocal microscopy; spots were isolated using the "find spot" tool in Volocity©. B &C) Between 12-15 cells were scored for each condition, monitored over 3 repeats. Unpaired Student t-test was conducted, but no statistical significance found. Scale bar is 3µm. Error bars represent standard error of the mean.

3.2.6 Generation of an HL-60 cell line to study the contribution of L-selectin shedding in regulating neutrophil migratory behavior

A major aim of this section was to generate a cell line that was genetically tractable, which is impossible to undertake in primary human neutrophils. However, it was important to understand beforehand how primary human neutrophil migratory behaviour is affected in the context of blocking L-selectin shedding. Primary neutrophils, although informative, have limitations in what they can be subjected to. All of the studies above have so far used the sheddase inhibitor, TAPI-0, which does not exclusively block L-selectin shedding. The sheddase that TAPI-0 targets at 10 μM, ADAM17, has many other substrates (e.g. TNF and the β2 subunit of the integrin LFA-1)(312)(313)(314). It is therefore difficult to assign any of the phenotypes that have shown significance between the TAPI-0 and DMSO treatment groups as being exclusively due to the blockade of L-selectin shedding. To ratify the phenotypes observed in primary human neutrophils it was important to generate a human neutrophil cell line, in which molecular mechanisms could be probed at the genetic level. Importantly, L-selectin is not expressed in HL-60 cells unless transiently stimulated with retinoic acid (personal communication: Dr. Alun Brown, KCL). This made investigating the contribution of mutant forms of L-selectin easy to compare with WT. In previous work from the Ivetic group, tagging L-selectin with Green Fluorescent Protein (GFP) did not affect L-selectin-dependent adhesion, shedding and interaction with ERM and calmodulin – two known binding partners of L-selectin(315)(212).To this end HL-60 cells were transduced with lentiviral constructs, containing either GFP alone (as a control), WT L-selectin-GFP, or a non-cleavable form of L-selectin called ΔMN–GFP. ΔMN refers to the 8 amino acids that have been deleted between the cleavage site and the amino acid closest to the extracellular face of the plasma membrane ($_{NH2}$-MIKEGDYN-$_{COOH}$). For a detailed description of generation of lentiviral particles and the MOI used for each cell line, see ***section 2.7***.The newly generated cell lines were FACs sorted to ensure protein levels were matched between cell lines, and to also remove contaminating non-fluorescent cells. After sorting, GFP-positive cells were above 98% for all cell lines, which were confirmed by flow cytometry (see ***section 2.7.4***).

Deleted: can be

Deleted: Based on

Quantification of GFP intensities for WT L-selectin-GFP and ΔMN L-selectin-GFP cell lines were comparable: 19274 (A.U) and 21082(A.U.), with no significant differences (***figure 3.9***). However, HL60 cells expressing GFP alone cells expressed over a 3-fold increase in fluorescence intensity: 72521(A.U) (***figure 3.9***). The HL-60 cell lines WT L-selectin–GFP, ΔMN L-selectin–GFP and GFP alone will from now be termed: **WT**, **ΔMN** and **GFP**, respectively.

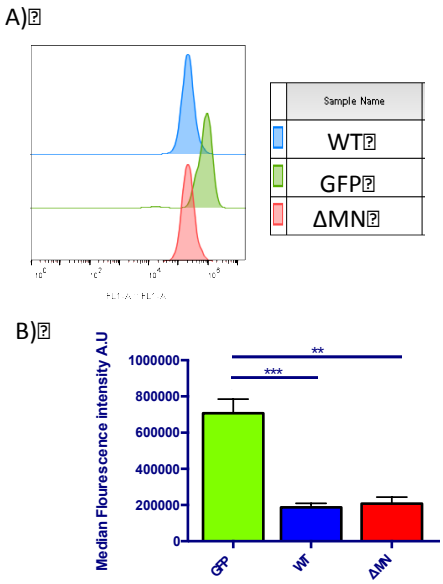

Figure 3.9: Fluorescence intensity measurements of GFP in HL-60 cell lines
Post-sorting, HL-60 cells expressing WT, ΔMN or GFP were subjected to flow cytometry to monitor GFP intensity values. Each cell line was investigated on three separate occasions. A) Representative histogram. B) Quantification, one-way ANOVA, followed by Tukey's multiply comparisons test. *** $p<0.001$, ** $p<0.01$.

3.2.7 Differentiation of HL-60 cells with DMSO

To terminally differentiate HL-60 cells into a neutrophil like phenotype, 1.3% (v/v) DMSO was added to HL-60 media for 4-5 days prior to experimentation. Differentiated cells are phenotypically unique to their undifferentiated counterparts being smaller and less spherical. The scatter plots in ***figure 3.10*** reveals that differentiated cells are much smaller in size, corresponding to a leftward shift in the FCS axis (forward scatter). As mentioned before HL-60 cells

Deleted: .

do not express endogenous L-selectin, this was confirmed in cells prior to lentiviral transduction through flow cytometry (***figure 3.11 A&Ai***). Additionally, DMSO-induced differentiation does not promote endogenous expression of L-selectin (***figure 3.11 A&Ai***).

As experiments were conducted on day 4 and day 5 of differentiation it was important that in this 24-hour window L-selectin surface levels were not significantly different. For this WT (L-selectin GFP) cells were differentiated for either 4 or 5 days with 1.3% (v/v) DMSO. L-selectin levels were confirmed via flow cytometry. Importantly, there was no significant difference between surface levels at days 4 or 5 (***figure 3.11 B&Bi***). Interestingly, when compared to non-differentiated cells, DMSO treatment induced ~35% (an average between day 4 and day5) drop in L-selectin expression levels. It is likely that as cells differentiate, more basal shedding occurs.

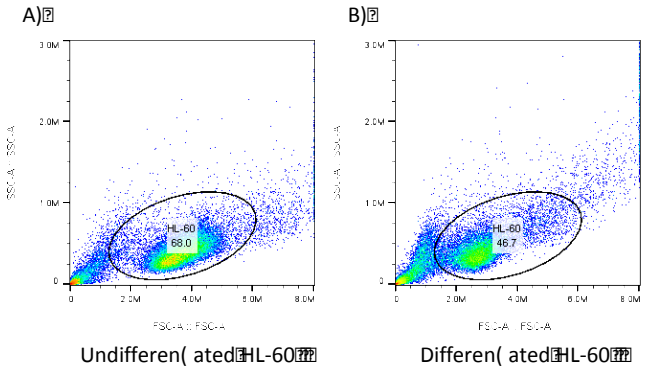

Figure 3.10: GFP levels in the HL-60 cell lines
HL-60 cells either undifferentiated or DMSO differentiated were subjected to flow-cytometry. Forward light scatter (FSC) along the X-axis is proportional to the cell area or cell size, while the side light scatter (SSC) along the Y-axis is proportional to cell granularity. Oval gate represents the HL-60 population.

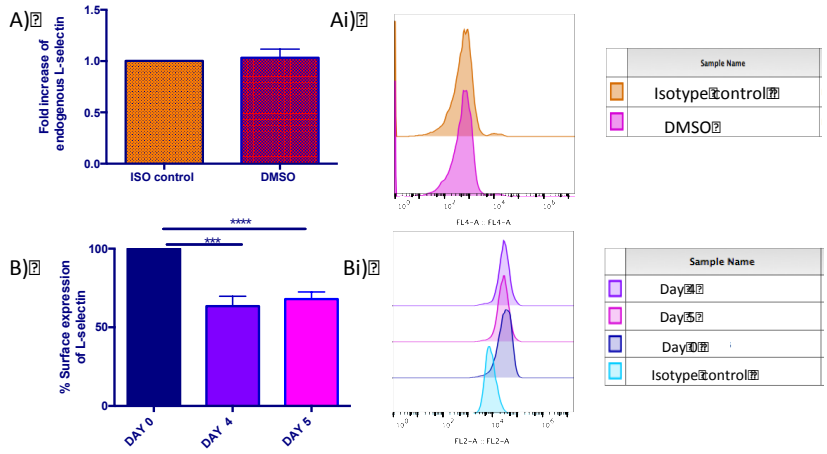

Figure 3.11: The impact of DMSO treatment on L-selectin-GFP expression in HL60 cells
A) Untransduced differentiated HL-60 cells were labelled with either DREG-56 followed by an Alexafluor©633 secondary antibody or appropriate isotype control. Endogenous L-selectin levels were normalised against the isotype control. Data in graph represents three independent experiments, each conducted in triplicate. Student t-test was performed. Ai) Histograms show relative expression levels of endogenous L-selectin. B) WT cells were differentiated for 0, 4 and 5 days in 1.3 %(v/v) DMSO. L-selectin levels were monitored with DREG-56 conjugated with phycoerythrin (PE). Percentage surface expression was quantified through removal of isotype median fluorescent values then normalised against median fluorescent values for day 0. Data in graph represents three independent experiments, each conducted in triplicate. One-way ANOVA, followed by Tukey's multiple comparisons test. **** p<0.0001 ***p<0.001. Bi) Histograms show relative expression levels of L-selectin-GFP.

3.2.8 Blocking L-selectin shedding reduces fMLP chemotaxis

Previous work in THP-1 monocyte cell lines expressing either WT L-selectin-GFP or ΔMN L-selectin-GFP revealed that blocking the shedding of L-selectin dramatically impacted the polarisation towards chemotactic gradient of monocyte chemoattractant protein-1 (MCP-1 or CCL2) (212). Much work has been published in HL-60 cell chemotaxis towards the end-stage chemoattractant, fMLP. As HL-60 cells cannot chemotax effectively towards CCL2, they were challenged with fMLP in micropipette assays (see ***section 2.10***). Fluorescent FITC-dextran (10kDa) supplemented into the chemoattractant media allowed the fMLP gradients to be approximated (***figure 3.12***). Cells were imaged and tracked using the manual tracking software MTrackJ (Fiji) for ten minutes, with an image

being taken every 20 seconds (***figure 3.12***). The micropipette was centred into the FOV, and all adhered cells within the FOV were tracked (***figure 3.13***). For each cell track, directionality was assessed at each time point. At time 0 the straight distance between the micropipette tip and the cell was recorded, ($D0_i$), at each twenty-second interval the new distance (D_i) was divided by $D0_i$. A cell migrating directionally towards the pipette tip will over time display a reduced $D_i/D0_i$ ratio, whereas a cell randomly migrating or undergoing chemorepulsion will display over time a $D_i/D0_i$ ratio close to 1 or a $D_i/D0_i$ ratio higher than one, respectively (***figure 3.14 A***). The individual $D_i/D0_i$ ratios for cells within each cell line were averaged to display the generalised behaviours towards the 200nM fMLP source within the ten-minute period, (***figure 3.14 B***). Quantifying directionality at the final minute (tenth minute) showed that both WT and GFP cells migrated directionally to the micropipette tip, while ΔMN cells showed a significantly reduced ability to migrate to the source of fMLP, (***figure 3.14 Bi***). At this time point the $D_i/D0_i$ ratio for WT, GFP and ΔMN was 0.69 +/- 0.02, 0.57+/- 0.05 and 0.88 +/- 0.03, respectively. Taken together, blocking L-selectin shedding dramatically impacts HL-60 cell chemotaxis towards fMLP.

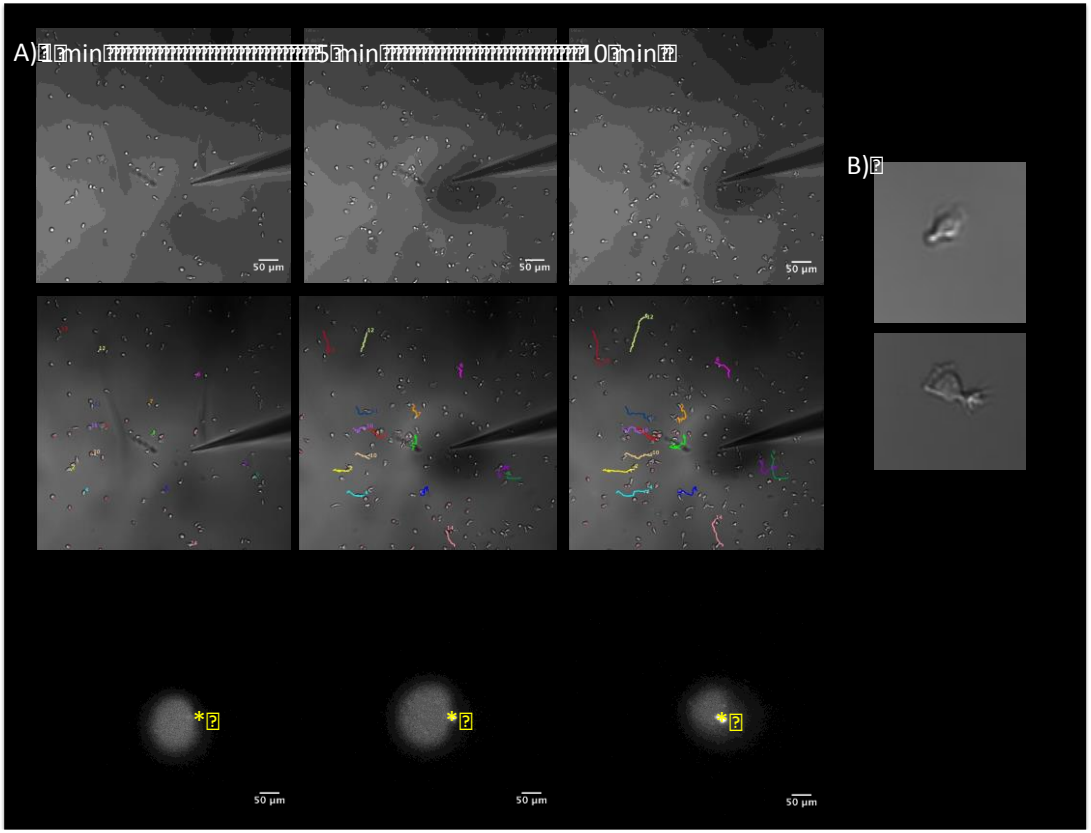

Figure 3.12: Micropipette assay

Assays were conducted using an FV-1000 scanning laser confocal microscope (Olympus), inverted 20x objective, A) Top row image series showing cells chemotaxing over time. Middle row - cells were manually tracked using MTrackJ and traces are shown in different colours to represent unique tracks. Bottom row - fluorescent dextran within the expelled micropipette media models the chemoattractant gradient; yellow asterisk denotes position of micropipette tip. B) Stills showing examples of polarized HL-60 cells chemotaxing towards fMLP. Scale bar is 50 µm.

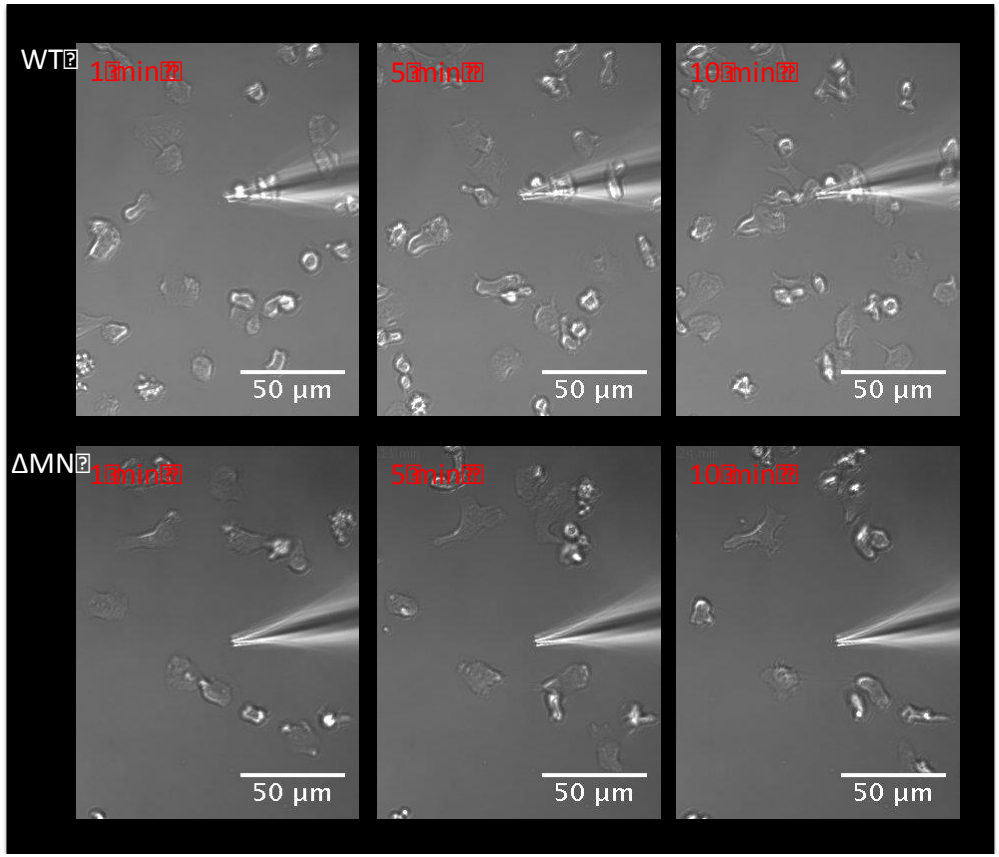

Figure 3.13: Blocking shedding of L-selectin inhibits chemotaxis towards fMLP
HL-60 cells adhered to fibronectin-coated glass bottomed dishes. WT, ΔMN or GFP cells were challenged with 200nM fMLP. Each ten-minute experiment was observed using an FV-1000 scanning laser confocal microscope (Olympus), 20x objective. All cells within the field of view (FOV) were scored.

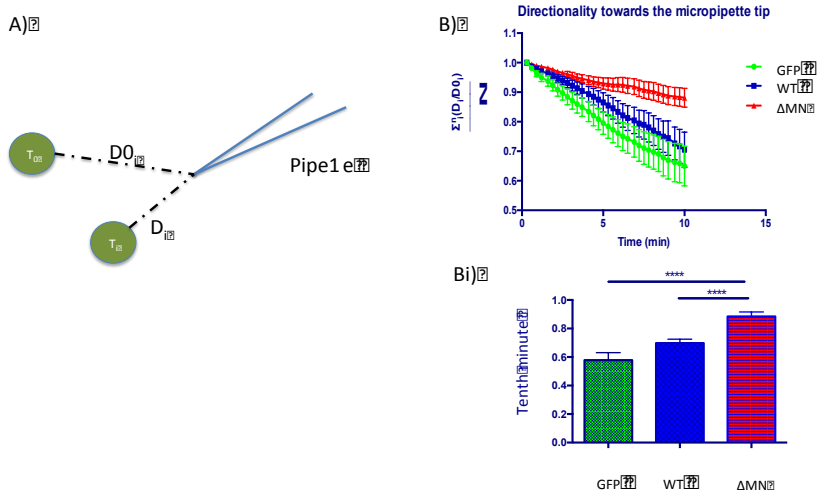

Figure 3.14: Blocking shedding of L-selectin inhibits chemotaxis towards fMLP
WT, GFP and ΔMN cells were allowed to adhere to fibronectin-coated glass-bottomed dishes and were then challenged with 200nM fMLP released from a pressurized micropipette tip. A) Schematic describing the straight distance measured at time 0 ($D0_i$) and the new distance measured at a time ($_i$) time point (D_i). B) Averaged $D_i/D0_i$ ratio for each cell line, a total of 88, 116 and 112 cells were analysed for GFP, WT and ΔMN, respectively. Bi) The $D_i/D0_i$ ratio represented for the final minute of the chemotaxis experiment (10^{th} minute), a total of 88, 116 and 112 cells were analysed for GFP, WT and ΔMN in at least 8 independent experiments. Statistical analysis, one-way ANOVA followed by Tukey's multiple comparisons test. ****p<0.0001.

Deleted: prevents

Upon chemotaxis, L-selectin-GFP underwent a dramatic re-localisation; concentrating at the uropod (***figure 3.15***). A similar phenomenon was reported, but in neutrophils rolling on either purified E-selectin or on IL-1β activated HUVEC monolayer. Under these conditions, L-selectin was enriched at the rear of the cell, and this was followed by the relocation of ADAM17 to a similar part of the neutrophil(265). By grouping L-selectin to the rear of the cell, along with ADAM-17 the authors proposed that transmigration would ensue upon shedding of L-selectin(265).

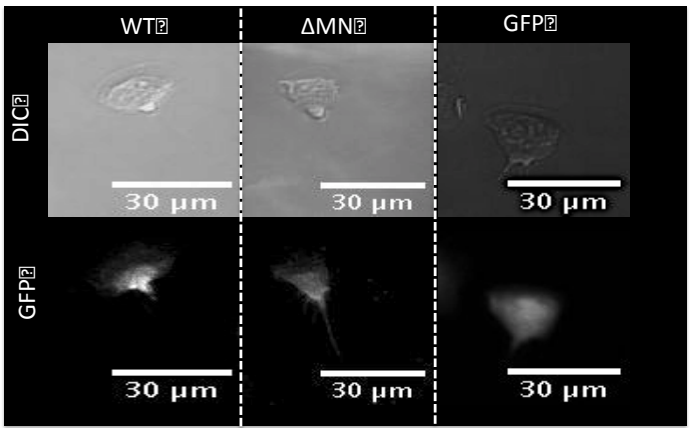

Figure 3.15. L-selectin subcellular localisation during chemotaxis
Cells were observed using an FV-1000 scanning laser confocal microscope (Olympus), 20x objective, using DIC and 488-laser excitation. Representative images for each cell line, WT, ΔMN and GFP depicting GFP signal localization.

In order to assess whether enrichment of L-selectin-GFP at the uropod was similar between WT and ΔMN cells, line profiles, 30 pixels wide, were drawn through the longitudinal axis of polarised cells (***figure 3.16 Ai***). The polarised cells were on a fibronectin substrate. GFP fluorescence intensities were internally normalised in each cell with respect to the pixel with the highest GFP intensity, F1/F0. Prior to this background fluorescence intensities (Fb) were also removed. Line profile intensities were then stretched to conform to a uniform length of 100 pixels (***figure 3.16 A&Ai).*** GFP fluorescent intensities were taken at the mid (40-60 pixel location) and rear (70-90 pixel location) of the longitudinal axis and quantified (***figure 3.16***). Cells transduced with GFP alone were used to control for cell volume changes in the 2D assay, as the GFP signal is cytoplasmic. There was no significant difference between the fluorescent signals corresponding to the mid-body and rear of GFP cells (***figure 3.16 B***). However, both WT and ΔMN cells displayed significantly higher distribution of GFP signal to the rear compared to their respective mid regions, (***figure 3.16 B***). Additionally, both WT and ΔMN had significantly higher levels at the rear to GFP cells (***figure 3.16 C***). Interestingly, the magnitude in the fluorescence intensities between WT and ΔMN was not

Deleted: or squeezed

Deleted: address

Deleted: address

profoundly different, suggesting that blocking L-selectin shedding does not alter the distribution of L-selectin in polarised cells. Indicating that the localisation of L-selectin might not influence the defect in chemotaxis towards fMLP ***figure 3.14***.

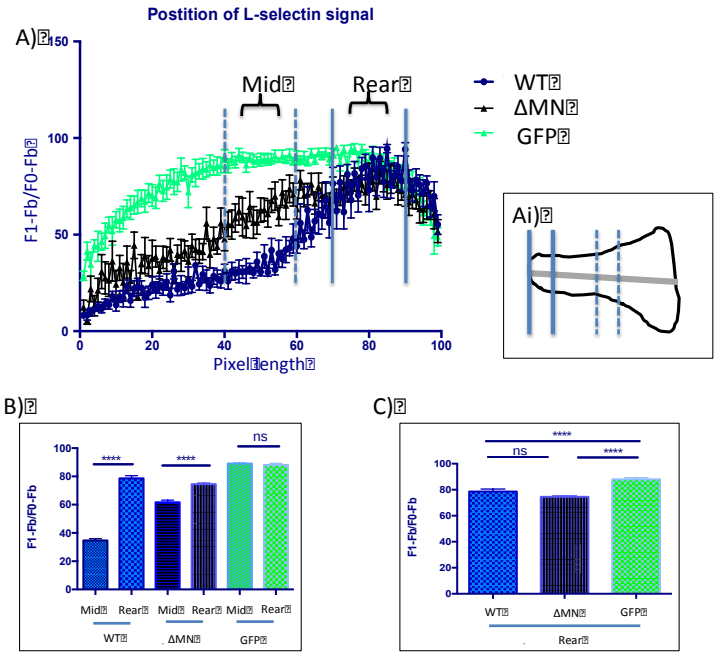

Figure 3.16 L-selectin is localised at the uropod
GFP fluorescence intensities were monitored using the Fiji line profile tool. Ai) Line profiles were taken from 80 polarised cells in the front-back axis, for each cell line A) Data from all GFP fluorescence intensity line profiles were stretched using a bespoke Matlab code, generating a uniform cell length of 100 pixels. Individual line profiles were normalised and background fluorescence removed. B) Direct comparisons of fluorescence intensities of the mid and rear regions within each cell. Unpaired Student t-test, ****p<0.0001 C) Fluorescence intensities at the rear of each cell are compared between cell lines. Statistical analysis, One–way ANOVA, followed by Turkeys post test ****p<0.0001.

3.2.9 CXCR2 is essential for HL-60 TEM

To generate a valid cellular model of neutrophils, it was vital that the HL-60 cells could undergo fTEM. To test this, WT cells were perfused over TNF-α-activated HUVEC monolayers. Over a 30-minute period of perfusion, very few fTEM events were recorded (see ***figure 3.19***). However, of the HL-60 cells that adhered to later

Deleted: sub-cellular

Deleted: either

Deleted: or squeezed

Deleted: m

Deleted:

Formatted: Font: Bold, Italic

Deleted: later

HUVEC under flow, they were observed to actively crawl along the apical aspect of the endothelium. This observation implied that HL-60 cells were lacking a vital component of a "TEM-sensing" cue.

TNF-α activation of endothelial monolayers induces the expression of the cell adhesion molecules E- and P-selectin, alongside expression of the chemokine Interleukin-8 (IL-8 or CXCL8) (316) . IL-8 has been shown to act as an important driver of neutrophil TEM (317)(318)(319), by acting on the receptor CXCR2. As CXCR2 is absolutely required for TEM, HL-60 cells were tested by flow cytometry for the presence of this receptor. Surprisingly, little to no CXCR2 was detected on the surface of HL-60 cells and could explain the inability of these cells to undergo TEM. In order to test this hypothesis, HL-60 cells expressing CXCR2 were obtained from Prof. Anne Richmond's Lab, Vanderbitt University, Tennessee, U.S.A. In addition, HL-60 cells expressing a signalling-defective form of CXCR2 – called CXCR2 ILAA – were also obtained as negative control cells. Briefly, two amino acid substitution mutations, I323A and L324A, which fall within the LLKIL motif of CXCR2, produced a 50% drop in ligand induced receptor internalisation and abolished chemotaxis towards IL-8 gradients (320)(321). For clarity in nomenclature, these new cell lines will be termed hereon as: **CXCR2 WT** and **CXCR2 ILAA**.

To confirm the newly acquired HL-60 cells were expressing CXCR2 at the plasma membrane, median fluorescence intensity values were acquired through flow cytometry. For a detailed description of sample preparation and analysis see ***section 2.4***.Median fluorescence intensity values were normalised with respect to HL-60 cells. Quantification revealed a 33.5 +/- 2.39 fold increase of CXCR2 expression in CXCR2 WT cells, and a 16.8 +/- 1.25 fold increase of CXCR2 in CXCR2 ILAA (***figure 3.17***) compared to HL-60 previously used. CXCR2 expression is therefore two-fold higher than CXCR2 ILAA (***figure 3.17***).

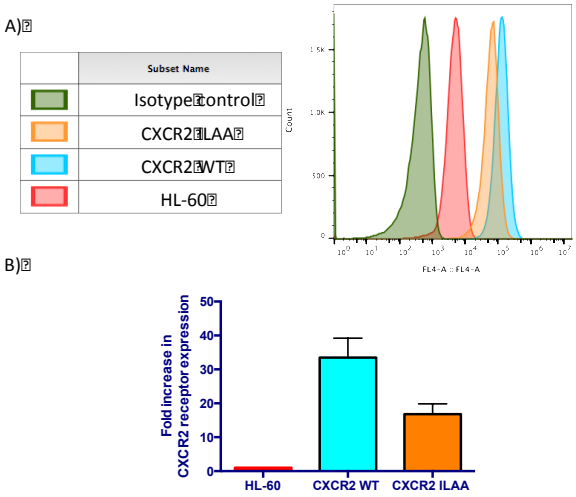

Figure 3.17: Relative expression levels of CXCR2 in the different HL-60 cell lines
The HL-60 cells: CXCR2 WT, CXCR2 ILAA or no overexpression (HL-60) was labelled with anti-CXCR2 or an appropriate isotype-matched control antibody. Secondary antibodies were APC conjugated. Surface expression was measured by flow cytometry. A) Histograms show expression levels of CXCR2. B) Comparison of CXCR2 expression between the cell lines, which is presented as fold increase. Results were obtained from median fluorescence intensities, after subtraction of the IgG isotype control values and then normalised against the endogenous levels of CXCR2 in HL-60. Data in graph represents mean +/- SEM. No statistical tests could be performed as the data represents two independent experiments, each performed in triplicate and three times on separate days.

Deleted: were

Deleted: .

To assess if overexpression of CXCR2 increased the percentage of TEM, perfusion experiments were conducted as described in ***section 2.5.1***. As in ***section 3.2.2***, HL-60-HUVEC interaction was monitored at 6 minutes, 10 minutes and 30 minutes during the course of the perfusion experiments. Cells were scored as being: bound, crawling, mid-transendothelial migration (mTEM) and full transendothelial migration (fTEM) (***figure 3.18***). A striking difference in TEM was detected as early as 6 minutes in HL-60 CXCR2 WT cells: 12.5 % +/- 4.01 compared to 0% of HL-60 cells undergoing fTEM (***figure 3.19 A***). At the final time point, 30 minutes, the majority of the recruited HL-60 cells were crawling, 83.4% +/- 4.41 only 2.67% +/- 0.93 beneath the endothelium (***figure 3.19 C***). In stark

Deleted: 46

Deleted: 36

contrast, only 4.58% +/- 1.23 of CXCR2 WT were crawling and 61.3% +/- 4.88 had undergone fTEM (***figure 3.19 C***). Repeating flow experiments in CXCR2 ILAA cells revealed the importance of expressing functional CXCR2 in HL60-cells. At 30 minutes only 11.2% +/- 3.92 of CXCR2 ILAA cells underwent fTEM (***figure 3.19 D***). It is believed that the dramatic reduction in fTEM of CXCR2 ILAA may be reflective in the 50% drop of surface expression compared to the WT form, but this cannot fully explain the 5-fold increase in fTEM in HL-60 cells expressing CXCR2 WT.

Deleted: 2

Deleted: 4

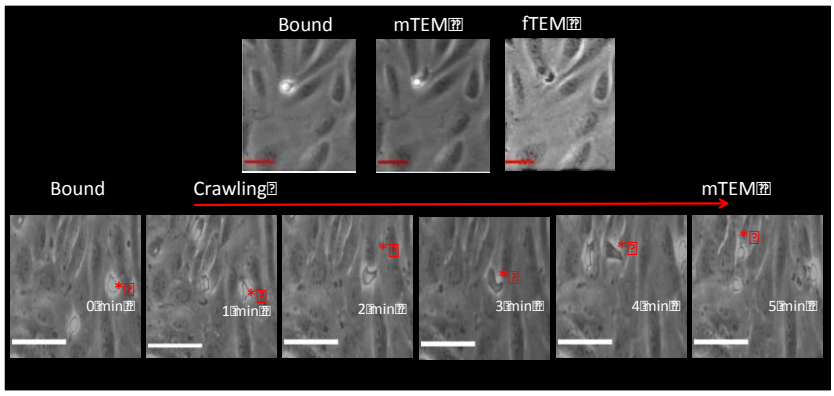

Figure 3.18: Stills from a time-lapse movie showing HL-60 cells crawling along the apical aspect of TNF-activated HUVEC.
HL-60 cells underwent transendothelial migration in stages; bound, mid-transendothelial migration (mTEM), luminal crawling, and full transendothelial migration (fTEM). Red scale bar is 50 μm. White scale bar is 30μm. Red asterisk denotes cells crawling for approximately 5 minutes prior to initiating TEM.

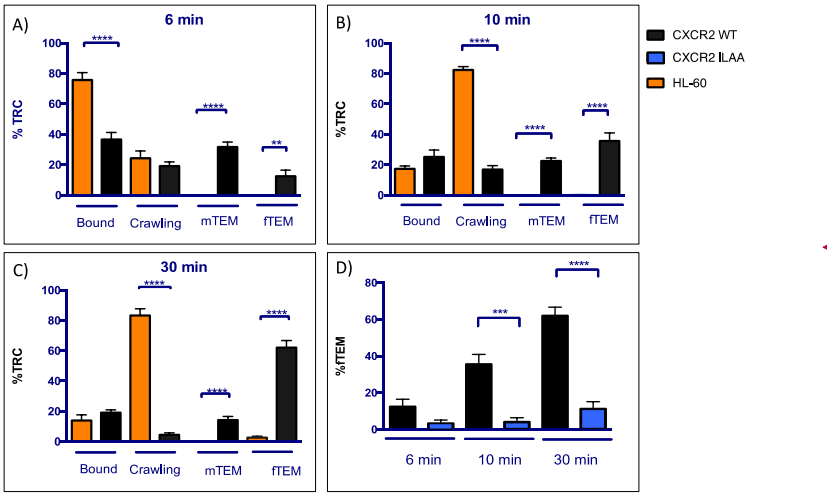

Figure 3.19: The importance of CXCR2 expression on HL-60 TEM behaviour.
HL-60, CXCR2 WT and CXCR2 ILAA cells were perfused over TNF-α-activated HUVEC monolayers for a total of 30 minutes. Cells were scored as; bound, crawling (along the apical aspect of the endothelium), mTEM or fTEM. Interactions were scored at 6, 10 and 30 minutes and recorded as a percentage of the total recruited cells (TRC) in any given field of view (FOV). Experiments were conducted in triplicate with 3 FOV per repeat. A total of 327, 376, 369 cells were scored for HL-60, CXCR2 WT and CXCR2 ILAA, respectively. Error bars represent standard error of the mean. Statistical significant was assessed through unpaired Student t-test, comparing the different cell lines at each separate stages of the adhesion cascade. **p<0.01, ***p<0.001 and ****p<0.0001.

3.2.10 Expression of CXCR2 does not prevent chemotaxis towards fMLP

Although CXCR2 and FPR1/2 have been shown to signal through PI3K/Akt and p38 MAPK pathways, respectively, for the purposes of this study it was essential to test that the CXCR2 WT cells responded to both end-stage and intermediate-stage chemoattractants (e.g. IL-8 and fMLP). Ultimately, the intention of this thesis is to challenge HL-60 cells and primary human neutrophils with conflicting intermediate-stage and end-stage chemoattractants within 3D collagen scaffolds (see ***chapter 5***).

Each cell line was plated onto a fibronectin coated glass-bottomed dishes, and then challenged with either 200nM fMLP or 100ng/mL IL-8 in micropipette assays, see ***section 2.10*** for a more detailed set up description. First the percentage of migrating and non-migrating cells (also termed bound) was scored to confirm that there was no difference in the populations of cells that had

Formatted: Font: 10 pt
Formatted: Line spacing: Multiple 1.15 li
Deleted: ¶
Deleted:) .
Deleted: or
Deleted: in micropipette

undergone DMSO induced differentiation. For both cell lines (CXCR2 WT and CXCR2 ILAA) there was no significant difference in the percentage of randomly migrating cells in response to either IL-8 or fMLP (***figure 3.20 A & figure 3.21 A***). Additionally, neither cell lines displayed significant differences in cell speeds when migrating cells were scored (irrespective of cell direction) (***figure 3.20 B & figure 3.21 B***). Interestingly, fMLP promoted significantly higher cell speeds than IL-8 in both cell lines (***figure 3.21 D***). Heit et al, demonstrated in neutrophils that fMLP driven chemotaxis was p38 MAPK dependent while IL-8 driven chemotaxis was PI3K dependent, this could be responsible for the different cell speeds observed when subjected to IL-8 and fMLP (111). Alternatively, cell response to chemoattractants could be due to the "steepness" of the gradient produced, which in turn will depend on the diffusion of the chemoattractant. The diffusion of a smaller molecule will be more rapid. IL-8 size is ~11kDa while fMLP is ~437Da, therefore fMLP will produce a swallower gradient. Several groups using the model organism Dictyostelium demonstrated chemotaxis towards a steep gradient of cyclic adenosine monophosphate (cAMP) was PI3K dependent. (322)(323) However, in the same organism Andrew et al., demonstrated in the presence of a shallow cAMP gradient PI3K was not required for migration. Suggesting that chemotaxis occurs via a variety of mechanisms, and a chemoattractant gradient may be an important determinant (324). Importantly, directed migration towards IL-8 was only impaired in CXCR2 ILAA cells, and both lines migrated efficiently towards the micropipette tip dispensing fMLP (***figure 3.20 & figure 3.21***). Directed migration was analysed through the $D_i/D0_i$ ratio, see ***section 3.2.8*** for more details.

Deleted: k

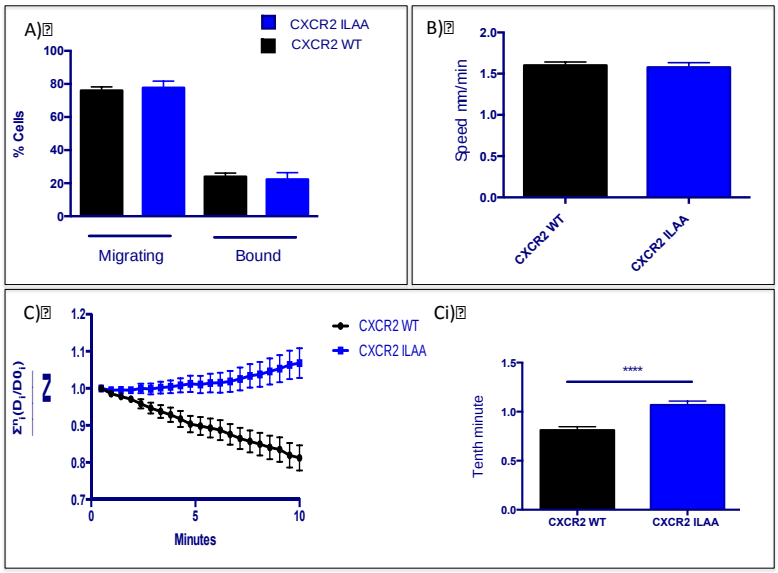

Figure 3.20: Chemotaxis towards IL-8

CXCR2 WT or CXCR2 ILAA cells were left to adhere to a fibronectin coated glass bottom dish and were then challenged with 100ng/mL IL-8. Each ten-minute experiment was observed using an FV-1000 scanning laser confocal microscope (Olympus), 20x objective. All cells within the field of view (FOV) were scored. A) The cells were scored for their ability to migrate, (assessed through uropod contraction and uropod movement of >6µm). Migrating cells within the FOV were manually tracked and speed, (B) and directional information obtained, (C). Directionality was defined by the $D_i/D0_i$ ratio, see ***section 3.2.8***. Ci) Directionality was statistically assessed using the final minute, (10^{th}). In total 89 and 101 migrating cells were tracked for CXCR2 WT and CXCR2 ILAA, respectively. Statistical analysis was conducted through unpaired Student t-test, ****p<0.0001. Experiments were conducted three times on three independent occasions.

Deleted: 8

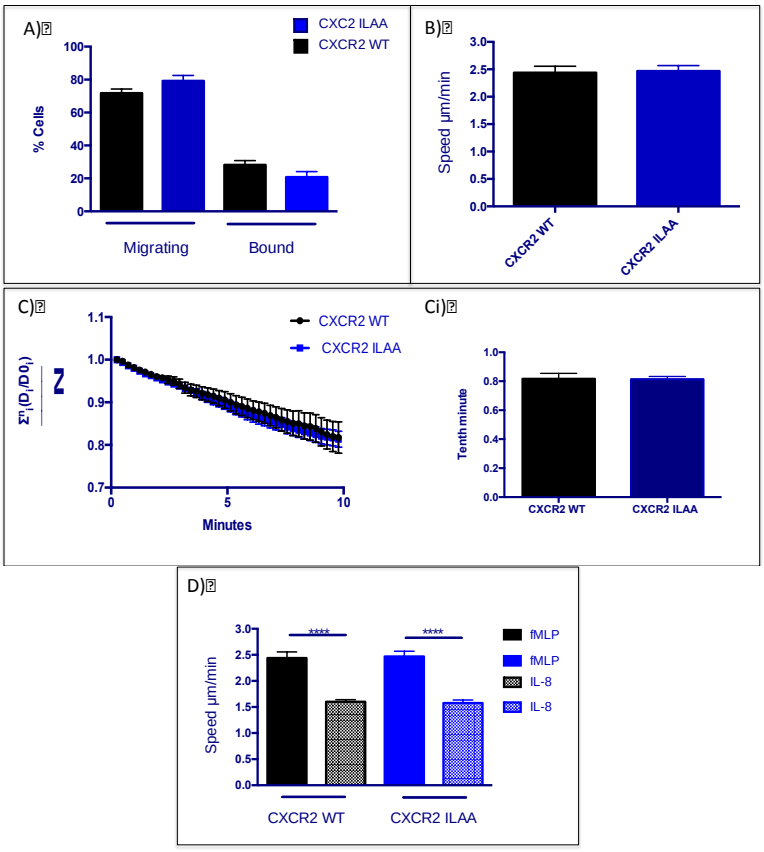

Figure 3.21: Chemotaxis towards fMLP
HL-60 cells were left to adhere to a fibronectin coated glass bottom dish. CXCR2 WT or CXCR2 ILAA cells were challenged with 200nM fMLP. Each ten-minute experimentation was observed using a FV-1000 scanning laser confocal microscope (Olympus), 20x objective. All cells within the field of view (FOV) were scored. A) The cells were scored for their ability to migrate, (assessed through uropod contraction and uropod movement of >6µm). Migrating cells within the FOV were manually tracked and speed, B) and directional information obtained, C). Directionality was defined by the $D_i/D0_i$ ratio, see ***section 3.2.8.***Ci) Directionality was statistically assessed using the final minute, (10^{th}) In total 92 and 98 migrating cells were tracked for CXCR2 WT and CXCR2 ILAA, respectively. Statistical analysis was conducted through unpaired Student t-test. D) Comparison of the cell speeds with respect to the chemoattractant stimuli, unpaired Student t-test used. **** $p<0.0001$. Experiments were conducted three times on three independent occasions.

Deleted: 8

To conclude the increased expression (~33.5 fold increase) of CXCR2 dramatically encourages neutrophil fTEM, which allows chemotaxis towards IL-8, and does not

inhibit chemotaxis towards fMLP. Therefore L-selectin constructs were introduced into the CXCR2 WT cells. From now on all new cell lines, unless stated otherwise will be overexpressing CXCR2 WT. HL-60 cell lines with no overexpression of CXCR2 will no longer be used for experiments in this thesis.

Deleted: will be

Deleted: , it is to be assumed that

Deleted: without a

Deleted:

Deleted: be used in this thesis

3.2.11 Engineering WT L-selectin and mutants into HL-60 cells expressing functional CXCR2.

Based on the high proportion of fTEM events observed in HL-60 cells stably expressing CXCR2, the main objective for this section of the study was to introduce WT and mutant forms of L-selectin-GFP using approaches previously described in ***section 2.7***. To simplify the definition of cell lines from hereon, all the cells used beyond this point will be stably expressing CXCR2. For simplicity the new cell lines all overexpressing CXCR2 WT are renamed: WT L-selectin–GFP cell line will be referred to as **WT**; ΔMN-GFP as **ΔMN**, ΔMN SSAA-GFP as **ΔMN SSAA,** ΔMN SSDD-GFP as **ΔMN SSDD** and **GFP** remains unchanged. The new cell lines ΔMN SSAA-GFP and ΔMN SSDD-GFP will be discussed in more detail later in this chapter. The GFP alone cell line, controls for the action of lentiviral stress on the cell. See ***table 2.4*** for details on MOI. To ensure that their protein expression was similar to prevent bias cells were FACS sorted. L-selectin levels were compared by flow cytometry in all the L-selectin-GFP constructs (***figure 3.22***). All cell lines expressing WT and mutant forms of L-selectin-GFP constructs displayed no significant differences in expression levels between one another. This is important for future experimentation to accurately attribute phenotypes to mutations of L-selectin, rather than variations in protein levels.

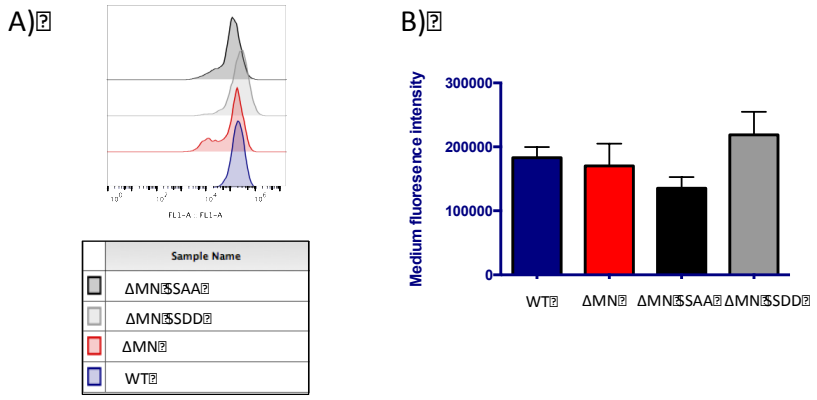

Figure 3.22: Comparison of WT and mutant L-selectin-GFP fluorescence intensity values in HL-60 cells stably over expressing CXCR2
After FACs sorting HL-60 cells stably expressing WT, ΔMN, ΔMN SSAA and ΔMN SSDD were subjected to flow cytometry to monitor their relative GFP fluorescence intensities. Each cell line was investigated on three separate occasions. A) Histogram of superimposed FACS profiles. B) Quantification of fluorescence intensities based on the GFP tag, one-way ANOVA, followed by Tukey's multiple comparisons test. Error bar represents standard error of the mean.

In order to establish if these newly developed HL-60 cell lines reflect primary neutrophil behaviour, the HL-60 cells were subjected to assays that interrogate: TEM behaviour, TEM rates, and the directionality and morphology of fTEM cells.

To first interrogate TEM behaviour; WT, ΔMN and GFP cells were perfused over TNF-activated HUVEC as described before. The most striking observation was at the 30-minute time point; WT and ΔMN had significantly higher percentages of fTEM, compared to GFP alone cells (***figure 3.23***). The percentage of fTEM at 30 minutes was 64.8% +/- 2.78, 63.9% +/- 2.67 and 52.4% +/- 2.81 for WT, ΔMN and GFP respectively (***figure 3.23***). In accordance with this observation, a significantly higher proportion of GFP cells were undergoing mTEM at 10 min and 30 min compared to WT and ΔMN cells. These results suggest that the expression of L-selectin-GFP in HL-60 cells drives the invasive potential in neutrophils, additionally this mimics what has already been described in THP-1 monocytes(212).

Deleted: truly

Deleted: 78

Deleted: 88

Deleted: 36

Deleted: confirmed

Deleted: ,

Deleted: and suggests that the expression of L-selectin-GFP in HL-60 cells also drives the invasive potential in neutrophils.

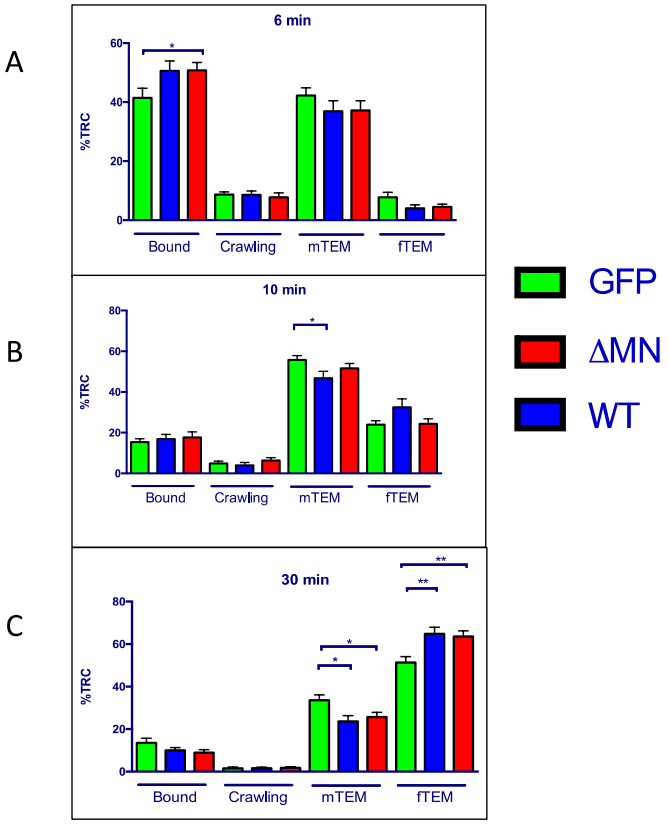

Figure 3.23: Monitoring HL-60 TEM behaviour and the contribution of L-selectin shedding to this mechanism

WT,ΔMN and GFP cells were subjected to 30-minute perfusion over TNF-α-activated HUVEC monolayer. Cells were scored at 6 minute, 10 minute and 30 minutes intervals, interactions between the leukocyte and the endothelium was described as either: bound, crawling, mTEM or fTEM. Total recruited cells were enumerated per each field of view (FOV). Experiments were conducted in triplicate with 3 FOV per repeat. A total of 254, 288,291 cells were scored for WT, ΔMN and GFP, respectively. Error bars represent standard error of the mean. Statistical significant was assessed through one-way ANOVA followed by Tukey's post test, different cells lines were compared with respect to a stage of the adhesion cascade. * $p<0.05$ ** $p<0.01$.

To investigate whether blocking L-selectin shedding altered the rate of TEM, as described before, HL-60 cells were timed from their initial capture from flow up until fTEM. There was no significant difference between the cell lines rate of TEM, with all cell lines taking between 4.6-5.8 minutes (***figure 3.24 A***). HL-60 TEM rate is over 2.19-2.76 times slower than observed for primary neutrophils. This difference is likely due to two reasons; firstly a percentage of HL-60 cells

underwent crawling prior to TEM, and secondly, the average HL-60 diameter is ~11µm while primary neutrophils have a smaller diameter, ~7µm. Additionally, primary neutrophils have a multi-lobed nucleus giving a higher degree of deformability to "squeeze" faster through cell junctions.

Once cells had undergone fTEM, they were manually tracked as previously described in ***section 2.5.2***. WT cells were significantly more directionality than both the GFP and ΔMN cells (***figure 3.24 B***). The directionality ratios were: 0.61+/- 0.02, 0.49+/- 0.03 and 0.43 +/- 0.02, for WT, ΔMN and GFP, respectively. Conversely the speed of the GFP cells was significantly faster compared to the other two cell lines, (***figure 3.24C***). Interestingly, clustering of fTEM HL-60 cells was not observed and may suggest defective mechanisms in swarming.

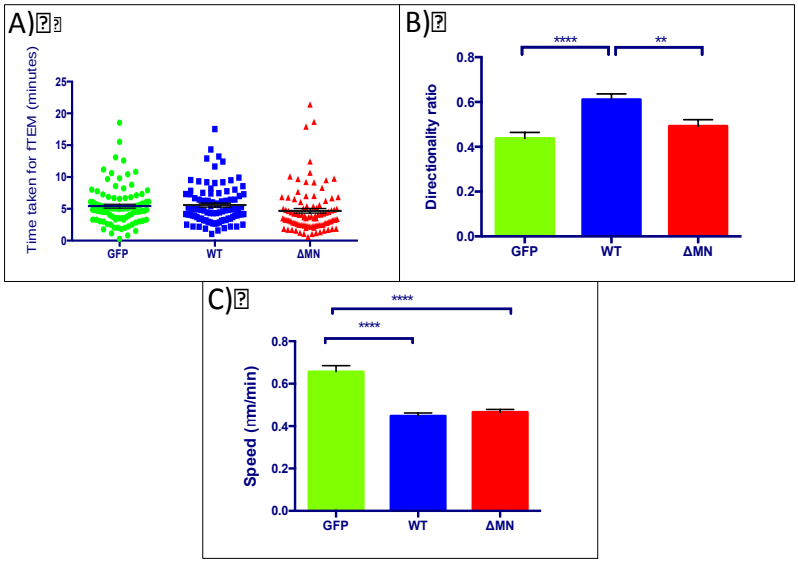

Figure 3.24: HL-60 dynamics beneath the endothelium
WT, ΔMN and GFP were perfused over TNF-α-activated HUVEC and recorded under phase contrast (10x objective lens) with an inverted time-lapse microscope. (A) The rate of TEM was calculated from the time taken from initial capture to complete TEM. 80 cells were scored for each condition. One-way ANOVA carried out. (B&C): Over 250 fTEM cells were tracked for 15 minutes for each condition over three separate experiments. B: Mann-Whitney test, **** p<0.0001, ** p <0.01. C: One-way ANOVA, **** p <0.0001.

Deleted: A
Deleted: increase in
Deleted: was observed only in WT cells, whereas
Deleted: showed no significant changes in directionality from one another
Deleted: y the
Deleted: speed at which fTEM cells migrated were
Deleted: in GFP cells
Deleted: condition. Student t-test carried out
Deleted: .

The fTEM cell morphologies; cell area and circularity (described in ***section 3.2.4***) phenocopied observations seen in primary neutrophils: ΔMN had lower circularity ratio than WT (***figure 3.25 A&B).*** ΔMN cells were elongated with indistinguishable front/back polarity, while WT cells appeared to have a rounded uropod. Interestingly, the cross-sectional cell area was smaller in GFP cells than WT or ΔMN cells (***figure 3.25 C***). The cell area was; 241.3 μm^2 +/- 7.6, 244 μm^2 +/- 8.2 and 194.4 μm^2 +/- 4.3 for WT, ΔMN and GFP, respectively. Change in cell area is a direct consequence of cell spreading; L-selectin has never before been seen to effect cell spreading. However, it is known that many ligands for L-selectin can be found in the ECM, e.g Biglycan (241)(325). High-density ligand binding leads to clustering of L-selectin. Subsequently, L-selectin clustering through GlyCAM-1 ligand binding or enforced monoclonal antibody (mAb) cross-linking has lead to β1 integrin activation (214). β1 integrins are responsible for binding fibronectin, the substrate pre-coated on the glass coverslips(326). Taken together, it is plausible that once the L-selectin positive cells have undergone fTEM, L-selectin binding to available ligands within the ECM, leads to clustering and L-selectin dependent β1 integrin up regulation/activation which successively leads to cell spreading.

Deleted: dramatically

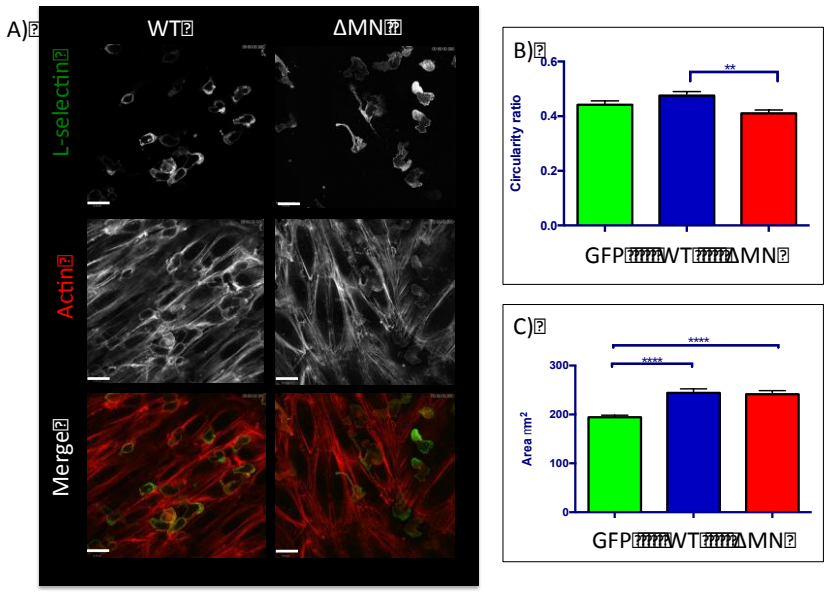

Figure 3.25: Characterisation of HL-60 circularity and cross-sectional area of fTEM HL-60 cells

WT, ΔMN and GFP were perfused for 30 minutes over TNF-α-activated HUVEC and subsequently fixed in 4% PFA treatment. Following permeabilisation, F-actin was stained with TRITC-phalloidin. Thin optical (0.75 micron) z-plane images were acquired by confocal microscopy and cell size parameters measured by using the free hand drawing tool, Fiji. A) Cells were individually traced, using the phalloidin signal as a marker. B&C) 55 cells were scored for each condition. A one-way ANOVA conducted, **** p<0.0001, ** p =0.01. Scale bar is 13μm.

Deleted: n unpaired Students t-test conducted

3.2.12 L-selectin-GFP is deposited from the uropod as HL-60 cells complete TEM

During perfusion assays, it was observed that WT and ΔMN cells undergoing fTEM detached fragments of their uropods. As these "uropod spots" were GFP-positive, it strongly suggested that they were enriched in L-selectin (***figure 3.26***). The frequencies of uropod spots deposited were scored in fTEM HL-60 cells only. Cells did not deposit more than one uropod spot. Frequency is scored between 0-1, with 0 being 0% percentage of the fTEM population depositing uropod spots, while 1 is equivalent to 100% of the fTEM population depositing uropod spots. Enumeration revealed that the frequency of uropod deposition was 0.41 +/- 0.04 in WT, 0.34 +/- 0.03 in ΔMN and 0.01 +/- 0.01 in GFP cells (***figure 3.27***). Therefore, as exogenous expression of WT or ΔMN L-selectin, but not GFP alone, increased the likelihood of the deposition of uropod spots; it strongly suggests the phenomenon is specific to L-selectin expression.

Deleted: Scoring of HL-60 cells undergoing fTEM revealed that these uropod spots occurred with a frequency (scored between 0-1) of

Deleted:

Deleted: in

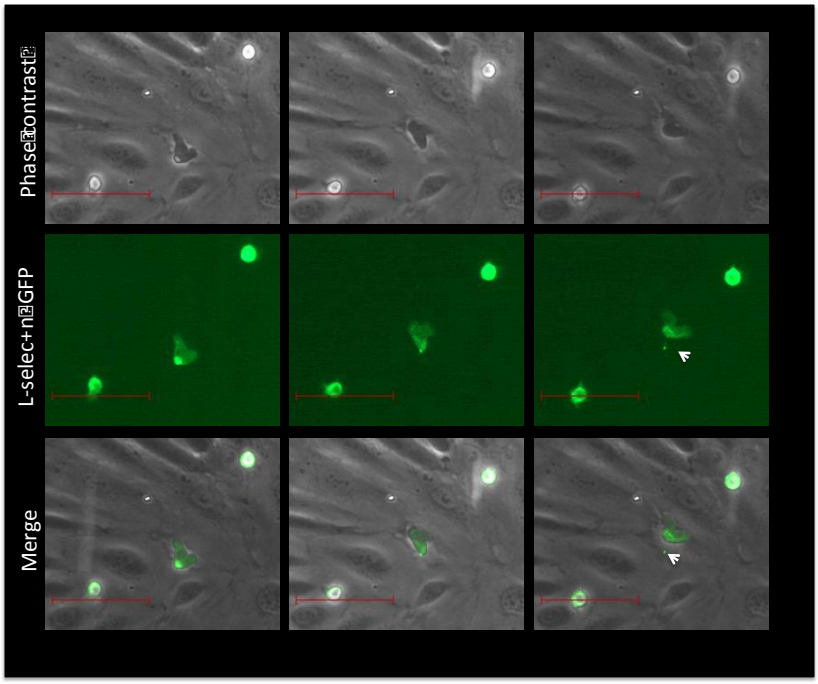

Figure 3.26: Deposition of uropod spots during TEM
Transmigrating HL-60 cells deposited uropod spots only when WT L-selectin-GFP or ΔMN L-selectin-GFP was expressed. WT L-selectin-GFP cells are shown in this figure. Uropod spots were observed by inverted fluorescence time-lapse microscopy, using a 10x dry lens objective. Phase contrast, GFP and merged channels are shown in time series from left to right. Scale bar is 60μm. White arrows indicate the precise moment when uropods are deposited as spots.

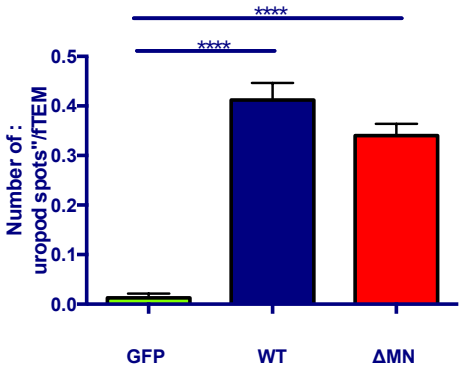

Figure 3.27: Frequency of uropod spots formed in HL-60 cell lines. WT, ΔMN and GFP cells were perfused over TNF-α-activated HUVEC, as described in ***section 2.5.1***. The frequency of uropod spots deposited by fTEM HL-60 cells increased significantly if either WT or ΔMN L-selectin was expressed. At least 3 independent flow assays were conducted per cell line, each with 3 FOV. A total of 190, 213, 183 cells were scored for WT, ΔMN and GFP respectively. A one-way ANOVA followed by Tukey's multiple comparison was conducted. **** P <0.0001. Mean and +/- SEM are shown.

Deleted: between cell lines

3.2.13 Understanding the role of the L-selectin cytoplasmic tail in contributing to the phenotypic changes observed in ΔMN cells

The cytoplasmic tail of L-selectin is composed of a 17 amino acids, two of which are serine residues at positions S364 and S367 (RRLKKGKK**S**KR**S**MNDPY). Phosphorylation of S364 and S367 was shown to be mediated by PKC isozymes alpha, theta and iota(226). Activation of classic PKC isoforms with PMA is known to promote robust shedding of L-selectin, and mutation of S364 to alanine (S364A) significantly reduces the shedding response. This suggests that the serine residues within the L-selectin tail undergo dramatic changes in phosphorylation and dephosphorylation – some of which act to promote the shedding of L-selectin (***section 1.7***). Additionally, phosphorylation of the L-selectin tail also occurs in response to stimulation with the chemoattractants fMLP and IL-8 (327).

Deleted: has been

Calmodulin (CaM) has been shown to negatively regulate L-selectin shedding (328) (329). Recently, phosphorylation of S364 was shown to promote the dissociation of CaM from L-selectin and culminates in L-selectin shedding (212). The serine S364, but not serine S367, is conserved in both mice and humans, suggesting conserved evolutionary mechanisms at this site. Although ΔMN L-selectin cannot be cleaved, it is highly likely that the phenotype presented in HL-

Deleted: s

Deleted: s

60 cells expressing this mutant form of L-selectin is driven by altered phosphorylation of S364 and S367 as previously shown in THP-1 cells. This in turn could impact on downstream signalling events. To address this question in more detail, two cell lines were generated to express ΔMN L-selectin with non-phosphorylatable alanines (A) or phospho-mimicking aspartates (D) at positions S364 and S367. The serine mutant ΔMN cell lines were generated as described in ***section 2.7***, and termed **ΔMN SSAA** and **ΔMN SSDD** for simplicity. Cell sorting, followed by flow cytometry, was used to ensure the cell lines (WT and ΔMN) had similar expression levels of L-selectin-GFP (***figure 3.22***). Quantification revealed no significant differences between in L-selectin surface expression levels in all L-selectin-GFP cell lines.

In order to establish a possible role that phosphorylation of the S364 and S367 serines have in ΔMN, ΔMN SSAA and ΔMN SSDD cells were subjected to the same experiments as previously documented for primary human neutrophils and for the GFP, WT and ΔMN HL-60 cell lines. The frequency of fTEM events, rate of TEM, directionality of fTEM cells, and the morphology of fTEM cells were all elucidated and compared directly to the ΔMN cell line. As described in ***section 2.5.1*** the ΔMN SSAA and ΔMN SSDD were perfused over TNF-α-activated HUVEC monolayers for 30 minutes to firstly quantify the frequency of fTEM events. As before, videos were acquired and analysed at the 6 minute, 10 minute and 30 minutes time points. Statistically significant differences in TEM behaviour were observed between ΔMN, ΔMN SSAA and ΔMN SSDD cells. Firstly, ΔMN SSAA and ΔMN SSDD both displayed significantly more crawling behaviour compared to ΔMN cells at all three time points (***figure 3.28***). The average percentage crawling at 10 minutes was 24.30 %+/- 2.43, 29.4% +/- 4.72, 7.8% +/- 1.66 for ΔMN SSAA, ΔMN SSDD and ΔMN, respectively (***figure 3.28 B***). Cell crawling on the apical aspect of the endothelium was apparent in HL-60 cells lacking CXCR2 expression (see ***figure 3.19***). To determine that crawling observed in ΔMN SSAA and ΔMN SSDD cells was not a hallmark of surface CXCR2 expression loss flow cytometry was used to re-measure surface levels of CXCR2 between cell lines. CXCR2 surface levels remained unchanged (data not shown). At the thirty minute time point

Deleted: .

Deleted:

Deleted: matched

Deleted: WT and ΔMN cell lines

Deleted: all cell lines

Deleted: .

Deleted: ’

ΔMN SSDD cells portrayed a lower percentage of fTEM events, 47.9% +/- 2.75 which was significantly different to both ΔMN 63.7% +/- 2.70, and ΔMN SSAA 66% +/- 2.46 fTEM events (***figure 3.28 C***). Interestingly, the percentage of fTEM at all time points was indistinguishable for ΔMN SSAA and ΔMN (***figure 3.28***).

Deleted: 5

Deleted: 68

Deleted: 5.99

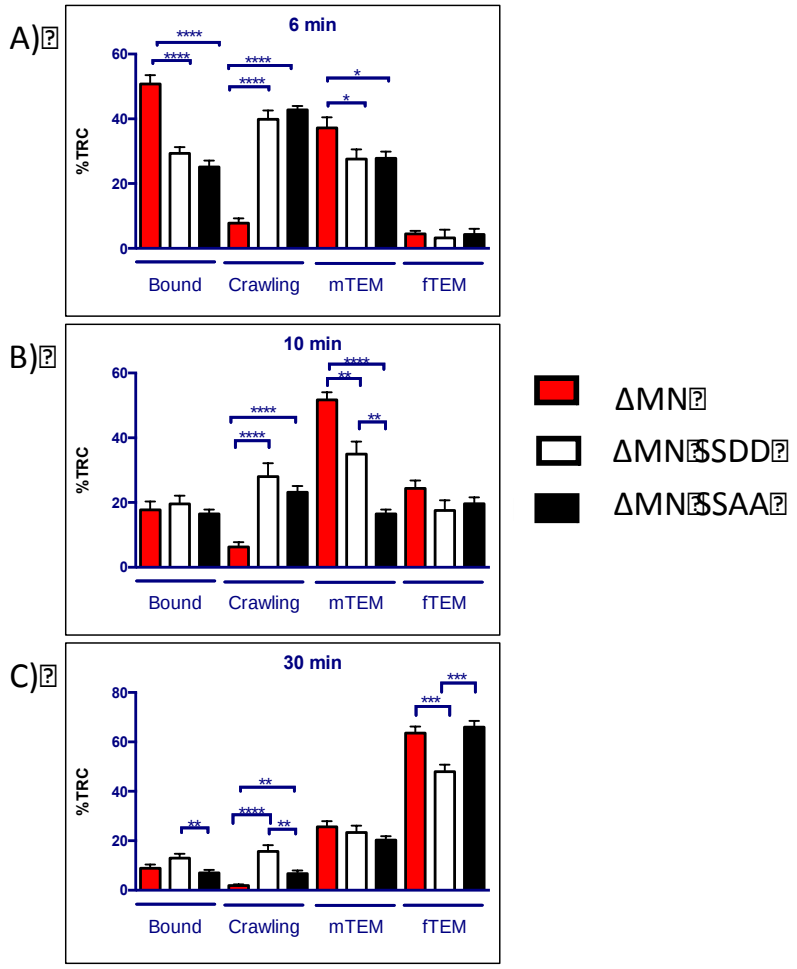

Figure 3.28: Defining the contribution of S364 and S367 in regulating TEM behaviour in HL-60 cells expressing ΔMN L-selectin-GFP

ΔMN SSAA, ΔMN SSDD and ΔMN were subjected to a 30-minute perfusion over TNF-α-activated HUVEC monolayers. Cells were scored at 6 minute, 10 minute and 30 minutes intervals, and TEM behaviour was defined as: bound, crawling mTEM or fTEM. Data expressed as the percentage of

the total number of recruited cells (TRC), which was performed over 3 independent experiments. Experiments were conducted in triplicate with 3 FOV per repeat. A total of 272, 298, 235 cells were scored for ΔMN SSAA, ΔMN SSDD and ΔMN, respectively. Error bars represent SEM. Statistical significant was assessed through one-way ANOVA followed by Tukey's post test, cell lines were compared with respect to the stage of the adhesion cascade. * p<0.05 **p<0.01. ***p<0.001 ****p<0.0001.

Next, the TEM rates were assessed more closely between cell lines, which may help understand some of the phenotypic differences observed in (***figure 3.28***). The increased crawling behaviour of ΔMN SSDD likely reflected the increased time taken for TEM, averaging ~ 8 minutes. In contrast, the time taken for ΔMN SSAA averaged ~6 minutes (***figure 3.29 A***). Both of these TEM rates were significantly higher than ΔMN cells, suggesting that altering the phosphorylation status of the L-selectin tail significantly impacts TEM behaviour. Or, in other words, the cytoplasmic tail of ΔMN L-selectin is under continued dynamic change of serine phosphorylation/dephosphorylation.

Next, the speed and directionality of fTEM HL-60 cells were analysed within the sub endothelial space. Both ΔMN SSDD (0.39μm/min +/- 0.00) and ΔMN SSAA(0.32μm/min +/- 0.00) cell speeds were significantly reduced compared to ΔMN (0.47μm/min +/-0.01)(***figure 3.29 B***). Interestingly, differences in the directionality ratio and circularity ratio of fTEM ΔMN SSAA and ΔMN cells were not significant (***figure 3.29 C*** and ***figure 3.30***). The circularity ratio of ΔMN SSAA and ΔMN cells was 0.39+/- 0.01 and 0.41+/-0.10, respectively. The directionality ratio of ΔMN SSAA and ΔMN cells was 0.52 +/- 0.01 and 0.49+/- 0.02, respectively. Together, this suggests that removal of phosphates at the serines S364 and S367 could contribute to the cell polarity defects and unsuccessful directional migration observed in ΔMN cells. However, in ΔMN SSDD cells, fTEM cellular behaviour was significantly different to ΔMN SSAA and ΔMN cells, with a directionality and circularity ratio of 0.39+/-0.02 and 0.36+/-0.01, respectively. This implies that if the cytoplasmic tail is permanently phosphorylated this negatively alters cell morphology, (more so than ΔMN) producing a more elongated cell underneath the endothelium and a less directed travel (***figure 3.29 C*** & ***figure 3.30***). Cell area remains unchanged between the cell lines (***figure 3. 30 C***). The study implies that blocking dynamic phosphorylation of the serine's does

Deleted: of

Deleted: the

Deleted: ratio and

Deleted: ly

Deleted: different

Deleted: While t

Deleted: .

not alter cell spreading. In summary, blocking dynamic phosphorylation encourages cell crawling. Once beneath the endothelium, ΔMN behaviour is close to ΔMN SSAA, indicating ΔMN within this stage of the adhesion cascade possibly remains largely un-phosphorylated. Interestingly, the amount of "uropod spots" produced decreased in ΔMN SSAA, yet ΔMN SSDD resembled WT and ΔMN cells in the frequency of "uropod spot" deposition, supporting the idea that phosphorylation can change dramatically, perhaps dependent on L-selectin ligand interactions (***figure 3.31***).

Deleted: MN behaviour

Deleted: uropod

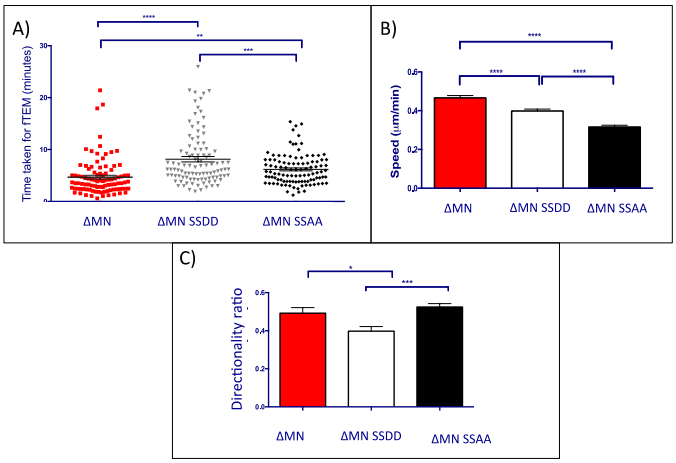

Figure 3.29: Monitoring migratory behaviour of fTEM HL-60 cells within the sub endothelial space

ΔMN SSAA, ΔMN SSDD and ΔMN cells were perfused over TNF-α activated HUVEC and recorded under phase contrast (10x objective lens) using an inverted time-lapse microscope. A) The rate of TEM was calculated from the time taken from initial capture to fTEM. At least 80 cells were scored for each condition. One-way ANOVA conducted for the statistical analysis. B&C: Over 250 fTEM cells were tracked for 15 minutes for each condition over three separate experiments. B: one-way ANOVA, **** p<0.0001 C: Mann-Whitney test, *** p <0.001 * p <0.05. Figures display the mean and SEM for each data set.

Deleted: Student t-test was

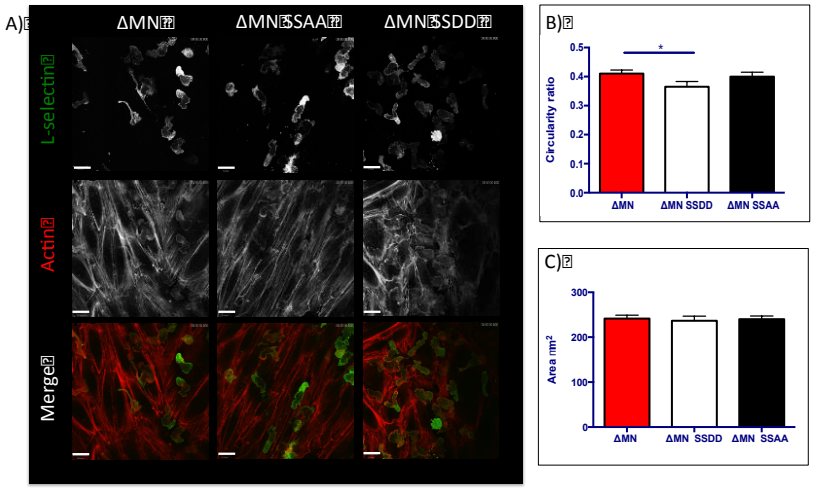

Figure 3.30: Assessment of cell morphology in fTEM HL-60 cells within the sub endothelial space

ΔMN SSAA, ΔMN SSDD and ΔMN cells were perfused for 30 minutes over TNF-α-activated HUVEC monolayers. Specimens were fixed in 4% PFA, and permeabilised so that the F-actin was cytoskeleton could be visualised using TRITC-phalloidin. Single z-plane images were acquired by confocal microscopy and cell size parameters measured by using the free hand drawing tool, Fiji. A) Cells were individually traced, using the phalloidin signal as a marker. B&C) 55 cells were scored for each condition. A one-way ANOVA was conducted, * p ≤0.01. Scale bar is 13μm. Figures display the mean and SEM.

Deleted: =

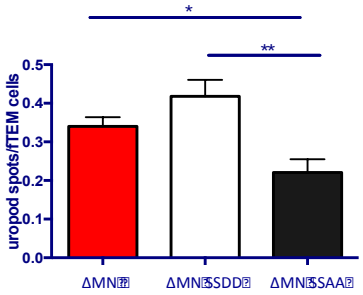

Figure 3.31 Frequency of uropod spots deposited by fTEM HL-60 cells

ΔMN SSAA, ΔMN SSDD and ΔMN were perfused over TNF-α-activated HUVEC monolayers, as described in ***section 2.5.1***. The frequency of uropod spot deposition from all fTEM cells was scored over a 30-minute period. Data are representative of 3 independent experiments, conducted in triplicate per day (each assay contains 3 FOV). A total of 197, 203, 193 cells were scored for ΔMN SSAA, ΔMN SSDD and ΔMN, respectively. One-way ANOVA followed by Tukey's multiple comparison was conducted. ** p<0.01. *p<0.05 .Mean and +/- SEM are shown.

Deleted: P

3.2.14 Chemoattractant stimulated shedding of L-selectin in primary neutrophils

Neutrophils are continually challenged with conflicting chemoattractants derived from intermediary and end-stage sources: e.g. IL-8 and fMLP, respectively. Although L-selectin shedding typically follows cell stimulation, its response to different types of chemoattractants has not been well studied. To better understand the extent of L-selectin shedding in response different types of chemoattractants, primary neutrophils were isolated from healthy volunteers and exposed to a given chemoattractant in suspension for 30 minutes at 37°C, after which cells were prepared for flow cytometry (see ***section 2.4*** for details). Neutrophils were also challenged with DMSO or 100nM PMA for 30 minutes, as respective negative and positive controls for shedding. Quantification revealed significant differences in surface levels of L-selectin in fMLP-stimulated neutrophils compared to the DMSO carrier treatment. However, based on the concentration range of fMLP used, no dose response in respect of L-selectin shedding was observed (***figure 3.32 A&B***). Additionally, IL-8 stimulation promoted L-selectin shedding, which did appear to slightly change across the range of concentrations used in the assay (***figure 3.32 C&D***). Finally, no L-selectin shedding was observed when primary human neutrophils were challenged with 100ng/ml - 1μg/ml of Gro-α (***figure 3.24 E&F***). In fact, the L-selectin surface expression increased slightly in response to Gro-α challenge, perhaps due to prevention of either basal shedding or increased mobilisation of L-selectin to the plasma membrane, or both. In conclusion, L-selectin shedding is remarkable different between different chemoattractants used.

Deleted: this

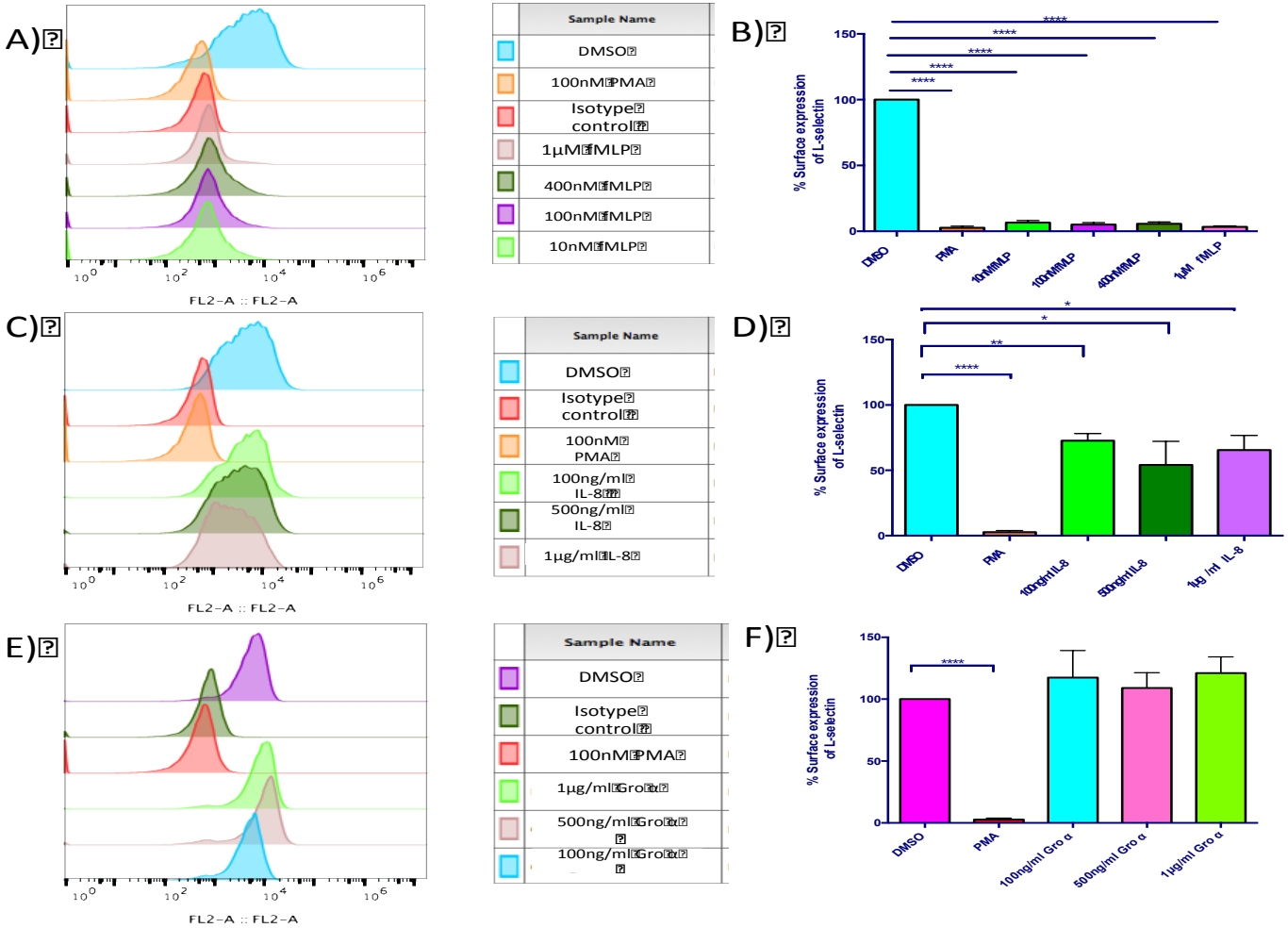
A)
Sample Name
DMSO
100nM PMA
Isotype control
1µM fMLP
400nM fMLP
100nM fMLP
10nM fMLP
FL2-A :: FL2-A
B)
% Surface expression of L-selectin
DMSO
PMA
10nMfMLP
100nMfMLP
400nMfMLP
1uM fMLP
C)
Sample Name
DMSO
Isotype control
100nM PMA
100ng/ml IL-8
500ng/ml IL-8
1µg/ml IL-8
FL2-A :: FL2-A
D)
% Surface expression of L-selectin
DMSO
PMA
100ngml IL-8
500ngml IL-8
1ug /ml IL-8
E)
Sample Name
DMSO
Isotype control
100nM PMA
1µg/ml Gro α
500ng/ml Gro α
100ng/ml Gro α
FL2-A :: FL2-A
F)
% Surface expression of L-selectin
DMSO
PMA
100ng/ml Gro α
500ng/ml Gro α
1ug/ml Gro α

Figure 3.32: fMLP induces L-selectin shedding in primary neutrophils
Primary neutrophils were stimulated for 30 minutes with increasing concentration of either fMLP (A&B), IL-8(C&D), Gro-α(E&F). DMSO treatment defined a non-shed control, while treatment with 100nM PMA defined a positive shed control. L-selectin was labelled using a PE-conjugated DREG-56. B&D&F) Representative histograms: depicting the surface expression of L-selectin after the specific treatments. Percentage surface L-selectin expression was calculated from median fluorescence values, after removal of IgG isotype control value, and normalisation to the DMSO non-shed control. Each data bar represents 3 health volunteer donor samples, the experiment was conducted in triplicate, bar graph represents mean +/- SEM. Statistical analysis; One –way ANOVA with Dunnett's comparative testing. **** p<0.0001, **p<0.01 and *p<0.05.

3.2.15 fMLP induces phosphorylation of p38 MAPK in primary neutrophils

L-selectin shedding can occur via two alternate kinase-dependent pathways; PKC or p38 MAPK, see ***section 1.9.2***. The p38 MAPK-dependent pathway involves activation of TACE by phosphorylation of its cytoplasmic tail, which leads to increased mobilisation of TACE to the plasma membrane (209). As fMLP was previously shown to activate p38 MAPK it was important to determine if this finding could be reproduced in this project (330). Briefly, primary neutrophils were stimulated for 30 minutes in 200nM fMLP (a concentration that is known to robustly promote L-selectin shedding, (***figure 3.32 A&B***). Immediately after stimulation, lysates were generated and resolved on polyacrylamide gels so that changes in phospho-p38 MAPK could be detected in Western blots. Due to the similarity of molecular weights of phospho-p38 MAPK (43kDa) and p38 MAPK (40kDa), cell lysates were resolved on separate polyacrylamide gels and subsequently Western blotted on separate membranes. To normalise any changes in protein levels, p38 MAPK and phospho-p38 MAPK were normalised against β-actin within each Western blot. As shown in ***figure 3.33***, stimulation of neutrophils with fMLP induced a significant increase in phospho-p38 MAPK levels (78.56% +/- 2.55) compared to cells challenged with just DMSO carrier (35.69% +/- 5.49). These data suggest that, following fMLP stimulation, p38 MAPK is activated upstream of L-selectin shedding.

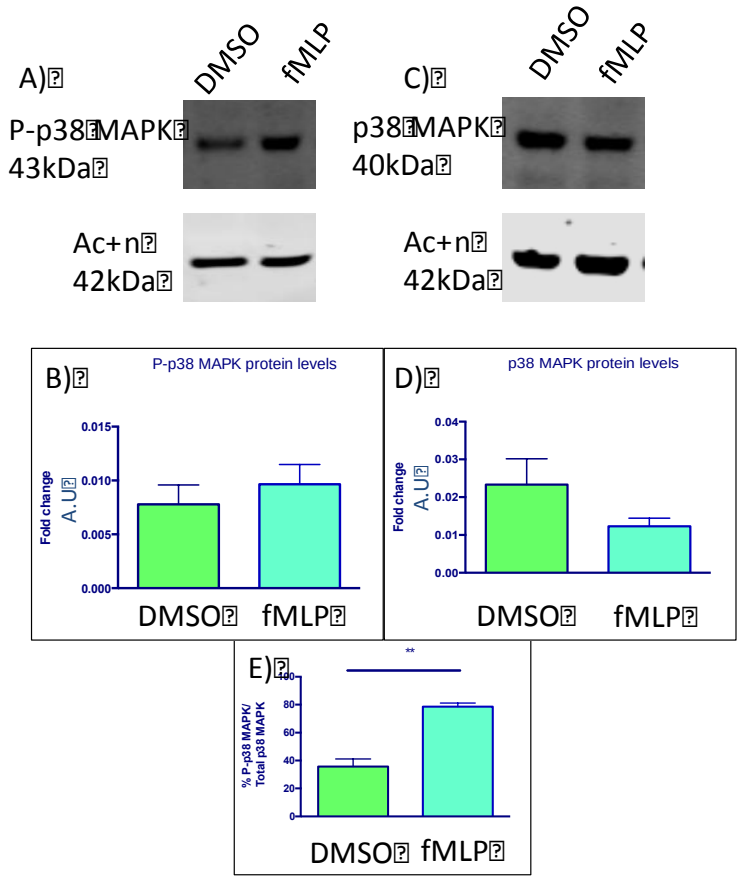

Figure 3.33: Stimulation of primary human neutrophils with fMLP activates p38 MAPK
Primary neutrophils were isolated from healthy donors and stimulated for 30 minutes with 200nM fMLP or a DMSO carrier. After stimulation, cells were lysed and whole cell lysates were resolved on polyacrylamide gels before being transferred to nitrocellulose filters for Western blotting. Phospho-p38MAPK, (A) and p38 MAPK, (C), were probed for on separate membranes. Proteins were identified using LI-COR compatible antibodies. B&D) Fold change was quantified by densitometric changes in protein bands corresponding to p38 MAPK and phospho-p38 MAPK, following normalisation against β-actin levels. E) Relative percentages of p38 MAPK and phospho-p38 MAPK were compared. Statistical analysis, unpaired Student t–test, ** $p<0.01$. A.U=Arbitrary units.

Deleted: <object>¶
¶
¶

Deleted: ¶
¶
¶
¶
¶
¶
¶
¶
¶
¶
¶
¶
¶
¶
¶
¶
¶
¶
¶
¶
¶
¶
¶
¶
¶
¶

3.2.16 PMA stimulates L-selectin shedding in WT but not ΔMN cell lines

To confirm WT cells could undergo *bonafide* L-selectin shedding, and, conversely, that ΔMN cells do not in order to definitively mimic the abilities of the DMSO and TAPI-0 treated primary neutrophils respectively. Each cell line was stimulated with 100 nM PMA as this is a potent PKC activator, PKC has been reported to induce L-selectin shedding in multiple leukocytes subtypes(202). Cell lines were incubated in PMA for 30 minutes and flow cytometry was used to measure the remaining surface L-selectin. In the presence of DMSO, L-selectin surface levels remained at 100% (-PMA), but decreased dramatically to 2.3% +/- 2.3 in the presence of 100 nM PMA (***figure 3.34***). Importantly, surface levels of ΔMN L-selectin remained unchanged irrespective of PMA stimulation (***figure 3.34***).

Deleted: It was important to

Deleted: .

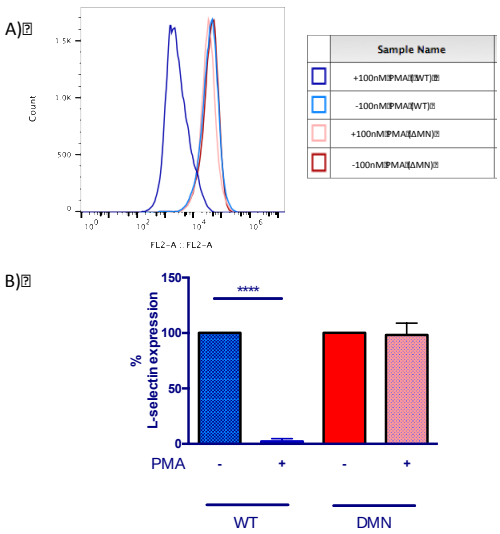

Figure 3.34: PMA stimulation of HL-60 cells expressing WT and ΔMN L-selectin
HL-60 cells stably expressing WT and ΔMN L-selectin cells were incubated with 100nM PMA for 30 minutes at 37°C. Cells were labelled with PE-conjugated DREG-56 antibody and L-selectin expression levels analysed by flow cytometry. A) Representative histograms depicting the surface expression of L-selectin after DMSO (-) or PMA (+) treatment. B) For each cell line, percentage L-selectin expression was calculated from median fluorescence values after subtraction of the IgG isotype-matched control values and normalisation to DMSO control. Experiments were conducted three times, each in triplicate. Statistical analysis performed using unpaired Student t test, ****p<0.0001.

Shedding of L-selectin with 100nM PMA, peaked at 5 minutes, as shown through Western blot analysis (***figure 3.35***). Interestingly, at 15 minutes the intensity of the cleaved/ stump band (35kDa) decreased suggesting the molecule turn over rate (***figure 3.35***). There is also a band at 25kDa MW, which doesn't fluctuate in density over time. The band corresponds to the molecular weight of GFP (27kDa), it is possible that is a product of degradation, or alternatively, the GFP protein may be being translated off an internal ATG start codon (***figure 3.35***).

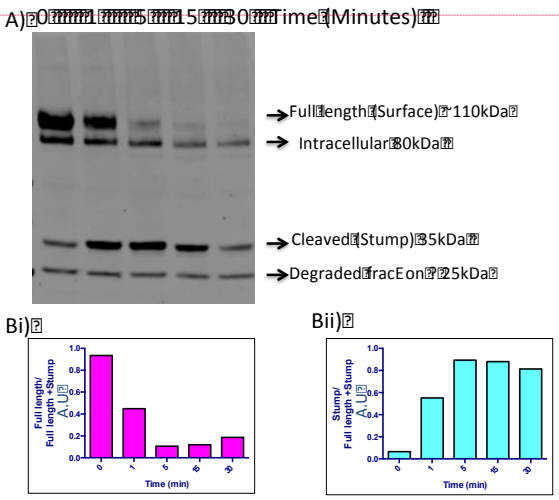

Figure 3.35: Time course of PMA-induced shedding of L-selectin by Western blotting
HL-60 cells stably expressing WT L-selectin-GFP were stimulated with 100nM PMA for time periods of 0, 1, 5, 15 and 30 minutes. After stimulation, cells were lysed and whole cell lysates were resolved on polyacrylamide gels before transfer onto nitrocellulose filters for analysis by Western blot. A) Western blots were probed with anti-GFP antibodies to detect both the full-length and the cleaved forms (stump) of L-selectin. B) Proteins were identified using LI-COR compatible secondary antibodies. Full-length and stump levels were normalised against the total full length and stump fractions at the corresponding time point. No statistical analysis was conducted as this data represents an N = 1. A.U=Arbitrary units.

3.2.17 Activation of the p38 MAPK-dependent pathway in WT cells

A previous study reported by Killock and Ivetic demonstrated that cell stimulation with PMA or the PP1/PP2A inhibitors: cantharidin and calyculin A

respectively promoted L-selectin shedding via PKC or p38 MAPK (209). Therefore to confirm L-selectin-GFP could be cleaved in WT cells via p38 MAPK, cells were treated with either 250 μM of cantharidin or 25nM of calyculin A for 30 minutes. Shedding was assessed through flow cytometry. L-selectin levels were dramatically reduced in response cantharidin and calyculin A, with only 7.2 % +/- 2.6 and 9.5% +/- 4.7 remaining, respectively (***figure 3.36***).

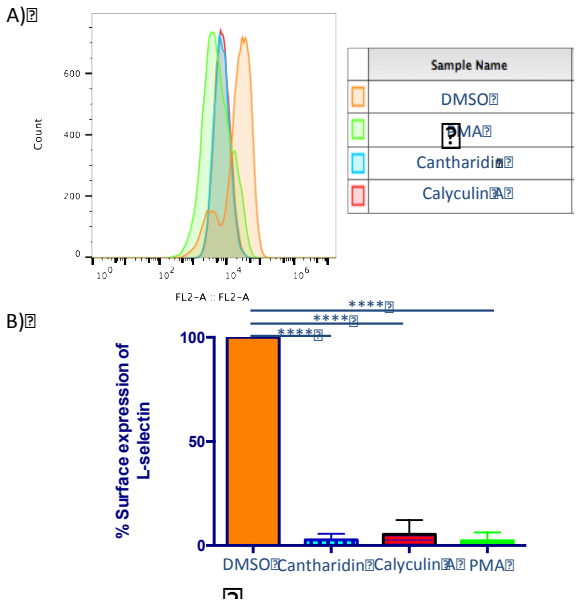

.

Figure 3.36: WT L-selectin-GFP is shed in response to stimulation with cantharidin or calyculin A

WT cells were incubated for 30 minutes with either 250μM cantharidin or 25nM calyculin A. A DMSO carrier treatment was used as control and values normalised to 100% surface expression. Treatment with 100nM PMA was used as a positive control. L-selectin was labelled using a PE-conjugated DREG-56. Surface expression was measured by flow cytometry as described in ***section 2.4.*** A) Overlaid histograms depicting the surface expression of L-selectin after challenging WT cells with various treatments. B) Percentage surface L-selectin expression was calculated from median fluorescence values, after removal of IgG isotype control value, and normalisation to the DMSO carrier control. Experiments were conducted three times each in triplicate, bar graph represents mean +/- SEM. Statistical analysis; one–way ANOVA with Tukey's comparative testing. **** $p<0.0001$.

3.2.18 Monitoring L-selectin shedding in WT HL-60 cells undergoing TEM

Earlier in this results chapter, L-selectin shedding was shown to occur in primary human neutrophils undergoing TEM. Performing similar assays using HL-60 cells is more difficult, as the L-selectin is tagged to the C-terminus with GFP. Additionally, the LAM1-14 monoclonal antibody used in ***figure 3.1*** is not commercially available and is in very limited supply (obtained through a materials transfer agreement with Prof. Thomas. F. Tedder – Duke University, USA). To quantify the extent to which L-selectin-GFP is cleaved during TEM of HL-60 cells, WT cells were subjected to static TEM assays; see ***section 2.9.2*** for more details. In short, WT or ΔMN cells were co-cultured with TNF-α-activated HUVEC monolayers for 45 minutes. After removal of unbound leukocytes, whole cell lysates were made from the remaining leukocytes/HUVEC co-culture, and L-selectin-GFP was detected by Western blot. As GFP is associated with both the full-length and cleaved forms of L-selectin, this approach allowed the extent of L-selectin shedding to be quantified. Quantification through densitometry measurements of anti-GFP bands, corresponding to full-length and cleaved forms of L-selectin, revealed there was a significant difference in shedding WT and ΔMN cells. The percentage of "stump" with respect to total L-selectin level (see below for formula) generated in WT cells was 12.6 % +/-2.10, while ΔMN cells had approximately 6-fold less: 2.11% +/- 0.3 (***figure 3.37 A&B***). To determine if the activated HUVEC monolayer played a significant contribution in the shedding process, WT cells were incubated for 45 minutes in cell culture media and lysed to monitor the extent of L-selectin-GFP shedding by Western blot. Quantification of densitometry revealed there was a significant difference in the % stump /(stump+ full length) WT cells co-cultured with HUVEC and those suspended in cell culture media (***figure 3.37 C&D***). The percentage of stump levels for TEM WT cells was 12.6%+/-2.10, while percentage stump levels for WT cells in suspension was only 4.15%+/- 0.30. The data implies that TEM of HL-60 cells also triggers L-selectin shedding; mimicking the behaviours observed in primary human neutrophils (***figure 3.1***).

Deleted: 56

Deleted: 56

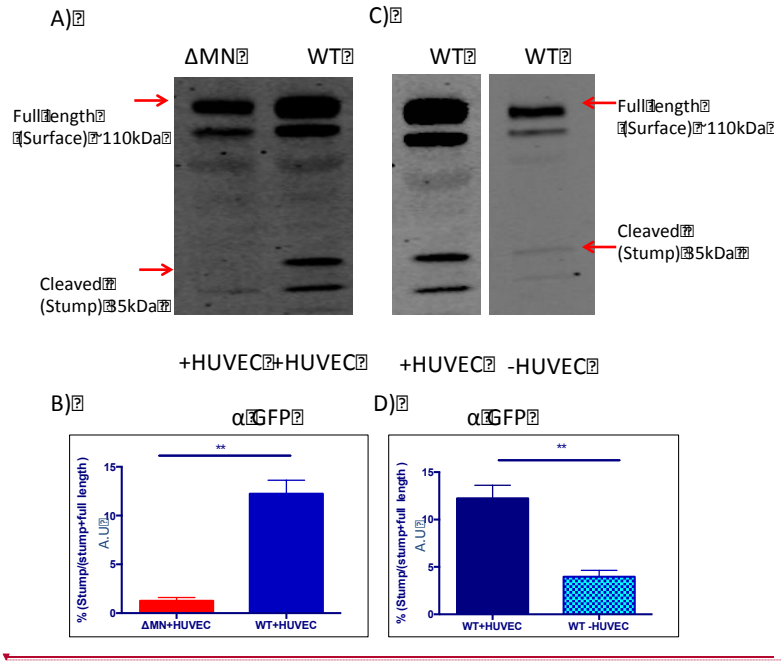

Figure 3.37: Monitoring L-selectin shedding in WT cells subjected to static TEM assays
WT or ΔMN were co-cultured with TNF-α-activated HUVEC monolayers for 45 minutes at 37°C (see ***section 2.9.2*** for details). After removing unbound cells, the remaining monolayer was lysed and the proportion of WT or ΔMN L-selectin-GFP was monitored by Western blotting (A). In a separate assay (C), cells expressing WT cell suspensions were lysed after incubation in media for 45 min. B&D) Densitometric analysis of bands corresponding to full-length and cleaved forms of L-selectin-GFP. The ratios of full length and cleaved/stump levels for each sample assessed the percentage of shedding in each condition/cell line. Three separate cell lysates carried out on three separate occasions complete a data set. Statistical analysis conducted, unpaired Student t –test, ** p<0.01. A.U=Arbitrary units.

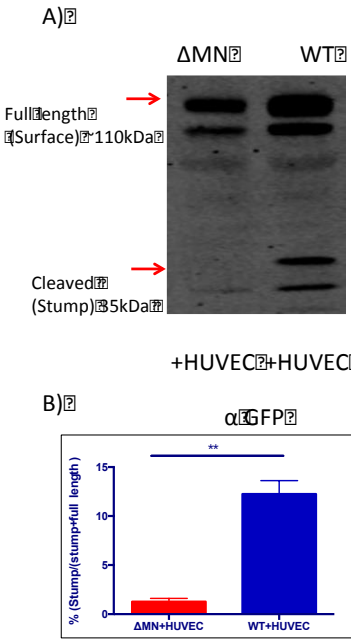

Deleted:

3.2.19 fMLP does not promote L-selectin shedding in HL-60 cells

Although the phosphatase inhibitors Calyculin A and cantharidin can indirectly activate p38 MAPK, this mechanism bypasses any signalling to p38 MAPK that might occur naturally, e.g. downstream signalling of FPR1/2 (fMLP receptors) post fMLP stimulation, To understand whether HL-60 cells responded to fMLP in a similar manner to primary neutrophils (see ***figure 3.32 B***) WT cells were stimulated with a range of fMLP concentrations (10nM- 1μM) for 30 minutes at 37°C. Cells were subsequently monitored for L-selectin surface expression by flow cytometry, using DREG-56 conjugated to PE. Quantification revealed no

Deleted: of fMLP stimulation of the FPR1/2 receptor

Formatted: Font: Bold, Italic

significant difference in surface expression of L-selectin between fMLP and DMSO controls (***figure 3.38***). This was surprising given the dramatic shedding seen when primary neutrophils were subjected to fMLP, and the extent to which both cantharidin and calyculin A could promote shedding in HL-60 cells (***figure 3.36***).

As stimulation of primary neutrophils with fMLP induced robust phosphorylation of p38 MAPK in primary human neutrophils (***figure 3.33***), it was important to understand if fMLP could induce the same response in HL-60 cells. WT cells were stimulated for 30 minutes with either 200nM fMLP or 250 μM cantharidin. As Cantharidin triggers robust p38 MAPK phosphorylation in HL-60 cells (***figure 3.39***), this was used as a positive control. No difference between the DMSO and fMLP groups was detected, yielding values of: 2.43% +/-0.74 and 1.71% +/- 0.68, respectively (***figure 3.39***). In contrast, a significantly higher increase in phospho-p38 MAPK was induced with cantharidin: 38.9% +/-5.52 (***figure 3.39***). Taken together, one can conclude that defective signalling pathway between FPR1/2 and p38 MAPK has been unearthed, which can be bypassed by the use of PP1/PP2A phosphatase inhibitors. It is important to note, DMSO treated primary neutrophil have ~38% of p38 MAPK in a phosphorylated state (***figure 3.33***), while WT HL-60 cells only have ~3% of p38 MAPK in its phosphorylated state (***figure 3.39***). This clearly illustrates differences in behaviour (basal kinase activity) between the cell line and primary cells.

Deleted: 81

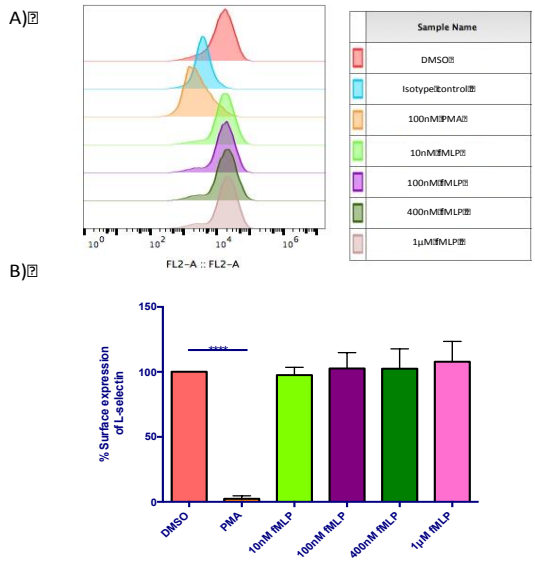

Figure 3.38: L-selectin-GFP is not shed from HL-60 cells stimulated with fMLP
WT cells were stimulated for 30 minutes with a range of fMLP concentrations and flow cytometry was used to monitor the remaining L-selectin at the cell surface. DMSO treatment acted as a negative control, while treatment with 100nM PMA was used as a positive control. L-selectin was detected with PE-conjugated DREG-56. A) Histograms depicting the surface expression of L-selectin after the specific treatments. B) Percentage surface L-selectin expression was calculated from median fluorescence values, after removal of IgG isotype control value, and normalisation to the DMSO non-shed control. Experiments were conducted three times, each in triplicate. Bar indicates statistical significance and represents mean +/- SEM. Statistical analysis; one–way ANOVA with Dunnett's comparative testing. **** $p<0.0001$.

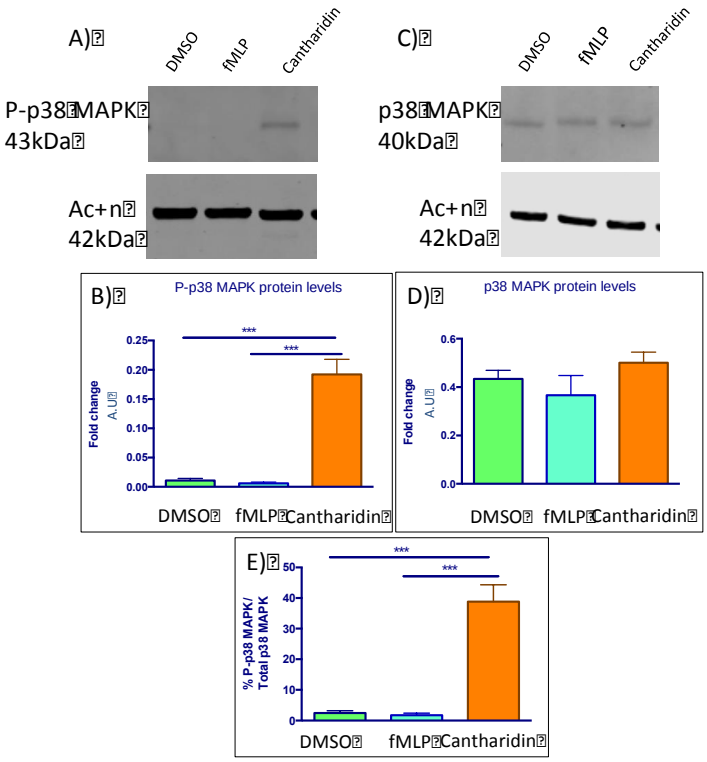

Figure 3.39: Stimulation of HL-60 cells with fMLP induces p38 MAPK phosphorylation
WT cells were stimulated for 30 minutes with DMSO, 200nM fMLP or 250μM Cantharidin. After stimulation, whole cell lysates were generated and phospho-p38 MAPK levels were determined by Western blotting. Phospho-p38MAPK, (A) and p38 MAPK, (C), were probed for on separate membranes. Proteins were identified using LI-COR compatible antibodies. B&D) Fold change was determined by densitometric analysis of protein bands corresponding to p38 MAPK and phospho-p38 MAPK, after normalisation to β-actin. E) Percentage of phospho-p38 MAPK was compared between treatment groups. Statistical analysis, one-way ANOVA followed by Turkeys multiple comparison test, *** p<0.001. A.U=Arbitrary units.

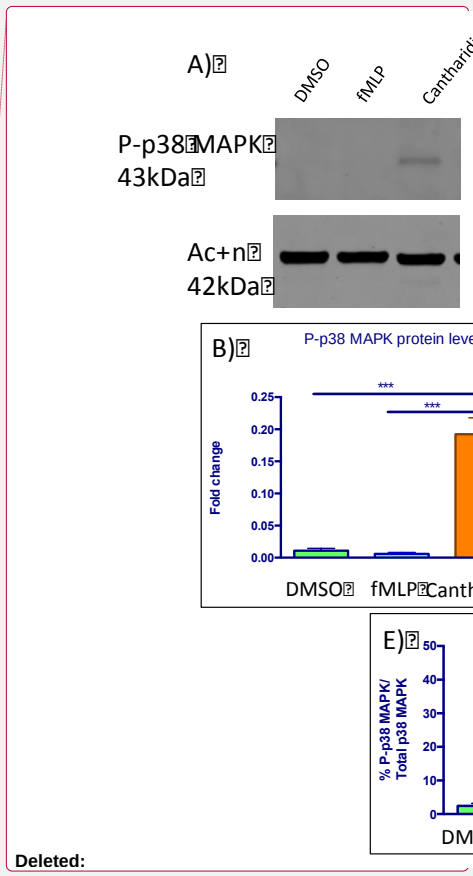

Deleted:

3.2.20 Regulation of FPR1/2 receptor expression in WT and ΔMN HL-60 cells

Earlier in this chapter, chemotaxis of HL-60 cells towards fMLP was shown to be hindered in ΔMN cells, but not WT cells (***section 3.2.8***). This observation suggests defective chemoattractant sensing, only when L-selectin shedding is blocked. This finding corroborates with an earlier report, where rendering L-selectin non-cleavable *in vivo* profoundly impacts chemotaxis towards the intermediary chemoattractant, KC (a mouse CXCR1 agonist, called Gro-α in humans). One possibility in the defective chemotactic ability of ΔMN cells towards fMLP gradients in micropipette assays could be because of defective FPR1/2 expression. Homo sapiens express three paralogues of the formyl peptide receptor; FPR1, FPR2 and FPR3. All three genes are located adjacently on chromsome 19. Neutrophils express only FPR1 and FPR2, which share a 69% sequence homology, FPR1 is the high affinity receptor for fMLP (Kd~10nM), while FPR2 is the low affinity receptor for fMLP (Kd~1μM)(331) (332).

Deleted: 2

To monitor surface levels of FPR1 and FPR2, WT, ΔMN and GFP cells were exposed to 200nM fMLP for 20 minutes, then prepared as described in ***section 2.4*** for flow cytometry. Quantification of median fluorescence intensities (MFI) values revealed that WT cells expressed significantly higher levels of FPR1 and FPR2 (1.26-fold and 1.22-fold increase, respectively) compared to ΔMN cell line (***figure 3.40***).

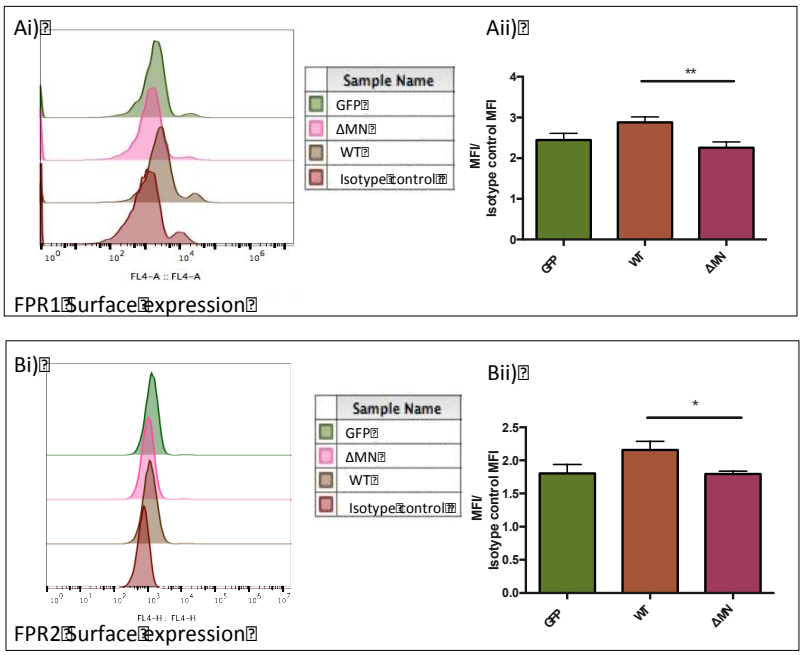

Figure 3.40: Formyl-peptide receptors surface expression is increased in WT HL-60 cells
WT, ΔMN or GFP cells were stimulated for 20 minutes with 200nM fMLP. Cells were prepared for flow cytometry through primary labelling with either anti-FPR1 or anti-FPR2; secondary antibodies were conjugated with AlexaFluor® 633. In parallel isotype controls were conducted. Ai&Bi) Representative histograms depicting the surface expression of FPR1 (Ai) and FPR2 (Bi), after fMLP treatment. Aii&Bii) Percentage surface expression was calculated from median fluorescence intensity (MFI) values, normalised against their respective isotype controls. Experiments were conducted three times each in triplicate, bar graph represents mean +/- SEM. Statistical analysis; one–way ANOVA with Tukey's comparative testing. ** $p<0.01$, *$p<0.05$.

Western blotting was next used to determine if the difference in surface expression was due to: (i) overall decrease in protein expression or (ii) defective receptor trafficking to the plasma membrane. Briefly, each cell lines was stimulated, for twenty minutes at 37°C with 200nM fMLP, and whole cell lysates probed for FPR1/2 expression by Western blotting. Importantly, the normalised levels of FPR1 and FPR2 were not significantly different in either of the three cell lines (***figure 3.41***). This strongly implies that expression of WT, but not ΔMN, L-selectin augments the surface expression of both FPR1 and FPR2.

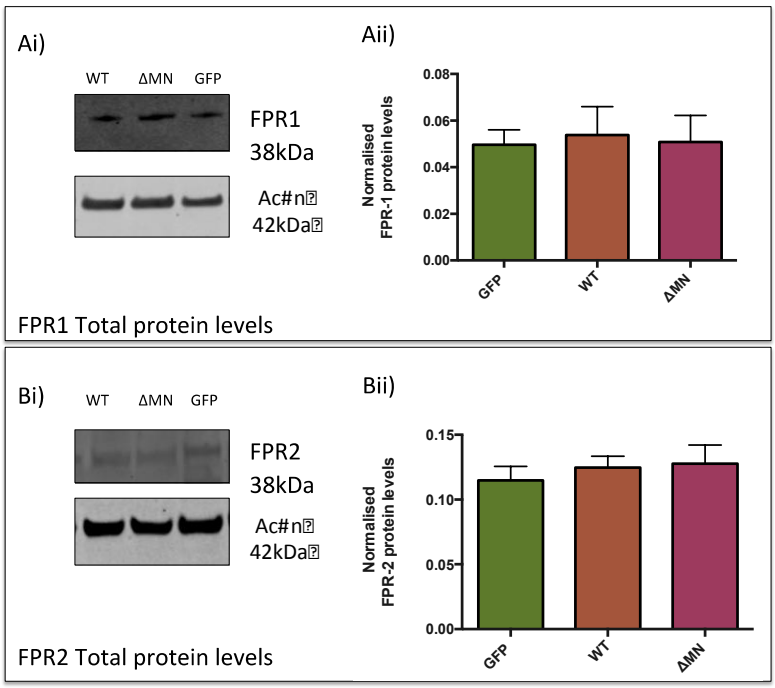

Figure 3.41: Total protein levels of FPR1 and 2 are not altered between WT, ΔMN and GFP cells

WT, ΔMN or GFP cells were stimulated for 20 minutes with 200nM fMLP and whole cell lysates were resolved on polyacrylamide gels, transferred to nitrocellulose filters and probed by Western blotting. A single Western blot of FPR1 is represented in (Ai), and densitometric analysis was performed on at least 3 independent Western blots (A ii). Total protein levels were normalised to β-actin for both receptors. Similar procedures applied for the detection and quantification of FPR2: (Bi) and (Bii). Statistical analysis was one-way ANOVA followed by Tukey's post test.

3.3 Discussion

The main aim of this chapter was to determine if the shedding of L-selectin in neutrophils occurs specifically during TEM, which was recently reported in primary human monocytes(212) .This indeed was the case, which then led to the establishment of a cellular model that could be used to genetically dissect some of the pathways that might be critical in controlling this process. As this project is heavily weighted towards studying L-selectin shedding, the use of sheddase inhibitors (such as TAPI-0) is an extremely useful tool when working with non-genetically tractable cells, such as primary human neutrophils. However, the specificity of such small molecule inhibitors are often limiting as they can have uncharacterised off-target effects. This is why a great effort has been invested in establishing a cellular model.

Generating cell lines to faithfully reproduce neutrophil behaviour is equally fraught with limitations, as cell lines are typically highly proliferative with doubling times reaching 1-2 days. The nature of increased proliferation is likely to impact the type of kinases and phosphatases that are active during cellular processes such as TEM, which may not be equally active in primary human neutrophils. This chapter has therefore generated and characterised HL-60 cell lines that express GFP alone or the non-cleavable ΔMN to act as suitable controls for understanding HL-60 cells that express WT L-selectin-GFP.

Deleted: that

Deleted: s

3.3.1 L-selectin shedding during TEM and beyond: similarities and differences in monocytes and neutrophils

This study has shown that, as in monocytes, L-selectin is cleaved from neutrophils specifically undergoing TEM. There are however a number of fundamental similarities and differences with primary human monocytes, which will be described in smaller sections below:

3.3.1.1 The role of p38 MAPK and L-selectin shedding during TEM

It is clear from the work documented in this chapter that L-selectin shedding is activated specifically in response to TEM, and not before. This observation applies to both primary human neutrophils (***figure 3.1***) and HL-60 cell lines (***figure3.37***). Importantly, these observations corroborate well with what has been reported in

Formatted: Font: Not Italic

Formatted: Font: Bold, Italic

monocytes and suggests a conserved mechanism between different leukocyte subsets. Currently, it is not known which kinase (PKC, p38 MAPK or both) triggers L-selectin shedding during TEM. However, it appears that the extent to which L-selectin is shed during TEM is very different between primary human neutrophils and HL-60 cells. It is likely that the difference in the degree of phosphorylation of p38 MAPK is responsible for the disparity in L-selectin shedding. In support of this, stimulating primary human neutrophil suspensions with fMLP leads to robust L-selectin shedding (***figure 3.32***), which is not detectable when HL-60 cells are challenged in the same way. However, when HL-60 cells are incubated with cantharidin or calyculin A, both activators of p38 MAPK, L-selectin shedding is robust. Further work using inhibitors of p38 MAPK, MEK/ERK and PKC, as shown by Killock and Ivetic (209) should be implemented in this study to better understand the role these kinases play in promoting L-selectin shedding during TEM. As endothelial cells will also come into contact with these inhibitors, one should be aware that this approach might not provide a fully conclusive result.

Deleted: This process is overcome

Deleted: when

Deleted: , suggesting that

Deleted: can be activated and that shedding downstream of this activation event is very robust.

3.3.1.2 Blocking L-selectin shedding and its impact on chemotaxis and cell polarity

Based on the data outlined in ***figure 3.13*** and ***figure 3.14***, it is clear that HL-60 cells expressing ΔMN L-selectin do not polarise or chemotax towards fMLP gradients as effectively. Similar phenotypic observations have been published in monocyte-like THP-1 cells, which fail to polarise efficiently towards micropipettes dispensing MCP-1 when ΔMN, but not when WT L-selectin is expressed (212).As MCP-1 is an intermediary chemoattractant and fMLP is an end-stage chemoattractant, this would suggest that blocking L-selectin shedding could indeed impact chemotaxis irrespective of the chemoattractant. It also suggests that blocking L-selectin shedding impacts chemotaxis in different leukocyte subsets. However, nothing is known about how this happens at a mechanistic level.

Deleted: fail to

Deleted: and

Deleted: .

Blocking L-selectin shedding in primary human monocytes and neutrophils affects cell polarity within the sub endothelial space, but in rather different ways. ***Figure 3.7*** shows that TAPI-0-treated primary human neutrophils present an elongated phenotype, which is similar to primary human monocytes treated with

Deleted: a

Deleted: bipolar

Deleted: very different

TAPI-0 (monocyte treated with TAPI-0 displayed a significantly increased longest axis compared to control cells). Interestingly, HL-60 cells expressing ΔMN L-selectin can phenocopy the bipolar phenotype, suggesting that the effects of TAPI-0 in neutrophils could be specifically targeting L-selectin shedding. In contrast to neutrophils, monocytes have been shown to present a "multi-protrusion" phenotype. Although the molecular mechanism underlying differences in monocyte and neutrophil polarity have not been investigated in any detail, it indicates two possibilities: (i) the cytoskeletal machinery regulating migration is "hard-wired" differently in monocytes and neutrophils, (ii) blocking L-selectin shedding in monocytes and neutrophils impacts different aspect of cytoskeletal regulation, resulting in different polarity phenotypes.

Deleted: .

3.3.1.3 The contribution of S364 and S367 in driving phenotypic differences in WT and ΔMN cells

The serine residues within the tail of L-selectin are known to regulate the binding of calmodulin(212). It is known that mutation of S346 to alanine or aspartate not only decreases CaM binding to L-selectin, but also L-selectin shedding. Therefore it is likely that the ERM proteins, which also interact with the L-selectin tail, are similarly affected by L-selectin serine phosphorylation, but this is currently speculation. Nonetheless, altering the capacity of these serine residues to be phosphorylated by mutating them to non-phosphorylatable alanines or phospho-mimicking aspartates has revealed some interesting phenotypic differences. Single alanine/aspartate mutants of L-selectin at S364 or S367 may pinpoint more accurately which residue is more important. As serine S364 is conserved between mice and humans, it is likely that this residue plays a dominant role in regulating signal transduction events.

Deleted: affects

Deleted: I

Deleted: profound

3.3.2 L-selectin enrichment at the cell rear

L-selectin was found to localise at the uropod of the cell, upon chemotaxis on a fibronectin substrate and immediately prior to TEM. During TEM this uropod enrichment of L-selectin often corresponded with detachment of uropod microparticles. Preventing L-selectin shedding did not alter the frequency of the uropod spot formation. ΔMN SSAA significantly reduced the amount of uropod spots deposited, suggesting that at this stage in the adhesion cascade L-selectin

Deleted: detected

Deleted: organise

Deleted:

Deleted: produced

localised to the uropod is predominantly phosphorylated. The uropod may be a location of serine phosphorylation or have a lower concentration of serine phosphatases. Interesting, no uropod spots were observed in GFP alone-transduced HL-60 cells, indicating that uropod spots could be composed exclusively of cell membrane. To confirm this is not the case, GFP cells could be stained with a membrane dye and re-measured for uropod spots. The function of these uropod spots remains elusive, they could act to temporarily seal the endothelial junctions after a TEM event has occurred, or could act as signalling molecules to indicate sites permissive for transmigration. To investigate these hypothesis', junctional permeability could be monitored using fluorescent dextrans, and multiple waves of leukocyte perfusions could indicate if TEM occurs more frequently at the deposition site of these uropod spots.

Deleted:
Deleted: this scission process
Deleted: exclusive
Deleted: elusive. It has been suggested that they
Deleted: or could
Deleted: s
Deleted: '
Deleted: the
Deleted: address of
Deleted:

3.3.3 L-selectin clustering in fTEM primary neutrophils

Previous observations in the human monocytic cell line THP-1, where WT L-selectin GFP was expressed, demonstrated that L-selectin organised into punctate spots specifically within the transmigrated pseudopods. The spots were hypothesised to form as a consequence of ligand induced L-selectin clustering, likely through the proteoglycans vinculin and biglycan, known ligands of L-selectin, and present beneath the basal surface of the endothelium. L-selectin clustering was severely reduced in THP-1 cells when L-selectin shedding was genetically blocked (212).To this end full-length L-selectin "spot" organisation was observed and quantified in fully transmigrated primary neutrophils. Strikingly, no significant difference in spot size and number of spots per cell were observed between DMSO and TAPI-0 treated cells. The antibody LAM1-14 detected L-selectin, however, this antibody recognises only the extracellular domain, and thus does not highlight the behaviour of the cleaved stump. Additionally, cells were permeabilised prior to immunostaining, therefore it cannot be exclusively ruled out that the spots are intracellular. The cause of these "spots" are currently unknown, however they could occur as a consequence of = i) molecule trafficking, ii) membrane organisation or iii) in response to ligand clustering. Each will be briefly discussed below:

Deleted: s
Deleted: ce
Deleted: as

As a consequence of molecular trafficking

The spots observed could be a result of L-selectin turnover, internalisation for degradation or trafficking to the membrane. Investigating co-localisation of L-selectin with endosomal markers, such as CD63, EEA1 and RAb1, could be conducted in future studies to fully elucidate the exact function of this L-selectin enrichment (333) (334) (335).

As a consequence of membrane organisation

As the spots were only observed in fTEM primary neutrophils the spots could be a result of membrane reorganisation post TEM. In neutrophils L-selectin has a bimodal distribution (~51% +/- 7 found in lipid rafts and ~33% +/- 7 found in none raft fractions) (336). TEM might encourage movement of L-selectin into lipid rafts. Lipid rafts are thought to be regions of L-selectin shedding as these rafts have a 2-3-fold elevation of the negatively charged phosphatidylserine compared to the plasma membrane. Here, the basic rich cytoplasmic tail of L-selectin may strongly interact with the highly anionic rich inner leaflet of the lipid raft plasma membrane, preventing calmodulin interaction and thus encouraging L-selectin shedding (337),(338),(339).Additionally, ADAM-17 is found in lipid rafts, further supporting the notion that L-selectin is shed within these membrane domains. To address this hypothesis, the cell lines WT and ΔMN could be used and stained with LAM1-14. Here, co-localisation between the C-terminally fused GFP and N terminally bound LAM1-14 signal will indicate whether the shed form of L-selectin residues in similar clusters. Investigating co-localisation of L-selectin with known lipid raft associated proteins for example flotillins may also confirm whether the L-selectin clustered signal is within a lipid raft.

As a consequence of ligand clustering

L-selectin clustering could be a prerequisite for shedding. Several studies have shown that mAb cross-linking induced L-selectin clustering has resulted in L-selectin shedding (340)(341)(342). Furthermore, densely arranged sulphated ligands, similar to ECM sulphated proteoglycans have been shown to cluster and ultimately shed L-selectin (343)(344).

3.3.4 Final thoughts

Finally, all cell migratory behaviours post transendothelial migration have been monitored in the sub endothelial space. This two-dimensional space between

endothelial monolayer and glass cover-slip substrate is ~1 micron in height, and constricts the neutrophils in a manner non-reflective of the heterogeneous flexible ECM fibre meshworks. The following results chapters is concerned with generating and optimised a device to monitor the entire leukocyte adhesion cascade, in order to better address how L-selectin regulates migration past the endothelium.

.

4. Generating microfluidic devices to monitor neutrophil migration in complex environments

4.1. Generation of a 2D device to monitor leukocyte behaviour when responding to conflicting gradients of chemoattractants

4.1.1. Biological rationale behind the design of the 2D device

Understanding how a leukocyte decides which signal to follow within a tissue is complex and little is known about the "guidance hand-over" between intermediary and end-target chemoattractants occurs. Therefore, to interrogate how leukocytes respond when challenged to both an end-target and intermediary chemoattractant simultaneously a reductionist approach was required. The first section of this chapter is concerned with designing and generating a microfluidic device to view how leukocytes respond to conflicting chemotactic cues. The device is a modification of gradient generating devices (345)(346)(347). The design and optimisation stages will be discussed in detail below. For simplicity, the device will now be referred to as the "2D device" because migration takes place only in 2D.

Deleted: how

Deleted: similar devices proposed by several others

4.1.2 Designing and generating the 2D device

Briefly, the device (***figure 4.1 A***) is composed of a central 300µm wide main channel. Running parallel, on either side of this main channel, are side channels. The side channels are connected to the main channel through a series of smaller perpendicular microchannels (***figure 4.1 A***). The device has 7 openings numbered 1-7 (***figure 4.1***). The openings will be referred to later in the text as inlets or outlets for the passage of cell culture media, in certain cases carrying cells or chemoattractants. The openings 1-4 are inlets for the introduction of media while the openings 5-7 are outlets for the removal of media.

Deleted: e

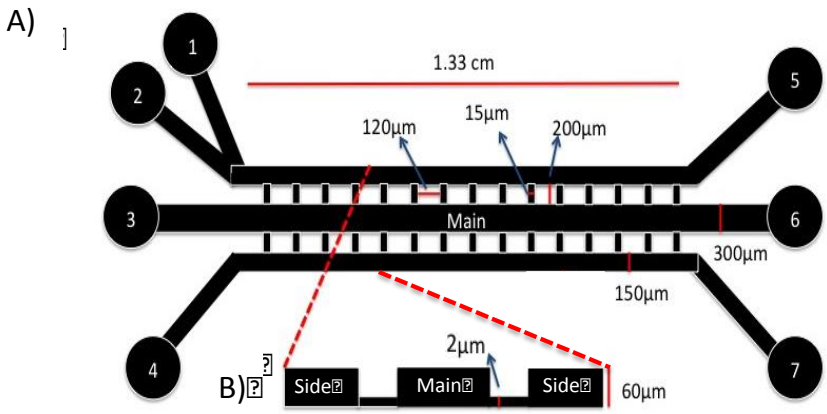

Figure 4.1: Schematical representation of the 2D device.
A) Ariel view of the 2D device with appropriate dimensions. Numberings identify inlets (1,2,3,4) and outlets (5,6,7). B) Cross sectional view of the 2D device within the red-hatched lines, the dimensions here indicate the relative heights of the main and side channels (both 60µm) compared to the small microchannels (2µm).

Prior to fabrication, the design (***figure 4.1***) was drawn to scale using AutoCAD, and printed onto two black emulsion masks at 40,000 dots per inch (dpi) (JDphotodata). The masks were printed in inverted contrast where all the features of the device (channels and inlets) were transparent; allowing light to penetrate through, in the same way a stencil would be generated (***figure 4.2***).

Deleted:

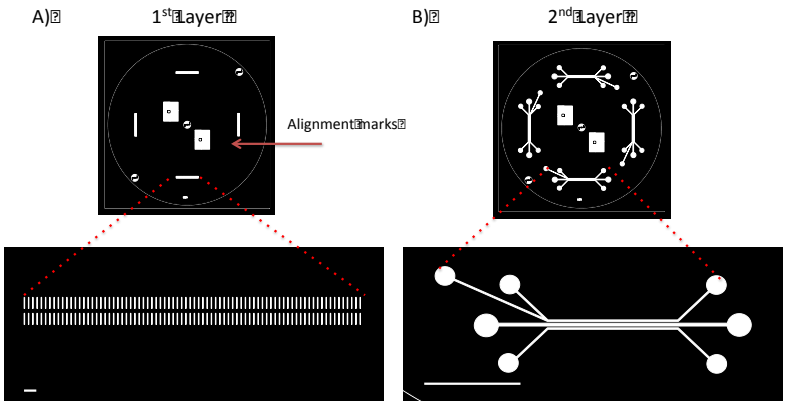

Figure 4.2: Black emulsion masks for the 2D device
A) 1st Layer: small microchannels. Scale bar is 120 µm. B) 2nd Layer: main and side channels with corresponding inlets and outlets. Scale bar on both images is 1cm. Each black emulsion mask has four devices. The central rectangles are identical in position in both the 1st and 2nd layers of the black emulsion masks -these features are alignment marks.

Once checking for geometric and printing errors within the black emulsion masks was complete, the initial stage of the device fabrication could commence. The 2D device was constructed using a staged approach, summarised in the following schematic figures (***figure 4.3 &figure 4.4***). In summary, the first stage (***figure 4.3***) uses ultraviolet (U.V) light to crosslink a photosensitive resist in the desired pattern onto a silicon wafer. This process is termed photolithography. The second stage (***figure 4.4***) uses the previously generated patterned silicon wafer to act as a master mould to cast inverted replicated stamps. These replica stamps are cast using an elastomeric material, Polydimethylsiloxane (PDMS). This second stage of the device design is termed soft lithography.

All photolithography work was carried out in a class 1000 (ISO 6) cleanroom at the London Centre of Nanotechnology (LCN). Temperatures, timings and spin speeds were all optimised using guidance from the photoresist manufacturer Microchem.

To start the fabrication process a 3-inch circular silicon wafer (WRS materials) was cleaned sequentially with 100% acetone and 100% isopropanol, then

dehydrated for 20 minutes at 200°C to remove any residual alcohol (***figure 4.3 stage 1***). Once dry, an epoxy-based negative photoresist, SU8 2002 (Microchem), was spin coated onto the wafer, this spin coating results in the first layer of device, producing the 2µm high microchannels. The thickness of the layer of photoresist on the wafer is determined by resist type, spin speed and spin duration. Later, (see below) a second layer of photoresist is applied to the wafer; this results in features of 60µm height. To apply the SU8 2002 the wafer was spun at 3000 rpm for 1 minute to obtain a 2µm thickness. This thickness determines the size of the first set of features (microchannels) imprinted onto the wafer (***figure 4.3 stage 2***). The coated wafer was baked for 1 minute at 95°C to remove solvent from the photoresist, in turn increasing the viscosity (***figure 4.3 stage 3***). The wafer was then aligned with the black emulsion mask directly above the wafer. Aligning both the emulsion mask and the pre-coated wafer was carried out using a Karl Suss MJB3 mask aligner. The wafer was then exposed to U.V for 4 seconds at 20 mJ/cm^2. The U.V light travels through the "clear" regions of the 1st emulsion mask (***figure 4.2 A***) to hit the photoresist. U.V exposure cross-links the photoresist making it adherent to the silicon wafer (***figure 4.3 stage 4***). Post exposure baking of the wafer was then conducted for 2 minutes at 95°C (***figure 4.3 stage 5***). Uncross-linked SU8 2002 photoresist was chemically removed from the wafer through incubation with Microposit EC solvent-11 for 1 minute (***figure 4.3 stage 6***). The cross-linked microchannel features remain present on the silicon wafer.

To generate the main and side channels a second round of photolithography was employed onto the patterned wafer described above. The wafer was spin coated with a second SU8 photoresist (SU8 2025) and re-spun at 1500 rpm to obtain a 60µm thickness (***figure 4.3 stage 7***). The more viscous a photoresist, the thicker the coating produced onto the silicon wafer. SU8 2025 photoresist was used for this second spin due to its increased viscosity compared to SU8 2002. The coated wafer was baked (pre-exposure) for 2 minutes at 65°C and 7 minutes at 95°C (***figure 4.3 stage 8***). The second black emulsion mask (***figure 4.2 B***) was positioned above the silicon wafer using the Karl Suss MJB3 mask aligner, the wafer was exposed to 12 seconds at 20 mJ/cm^2, the longer exposure time

Deleted: will be

Deleted: will

Deleted: ’

Deleted:

reflected the thicker resist layer. Prior to exposure, alignment marks previously created onto the wafer (***figure 4.2***) from the previous exposure were used to align the two layers of features to ensure that the small microchannels would correctly connect with the side and main channels (***figure 4.3 stage 9***). Post-exposure bake time was 1 minute at 65°C and 6 minutes at 95°C (***figure 4.3 stage 10***). The wafer was then developed in Microposit EC solvent-11 for 5 minutes (***figure 4.3 stage 11***). Finally, to preserve the longevity of the features patterned on the wafer, the patterned wafer was hard baked at 180°C for 5 minutes and inspected using light microscopy to ensure all the features were accurate and well developed (***figure 4.3 stage 12***). The final product from this stage of the fabrication process was a silicon wafer patterned with both 2µm high features (small microchannels), and 60µm high features (main and side channels).

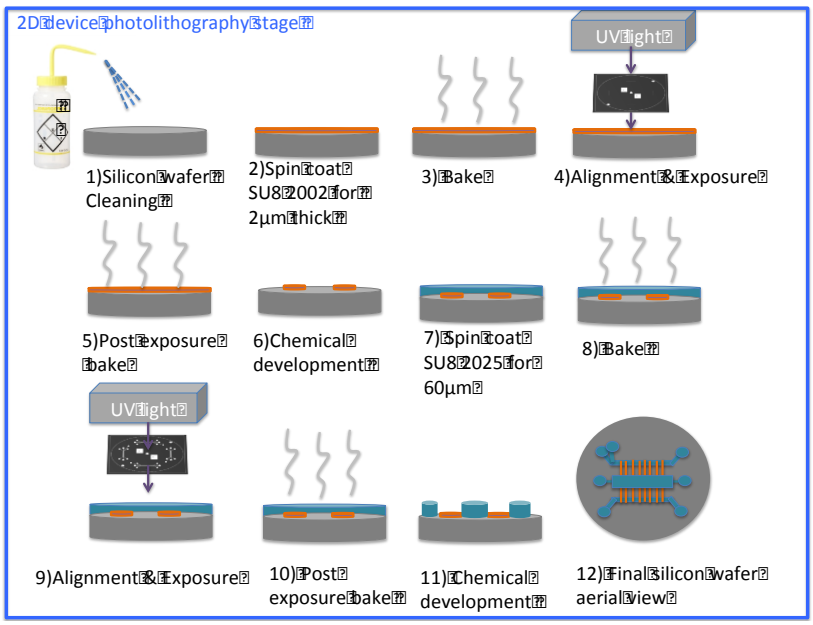

Figure 4.3: Schematic representing the 12 stages of the photolithography process for the 2D device fabrication
1) The silicon wafer is cleaned. 2) The silicon wafer is spin-coated with a SU8 2002 photoresist to produce an even layer 2µm thick. 3) The silicon wafer is baked. 4) Silicon wafer is aligned with the black emulsion mask and then exposed to U.V light. U.V only passes though transparent areas of

the black emulsion mask generating permanent features on the wafer, this occurs through U.V dependent cross-linking of the photoresist. 5) The silicon wafer is baked. 6) Chemical development to remove uncross-linked photoresist. 7) The silicon wafer is spin-coated with a SU8 2025 photoresist to produce a 60µm thick layer. 8) Silicon wafer is baked. 9) Align a second black emulsion mask and expose to U.V. 10) Bake. 11) Chemical development. 12) Visual inspection.

The patterned wafer is placed into a petri dish to act as a master mould. PDMS is poured on top of the silicon wafer. PDMS is a polymer made by mixing elastomer and curing agent in a 10:1 ratio of elastomer: curing agent. PDMS is frequently used to generate biological devices, as the polymer is biocompatible and optically transparent. The PDMS is cured for a minimum of 2 hours at 60°C (***figure 4.4 A***). Once set, PDMS devices are released from the master mould. Inlet and outlet holes are bored using a 0.75mm diameter biopsy punch, to excise cylindrical PDMS from the PDMS stamp. The PDMS device is irreversibly bonded feature side down to a cleaned 5cm diameter glass. To bond, oxygen plasma is passed over the surfaces of both the PDMS and glass coverslip and immediately placed together. Oxygen plasma converts the silicon bonded methyl groups on the PDMS surface to silanol terminations (SiOH) and the oxygen plasma oxidises the glass coverslip. Together the functionalised PDMS and glass adhere covalently by producing Si-O-Si bonds. To ensure a strong PDMS to glass bond formation, the 2D device is left at 60°C overnight. The following day, the inlets and outlets are then fitted with tygon tubing (***figure 4.4 B)*** to allow for the introduction of fluids for 2D device priming (see ***section 4.1.3***) and ready for the introduction of cells into the main channel (***figure 4.4 C***).

Deleted: then

Deleted: then

Deleted: left to

Deleted: then can

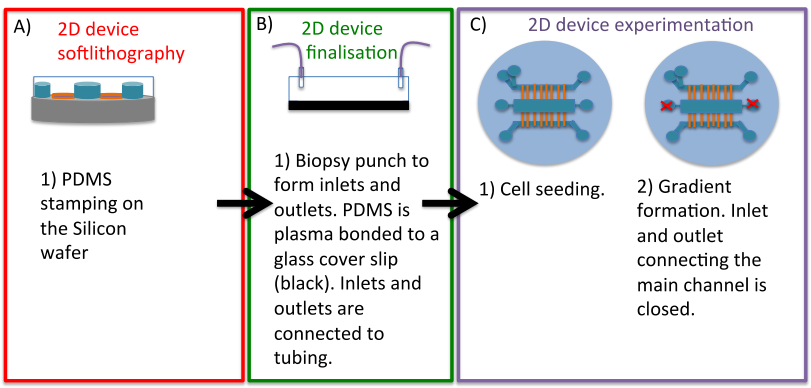

Figure 4.4: Schematic representing the soft lithography and 2D device assembly process. A) PDMS is poured onto the patterned silicon wafer, which acts as a master mould. The PDMS is left to polymerise, once set the PDMS can be cut free. B) Inlets and outlets are generated using a biopsy punch. The PDMS is irreversibly bonded to a glass coverslip, feature side down to generate the channels. Tubing is then introduced. C) Cells and fluids can be introduced from the inlets into the device.

4.1.3 Quality control testing of a chemoattractant gradient

Chemotaxis of leukocytes within the 2D device is strictly dependent on the correct establishment of a diffusion gradient. Basic linear gradients are generated in the main channel - the location where the leukocytes are seeded. To generate gradients in the main channel, chemoattractants are introduced into the side channel inlets under low pressure (between 9-13 mbar). Under this low pressure, fluid velocity is low, and the fluids travel in laminar flow. Laminar flow describes fluids flowing in parallel, where different fluids mix solely through lateral diffusion at the interface. For fluid to enter the main channel it must move from the side channels to the microchannels, the height difference between the microchannels (2µm) and the side and main channels (60µm) restricts fluid movement. During a chemotaxis experiment the inlet and outlet corresponding to the main channel is sealed. Therefore, the movement of fluid from the microchannel and into the main channel is governed by diffusion and the little internal convection that is present. To monitor gradient formation, medium supplemented with fluorescently labelled dextrans was introduced into the side channel inlets (1,2&4) (***figure 4.1***). Each inlet introduced a uniquely labelled dextran; FITC-dextran, TRITC–dextran and Alexa647-dextran. To accurately model diffusion of the physiologically relevant chemokines, the molecular weights of all dextrans were 10kDa as this reflected the average weight of a chemokine (~8-11kDa). Additionally, to maintain consistent comparative fluorescence intensities throughout different 2D devices, dextrans were used at a working concentration of 0.1mg/mL and microscope settings and parameters were kept constant.

The ultimate aim of the 2D device was to initially expose cells to only one chemoattractant (either an end-target or intermediary), and then confront cells to a second chemoattractant gradient from the opposite direction. To this end, cell

Deleted: is

behaviour can be monitored in response to a single signal; this behaviour can then be directly compared (looking at the same cell population) when immediately presented with a choice of chemical cues (***figure 4.5***).

Deleted: will be

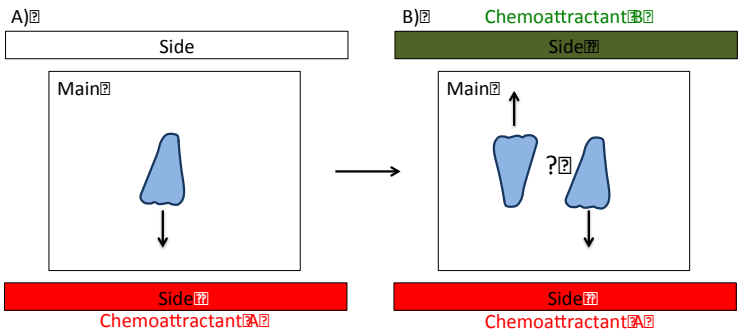

Figure 4.5: Schematic of chemoattractant competition experiment
A) Leukocytes are seeded within the main channel and subjected to the first chemical cue - chemoattractant A. B) A second chemical cue is introduced – chemoattractant B. Leukocytes within the main channel are now subjected to two opposing gradients. For simplicity, the microchannels are not represented in this schematic; this is a representative depiction of the middle section of the 2D device, omitting inlets and outlets.

To achieve the setups demonstrated in ***figure 4.5 A&B,*** inlets 1,2 and 4 were individually pressurised using a Fluigent system (MFCS-8C). The Fluigent system is a pressure driven flow controller, which is capable of individually controlling 8 unique pressure values. The MFCS-8C instrument works through positive pressure at a value range of 0-1000mbar. To create the set up in ***figure 4.5 A*** each of the three inlets were pressurised: Inlet 4 (10.5mbar) and inlet 1 (9mbar) introduce different chemoattractants, while inlet 2 (10mbar) introduces cell culture media only. Initially cells within the main channel sense only the chemoattractant gradient supplied from inlet 4 due to the bifurcation channel (***figure 4.5 A & figure 4.6 A***). The bifurcation channel (a forked channel where two separate liquids are introduced from two separate inlets and converge into one side channel) allows the fluids introduced from inlet 1 and 2 to run in parallel laminar flow in the side channel. The cell culture media introduced from inlet 2 shields the cells from the chemoattractant supplied from inlet 1 (***figure 4.6 C***). To allow the cells to sense both chemoattractants, the influx of medium from inlet 2

is stopped, and inlets are re-pressurised. I will refer to this step as a pressure switch as it typically can be achieved in a few milliseconds. The new pressure values are as follows: Inlet 1 (13mbar), Inlet 2 (0mbar) and Inlet 4 (10.5 mbar). Again, the rapid change in fluid pressure is achieved through the use of the Fluigent system. One minute after the re-pressurising of the inlets, a chemoattractant gradient produced from inlet 1 is visible in the main channel (***figure 4.6 B & figure 4.7***). Importantly, this pressure switch does not alter the pre-existing gradient formed within the main channel from inlet 4 (***figure 4.6 B & figure 4.7)***. The leukocytes are now exposed to two opposing chemoattractant gradients (***figure 4.5.B***). Pressure values for each inlet were determined empirically.

Gradient formation within the device was monitored live using an inverted fluorescence microscope. Two separate fields of view (FOV) were taken along the main channel. The two FOV were positioned ~50µm and ~250µm from the start of the main channel, respectively. It was important to include both of the side channels in the FOV to calculate initial fluorescence intensity for each dextran, prior to dextran dilution within the main channel. This initial fluorescence value will normalise fluorescence intensity values in the main channel, to gauge the relative concentration of chemoattractant. Fluid movement coming from each inlet (1,2&4) could be identified through their unique fluorescence wavelength. Fluid from inlet 1 contained FITC-dextran, inlet 2 contained Alexa 647-dextran and inlet 4 contained TRITC-dextran. These were visualised using excitation at the following wavelength: 488nm, 543nm and 633nm, respectively. Images were acquired every minute using a 10x objective for a total duration of 45 minutes. The pressure switch occurred at the 23rd minute of experimentation (***figure 4.7***).

Deleted: l

To analyse gradient formation over time, post acquisition analysis was performed in the middle of the two FOV for each device using Fiji. A total of four devices were used to characterise the gradient behaviour. To determine fluorescence intensity values, a line profile was drawn across the width (transverse section) of the main channel in both FOVs. Intensity values, from the line profile were recorded over time separately for each wavelength. Line profiles were averaged over a 30-pixel

width to reduce noise. For each fluorescent dextran, fluorescence intensity values from each line profile at each time point were internally normalised, (F1/F0). Here, F0 is the fluorescence intensity within the side channel, prior to dextran diffusion. Fluorescence normalisation controlled for slight differences in laser intensities between experiments. All fluorescence intensities were subjected to background fluorescence removal (Fb) (***figure 4.***7). Background fluorescence occurs through auto fluorescence of sample (e.g. from the 2D device or media), or from noise from the excitation light. Background fluorescence was measured for each unique fluorescent dextran using the appropriate laser excitation when no fluorescent dextran was present within the 2D device. ***Figure 4.7*** show that two opposing gradients can be reproducibly generated at the two FOVs. The gradients also remain stable for a period greater than 20 minutes, an appropriate time scale to monitor leukocyte migratory behaviour.

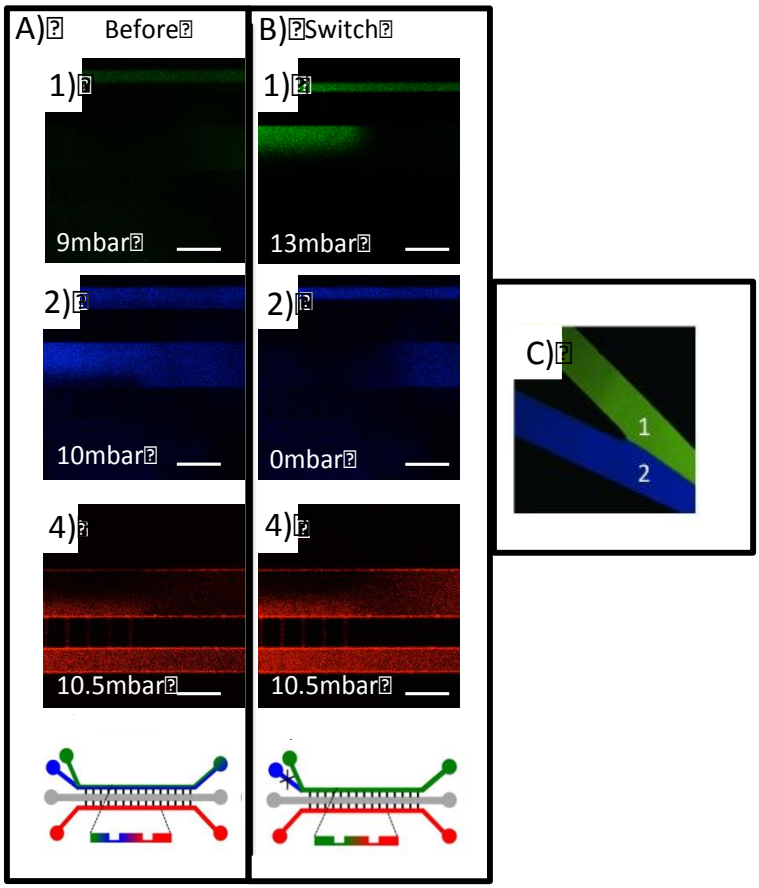

Figure 4.6: Diffusion within the 2D device
Confocal microscopy monitored the movement of each of the three dextrans into the main channel from the side channels. A&B) Numbers on top left hand side of image denote inlet specific dextran. A) A Confocal image before the pressure switch: inlets were pressurised as follows: 9mbar for inlet 1 (FITC-dextran), 10 mbar for inlet 2 (Alexa647-dextran), and 10.5mbar for inlet 4 (TRITC-dextran). B) A Confocal image after the pressure switch: inlets were pressurised as follows: 13 mbar for inlet 1 (FITC-dextran), 0 mbar for inlet 2 (Alexa647-dextran) and 10.5mbar for inlet 4 (TRITC-dextran). C) Confocal still demonstrating the bifurcation channel, here fluids are introduced from inlet1 and inlet 2, and the liquids converge into the same channel however both liquids flow side by side. Scale bar is 300μm. Switch occurs after 23 minutes of dextran introduction into the inlets.

Ai)

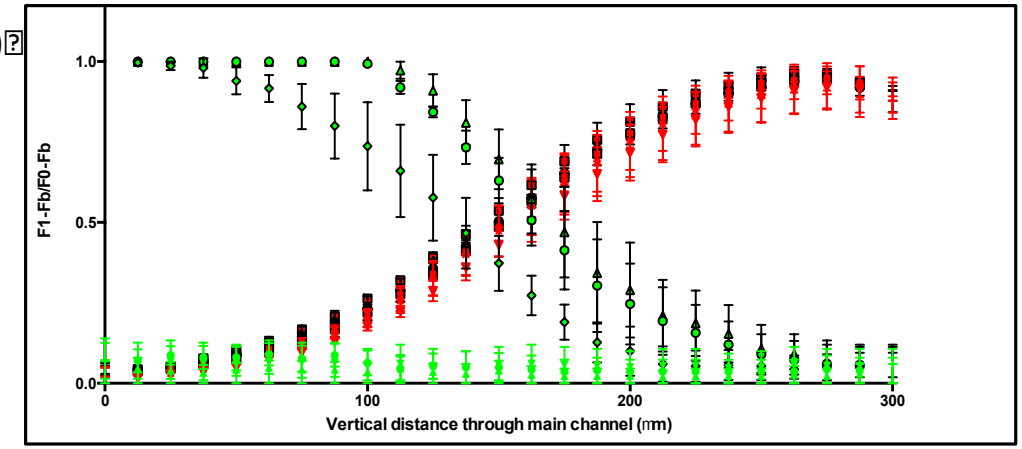

Aii)

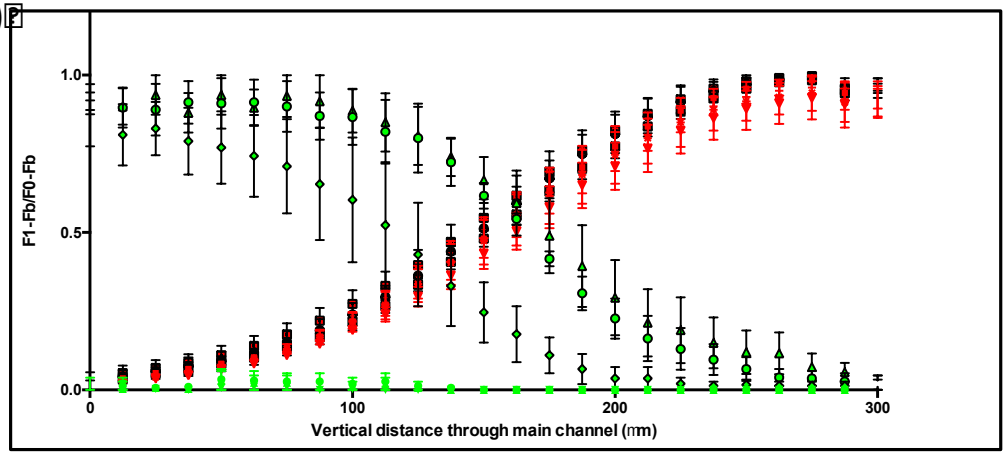

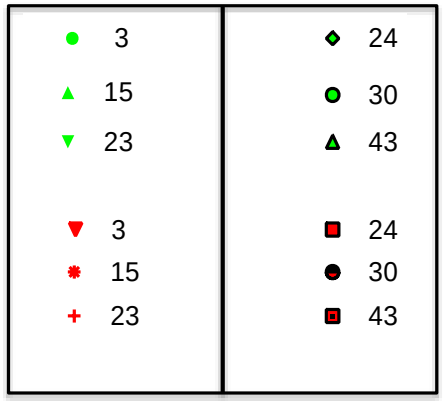

Legend – Minutes

Figure 4.7: Fluorescence intensity line profile through the main
Gradients profiles of the fluorescent dextrans, FITC dextran (inlet 1) & TRITC dextran (inlet 4) were monitored from images acquired from an inverted fluorescent confocal microscope. Two FOV located at ~50μm(Ai) and ~250μm(Aii) from the start of the main channel were imaged over time for each device. Diffusion profiles from a total of four devices generated the data represented in the graphs. Images were acquired every minute. Fluorescent dextran diffusion was assessed post image acquisition. A line profile was taken across the transverse section of the main channel (the width) to generate intensity values for each fluorescent dextran. Fluorescence background (Fb) intensities levels were removed from all fluorescence intensities values. Fluorescent intensity (F1) values along the line profile of the main channel were normalised with respect to the corresponding fluorescence intensity in the side channel, (F1-Fb/F0-Fb). Green symbols represent dextran movement from inlet 1. Red symbols represent dextran movement from inlet 4. Error bars represent standard deviation from the mean and represent four devices. Red and Green symbols with a black outline represent dextran movement after the pressure switch. The pressure switch occurs at minute 23. For the pressure values of each inlet before and during the pressure switch see ***figure 4.6***.

4.1.4 Cell seeding within the 2D device

Prior to cell introduction, the device was primed with a 1x PBS solution. Priming the device minimised the risk of trapped air in the small microchannels. The best results were achieved when the device was fully submerged in PBS and left overnight before any experimentation was conducted to remove any gas dissolved with the gas-permeable PDMS. Care was taken to de-gas media before introduction into the device. Next, PBS containing 10μg/mL fibronectin was introduced into the device to provide a substrate for cell adhesion. The device was incubated for 1 hour at 37° C with this solution. This was then washed out with PBS.

Deleted: u

A bespoke cell seeding method was devised to position the cells in the centre of the main channel and prevent cell movement and aggregation at the entrance of the microchannels. Blockage of the microchannels would hinder delivery of the chemoattractant. Cells were introduced into the device (inlet 3) at a high concentration, (10-15x10^6/mL). Inlet 1 and Inlet 4 introduced media at high pressures (~200mbar), while inlet 2 was blocked. All outlets were left open. High fluid flow entering the main channel from the microchannels focused cells into a central stream within the main channel. At this point all tubing connecting inlets and outlets were then rapidly blocked with the aid of arterial surgical clamps.

This rapid blockade of internal flow allowed cells to settle through gravity and adhere to the fibronectin substrate. ***Figure 4.8 A*** is an example of cell focusing then subsequent settling through gravity, while ***figure 4.8 B*** is an example of cell settling in an environment where there is internal flow, e.g. inlets and outlets have remained open. Unfortunately, due to time constraints no chemotaxis experiments could be performed using this device.

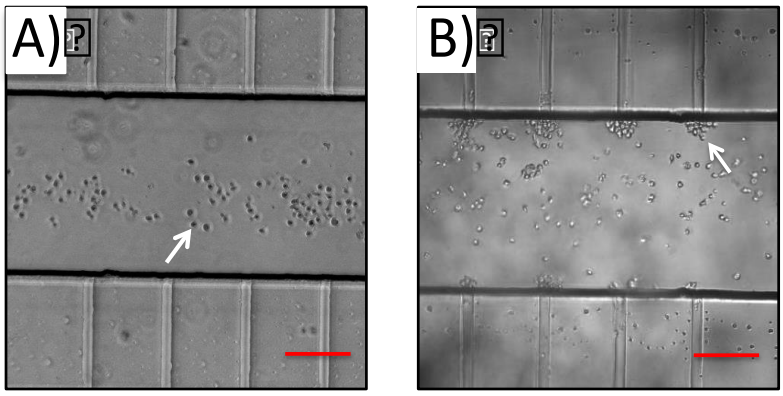

Figure 4.8: Alternative cell seeding approaches in the 2D device
Cells were introduced into the main channel of the 2D device. Cell seeding was imaged using brightfield and a 10x objective. A) Cell seeding in the main channel, inlet 1 and inlet 4 are pressurised at high pressure, ~200mbar, to encourage cells to focus into the middle of the main channel. Once focused all inlets and outlets are rapidly closed to allow cells to settle through gravity. B) Cell seeding in the main channel, all inlets and outlets remained open after cell introduction, resulting in cell displacement towards the edge of the main channel and accumulation at the entrance of microchannels. White arrows indicate cells. Scale bar is 100µm.

4.2 Generation of a 3D device to monitor the entire leukocyte adhesion cascade from capture to chemotaxis

4.2.1 Biological rationale behind the design of the 3D device

Currently, the methodology used to study the multi-step leukocyte adhesion cascade of primary human leukocytes is limited and slow evolving. Scientists routinely use the parallel plate flow chamber. In this setup, leukocytes are perfused over activated endothelial monolayers under physiological shear stress and cellular behaviour is recorded in real-time. Traditionally, a confluent endothelium is grown on fibronectin-coated coverslips, which provides a limited space (~1 micron) between the endothelial cells and the underlying glass for the

leukocytes to migrate. As such, the current setup does not provide an accurate representation of migration of leukocytes in the extravascular connective tissue observed *in vivo*. Leukocytes will typically sense different chemoattractants as they pass from the blood into tissue, which is not featured in any current parallel plate flow chamber model. Cain et al., recently developed a transmigration assay that was devoid of flow, but allowed transmigrating leukocytes to move directionally through a 3D collagen scaffold (348). Briefly, liquid collagen was polymerised within transwell inserts containing polycarbonate filters. Once an endothelial cell monolayer was established on top of the collagen matrix, the entire insert was placed into a well containing a known quantity of chemoattractant. Timed incubations showed that leukocytes would transmigrate and move directionally towards the highest source of chemoattractant. Although this technique was the first of its kind, it did not incorporate shear stress and did not permit live cell imaging, as the polycarbonate filter acted as an optical barrier for imaging with inverted microscopes.

As explained above the study of the leukocyte adhesion cascade is disjointed, with separate assays to monitor leukocyte behaviour before and after transendothelial migration. The second part of this chapter will focus on the design and optimisation of a device, which will permit visualisation of the entire multi-step adhesion cascade: from initial tethering to interstitial chemotaxis through a 3D collagen scaffold. For simplicity, this device will be referred to as the "3D device".

Deleted: .

4.2.2 Design and fabrication of the 3D device

The 3D device was designed around fixed specifications, summarised below (***table 4.1***). This table will be referred to continually throughout the section.

Specification	Justification
ECM component able to support a HUVEC monolayer.	A confluent endothelial monolayer is required to mimic transendothelial migration.
3D ECM permissible for neutrophil migration.	Non-optimal matrix porosity will hinder migration.
Stable chemoattractant gradient formed within the ECM.	Allow neutrophils to follow a graded response to a chemoattractant source.
Couple to a pre-existing parallel plate flow chamber.	Allow introduction of neutrophils across the endothelium at physiological stress.
ECM thickness ~ 125µm in the 3D device.	Thickness will enable sufficient depth for neutrophil migration and acquisition of z-stacks at high magnification using a confocal microscope.

Table 4:1: The specifications and justifications for the design of the 3D device.

Briefly, the device consists of a thick PDMS frame irreversibly bonded to a glass coverslip. This frame supports a collagen matrix, which in turn supports an endothelial monolayer (***figure 4.9***). Within the frame, there are two microchannels, which can be used to introduce chemoattractant/s into the collagen (***figure 4. 9***). The device is open top, allowing it to be easily interfaced with the pre-existing parallel plate flow chamber within the Ivetic lab (***figure 4.9& table 4.1*).** Dimensions for the device were imposed by the need for compatibility with the present experimental setup. For example, the diameter (1.8cm) of the plastic parallel plate flow chamber dictated the distance between the microchannel inlet and the collagen trough, (***figure 4.9***), while the 5cm diameter glass which formed the base of the device, dictated the maximal device size.

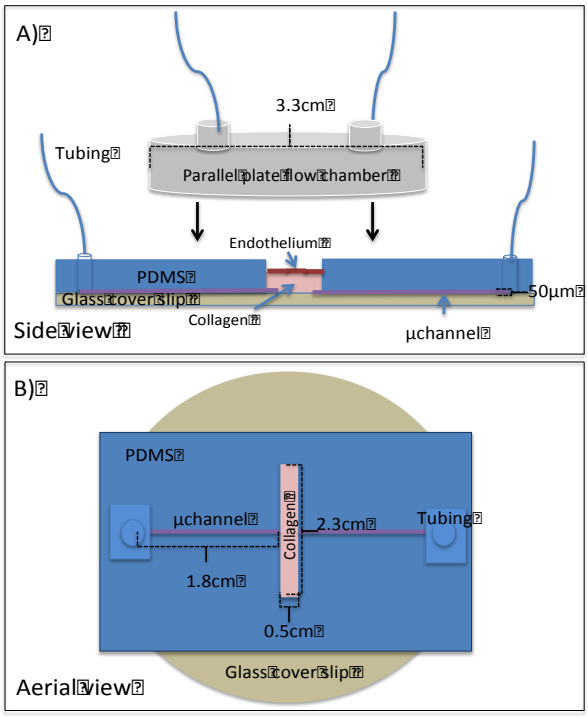

Figure 4.9: Schematic of 3D device design.
A) Side view of the 3D device interfacing with the parallel plate flow chamber. B) Aerial view of the 3D device. Dimensions represent the true dimensions of the 3D device. Endothelium and parallel plate flow chamber not shown for simplicity.

Deleted: ¶

Prior to fabrication of the 3D device, the design with the above dimensions (***figure 4.9***) was drawn using AutoCAD and transferred onto a black emulsion mask (JDphotodata). In the black emulsion mask, features to be patterned onto the silicon wafer are transparent (***figure 4.10***).

Deleted: As for the 2D device, prior

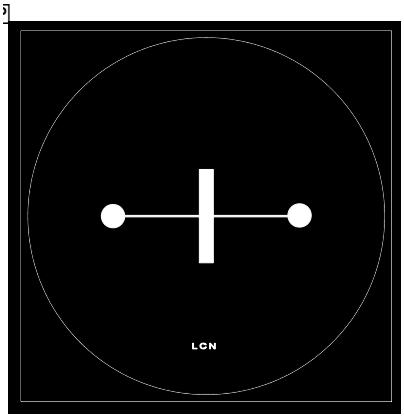

Figure 4.10: Black emulsion mask for the 3D device

The 3D device was constructed using a staged approach, summarised in schematic figures ***figure 4.11 &figure 4.12***.

Fabrication is initiated with the cleaning of a 3-inch silicon wafer (WRS materials), as described in ***section 4.1.2,*** (***figure 4.11 stage 1***). An epoxy-based negative photoresist, SU8 2025 (Microchem), was spun coated at 1750 rpm to achieve a 50μm thick layer. This thickness determined the microchannel feature in the 3D device (***figure 4.11 stage 2***). After, the coated wafer was baked (pre-exposure) for 2 minutes at 65°C and for 5 minutes at 95°C (***figure 4.11 stage 3***). The features were then cross-linked onto the wafer. For this, the emulsion mask (***figure 4.10***) was aligned with the wafer using the Karl Suss MJB3 mask aligner. The wafer was exposed to U.V light for 10 seconds at 20 mJ/cm^2 (***figure 4.11 stage 4***). U.V light passed through the transparent regions of the emulsion mask and cross-linked the photoresist to form irreversible features adhered to the silicon wafer. The wafer was baked (post exposure) for 2 minutes at 65°C and 5 minutes at 95°C (***figure 4.11 stage 5***). Finally, the wafer was developed in Microposit EC solvent-11 for 5 minutes until all residual resist was removed, and hard baked at 150°C for 4 minutes (***figure 4.11 stage 6***). The wafer was then visually inspected (***figure 4.11 stage 7***).

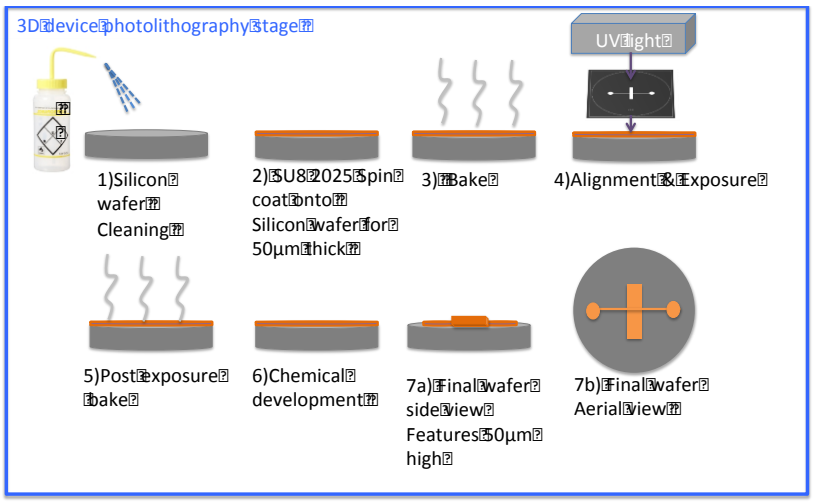

Figure 4.11: Schematic representing the 7 stages of the photolithography process for the 3D device fabrication
1) The silicon wafer is cleaned. 2) The silicon wafer is spin coated with a SU8 2025 photoresist to produce a 50µm thick layer. 3) Silicon wafer is baked. 4) Silicon wafer is aligned with the black emulsion mask and then exposed to U.V light. U.V only passes though transparent areas of the black emulsion mask generating permanent features on the wafer, this occurs through U.V dependent cross-linking of the photoresist 5) Silicon wafer is baked. 6) Chemical development to remove uncross-linked photoresist. 7) The silicon-patterned wafer is visually inspected.

The patterned wafer can then act as a master mould. PDMS was poured over this master mould (***figure 4.12 A***). Prior to covalent plasma bonding of the PDMS to the glass coverslip, a rectangular PDMS cuboid 2.3cm (h) x 0.5cm(w) is excised with a scalpel from the central part of the device (***figure 4.12 B***). Biopsy punching. After plasma bonding to the glass, two microchannels are formed, separated by a large rectangular void. This excised region now acts as a trough, in which collagen can be polymerised to provide a substrate for endothelial cells (***figure 4.12 B***).

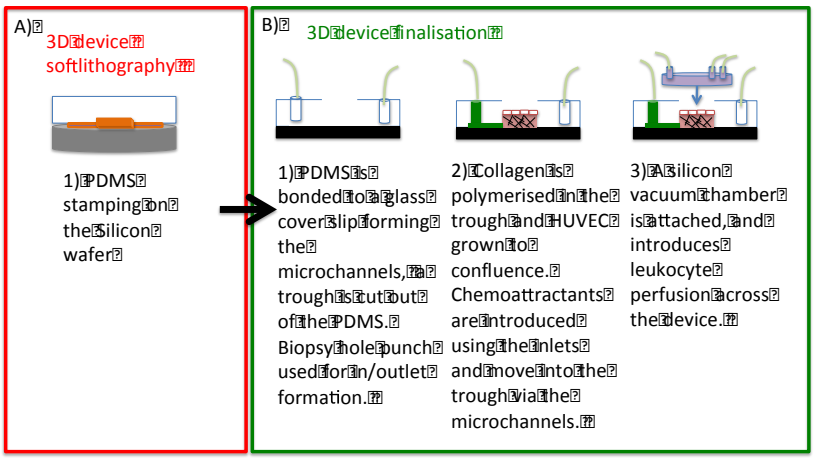

Figure 4.12: Schematic representing the soft lithography and 3D device assembly process. A) PDMS is poured onto the patterned silicon wafer, which acts as a master mould. The PDMS is left to polymerise, once set the PDMS can be cut free. B) 1) Inlets are generated using a biopsy punch; a PDMS cuboid is excised from the centre of the device. The remaining PDMS is irreversibly bonded to a glass coverslip, feature side down, to generate the microchannels and a trough. 2) Collagen is placed into the trough and left to polymerise. The polymerised collagen gel can support an endothelial monolayer. Chemoattractant/s (green) are introduced into the trough from the microchannel/s (one inlet filled here). 3) Finally, the device is interfaced with a parallel plate flow chamber to perfuse leukocytes across the endothelium at physiological shear stress.

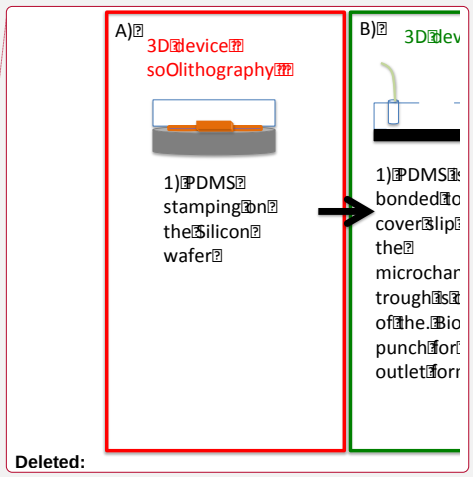

Deleted:

4.2.3 Optimising extracellular components to support a HUVEC monolayer

The extracellular matrix (ECM) is a non-cellular protein meshwork component surrounding all cells of the human body. In the interstitial space the ECM underlying the endothelium is produced through secretion by endothelial cells and pericytes (140),(141). Here, the two basic forms of the ECM are the basement membrane and the loose fibril-like interstitial matrix. Crucially, the ECM provides structural and signalling properties to support blood vessel formation and provides chemotactic properties to encourage leukocyte diapedesis (see ***section 1.4.2***). Therefore, it is important to not only generate a suitable ECM to provide a matrix where the HUVEC would reproducibly form a confluent monolayer (***table 4.1***) but also to encourage TEM events.

Deleted: The extracellular matrix (

Deleted:)

Deleted: consists of the protein meshwork

Deleted: . It

Deleted:

Deleted: The

To this end, the commercialised hydrogel Matrigel® was trialled. Matrigel® is the solubilised basement membrane fraction from Engelbreth-Holm-Swarm (EHS) mouse sarcoma, rich in laminins, collagen IV, nidogen and heparin sulphate

proteoglycans (a protein proven to aid diapedesis). Matrigel® was polymerised in bespoke cut PDMS troughs (as designed in ***section 2.12.4***) at a concentration range of 2-4 mg/mL. After 30 minutes polymerisation, HUVECs were seeded at a density of $0.5X10^6$/mL. In these conditions, HUVECs consistently failed to form cell-cell junctions, instead adopting an elongated "fibroblast like" phenotype (***figure 4.13 A***). It became apparent that Matrigel® contained undocumented factors, promoting HUVEC to differentiate and form tubules. To prevent this, Matrigel ® (25% (v/v)) was mixed with rat-tail collagen (75% (v/v)); this ECM composition did generally promote formation of a confluent HUVEC monolayer. However, confluent monolayers could not be reproducibly established. This is likely due to batch variability of the Matrigel ®. Thus, for ease of replication rat-tail collagen was used as the only ECM component within the troughs. Rat-tail collagen is prepared as described in ***section 2.12.1***. Collagen concentrations between 1.5-3mg/mL were tested and all promoted formation of confluent HUVEC monolayers (***figure 4.13 B***)***.*** As the device is open top, pericytes could be added in the collagen matrix in the future. This addition would aid endothelial cell derived basement membrane assembly(101).

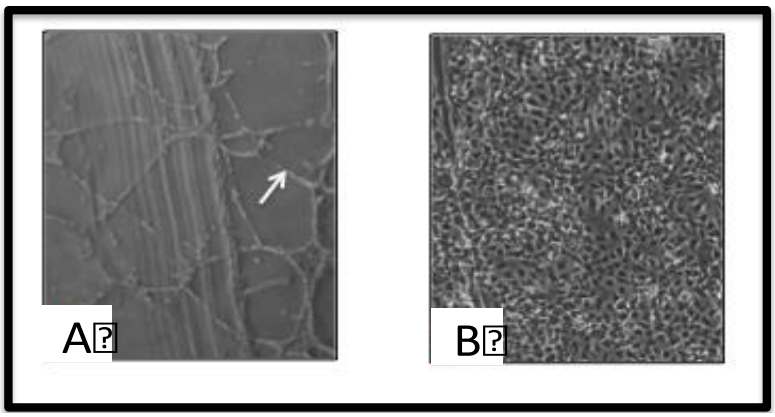

ECM composition (v/v)	Repeat number	Comments
A) 100% Matrigel®	3 troughs	Formed tubes
B) 100% Rat tail collagen	3 troughs	Good monolayer

Figure 4.13: HUVEC growth on different ECM components
Phase contrast images of HUVECs grown on either A) Matrigel® matrix or B) rat–tail collagen matrix, were acquired using a 10x objective. White arrow indicates, endothelial tube formation.
Table 4.2: HUVEC grown on different ECM components

4.2.4 Factors contributing to collagen pore size

Cell migration within a 3D environment depends on three factors: 1) matrix metalloproteinases (MMPs) driven ECM digestion, 2) the degree of cell deformability and 3) the physical tissue constraints. If MMPs are inhibited; an additional constraint for a cell moving through a 3D meshwork is nucleus deformability. As neutrophils have a multi-lobed nucleus, the cells and their nuclei have a high deformability and therefore can migrate through pore sizes larger than 2 μm^2. In contrast, T cells and cancer cells need a cross sectional space of 4μm^2 and 7μm^2 respectively (349)·(350). Previous work by Wolf et al., has shown that temperature and collagen concentration can affect the pore size of collagen gels (351). Therefore to assess how temperature and concentration of collagen contribute to the fibre density, reflection microscopy and post-acquisition binary processing was performed. Using this technique, the organisation of the collagen fibres could be assessed to give an indirect indication of pore size.

Deleted: If
Deleted: inhibited,

To analyse pore size, 50 µL of rat-tail collagen at concentrations of 1.5 mg/mL or 2 mg/mL were added to PDMS troughs and left to set for 30 minutes. The polymerisation temperature was also a variable: 20 or 37°C. The fibrous matrix architecture was imaged by confocal reflection microscopy (see ***section 2.12.1***). For each condition, 8 troughs were assessed at three optical z-planes: 10 µm, 30 µm and 60 µm above the glass substrate. To assess the pore size of each collagen preparation, a binary image of the collagen fibres was converted into a "distance map" provided within the tools of Fiji image analysis software. This is a Euclidian distance map also known as a distance transformation (***figure 4.14 A***) where each black pixel is replaced with a value, which directly correlates to its distance from the nearest white pixel. A black pixel that is further from a white pixel will have a higher value. This is simplified in ***figure 4.14 B***. The percentage of black pixels plotted against the transformed distance to the nearest white pixel gives an indication of how densely assembled the fibres are and the maximum distance between a black pixel (pore) to nearest white pixel (fibre). The distance in pixels is converted to µm to calculate the correct distances between black and white pixels. Hence, this method can act as a faithful indicator of pore size (***figure 4.15***). This analysis does not take into account the 3D nature of pores; instead it represents pores as 2D circular structures. For clarity, all analyses start at a minimal distance of 2.3µm to the nearest white pixel. The graph indicates that changing the gelling temperature of rat-tail collagen from 37°C to 20°C caused an increase in pore size, the same effect was observed when the protein concentration was decreased (***figure 4.15***). Encouragingly, Wolf et al obtained similar results in a study (351).It is important to note that collagen pore size and fibre thickness can be manipulated through other parameters for example pH and polymerization time (352)·(353). These variables where not varied within this thesis.

This section highlights how changing parameters can have a profound effect on pore size. In order to maintain the highest degree of reproducibility, when conducting experimentation using the 3D device, protein concentration and polymerization temperature were carefully controlled.

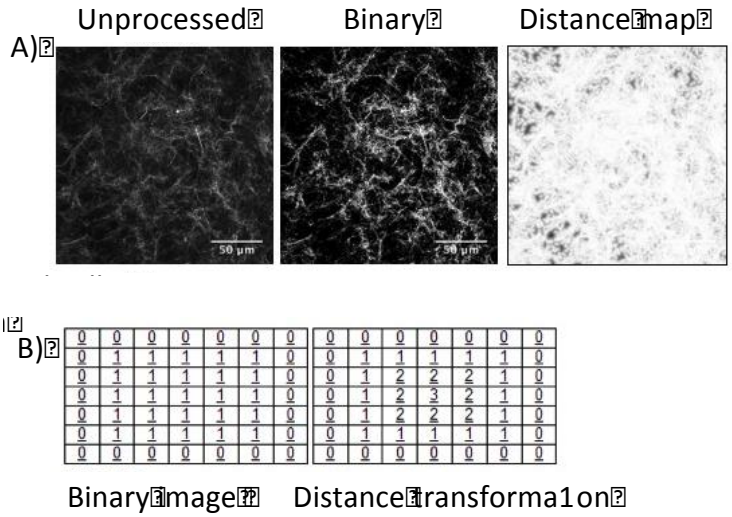

Figure 4.14: Image analysis for estimating collagen pore size
A) Polymerised rat-tail collagen was imaged using reflective confocal microscopy. Images were converted into binary where fibres were white and pores were black. Black pixels were given a value to representing their respective distance to the nearest white pixel (fibre); this can be represented as a distance map or tabulated as a distance transformation table. Scale bar is 50µm. B) A simplified example of a binary picture, 0 = white pixels and 1 = black pixels; when transformed the pixels in the centre that are furthest from the 0 border have a higher value, this value can be translated into distance using the pixel to µm scale of the image.

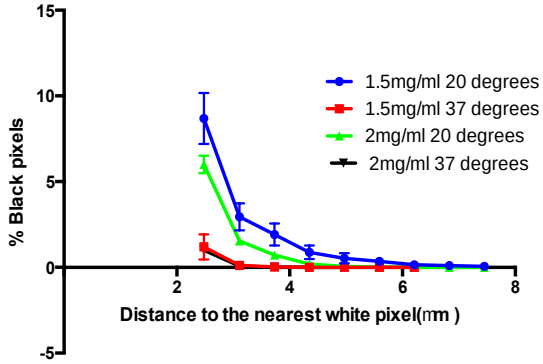

Figure 4.15: Graph demonstrating the effect of change in collagen concentration and polymerisation temperature on gel pore size.
Polymerised rat-tail collagen was imaged using reflection confocal microscopy. For each condition, a total of 8 experiments were conducted with 3 confocal z-slices per experiment. Post acquisition analysis was conducted as explained in ***figure 4.14***. The graph represents the percentage black pixels against the distance to the nearest white pixel. Error bars represent standard deviations

from the mean. This was a qualitative assessment, so no statistical analysis was conducted. For clarity data points where a black pixel had a distance less than 2.3 μm away from a white pixel was excluded, this represented the majority of pixels.

4.2.5 HL-60 migration through a collagen matrix

As shown in ***figure 3.10*** addition of 1.3% (v/v) DMSO into the cell culture media of the HL-60 cell line induced differentiation into a neutrophil-like cell line. Differentiated HL-60 cells have routinely been used as a neutrophil model to monitor migration through a collagen gel.

An important factor in the design specification was to ensure that the ECM components chosen, in this case rat-tail collagen, supported neutrophil migration (***table 4.1***). Thus, it was crucial to confirm that this cell line would successfully migrate within this matrix. To monitor cell migration, $1x10^6$ differentiated WT L-selectin–GFP HL-60 cells, also known as WT, were mixed into 100μL of 2.5mg/mL rat-tail collagen solution and placed into one well of a 96 well plate. The collagen–cell mix was placed in a cell culture incubator for 30 minutes to allow for gel polymerisation. To confirm gel polymerisation had occurred, collagen fibres were observed by phase contrast microscopy. To prevent the collagen/cell mix from drying out, 200μL HL-60 cell culture media was pipetted on top of the gel. Cell migration was monitored for 30 minutes with time-lapse microscopy. Imaging was conducted on three separate occasions; each time all cells in the FOV were tracked using the manual tracking software MtrackJ. Cells were only tracked if they remained in the FOV for the 30-minute window of imaging. The average speed of migration was 1.89 μm/min +/- 0.14 (***figure 4.16***).

As successful migration was observed in 2.5mg/mL collagen, this concentration of collagen was used in the trough of the 3D device. Due to time constraints, the pore size was not evaluated at this collagen concentration and no further examination of additional migration assays in alternative collagen concentrations were carried out.

Deleted: .

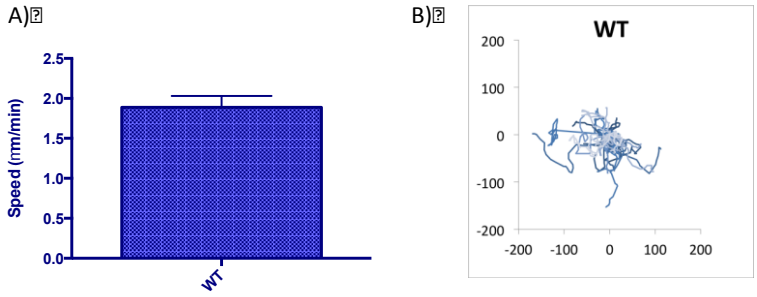

Figure 4.16: HL-60 migration through collagen gel
Differentiated WT L-selectin-GFP HL-60 cells (WT) were mixed into liquid collagen. Once the rat-tail collagen (2.5mg/mL) was polymerised, cell migration was observed using an inverted fluorescence microscope. The experiment was conducted on three separate occasions. In total 90 cells were tracked for a 30 minute period. A) The average speed was 1.89 μm/min +/-0.14; error bar represents the standard error of the mean. B) To visualise the length of cell trajectories, tracks were adjusted to have a 0,0 start point; X and Y-axis represent pixels.

4.2.6 Optimising the collagen depths with the 3D device

The depth of the collagen within the device was an important design feature (***table 4.1***). Indeed, the depth of the trough needed to allow neutrophil invasive migration for 1 or 2 hours, yet the depth needed to be compatible with the working distances of high magnification objectives in order to observe specific membrane protein localisation.

The working distance of an objective is the distance between the front edge of the objective lens and the specimen surface. In general, as the magnification of the objective increases the working distance decreases. Using the common working distance for a 60x oil immersion lens (Nikon) as 0.21mm, and taking into account the thickness of the coverslip (or base of the 3D device) as 0.085mm, the depth of the collagen should be no more than 0.125mm(0.21mm-0.085mm=0.125mm). By definition collagen is a hydrogel, capable of retaining large amounts of water within the three dimensional network. Therefore, it was important to monitor collagen depth experimentally. Three different volumes, 30μL, 50μL and 70μL of

2.5mg/mL rat-tail collagen were prepared as described in ***section 2.12.1***, and pipetted into the centre of the 0.5cm by 2.3cm trough. Prior to collagen deposition, devices were chilled on ice to prevent premature collagen polymerisation; the collagen was levelled by eye. Producing a level surface of polymerised collagen in a trough is problematic. Surface tension at the edges of the trough results in the collagen solution naturally forming a meniscus, setting thicker at the edges and thinner in the middle. To minimise this effect, the edges of the trough were lined with a hydrophobic barrier pen to reduce surface tension.

Once the collagen had polymerised within the troughs, HUVECs were seeded and left for 48 hours to form a confluent monolayer. Prior to imaging, HUVECs were stained with 1μM Celltracker™ Orange (see ***section 2.5.3***). Collagen depths were monitored with confocal microscopy using a line scan in Z. Using the stained endothelium and reflection microscopy for the collagen fibres the depth of collagen could be gauged. Line scans in Z were taken at four positions within each trough to determine collagen depths. Twelve troughs for each different collagen volume were analysed on three separate days. There were significant differences in the depths for each collagen volume. The mean depth for each volume was 132 μm +/- 22.9 (30μL), 536 μm +/- 29.2 (50μL) and 860 μm +/- 29.5 (70μL) (***figure 4.17***). Therefore, 30μL was used within the trough as this generated the optimal thickness to allow high-powered magnification imaging. Smaller volumes of collagen (10μL and 20μL) were trialled but were hard to manipulate, and frequently resulted in the collagen completely drying out and peeling away from the edges of the trough.

Deleted: μm

Deleted: 86μ

Deleted: 17

Deleted: .4

Deleted: 46

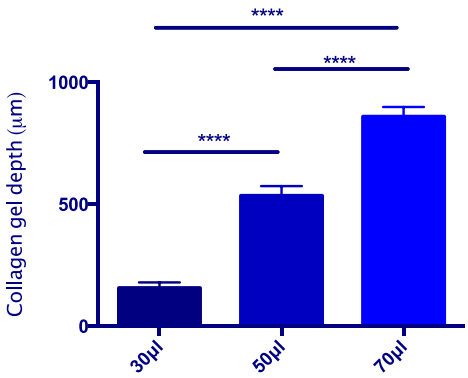

Figure 4.17: Optimising collagen depths within a trough
PDMS troughs (0.5cmx2.3cm) were filled with varying volumes of liquid collagen. Once polymerised the collagen supported a HUVEC monolayer. When confluent, this HUVEC monolayer was stained with 1µM Celltracker Orange. Collagen depths were assessed through confocal microscopy using a line scan in Z. Collagen fibres were imaged through reflection microscopy and the position of the endothelial monolayer was assessed through the Celltracker stain. For each collagen volume, 12 troughs were assessed with 4 line scans in Z for each trough. Statistical assessment was conducted using a one-way ANOVA followed by Tukey's multiple comparison tests. **** $p<0.0001$.

4.2.7 Generating a chemoattractant gradient within the 3D device

Another specification for the device was the production of a stable chemoattractant gradient produced in the collagen (***table 4.1***). To assess the gradient formation and stability in the 3D device, 30µL of 2.5mg/ml collagen was placed in the trough of the device and left to polymerise for 30 minutes. HUVECs were grown to confluence on top, prior to gradient assessment the monolayer was stimulated with TNF-α for 12-16 hours, to mimic the "leakiness" of the junction under inflammatory conditions. To visualise the HUVEC monolayer, the cells were stained with 1µM Celltracker™ Orange,(***section 2.5.3***). The gradient was formed using the source/ sink principle (***figure 4.18***). The source in these preliminary experiments was visualised with a 10,000 MW FITC-dextran. The weight of the dextran represents the average molecular weight of a chemokine ~8-11 kDa (***figure 4.9***). Introduction of the dextran was achieved through the use of a Harvard syringe pump, running at a rate of 0.2µL/min. The sink is the large reservoir of medium above the HUVEC monolayer. To establish a gradient, the volume of the sink must be either far larger than that of the source, or the sink

must be continually replenished to prevent accumulation of the FITC-dextran molecules. In experiments conducted in ***chapter 5***, cell medium above the HUVEC monolayer is continually being replenished by the parallel flow system. The HUVEC monolayer acts as a permeability barrier; dextran can only diffuse through the junctions between ECs. As a result, this physically constrains diffusion within the collagen gel, slowing down the release of the dextran from the gel into the medium.

To monitor the FITC-dextran movement through the collagen, line scans in Z were acquired using a 10X objective (***figure 4.18***). Confocal line scans were taken at regions proximal to the entrance of the microchannel either in XZ or YZ (***figure 4.19***). Images were acquired every minute for 60 minutes. The dimensions of the line scans were ~1.5 mm in the X or Y-axis and 150 μm in Z.

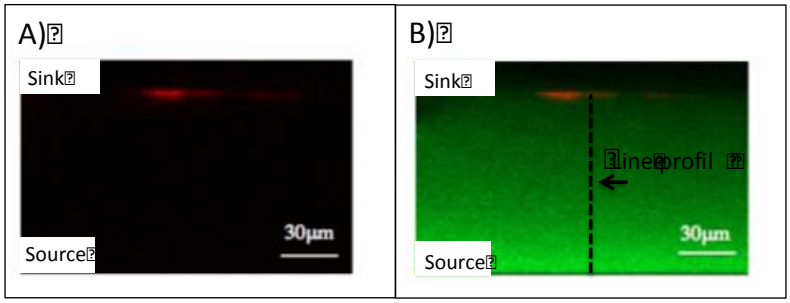

Figure 4.18: A line scan in XZ demonstrating FITC-dextran diffusion
Rat-tail collagen 2.5mg/mL (30μL) was added to the trough within the 3D device. Once polymerised, this matrix allowed formation of an endothelial monolayer. Prior to diffusion experiments, the endothelium activated and stained with 1μM Celltracker ™ Orange. FITC-dextran was introduced into one of the microchannels in the 3D device at a rate of 0.2 μm/min. Line scans in Z were taken to monitor diffusion profiles. A) Endothelium only. B) Dextran and endothelium. Post acquisition, line profiles (black dashed line) were taken through the transverse line scans Scale bar is 30μm.

Post acquisition, analysis was conducted on the line scans in XZ or YZ using a line profile intensity tool implemented in Fiji (***figure 4.18***). Fluorescence intensity values (F1) for each line profile were normalised with respect to the fluorescence intensity in the microchannel prior to diffusion (F0). In addition, background fluorescence (Fb) was subtracted from both F1 and F0. Three separate

experiments characterized the stability of the diffusion in time and along the XZ and XY axis (***figure 4.19***).

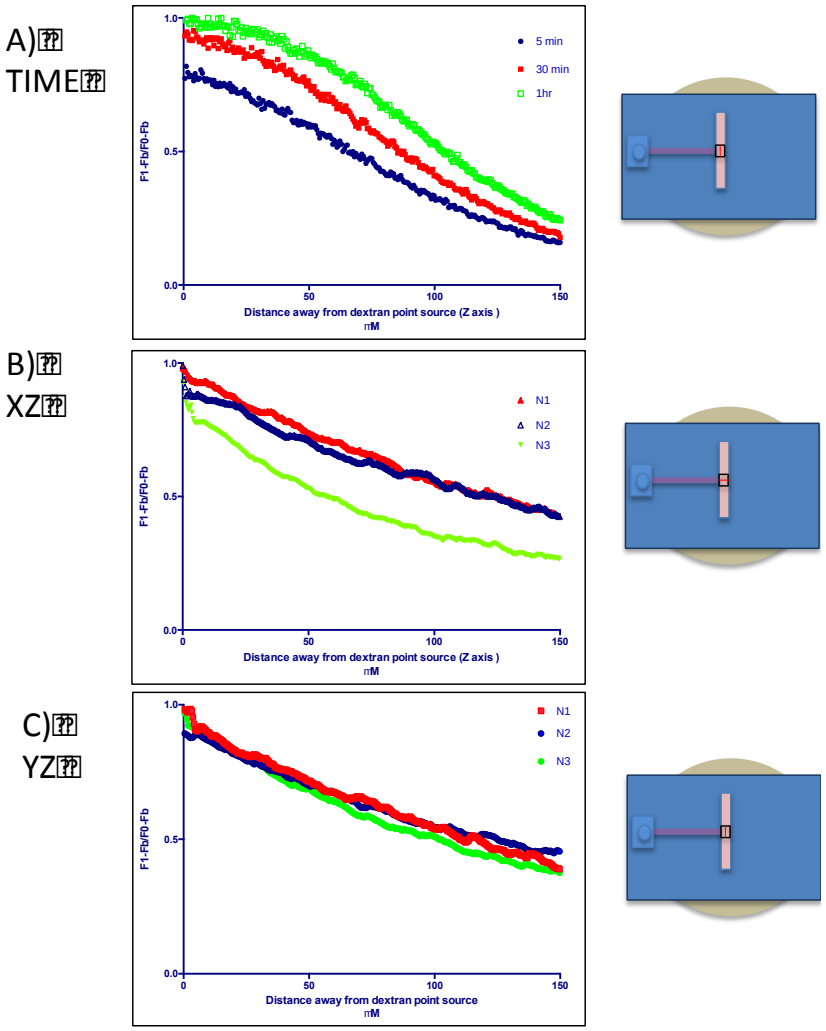

Figure 4.19: Fluorescence intensity line profiles demonstrating the establishment of a concentration gradient along the z axis.
A) A line scan in XZ (within the proximal region) was acquired every 1 minute. FITC-dextran diffusion over time was monitored by taking a line intensity profile (see black dashed line in ***figure 4.18 B***) from line scans in XZ at 5 minutes, 30 minutes and 1 hour. Background fluorescence values were subtracted from the fluorescence intensity values prior to normalisation. Data from one 3D device is shown. B) Three separate line scans in XZ were conducted within the

proximal region in three separate 3D devices. FITC-dextran diffusion was monitored 1 hour after dextran introduction by taking a line intensity profile (see black dashed line in ***figure 4.18 B)***. Fluorescence intensity values were normalised and background fluorescence removed. C) Experiments were conducted in the same way as B) except that a YZ line scan was acquired within the proximal region. Red line in each schematic right of the graph demonstrates the position of the line scan in z.

The FITC-dextran gradient remained relatively stable for 1 hour within the device (***figure 4.19 A***). Gradients formed in both the XZ and YZ were similar (***figure 4.19 B&C***) indicating that within this 1.5mm^2 region diffusion profiles were characterised. This 1.5mm^2 area will now be called the proximal region, and the far ends of the trough will be termed remote regions. The remote regions are expected to have a lower concentration of chemoattractant. Although this has not been fully explored using dextran modelled diffusion profiles, the diffusion of TRITC-dextran (10,000Da) in the proximal and remote positions have been observed using an inverted fluorescence microscope and show clear differences in fluorescence intensity (***figure 4.20***).

Deleted:

Deleted: fully characterised

Deleted: k

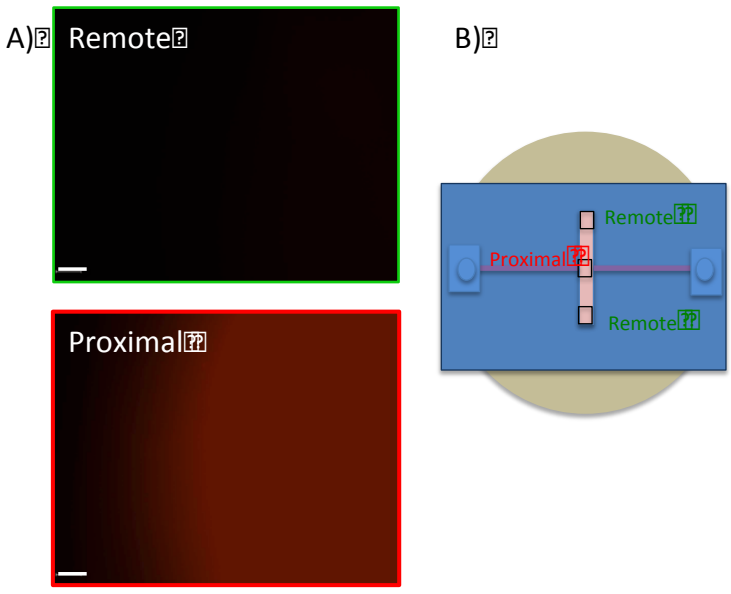

Figure 4.20: Gradient observation during flow assays
TRITC-dextran was introduced into a microchannel of the 3D device. Collagen and HUVEC are present, but not shown. TRITC-dextran could be observed in the proximal region of the 3D device, (B), but no TRITC-dextran could be observed in the remote region of the 3D device, (A). TRITC-dextran was observed using an inverted fluorescence microscope. Scale bar is 20µm. C) Schematic

indicating the locations of the remote and proximal regions (black rectangles) in the 3D device. Image acquisition parameters remained the same for both locations.

4.2.8 Optimising neutrophil recruitment under flow conditions

Introducing neutrophils under flow is important; shear stress is responsible for strengthening cell adhesion molecules, ***section 1.2.2***, (***table4.1***). Upon coupling the 3D device to the parallel plate flow chamber; it became apparent that the height of the PDMS in the 3D device played an important role in determining how the leukocytes interacted with the activated endothelium. When the PDMS height of the 3D device was > 4mm, HL-60 cells perfused through the device at 1.24 dynes /cm^2 failed to roll and form any interaction with the endothelium (***figure 4.21 B***). However, when the height of the device was controlled to ~2mm, HL-60 cells perfused across the 3D device were successfully captured from flow and underwent tethering and rolling (***figure 4.21 A***). Subsequently, the height of the 3D device was controlled through adding a constant volume of PDMS (~3mL) to the patterned wafer mould to yield devices with an approximate 2 mm height.

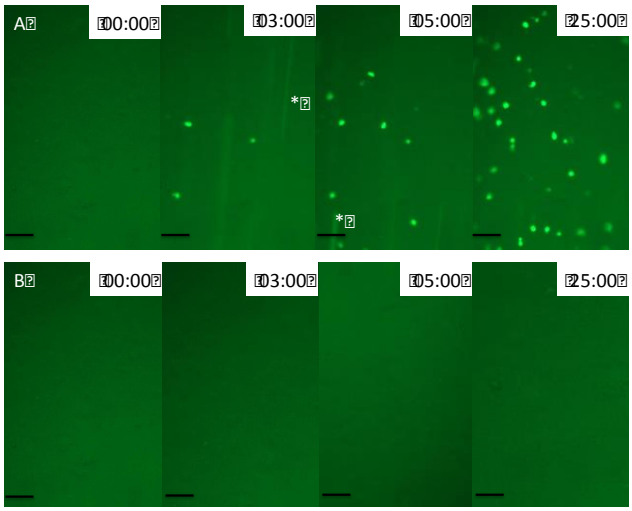

Figure 4.21: Leukocytes flowing across an activated HUVEC in the 3D device
Neutrophils (green) were perfused at 1.24 dynes /cm^2 across a cytokine activated endothelium within the 3D device. Neutrophil behaviour was monitored over time (0-25 minutes) using an inverted fluorescence microscope. A) A 3D device when the PDMS height is ~ 2mm. Neutrophils are captured from flow after 3-5 minutes. At 25 minutes, most neutrophils had been captured, and are firmly adhered to the endothelium and undergoing mTEM or fTEM events. B) When the PDMS

height was >4mm, neutrophils failed to be captured from flow. White asterisk denotes cells slowing down from the flow and starting to roll. Scale bar is 100μm. The timing of each panel is indicated in the right hand top corner.

4.3 Discussion

The ultimate aim of the work presented in this chapter was to design, manufacture and optimise two microfluidic devices to monitor a) cell migration when subjected to hierarchical chemical signals and b) the complete adhesion cascade coupled with interstitial chemotaxis.

4.3.1 The 2D device

The first aim of the project was to generate a device where leukocytes could be subjected to different chemoattractants with differential hierarchies. Through the use of a computerised flow control system, inlets can be independently and rapidly pressurised. The main channel of the device is connected via an array of microchannels to two side channels. A bifurcation channel allows two fluids to travel in parallel without mixing into one of the side channels. Through systematically altering the pressures at each inlet, an optimised inlet pressure protocol was empirically determined which allowed a rapid switch in the chemoattractants that the cells were exposed to (***figure 4.6***). Altering the pressures at the inlets connecting to the bifurcation channel allows a rapid exchange of fluids diffusing into the main chamber; the new fluid stabilises within 1 minute, becoming a stable linear gradient in the main channel (***figure 4.6 & figure 4.7***) with the previous fluid disappearing. Importantly, the gradient produced from the opposite side channel remains stable after the pressure switch and resultant fluid exchange in the opposite side channel. Here, the 2D device produces two stable linear gradients of opposite slopes for 20 minutes in the main channel (***figure 4.7***). The 2D device enables cells to respond to one chemoattractant initially (for 20 minutes) then be exposed to the other while still in the presence of the initial chemical cue (***figure 4.5***). The gradients were established through an empirical approach that was time consuming for both optimisation and analysis. To define diffusion, fluorescence intensities were analysed over time from two transverse line profiles taken across the width of the main channel at two FOVs (50μm and 250μm from the start of the first

microchannel). In order to interpret diffusion throughout the main channel, it would be advantageous to simulate this. COMSOL® is a software platform that is routinely used to model diffusion gradients within microfluidic devices. For this, the diffusion coefficient of the monitored chemokine would be required alongside the geometry of the device.

In future studies, the 2D device could be used to monitor the cellular response to both end-target and intermediary chemoattractants, paying particular attention to L-selectin shedding. To monitor L-selectin shedding in real time, neutrophils could be incubated with the fluorescently conjugated non-function blocking antibody LAM1-14 and their response to an array of chemotactic molecules could be investigated to understand if shedding is a prerequisite to chemotaxis towards certain molecules.

4.3.2 The 3D device

The 3D device will allow researchers for the first time to interrogate all aspects of the multi-step adhesion cascade. Currently, two disjointed experimental techniques are used to explore the adhesion cascade in humans: (i) recruitment from flow on to 2D endothelial monolayers and (ii) interstitial migration through 3D environments. It is highly likely that interstitial migration could be heavily influenced by mechanotransducive force. Indeed, exposure to shear stress may be an essential prerequisite to the molecular events that lead to interstitial migration. Thus, this device will allow investigation of fundamental questions that can only be explored *in vivo* while affording the user a higher degree of control over the environmental conditions than can be achieved *in vivo*.

The device was designed around a series of criteria to image the whole adhesion cascade as a continuous event (***table 4.1***). Devices were reproducibly manufactured with approximate 135μm vertical height of collagen to allow for high magnification imaging. Incorporation of a hydrophobic coating around the perimeter of the PDMS trough prevented formation of a collagen meniscus thus levelling the collagen within the 3D device.

To measure chemokine gradients, microchannels introduced 10,000Da fluorescent dextran into the collagen gel, which reliably produced a linear gradient in a 1.5mm^2 area, also known as the proximal region. The gradient was stable over a 60-minute period. However, it is important to note that the diffusion profiles of the dextran do not represent the diffusion profile of the end-target chemoattractant fMLP. Indeed, as the molecular weight of fMLP is 437.55 Da, fMLP would diffuse further than chemokines within the gel matrix. In the future, an alterative method of chemokine visualisation could be used. Incorporation of a fluorescent dye at the c-terminus of chemokines would allow direct monitoring of their gradients. This has already been achieved with the chemokines- CCL7, CCL1, CCL3 and CXCL8. These labelled chemokines displayed wild type behaviour in receptor binding and calcium mobilisation assays(354).

Deleted: k

Using reflection microscopy, collagen fibres were visualised and pore size diameters were estimated through pixel distance mapping. The importance of collagen concentration and polymerisation temperature was characterised. Differentiated HL-60 cells successfully migrated through 2.5mg/mL rat-tail collagen at an average speed of 1.89μm/min.

The device has also been successfully interfaced with the parallel plate flow chamber allowing capture of leukocytes by the endothelium from flow conditions.

4.3.3 Final thoughts

To conclude, this chapter has developed two proofs of principle devices, the 3D device will be used in chemotactic experimentation in the following chapter, ***chapter 5***.

Chapter 5. Understanding the role of L-selectin shedding in regulating neutrophil chemotaxis through 3D scaffolds.

5.1 Biological rationale

Interstitial leukocytes are required to undergo chemotaxis to arrive to their target site, a process that is highly dependent on cell polarity. Numerous chemoattractants are responsible for regulating chemotaxis. Over the past ten years, several studies have demonstrated that L-selectin is responsible for mediating a cell's chemotactic ability. Several studies have documented that the absence of L-selectin, and the prevention of L-selectin shedding inhibits directed migration towards chemoattractants (284)(212)(264), with little understanding of the mechanism behind these observations. Alternatively, L-selectin can act as a signalling molecule to enhance both CXCR4 and CCR7 driven chemotaxis, see ***section 1.11.2***, (292)(290). As very few chemoattractants have been studied in respect of L-selectin-dependent chemotaxis, it is not clear whether L-selectin also regulates chemotaxis towards end-target chemoattractants.

The data presented in ***chapter 3*** outlined that polarity and migration defects were produced in both primary human neutrophils and HL-60 cells when L-selectin shedding was blocked either pharmacologically or genetically. The data presented in ***chapter 4*** describes the fabrication and optimisation of a bespoke device that carries the potential to observe the entire multi-step adhesion cascade: from leukocyte capture from flow to chemotaxis within a 3D collagen matrix. The work from the two previous chapters will be integrated into this final chapter to understand how L-selectin shedding impacts chemotaxis towards intermediary or end-stage chemoattractants.

The main body of work discussed in this chapter uses the self-designed self-generated 3D device (***chapter 4***). This device is open top, allowing easy coupling of the parallel plate flow chamber to the collagen-supported endothelium, see ***figure 4.8***, for a more detailed description. The device has two feeder microfluidic channels, which allow chemoattractant to diffuse through the collagen. Leukocyte interactions with the apical surface of the endothelium can be monitored in real time, using an inverted fluorescence time-lapse microscope. Additionally,

Deleted: introduction into the

monitoring fluorescently conjugated dextran molecules enabled assessment of the chemoattractant gradient. Gradients were maintained using the source and sink principle. Here, chemoattractant introduced from the microchannel (source) is so small in volume compared to the constantly replenishing HL-60 media (sink) that the media will never become saturated with chemoattractant. In this system the cytokine activated HUVEC acts as a semi-permeable barrier between the source and sink see ***section 4.2.7.***

As shown in ***section 4.2.4***, collagen pore size is heterogeneous (no uniform pore size), and the size of the pores generated is highly dependent on protein concentration, polymerisation time and temperature. To control for this pore size heterogeneity the above conditions remained constant and co-perfusion of control and experimental cell lines were carried out where possible. Such co-perfusion studies could not be conducted using primary human neutrophils, as blocking the shedding of these cells could only be achieved using a the soluble synthetic inhibitor TAPI-0, here TAPI-0 was required to remain present throughout the assay time. Therefore, "minus inhibitor (DMSO)" experiments could not be conducted with "plus inhibitor (TAPI-0)" primary neutrophils. All studies conducted in this chapter use 2.5mg/mL rat-tail collagen, which is prepared as described in ***section 2.12.1***.

Deleted: ,

Deleted: co

Deleted: which was achieved through continued exposure.

Deleted: In other words

Deleted: inhibitor

Deleted: inhibitor

5.2 Results

5.2.1. Blocking L-selectin shedding alters directional migration of HL-60 cells within collagen matrices.

To comprehend if L-selectin shedding contributed to neutrophil migratory behaviour within the ECM, HL-60 cell expressing: WT or ΔMN L-selectin-GFP or GFP alone were individually mixed with liquid rat-tail collagen into wells within 96 well plates, see ***section 2.12.1*** for instruction on collagen preparation. Here, neutrophils had no prior exposure to endothelial cells or chemoattractants. Once the collagen had polymerised (to create a surrounding 3D scaffold), neutrophil movements were recorded for 30 minutes using an inverted time-lapse fluorescence microscope, 3 fields of view (FOV) were selected at random within each well of a 96 well plate. All the cells within each FOV were manually tracked

using the Fiji plugin, MtrackJ, to quantify cell speed and directionality, see ***section 2.5.2***.Cells exiting the FOV during the 30-minute imaging period were excluded from analysis.

Expression of either WT or ΔMN L-selectin-GFP into the HL-60 cells produced no significant difference in cell speed compared to GFP cells (***figure 5.1 A***). WT, GFP and ΔMN cells averaged a speed of 1.89 μm/min +/- 0.14, 1.83μm/min +/- 0.13 and 1.86μm/min +/- 0.16, respectively. Comparatively, there was a significant difference in the directionality of migration between the three cell lines (***figure 5.1 B&C***). WT Cells had the greatest directional persistence with an averaged directionality ratio of 0.42 +/- 0.04, while GFP and ΔMN displayed reduced straightness of travel, 0.29+/-0.03 and 0.25+/-0.03, respectively.

Deleted: dramatically

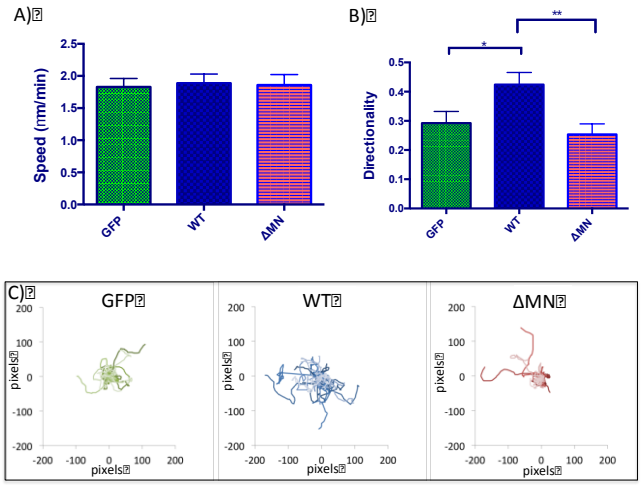

Figure 5.1: Expression of WT L-selectin augments directional migration of HL-60 cells within 3D collagen scaffolds.

WT, ΔMN or GFP cells were separately mixed into liquid rat-tail collagen (2.5mg/mL). Cells ($1x10^6$) were mixed into 100μL of collagen and introduced into a well of a 96 well plate. Collagen polymerisation took place at 37 °C under humidifying conditions for 30 minutes. Cell migration was imaged every 30 seconds and cells were tracked manually for 30 minutes with the Fiji plugin MtrackJ. A total of 90 cells were tracked for each cell line, conducted across 3 independent experiments. A) Cell speed. One-way ANOVA, followed by Tukey's multiple comparisons test. B) Directionality ratio. One-way ANOVA followed by Tukey's multiple comparisons test. * $p<0.01$, **$p<0.001$. C) Representative tracks (WT=41, GFP=32 ΔMN=25) from one experiment start of each track is superimposed at a 0,0 origin.

5.2.2 Blocking L-selectin shedding impairs invasion into collagen matrices under static conditions

As HL-60 cells expressing WT, and therefore cleavable, L-selectin displayed significantly greater directional persistence in migration within a 3D collagen matrix compared to GFP and ΔMN cells. Previous experiments outlined in ***figure 3.24 A*** revealed that little difference in TEM rates were observed between WT and ΔMN cells. This would suggest that, under static conditions, HL-60 cells undergoing TEM would likely be equal between WT and ΔMN cell lines, but possibly differ in respect of their invasion through collagen scaffolds. To gauge if blocking L-selectin shedding influenced cell invasion, the depths of migration through the collagen scaffold was measured at two time points: 1 hour and 4 hours. Experiments were initially conducted on primary human neutrophils (pre-treated for twenty minutes with either the DMSO carrier or 10μm TAPI-0). The TAPI-0 and DMSO treated primary neutrophils could not be used in conjunction with one another. This static assay was designed as described in ***section 2.12.4***, for simplicity a "trough" is manufactured from excising a cuboid of PDMS. The remaining PDMS frame is then plasma bonded onto a glass 5cm coverslip, within the "trough" 50μL of collagen is left to polymerise, after which acts as a scaffold for the HUVEC monolayer. For each of the two time conditions (1 hour or 4 hour) 3 separate static transmigration assays (or troughs) were conducted. Primary neutrophils were labelled with Celltracker Orange (see ***section 2.5.3***), for easy identification.

Deleted: -

Deleted: -

After 1-hour or 4-hours of neutrophil incubation with the endothelium, PBS was carefully introduced to remove any unbound neutrophils, then the sample was fixed with 4% PFA, permeabilised and then labelled with FITC phalloidin. Cell depths were monitored through spinning disk confocal microscopy, taking Z stacks directly below the endothelium. The Z stack position was chosen at random, with the only criteria that the endothelial monolayer was intact and complete. Stacks were discarded if the endothelium was not intact (which could have lifted off during fixation and staining procedures). To avoid bias, Z stack

position was chosen when only the endothelium was in focus to avoid preferentially picking areas rich or void of neutrophil migration. For each static assay (e.g. one trough) three Z stacks, were taken at random positions, each stack was composed of 200 slices each 1 µm thick. Taking multiple positions within a trough controlled for the heterogeneous nature of the collagen. Cell depths were manually enumerated post image acquisition at 10 µm increments, (equivalent to 10x 1 µm slices), ***figure 5.2 A***. In short, the 200µm stack was divided into 20 sub-stacks (each 10 µm in depth) and the amount of neutrophils in each sub-stack scored. To aid neutrophil visualisation a 16-colour scale heat map was applied. The heat map directly correlates to fluorescence intensity. Here, cells within the field of focus (higher fluorescence intensity) were distinguishable by a hotter colour e.g. red, compared to a cell not within the field of focus (lower fluorescence intensity), which had a colder colour e.g. blue (***figure 5.2 B***).

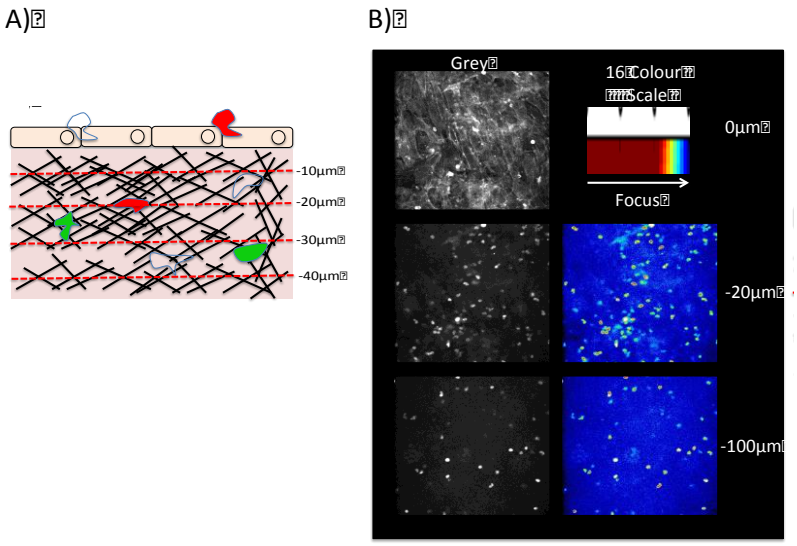

Figure 5.2: Cell invasion assay
Each assay was conducted in the 3D device, where TNF-activated endothelial monolayers were established on a bed of 2.5mg/mL rat-tail collagen. Static assays were conducted for either 1 or 4 hours, after which samples were fixed in 4 % PFA and stained with FITC-phalloidin. Neutrophils were observed through spinning disk confocal microscopy, using a 30x oil immersion lens. Three Z stacks (comprising of 200 slices each 1µm thick) were taken beneath the endothelium for each trough. (A) Schematic representing the uniquely stained HL-60 cell lines, which were labelled with separate distinct fluorescence dyes that could be distinguished with the spinning disc confocal

Deleted: unique

Deleted: fluorescence

microscope. Each 200µm stack was sub divided into 20 lots of 10µm stacks. Cell within each 10 µm subsection were scored. (B) To visualise neutrophils a 16-colour scale was applied to the acquired images, using the image visualising software, Fiji. Here, the colour scale directly correlates with the fluorescence intensity.

Quantification revealed that in the 1-hour assay primary neutrophils migrated significantly deeper in the collagen bed when treated with the DMSO carrier (***figure 5.3 A***). Pre-incubation with 10µm TAPI-0 appeared to decrease the "invasiveness" of neutrophils (***figure 5.3 A***). The averaged mean invasion depths at 1 hour were -36.4µm +/- 2.10 and -45.8µm +/- 3.30 for TAPI-0 and DMSO treatments, respectively. However, no recognisable differences where observed in the 4-hour static transmigration assay (***figure 5.3 B***). As TAPI-0 was present in the cell culture media throughout the duration of this assay it is not possible that the concentration of TAPI-0 was diluted. However, long-term effects of TAPI-0 incubation are unclear, it is possible that over time the inhibitor stability is compromised. To clarify whether preventing L-selectin shedding did reduce the "invasive behaviour", the assay was repeated using the HL-60 cell lines: WT, ΔMN and GFP. The assays were conducted as described above. However, unlike the primary neutrophil assay, here, all the three cell lines were mixed and co-introduced on to TNF-α-activated endothelial monolayers. Each cell line was uniquely labelled with different cell tracker dyes for easy identification (see ***section 2.5.3***). To avoid bias and prevent a dye producing an adverse effect on cell behaviour, dyes were exchanged periodically between lines for each repeat.

Deleted: 37

Deleted: 79

Deleted: 3.3 for

Deleted: "

Deleted: ¶
¶
¶

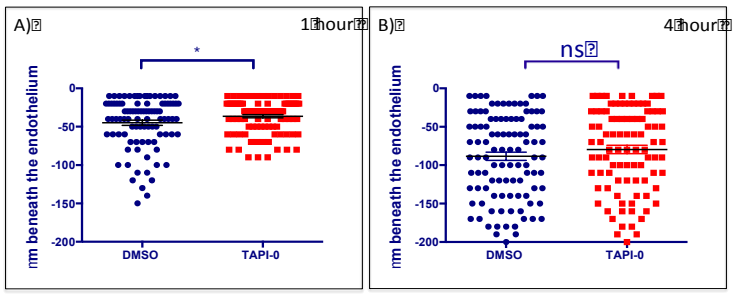

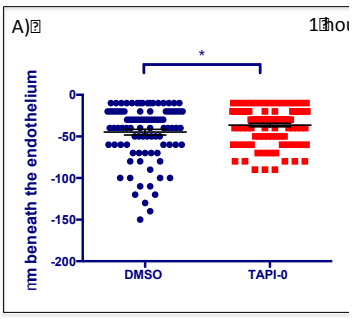

Deleted:

Figure 5.3: Blocking L-selectin shedding in primary neutrophils reduces invasion
Primary neutrophils were isolated and pre-treated with either a DMSO carrier or 10 µm TAPI-0 for twenty minutes. Neutrophils were incubated on a confluent TNF-α-activated endothelial

monolayer supported on a bed of rat-tail collagen. Static transmigration assays were conducted then fixed with 4 % PFA, permeabilised and stained with FITC-phalloidin. Neutrophil invasion was manually enumerated, as described in ***figure 5.2***. Error bars represent the standard error +/- of the mean. Each data set represents three separate static transmigration assays, where each assay has three 200µm deep stacks A) Distribution of migratory positions within the collagen after 1 hour static migration. A total of 150 and 146 cells were scored for TAPI-0 and DMSO conditions, respectively. Statistical analysis, unpaired Student t test, *p<0.01. B) Distribution of migratory positions within the collagen after 4-hour static migration. A total of 178 and 201 cells were scored for TAPI-0 and DMSO conditions, respectively. Statistical analysis unpaired Student t test.

Importantly, when the assay was conducted using the cell lines, a significant defect in invasion was observed in ΔMN cells (***figure 5.4***). This defect was observed in both the 1-hour and 4-hour time scales, possibly suggesting that the navigation of HL-60 cells is more cumbersome through the collagen scaffold than primary human neutrophils. Additionally, over the 4-hour assay the lack of L-selectin decreased invasion (***figure 5.4***).

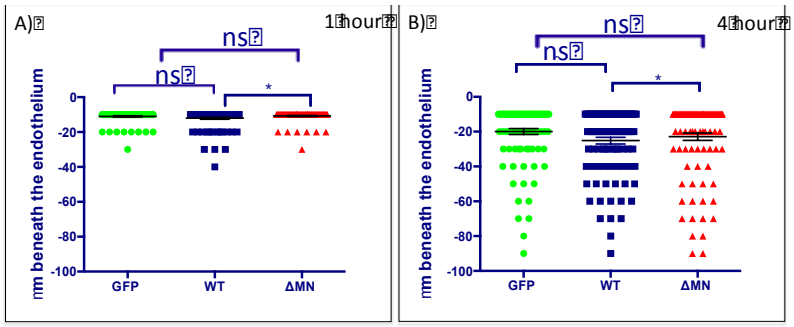

Figure 5.4: WT L-selectin increases invasiveness of HL-60 cells through collagen.
The HL-60 cell lines: WT, ΔMN and GFP were added to confluent TNF-α-activated endothelial monolayer, which were established on a bed of collagen. To ensure identification of each cell line, cells were labelled with 1 µM Celltracker ™(orange, far red or unlabelled). To protect against bias, Celltracker ™ dyes were interchanged between cell lines for each independent experiment. Static transmigration assays were conducted and then fixed and stained with 4 % PFA and FITC-phalloidin, respectively. Neutrophil invasion was manually scored, as described in ***figure 5.2.*** Error bars represent the standard error +/- of the mean. Each data set represents three separate static transmigration assays. A) Distribution of migratory positions within the collagen after 1 hour of adding HL-60 cells to activated endothelial monolayers. A total of 98, 94, 118 cells were scored for GFP, ΔMN and WT, respectively. Statistical analysis, one-way ANOVA followed by Tukey's multiple comparisons test, *p<0.01. B) Distribution of migratory position within the collagen after 4 hours of static migration. A total of 112, 123, 97 cells were scored for GFP, ΔMN and WT, respectively. Statistical analysis, one-way ANOVA followed by Tukey's multiple comparisons test, *p<0.01.

Deleted: ¶

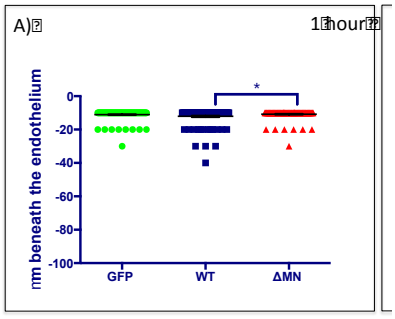

5.2.3 Understanding the effect of L-selectin shedding in regulating chemoattractant-driven invasion in primary neutrophils

Under static conditions, it was apparent that blocking L-selectin shedding decreased the neutrophil invasiveness through collagen matrices. Hydrodynamic shear stress is a fundamental feature of the leukocyte adhesion cascade. This could indeed act as a vital priming step for neutrophils prior to their exit from the circulation. To mimic a more physiologically relevant assay, the assay was conducted under flow conditions. In addition the following chemoattractants were perfused beneath the collagen gel: fMLP, IL-8 and Gro-α, as described in ***section 4.2.7***. All the remaining work described in this results chapter uses the 3D device, for full description see ***section 4.2***. It is noteworthy to mention that 30μL of collagen is present in each 3D device. The depth (measured between coverslip base to endothelium of this collagen) averaged 132 μm +/- 22.9, therefore often the 200 μm Z stack used imaged past the collagen and through to the cover glass. The large Z stack (200 slices x 1 μm thick) ensures that all cell invasions are recorded.

Deleted: 86

Primary neutrophils, pre-treated for twenty minutes with either the DMSO carrier or 10 μm TAPI-0, were introduced into the 3D device at 1.24 dynes/cm^2 for five minutes. Introducing neutrophils at a density of 0.5x10^6/mL ensured good binding to the underlying activated endothelium. After 5 minutes, neutrophil perfusion was ceased and replaced with cell culture media (supplemented with 10 μm TAPI-0, where appropriate). Chemoattractants were delivered using a Harvard syringe pump, at a flow rate of 0.2 μl/min, which was initiated after the 5-minute perfusion of neutrophils. It is noteworthy to mention that the gradient profiles were only characterised for a maximum of 1 hour, ***section 4.2.7***. Therefore gradient stability could only be guaranteed for 1 hour. Chemoattractants were used at a concentration of 200nM fMLP, 100ng/mL IL-8 and 100ng/mL Gro-α. The concentrations for fMLP and IL-8 had previously been used in micropipette assays, (***figures 3.20 & 3.21***), and successfully promoted HL-60 chemotaxis.

Controls assays were also performed using 3D devices without the presence of chemoattractant. After the 2-hour perfusion the 3D devices were prepared for spinning disk confocal imaging and analysis, as described in ***section 5.3.2***. For each 3D device, Z stack imaging was acquired in the trough at positions remote and proximal to the chemoattractant source, see ***figure 4.20***. For each 3D device, 6 Z stacks were imaged (3 proximal and 3 remote with respect to the chemoattractant source), unless stated otherwise data from these stacks are pooled. For each chemoattractant (fMLP /Gro-α/IL-8) a total of 3 separate 3D devices were used. As above in ***section 5.2.2***, Z stacks were only imaged if the endothelium was intact.

Treatment of primary neutrophils with 10 μM TAPI-0 led to a significant decrease in cell invasiveness compared to their DMSO controls in the presence of fMLP or Gro-α or absence of chemoattractant (***figure 5.5***). The average invasive depth of primary neutrophils chemotaxing towards a gradient of fMLP was -45.3 μm +/- 0.6 and -32.7 μm +/- 0.60 and, in the presence of DMSO and TAPI-0, respectively. Interestingly, blocking L-selectin shedding did not alter chemotaxis and therefore the invasiveness towards IL-8. This suggests IL-8-dependent chemotaxis is not influenced by L-selectin shedding (***figure 5.5***). The average invasive depth of neutrophils chemotaxing towards a gradient of IL-8 was -48.1 μm +/-1.08 and -46.5 μm +/-0.50, in the presence of DMSO and TAPI-0, respectively.

Deleted: device 6

Deleted: 2

Deleted: 68

Deleted: 06

Deleted: 46

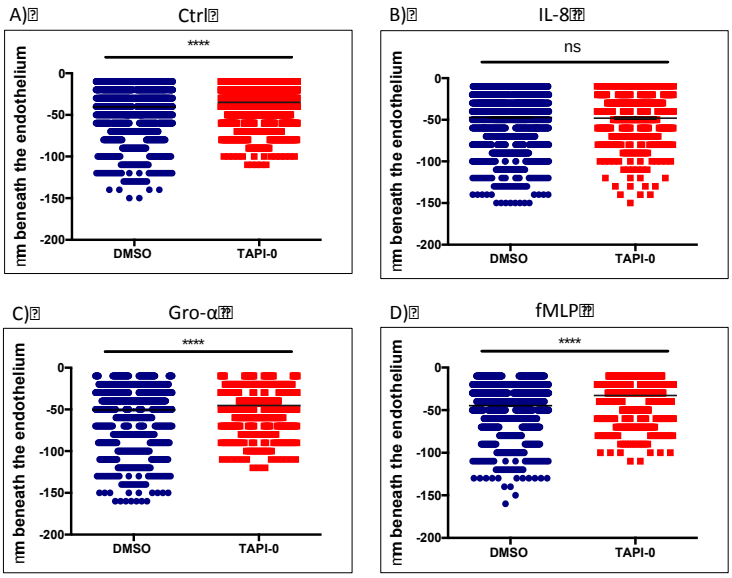

Figure 5.5: Blocking L-selectin shedding reduces invasiveness towards gradients of fMLP and Gro-α, but not IL-8.
Primary neutrophils were pre-treated for twenty minutes with either a DMSO carrier or 10μM TAPI-0. Prior to the assay neutrophils were labelled with 1 μM Celltracker ™ Orange for post acquisition analysis. Neutrophils were perfused across TNF-α- activated HUVEC monolayers. Each assay was conducted for 2 hours, after which the 3D devices were fixed in 4% PFA, and F-actin was labelled using FITC-phalloidin. Neutrophil position within the collagen gels were imaged using spinning disc confocal microscopy and manually scored, as described in ***figure 5.2***. Error bars represent the standard error +/- of the mean. Each data set represents the three independent experiments, and data sets are pooled from a minimum of 6 Z stacks. A) Invasion assay in absence of chemoattractant. A total of 3740 and 2985 cells were scored for TAPI-0 and DMSO treatments, respectively. Statistical analysis, unpaired Student t test **** $p<0.0001$. B) Invasion assay in the presence of 100ng/mL IL-8. A total of 2572 and 2286 cells were counted for TAPI-0 and DMSO treatments, respectively. Statistical analysis unpaired Student t test. C) Invasion assay in the presence of 100ng/mL Gro-α. A total of 820 and 1072 cells were counted for TAPI-0 and DMSO treatments, respectively. Statistical analysis, unpaired Student t test **** $p<0.0001$ D) Invasion assay in the presence of 200nM fMLP. A total of 989 and 1836 cells were counted for TAPI-0 and DMSO treatments, respectively. Statistical analysis, unpaired Student t test **** $p<0.0001$

Side-by-side comparisons of the invasive depths of neutrophils responding to chemoattractants revealed a significant increase in invasiveness in the absence of TAPI-0 (***figure 5.6A***). This data clearly showed that all chemoattractants were bioactive in the bespoke flow chamber assay. Although the use of TAPI-0

dramatically reduced the invasive depth of most of the conditions tested, the most affected by the treatment was when neutrophils were chemotaxing towards fMLP gradients (***figure 5.6B***). As previously shown in ***section 3.2.14*** challenging primary neutrophils with fMLP promotes robust L-selectin shedding. This suggests implies that L-selectin shedding is potentially linked to fMLP-dependent chemotaxis, whereas chemotaxis towards Gro-α or IL-8 may involve another mechanism that is only partially dependent on L-selectin shedding.

Deleted: all

Deleted: strongly

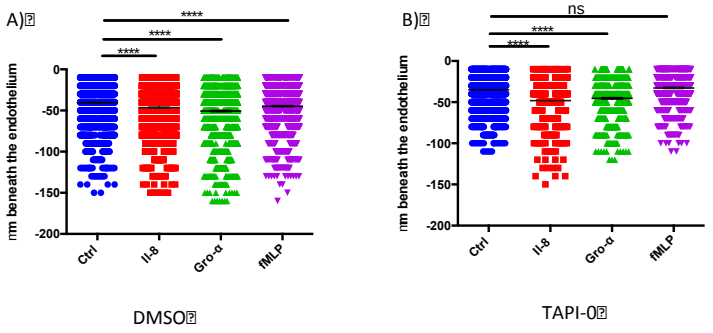

Figure 5.6. Side-by-side comparison of neutrophil invasiveness towards different chemoattractant gradients
The data generated in ***figure 5.5*** was reconfigured to confirm that the chemoattractants used were all biologically active. A) DMSO treated cells: a total of 2985, 2286, 1072 and 1836 cells were counted for the conditions: no chemoattractant (Ctrl), IL-8, Gro-α and fMLP, respectively. One-way ANOVA, followed by Dunnett's multiple comparisons test. **** $p<0.0001$. B) Invasiveness of TAPI-0-treated cells: a total of 3740, 2572, 820 and 989 cells were counted for the conditions: no chemoattractant (Ctrl), IL-8, Gro-α and fMLP, respectively. One-way ANOVA, followed by Dunnett's multiple comparisons test. **** $p<0.0001$.

As mentioned previously, based on the microfluidic delivery of chemoattractant to the "trough" of the 3D device, it is possible to designate regions that are proximal and remote to the source of chemoattractant (see ***figure 4.20***). To confirm that the observed invasiveness was dependent on the chemoattractant concentration, data from ***figure 5.5*** was reconfigured so that the invasive depths of neutrophils from the proximal and remote regions could be compared directly. Furthermore, under situations where no chemoattractant was used, the analysis of invasive potential of neutrophils at proximal or remote regions would allow an

insight into the contribution of variations in shear stress as a result of the geometry of the device. Interestingly, no significant difference in invasive depths was observed in regions that were remote or proximal when there was no chemoattractant present, validating that the geometry of the 3D device did not bias neutrophil invasiveness (***figure 5.7 A***). For DMSO treated cells the depth of migration was 48.7μm +/- 1.02 and 54.4μm +/- 1.83 for remote and proximal regions, respectively. Quantification of invasive depths of neutrophils responding to IL-8 revealed significantly greater invasive depth within proximal compared to remote regions. As shown in the pooled data (see ***figure 5.7 B***), inclusion of TAPI-0 in the assay did not affect neutrophil invasiveness towards a source of IL-8. This observation suggests that primary human neutrophil chemotaxis is independent of L-selectin shedding (***figure 5.7 B***). Neutrophil chemotaxis towards Gro-α appeared to be strongly dependent on concentration, as the invasive depths of neutrophils varied dramatically at proximal and remote areas in DMSO-challenged assays (***figure 5.7 C***). Although the statistical significance between proximal and remote regions of neutrophils chemotaxing towards Gro-α was higher in TAPI-0 than DMSO-treated cells (***figure 5.7 C***), the overall depth of invasiveness was greater in the remote regions – for both treatments DMSO or TAPI-0 (***figure 5.7 C***). For DMSO treated cells the depth of migration in response to Gro-α was 68.7μm +/- 5.2 and 56.1μm +/- 1.61 for remote and proximal regions, respectively. As increased invasive depth was confined to the remote region, it would suggest that the effect of Gro-α on primary human neutrophils is concentration-dependent. Neutrophil chemotaxis towards fMLP revealed no significant difference in invasiveness with DMSO-treated cells (***figure 5.7 D***). This could be explained through the comparatively small size of fMLP (~20 fold smaller than IL-8 and Gro-α). The size difference is likely to have a dramatic impact on the diffusion of fMLP through the collagen matrices. Although the effect of TAPI-0 led to reduction in neutrophil invasion in both remote and proximal regions, the effect of the inhibitor on neutrophils invading proximal regions of the 3D device was significantly higher (***figure 5.7 D***). These outcomes suggest that chemotaxis of neutrophils towards fMLP is concentration-dependent, but the effect of TAPI-0 could be more efficacious in proximal regions where the fMLP concentration is likely to be much higher than within remote regions.

Deleted: α was

Deleted: fold

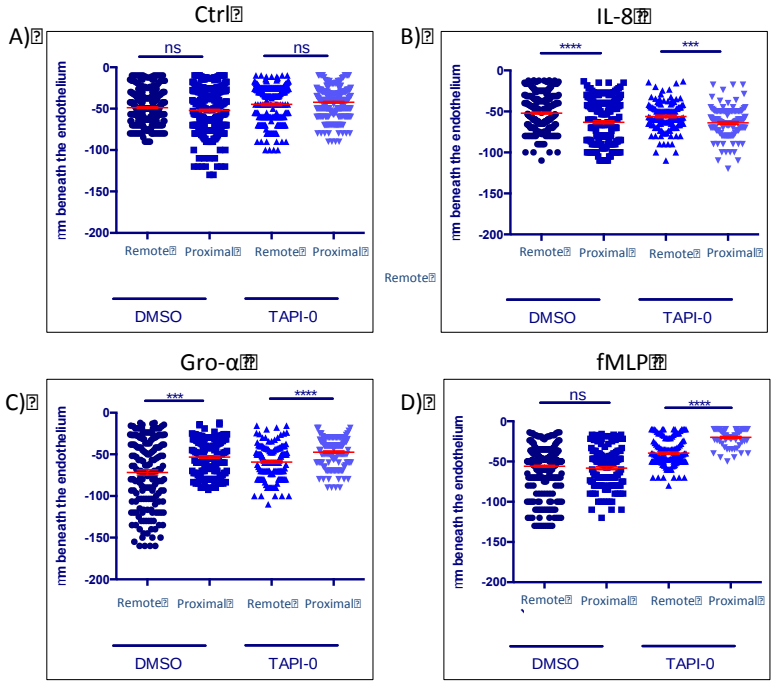

Figure 5.7: Primary neutrophil chemotaxis through collagen matrices is concentration-dependent.
The data generated in ***figure 5.5*** was reconfigured to gain further insight into the effect of chemoattractant concentration on neutrophil invasion. For each chemoattractant used, approximately 400-1200 cells were scored for each region (proximal or remote) of the 3D device. Statistical analysis: unpaired Student *t* test, comparing relative proximal and remote regions for the same cell treatment. ***p<0.001,****p<0.0001. A) No chemoattractant present (Ctrl). B) 100ng/mL IL-8. C) 100ng/mL Gro-α. D) 200nM fMLP

5.2.4. Understanding the effect of L-selectin shedding in chemotaxis of HL-60 cells through collagen matrices.

Blocking L-selectin shedding in primary neutrophils dramatically reduces 3D chemotaxis towards a gradient of fMLP (***section 5.2.3***). However, blocking L-selectin shedding did not significantly alter chemotaxis towards IL-8. As mentioned previously, fMLP and IL-8 have been categorised as an end-target and intermediary chemoattractant, respectively. ***Section 5.2.3*** suggests that chemotaxis towards fMLP is dependent on L-selectin shedding, while chemotaxis towards the intermediary chemoattractant; IL-8 (and possibly Gro-α) is

independent of L-selectin shedding. In order to determine if the effect of TAPI-0 was directly targeting L-selectin shedding and not a secondary target, similar experiments were conducted using the previously engineered HL-60 cell lines: GFP, WT and ΔMN. Experimentation and analysis was performed as described in ***section 5.2.2***. Unlike with assays using primary human neutrophils, all three HL-60 cell lines could be co-perfused. This co-perfusion tightly controlled for collagen gel heterogeneity within the 3D device. Analysis was performed as described in ***section 5.2.2***. Unfortunately, due to time constraints of the project, chemotaxis towards Gro-α was not conducted.

Expression of WT L-selectin promoted a significant increase in invasive depth of HL-60 cells, compared to GFP and ΔM-N cells (***figure 5.8 A***). This data corroborates with what has been shown for THP-1 monocytes, albeit using a slightly different parallel plate flow chamber assay(212). The average invasive depths of WT, ΔMN, GFP cell lines migrating without the presence of a chemoattractant was: –17.87 μm +/- 0.64, -15.28 μm +/- 0.63 and -15.59 μm +/- 0.62, respectively. Significant differences were observed between WT and ΔMN and WT and GFP. No difference was observed between ΔMN and GFP cells, indicating that the lack of L-selectin and preventing L-selectin shedding both hinder cell invasion depths, this data reflects ***figure 5.1 B***, where WT cells have a greater directional persistence irrespective of chemoattractant presence. Although expression of WT L-selectin promoted HL-60 cell invasiveness in the absence of chemoattractant (***figure 5.8 A***), no significant difference in chemotaxis towards fMLP was observed between WT and GFP cells (***figure 5.8 B***). In contrast, ΔMN cells were significantly less chemotactic towards fMLP compared to both WT and GFP cells (***figure 5.8 B***), suggesting, as shown in primary human neutrophils, that chemotaxis towards fMLP is strongly dependent on L-selectin shedding. The average invasive depth of WT, ΔMN, GFP cell lines migrating with the presence of fMLP was -21.52μm +/- 0.81μm, -16.65μm +/- 0.52, -20.52μm+/- 0.80, respectively. It appears that cell migratory behaviour towards fMLP is similar between GFP and WT cells. These results were also mirrored in the micropipette assay (see ***section 3.2.8***), where WT and GFP both migrated towards

the source of fMLP in a more directed manner than ΔMN. Therefore, although L-selectin shedding *per se* is not essential for fMLP-induced chemotaxis, blocking L-selectin shedding in cells that express it (e.g. neutrophils) dramatically impacts chemotaxis towards fMLP. Finally, there was little difference between WT and ΔMN migration through the collagen towards IL-8, (***figure 5.8 C***) with WT slightly more invasive 27.25 μm+/- 1.68 compared to ΔMN 23.95μm+/-1.23. There was no difference between GFP and ΔMN or GFP and WT. This closely resembles work in the primary neutrophils (***figure 5.5***) where blocking shedding did not affect invasive behaviour. Side-by-side comparisons of the invasive depths of neutrophils responding to chemoattractants clearly showed that all chemoattractants were bioactive in the bespoke flow chamber assay (***figure 5.9***). The general trend in all of the cell lines is that IL-8 is more potent at driving cell invasion although this is not significant in GFP cells (***figure 5.9 C***).

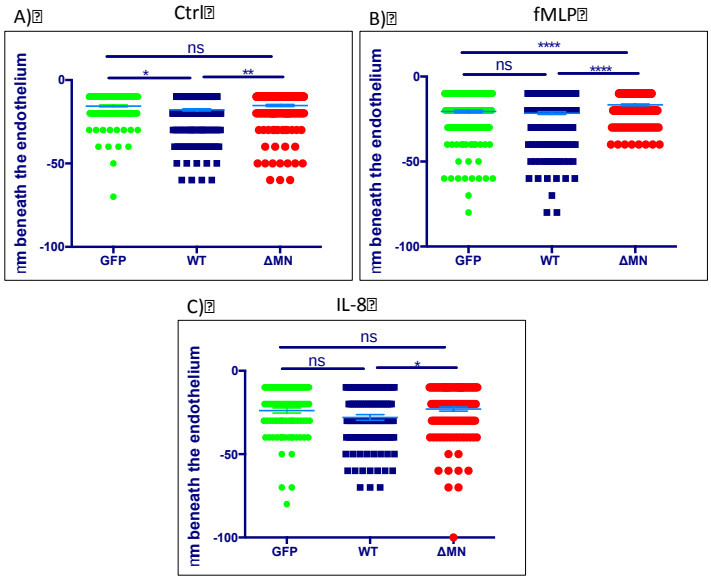

Figure 5.8: Investigating the contribution of L-selectin shedding in HL-60 cell chemotaxis through collagen matrices.

WT, GFP and ΔMN cells were uniquely stained with 1 μM Celltracker™ of different colours. Cells were perfused over the TNF-α activated HUVEC monolayer within the 3D device. To avoid bias and to overcome the possibility of the dye producing adverse effects on cell behaviour, Celltracker™ dyes were exchanged periodically between lines for each repeat. Each flow assay was conducted for a total of 2 hours, after which the 3D devices were fixed and stained for F-actin (using FITC-phalloidin). Neutrophil invasion was manually scored from images acquired using a spinning disk confocal microscope (as described in ***figure 5.2***). Error bars represent the standard error +/- of the mean. Each data set represents three independent experiments. For each device, a minimum of 6 Z stacks were collected from proximal and remote regions. A) Invasion assay in the presence of no chemoattractant (Ctrl). A total of 286, 179 and 252 were counted for WT, GFP and ΔMN cells, respectively. Statistical analysis, one-way ANOVA followed by Tukey's multiple comparisons test, ** $p<0.01$, *$p<0.05$. B) Invasion assay in the presence of 200nM fMLP. A total of 277, 251 and 233 were counted for WT, GFP and ΔMN cells, respectively. Statistical analysis, one-way ANOVA followed by Tukey's multiple comparisons test, **** $p<0.0001$. C) Invasion assay in the presence of 100ng/mL IL-8. A total of 111, 91 and 148 were counted for WT, GFP and ΔMN cells, respectively. Statistical analysis, one-way ANOVA followed by Tukey's multiple comparisons test, *$p<0.05$.

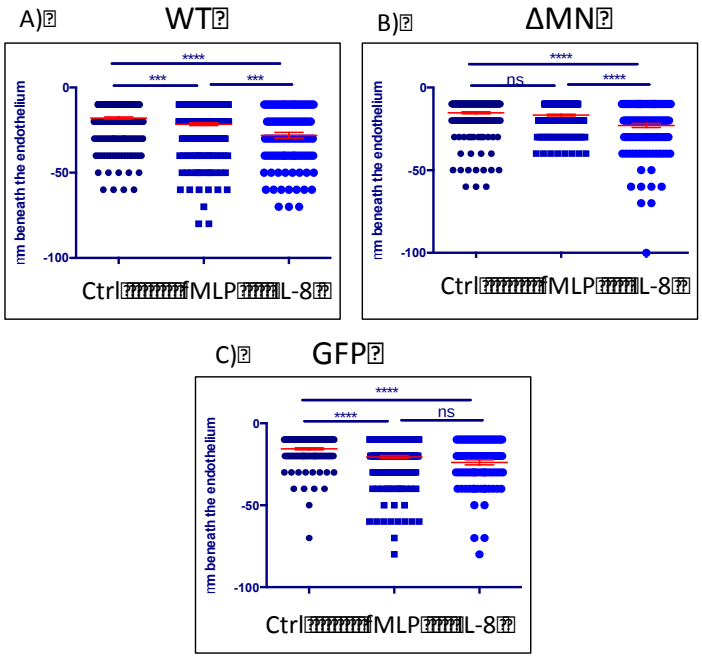

Figure 5.9. Side-by-side assessment of invasiveness in GFP, WT and ΔM-N HL-60 cell lines responding to different chemoattractants within the 3D device.
The data generated in ***figure 5.8*** was reconfigured to determine the extent of invasion between intermediary (IL-8) and end-stage (fMLP) chemoattractants. A) A total of 286, 277, and 111 WT cells were scored for the conditions: no chemoattractant (Ctrl), fMLP, and IL-8, respectively. One-way ANOVA, followed by Dunnett's multiple comparisons test. **** p<0.0001, ***p<0.001. B) A total of 252, 233, and 148 ΔMN cells were counted for the conditions: no chemoattractant (Ctrl), fMLP, and IL-8, respectively. One-way ANOVA, followed by Dunnett's multiple comparisons test. **** p<0.0001. C) A total of 179, 251, and 91 GFP cells were counted for the conditions: no chemoattractant (Ctrl), fMLP, and IL-8, respectively. One-way ANOVA, followed by Dunnett's multiple comparisons test. **** p<0.0001.

5.2.5 Understanding the contribution of the L-selectin tail in regulating HL-60 cell chemotaxis through collagen scaffolds.

So far, the data from this chapter shows that blocking shedding of L-selectin either in primary human neutrophils of HL-60 cell lines dramatically impacts invasion trough collagen matrices. In addition to acting as a cell adhesion molecule, L-selectin can also transduce intracellular signals following ligand binding (355). Previous reports have demonstrated that the cytosolic tail of L-

selectin can be phosphorylated at serine residues (RRLKKGKK**S**KR**S**MNDPY) in response to a variety of inflammatory agonists, including fMLP (327).

To determine if the ΔM-N phenotype could be reverted by altering the phosphorylation status of the L-selectin tail, two cell lines were generated that expressed ΔMN L-selectin, but where the serine residues were replaced with non-phosphorylatable alanines (ΔMN SSAA) or phospho-mimicking aspartates (ΔMN SSDD). Perfusion experiments within the 3D device were carried out and analysed as described in ***section 5.3.2***. Quantification of invasive depths for ΔMN SSAA and ΔMN SSDD compared to ΔMN revealed no significant difference when the cells were exposed to no chemoattractant, fMLP and IL-8 (***figure 5.10***). As before, the data was reconfigured to illustrate side-by-side comparisons of the invasive depths of neutrophils responding to chemoattractants (***figure 5.11***). ΔMN cells response to fMLP was not significantly different to their cellular response when no chemoattractant was present; yet, the presence of IL-8 dramatically encouraged migration into the collagen (***figure 5.11 A***). This replicates behaviour already seen in the WT/ΔMN/GFP experiments (***figure 5.8*** & ***figure 5.9 B***) Comparatively, the cell line ΔMN SSAA did respond significantly to both fMLP and IL-8 when compared to migration depths when no chemoattractant was present. ΔMN SSAA invasion depths when no chemoattractant, fMLP and IL-8 was present were: -13.7µm+/- 0.39, -15.4µm+/- 0.41 and -20.4µm+/-0.96 respectively (***figure 5.11 B***). Finally, mutating the serine residues to aspartates (ΔMN SSDD) produced an even greater response to fMLP to that than observed in ΔMN SSAA cells. ΔMN SSDD invasion depths when no chemoattractant , fMLP and IL-8 was present were: -13.3µm+/- 0.41, -15.5µm+/- 0.44 and -22.2µm+/- 1.11 respectively (***figure 5.11 C***) (***figure 5.11 C***). Together this work suggests that mutating the serine residues does not alter chemotaxis towards IL-8, however the role of serine phosphorylation in regulating the chemotaxis towards fMLP is still unclear.

Deleted: did not

Deleted: 68

Deleted: 4

Deleted: 36

Deleted: 1

Deleted: 1

Deleted: 1

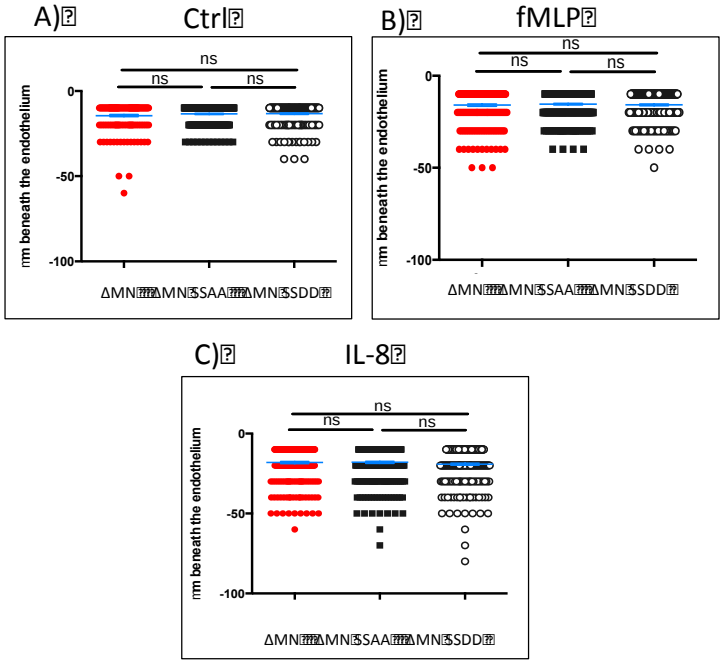

Figure 5.10: Understanding the contribution of the L-selectin tail in regulating chemotaxis through collagen matrices

ΔMN, ΔMN SSAA and ΔMN SSDD cells were uniquely stained with 1 μM Celltracker ™ of different colours. Cells were co-perfused across the TNF-α activated HUVEC monolayer of the 3D device. To avoid bias and to overcome the possibility of the dye producing adverse effects on cell behaviour, Celltracker™ dyes were exchanged periodically between lines for each repeat. Each flow assay was conducted for a total of 2 hours, after which the 3D devices were fixed and stained for F-actin (using FITC-phalloidin). Neutrophil invasion was manually scored from images acquired using a spinning disk confocal microscope (as described in ***figure 5.2***). Error bars represent the standard error +/- of the mean. Each data set represents three independent experiments. For each device a minimum of 6 Z stacks were collected from proximal and remote regions. A) Invasion assay in the presence of no chemoattractant (Ctrl) A total of 178, 285 and 239 were counted for ΔMN, ΔMN SSAA and ΔMN SSDD cells, respectively. Statistical analysis, one-way ANOVA followed by Tukey's multiple comparisons test. B) Invasion assay in the presence of 200nM fMLP. A total of 268, 285 and 291 were counted for ΔMN, ΔMN SSAA and ΔMN SSDD cells, respectively. Statistical analysis, one-way ANOVA followed by Tukey's multiple comparisons test. C) Invasion assay in the presence of 100ng/mL IL-8. A total of 281, 260 and 271 were counted for ΔMN, ΔMN SSAA and ΔMN SSDD cells, respectively. Statistical analysis, one-way ANOVA followed by Tukey's multiple comparisons test.

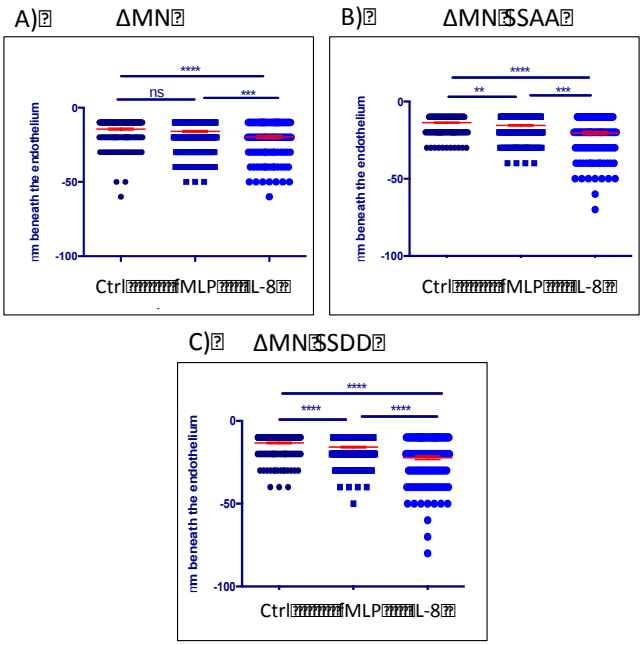

Figure 5.11: Side-by-side assessment of invasiveness in ΔMN, ΔMN SSAA and ΔMN SSDD HL-60 cell lines responding to different chemoattractants within the 3D device.
The data generated in ***figure 5.10*** was reconfigured to determine the extent of invasion between intermediary (IL-8) and end-stage (fMLP) chemoattractants. A) A total of 178, 268, and 281 ΔMN cells were scored for the conditions: no chemoattractant (Ctrl), fMLP, and IL-8, respectively. One-way ANOVA, followed by Dunnett's multiple comparisons test. **** p<0.0001, ***p<0.001. B) A total of 285, 285, and 260 ΔMN SSAA cells were scored for the conditions: no chemoattractant (Ctrl), fMLP, and IL-8, respectively. One-way ANOVA, followed by Dunnett's multiple comparisons test. **** p<0.0001. C) A total of 239, 291, and 271 ΔMN SSDD cells were scored for the conditions: no chemoattractant (Ctrl), fMLP, and IL-8, respectively. One-way ANOVA, followed by Dunnett's multiple comparisons test. **** p<0.0001.

5.3 Discussion:

The ultimate aim of this chapter was to understand how L-selectin regulates chemotaxis within collagen matrices – particularly in response to intermediary and end-stage chemoattractants. This was made possible through the use of the custom made 3D device that was fabricated in ***chapter 4***. The importance of L-selectin shedding, in chemotaxis towards either an end-target (fMLP) or intermediary (IL-8 & Gro-α) chemoattractants was illustrated through the use of human cell lines (HL-60) and primary neutrophils. In experiments L-selectin shedding was either genetically or pharmacologically inhibited respectively termed ΔMN or TAPI-0. The depth of cell penetration into the collagen past the

Deleted: ,

Deleted: , respectively

endothelium was enumerated after a 2-hour perfusion. This freeze frame in time does not give justice to cell movements within the XY axis. To overcome this, in the future, the 3D device can be easily interfaced with a spinning disk confocal during experimentation, and cells tracked in 4D (i.e. in 3D and over time). Imaging was conducted here using a 30x objective lens, however the collagen depth within the 3D device has been previously optimised (see ***section 4.2.6***) to allow for higher magnification (60x objective). This level of resolution would provide information on L-selectin subcellular localisation during TEM and chemotaxis. ***Chapter 3*** (see ***section 3.2.8*** and ***section 3.2.12)*** demonstrated that L-selectin has enriched at the uropod during chemotaxis and upon TEM L-selectin positive membrane was deposited, a higher imaging power will address whether these observations can be produced within a 3D environment.

5.3.1 Comparing cell invasion

The cell lines (WT, GFP, ΔMN, ΔMN SSAA and ΔMN SSDD) and primary neutrophils (pre-treated with TAPI-0 or DMSO), all demonstrated differences in cell speed and directionality when assessed in the sub endothelial space (***chapter 3***). Additionally, the cell lines WT, GFP, ΔMN exhibited substantial differences in directional persistence of migration when mixed into pre-polymerised collagen gel, (***figure 5.1***). These variables make it extremely difficult to clearly assess the contribution of L-selectin shedding in the 3D device invasion assays, where penetrative depth into the collagen gel is monitored. In the future a thorough investigation of cell directionality and speed of cells moving within collagen should be carried out, similar to the experimentation in ***figure 5.1***. This work will be important to clearly compare cell migration through the collagen plug between cell lines or cell treatments, and ensure that differences in depths observed are not a result of reduced cell speed. For this discussion it is assumed that between HL-60 cell lines or between primary neutrophils (+/-TAPI-0) there were small or no difference in cell speeds.

Deleted: cells "invasiveness" was recorded

Deleted: with a chemotactic score

Formatted: Font: Bold, Italic

Deleted: To overcome this, cells were given a chemotactic score. The chemotactic score is derived from the degree of significance (*p* value) obtained from invasive depths when compared between a specific cell line/primary cell treatment in a no chemoattractant environment to its respective cell line/ primary cell treatment in the presence of a chemoattractant gradient. For examples of these comparisons see ***figures 5.6, 5.9, 5.11***. A chemotactic score of 4, 3, 2, 1 would have p values of 0.0001,0.001,0.01 and 0.05, respectively. A chemotactic score of 0 would have no-significance. Thus, the higher the chemotactic score the greater the invasion of the specific cell line/primary cell in response to the particular chemoattractant. The chemotactic scores are represented in ***table 5.1***.

Deleted: ¶

Cell line /Cell treatments	fMLP
Primary neutrophil DMSO	4
Primary neutrophil TAPI-0	0
WT	3
DMN	0
GFP	4
DMN SSAA	2
DMN SSDD	4

5.3.1.1 Cell invasions in response to the intermediary chemoattractants IL-8 and Gro-α are L-selectin shedding independent

Pharmacologically blocking shedding in primary neutrophils does not affect the cells' ability to chemotax to both the intermediary chemoattractants IL-8 and Gro-α. Irrespective of the pre-treatment (DMSO/ TAPI-0) cells exposed to IL-8 and Gro-α, WT, ΔMN, GFP all successfully responded to IL-8 .Together this suggests that either removal of L-selectin or preventing L-selectin shedding does not impact migration towards these intermediary chemoattractants. However this data conflicts with two previous studies carried out. Firstly, in a recent report (2015), blocking L-selectin shedding in THP-1 cells (a monocyte cell line) prevented polarisation towards monocyte chemoattractant protein-1 (MCP-1), which, although not a neutrophil chemoattractant, could be classified as an intermediary chemoattractant, this conflicts with this current study in HL-60 neutrophils(212) .This highlights how a cell's response to blocking L-selectin shedding can be very much leukocyte-specific. Secondly, in another study *in vivo*, following a superfusion of the chemokine KC to the cremaster muscle, sheddase resistance neutrophils ($L(E)^{same}$) remained within a 50μm distance from the venule. In contrast neutrophil migration from the WT littermates extended over 150μm further from the venule (264).This study hypothesises that preventing L-selectin shedding prevents KC induced migration. However, the study does not provide dynamic information on neutrophil travel, the data is collected at one time point (120 minutes post superfusion), and moreover a superfusion does not provide a gradient, so migration towards KC cannot be defined as chemotaxis. Finally, imaging of the murine cremaster muscle requires detachment from the testicle, and spreading the cremaster radially as a flat sheet. Together, this handling and surgery inevitably produces local damage, releasing DAMPs (see ***section 1.1.1***). Therefore, this study cannot exclude the possibility that neutrophils are not responding to DAMPs, for example mitochondrial-derived fMLP. To summarise, given the difference in either cell type or experimental set up it is hard to draw direct comparisons.

Deleted: Table 5.1: The chemotactic scores¶
White numbering represents the chemotactic score given to the cell line/cell treatment (far left column) when exposed to a specific chemoattractant (top row). Bottom right: score key demonstrates how chemotactic scores are derived from *p* values. ¶
¶

Deleted: Above, ***table 5.1*** demonstrates that pharmacologically

Deleted: produced a chemotactic score of 4

Deleted: – achieving a chemotactic score of 4.

5.3.1.2 Cell invasions in response to the end-target chemoattractant fMLP are L-selectin shedding dependent

Strikingly, when L-selectin was blocked in both primary neutrophils and cell line models, exposure to an fMLP gradient resulted in diminished chemotaxis indicating there was no significant difference in invasion between their respective chemoattractant null controls. Flow cytometry data (see ***section 3.2.14***) further supports the notion that L-selectin shedding is involved in fMLP directed migration. When primary neutrophils were stimulated with a range of fMLP concentrations (10nM-1μM) all conditions produced a combined average of ~90% L-selectin shedding. In comparison ~37% of L-selectin was shed in response to IL-8 and no shedding was observed in response to Gro-α (both these chemokines were used at a the concentration range of 100ng/mL-1μg/mL) (see ***figure 3.32***). Therefore as L-selectin is only slightly shed and not shed at all in response to IL-8 and Gro-α respectively, it seems logical that blocking shedding does not alter invasive migration into the collagen gel for these intermediary chemoattractants. Interestingly, complete removal of L-selectin (in the GFP cell line) did not hinder a cells ability to migrate towards fMLP, this implies that it is the prevention of L-selectin shedding has a negative effect on fMLP mediated chemotaxis. ***Section 3.2.20*** demonstrated that surface expression of the fMLP receptors FPR1 and FPR2 were decreased in ΔMN cells in comparison to GFP and WT. Perhaps, this decrease in FPRs expression at the plasma membrane in the sheddase resistant cell line contributes to the lack of response towards fMLP. A hypothetical model will be discussed in ***chapter 6***.

5.3.2 Final thoughts

Although numerous responses have been shown to occur downstream of fMLP stimulation (phagocytosis and degranulation), currently, it is not known if blocking L-selectin shedding will impair neutrophil effector function. If blockage of L-selectin shedding in the presence of fMLP does prevent one or more of the neutrophil effector neutrophils this could have an enormous impact in neutrophil behaviour towards sterile injury sites for example the infarct zone in the early stages (days 1-3) of myocardial infarction (MI). See ***section 1.5.4*** for a description of neutrophils roles in MI.

Deleted: a

Deleted: c

Deleted: tic score of 0,

Formatted: Font: Bold, Italic

Deleted: , having a chemotactic score of 4,

Deleted: that

Deleted: *5.3.1.3 The ΔMN SSDD cell line rescues the ΔMN response to fMLP*¶
Interestingly, when the cytoplasmic tail serines were replaced with aspartates to mimic permanent phosphorylation (ΔMN SSDD) these cells produced a chemotactic score of 4 when exposed to fMLP, effectively rescuing the ΔMN response towards fMLP. While ΔMN SSAA cells only produced a chemotactic score of 2 when exposed to fMLP. The results imply that if L-selectin is expressed, prevention of serine phosphorylation hinders fMLP-driven chemotaxis. It is clear that L-selectin shedding and serine phosphorylation does not alter IL-8 directed chemotaxis. In order to fully understand the separate roles of L-selectin shedding and serine phosphorylation it would be of use to generate HL-60 cell lines where the L-selectin molecule is cleavage yet the serine residues have been exchanged with either alanine or aspartates. Alongside this, it would be important to decipher if L-selectin shedding regulates chemotaxis towards other chemoattractants. Neutrophil migration could be observed within the 3D device towards the complement protein C5a, another end-target chemoattractant.¶

6. General Discussion

The primary objective of this PhD thesis was to investigate the impact of blocking L-selectin shedding on neutrophil TEM and chemotaxis through 3D environments. The study used primary human neutrophils and HL-60 cell lines to explore neutrophil cellular behaviour responding to synthetic inhibitors (TAPI-0) and genetic manipulation of L-selectin-GFP. Using classic parallel plate flow chamber assays, ***chapter 3*** was designed to specifically explore how blocking L-selectin shedding impacted neutrophil TEM. The behavioural parameters analysed included: cell shape, directionality and TEM rate. L-selectin shedding was monitored during the course of TEM, to establish whether, as in CD14-positive monocytes, the process was triggered specifically during TEM (205). Primary human neutrophils and HL-60 cells were also challenged with various chemoattractants to determine if chemokines or fMLP, in isolation, could promote L-selectin shedding. Interestingly, challenge with Gro-α led to no L-selectin shedding, whereas challenge with IL-8 led to ~37 % shedding. In contrast, challenge with fMLP led to robust (almost 95%) L-selectin shedding.

Here, TEM assays were conducted using the parallel plate flow chamber. This experimental set up dictated that the endothelium was grown on a fibronectin substrate, and thus information regarding post TEM events (e.g. further interstitial migration) was limited. To fully explore interstitial migration and chemotaxis, a bespoke microfluidic device was designed and fabricated (***Chapter 4***). The device was modelled on strict criteria, ***table 4.1***, and successfully interfaced with the parallel plate flow chamber to introduce leukocytes into the device at physiological shear stress. The endothelium within the device is

Deleted: 50

Deleted: subtrate

Deleted: .The

supported on a collagen matrix, microchannels entering into the collagen deliver stable chemoattractant gradients. Finally, ***chapter 5*** amalgamates work from the previous two chapters; the neutrophils (primary and HL-60 cell lines) were introduced into the 3D device where the complete leukocyte adhesion cascade could be interrogated.

Taken together, this thesis has concluded that: (i) As with monocytes, L-selectin contributes to the invasive mechanism of neutrophils during TEM, (ii) L-selectin shedding occurs specifically during TEM and not before, (iii) L-selectin is dramatically shed in response to fMLP, but not to the chemokines IL-8, (iv) blocking L-selectin shedding hinders chemotaxis towards fMLP, but not to IL-8, in 3D environments, (v) FPR1 and FPR2 surface expression is impacted by L-selectin shedding. Below key findings are dissected in more detail with the use of graphical models.

Deleted: an

Deleted: chemokines

6.1 L-selectin shedding during TEM and chemotaxis

Chapter 3 demonstrates that L-selectin is shed in human neutrophils specifically during TEM, only previously documented using a skin blister model (312). The data within this thesis confirms what others have described, that L-selectin acts as a pro-invasive molecule, (see ***section 3.2.11***). Blocking L-selectin shedding in both primary neutrophils and a neutrophil cell line model reduced cell directional persistence in both 2D and 3D environments, see ***figures 3.6/3.24/5.1***. In keeping with this, the cell morphologies of fTEM cells were monitored and blocking L-selectin shedding altered cell polarity, typically producing an elongated cell with multiple membrane undulations, see ***figure 3.7*** & ***figure 3.25***. Leukocytes with impaired polarity frequency present with impaired chemotaxis (13).Indeed, blocking L-selectin shedding affects migration past the endothelium, and chemotaxis to the end-target chemoattractant fMLP, see ***section 5.2.3*** & ***section 5.2.4***.

Deleted: s

Deleted: the

Deleted: .

Deleted: shedding prevented

Recently, mice expressing a knock-in "sheddase resistant" form of L-selectin (where the cleavage domain of L-selectin is swapped with a similar non-cleavable region of E-selectin) have become available for use in the Ivetic lab (264). Isolating neutrophils from these mice will bypass the need for using TAPI-0 in

future flow experiments. Comparing these neutrophils against WT counterparts in the 3D device will allow one to determine if the mutant neutrophil phenocopy some of the behavioural responses seen in TAPI-0-treated human neutrophils or the ΔMN HL-60 cells. It will also allow one to determine if the impact of L-selectin shedding on neutrophil behaviour is conserved across species. Using TAPI-0 on neutrophils expressing the sheddase-resistant L-selectin could help determine if there are any additional phenotypes that are secondary to inhibiting L-selectin shedding. As ADAM-17 has many other substrates, this would be an extremely important question to address in light of the different phenotypes presented by primary human neutrophils and HL-60 cells. Consistency in phenotype, using this approach, would give confidence to the fact that TAPI-0 could be acting selectively to inhibit L-selectin shedding at 10 μM. The mice will hopefully open up an avenue of *in-vivo* work, for example neutrophil migration towards laser injury (mimicking sterile injury) could be observed.

Deleted: alongside

6.2 Putative mechanisms underpinning L-selectin regulation during TEM and interstitial chemotaxis

The first graphical summary, ***figure 6.1***, demonstrates L-selectin shedding dependent phenotypes in TEM, while the second graphical summary, ***figure 6.2***, illustrates the dynamic changes in serine phosphorylation in TEM.

Recent work in monocytes has revealed that the L-selectin that is present in transmigrating pseudopods is exposed to ECM components, such as biglycan, where it is clustered(212). The study concludes that clustering of L-selectin is likely to preceed shedding. Although not formally investigated, it is likely that clustering encourages a high density of surface L-selectin for ADAM17 to cleave. In neutrophils, the magnitude of L-selectin clustering was not as apparent as in monocytes (see ***section 3.2.5***). However, it is unclear whether the small clusters of L-selectin that are formed in neutrophils acts as a pre-requisite for shedding. It is possible that L-selectin clusters are shunted into lipid rafts (possibly through cytoplasmic tail phosphorylation), where ADAM-17 also resides (357) (358). p38 MAPK has been reported to become activated downstream of ligand induced

Deleted: gligan

Deleted: de

Deleted: corrals

clustering of L-selectin, opening up the possibility that L-selectin shedding within the sub-endothelium is p38 MAPK dependent(286). Blocking L-selectin shedding impairs fTEM cells to adopt normal polarity and migrate directionally within 3D scaffolds (***figure 6.1***). L-selectin shedding triggered by TEM could be initiated through K-Ras/SOS signalling; L-selectin clustering has been shown to activate Ras and SOS binding (209). Interestingly, K-Ras and SOS have both been shown to impact the phosphorylation of p38 MAPK (359) (360). Additionally, Ras has been shown to mediate tumour invasion, and recently its interaction with the PI3 kinase p110α was shown to induce Rac GTPase activation (224)(359).

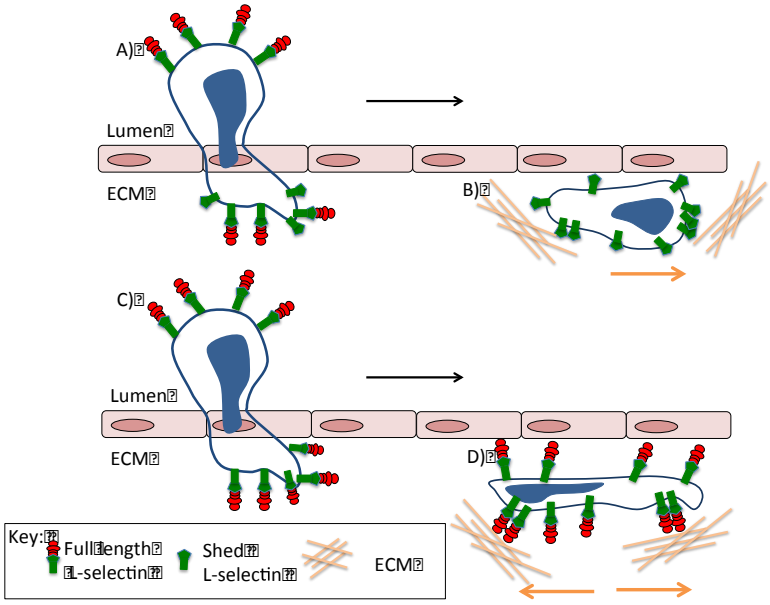

Figure 6.1: Schematic model representing the effects of L-selectin shedding on neutrophil polarity
This model was produced based on findings from HL-60 cells and primary neutrophils from within this thesis. A) During TEM, L-selectin within transmigrated pseudopods binds to ligands within the ECM (e.g. biglycan), which promotes L-selectin clustering. Although not proven, it is assumed that the signals transmitted downstream of L-selectin at this point are likely to "inform" the cell that it has entered the subendothelial space. L-selectin clustering could activate a pathway involving K-Ras/SOS and p38 MAPK signalling (212). B) L-selectin is shed upon completion of TEM, leading to neutrophils establishing front-back polarity, enabling successful directional migration. C) Blocking L-selectin shedding also promotes the formation of clusters with similar dimensions to WT L-selectin within transmigrating pseudopods. However, based on the

Deleted: .
Deleted: ing
Deleted: successful directional

phenotype presented in TAPI-0-treated neutrophils and ΔMN cells, the pathways that are activated downstream of L-selectin in this scenario is likely to be very different. D) Importantly, the signals induce a bipolar phenotype and loss in front-back polarity. Orange arrows indicate the cells direction.

Deleted: overall

The cytoplasmic tail of L-selectin bears no homology with its family members, E- and P-selectin, so there is a high probability that its regulation is highly unique. Chemoattractants, such as IL-8 and fMLP have been shown to induce serine phosphorylation of the L-selectin tail (260). As neutrophils respond to these very chemoattractants during an inflammatory response, it is likely that serine phosphorylation of the L-selectin tail is regulated dynamically during TEM and interstitial migration (where L-selectin shedding is blocked). In contrast to ΔMN cells, expression of ΔMN SSAA or ΔMN SSDD in HL-60 cells led to an increased dwell time of neutrophil crawling on top of endothelial cells. This would suggest that although blocking L-selectin shedding does not impact the TEM rate, the serine residues in the ΔMN tail are fundamental to driving TEM.

Deleted: would not be surprising to assume

Previous *in vivo* studies have shown that fragments of the uropod are detached from neutrophils upon completing TEM (361). This phenomenon was also observed in HL-60 cells expressing L-selectin-GFP. Interestingly, although the frequency of "uropod spots" did not differ between WT and ΔMN cells, locking the phosphorylation status of the ΔMN L-selectin tail (either to AA or DD) significantly impacted spot formation. ΔMN SSAA cells left significantly fewer L-selectin spots than ΔMN cells (***figure 6.2 B***). One reason for this observation could be that serine phosphorylated L-selectin allows preferential binding to ezrin and moesin, known L-selectin tail binding partners, which has been shown to localise to the rear of polarised leukocytes (362)(363). Once within the sub endothelial space, the fully transmigrated ΔMN and ΔMN SSAA cells behaved similarly, suggesting that blocking serine phosphorylation does not deviate from the ΔMN phenotype (***figure 6.2.D***).

Deleted: E

Deleted: RM proteins

Deleted: a

Interestingly, permanently mimicking serine phosphorylation (ΔMN SSDD) rescues chemotaxis towards fMLP, indicating WT cells may be preferentially

phosphorylated during chemotaxis towards fMLP (***figure 6.2 E***) although more work needs to be done to confirm this. To definitively understand the pathways leading towards L-selectin serine phosphorylation and shedding, and how they collectively impact cell behaviour, WT SSAA and WT SSDD cell lines should be engineered and characterised to complement this study. Serine phosphorylation incorporates a negative charge cloud on to the predominately basic cytoplasmic tail (RRLKKGKKSKRSMNDPY), which may alter binding of L-selectin with its partners or to phosphatidyl serines within the inner leaflet of the plasma membrane (211). Although there is still much work to be done to understand how serine residues in the L-selectin tail are regulated, it is clear that blocking L-selectin shedding in neutrophils can profoundly impact signalling proteins at the plasma membrane. The lack of polarity suggests that the recruitment or activation of Rho_GTPases is being impacted. More work is required to understand if blocking L-selectin shedding is therapeutically beneficial – particularly in the setting of sterile inflammation (see later).

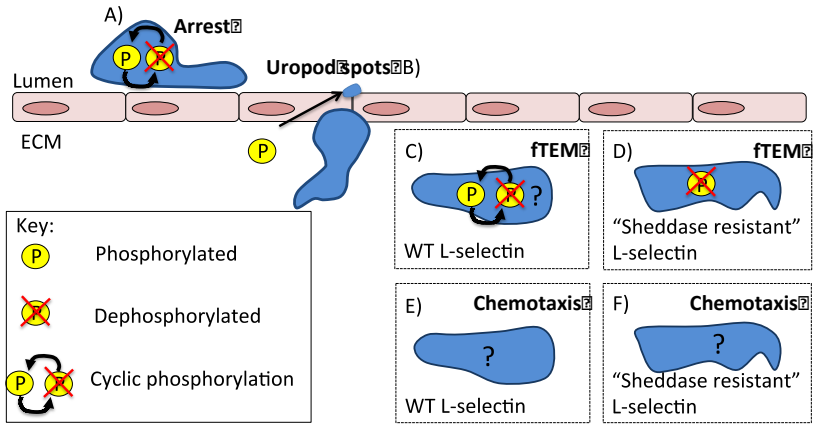

Figure 6.2: Schematic model representing the effects of L-selectin phosphorylation
This model was produced based on findings from HL-60 cells and currently available literature. A) Cyclic phosphorylation of the serine's (S364 and S367) in the cytoplasmic tail of L-selectin is required for timely firm arrest to the endothelium, preventing extensive intraluminal crawling. B) The uropod spot formation occurs more frequently when the serines within the cytoplasmic tail were converted to aspartic acids. C) It is likely that cyclic phosphorylation attributes to successful cell polarity and cell migrational persistence. D) The disrupted cell polarity and undirected migration is likely due to unphosphorylated serines. E&F) How phosphorylation events contribute to chemotaxis is still unclear.

Deleted:
Deleted: are
Deleted: profoundly
Deleted:
Deleted:
Deleted: introduced a negative charge
Deleted: '

6.3 Putative mechanism underpinning L-selectin shedding and chemotaxis towards fMLP

It is clear the blocking L-selectin shedding in neutrophils significantly impacts chemotaxis towards the end-target chemoattractant, fMLP. As demonstrated in primary neutrophils fMLP induces both p38 MAPK phosphorylation and L-selectin shedding. Previous work from the Tedder group has shown that serine phosphorylation of the L-selectin tail occurs soon after challenge with fMLP (260) (***figure 6.3***).

Deleted: have

Serine phosphorylation of the L-selectin tail, specifically at S364, has very recently been shown to promote the dissociation of calmodulin from the L-selectin tail (205). Killock and Ivetic had also shown that activation of p38 MAPK leads to the mobilisation of ADAM-17 to the plasma membrane (202) (***figure 6.3***). Others have shown that the catalytic activity, rather than increased expression of ADAM-17 at the plasma membrane, is upregulated in response to p38 MAPK activation(364). Both of these reports corroborate that neutrophils are better primed to drive L-selectin shedding following p38 MAPK activation.

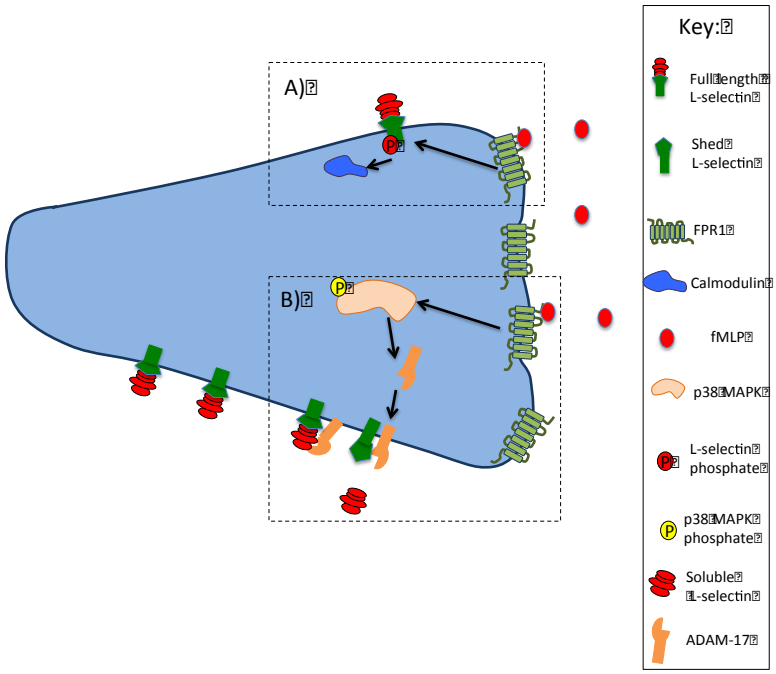

Figure 6.3: Schematic model representing L-selectin dependent FPR1 regulation
This model was produced based on findings from HL-60 cells and currently available literature [202][212]. A) fMLP stimulates L-selectin phosphorylation. Phosphorylation at S364 likely prevents calmodulin-binding rendering L-selectin susceptible to shedding. B) fMLP binding to its receptor stimulates p38 MAPK phosphorylation. Activated p38 MAPK mobilises ADAM-17 to the plasma membrane increasing surface expression. ADAM-17 is the prominent cleavage enzyme responsible for L-selectin shedding.

Deleted: calmodulin binding

Although this study has revealed for the first time that blocking the shedding of L-selectin impacts chemotaxis towards fMLP gradients in 2D and 3D environments, the mechanism underpinning this response remains poorly understood. ***Figure 3.40*** showed that HL-60 cells expressing WT L-selectin have significantly higher levels of surface-expressed FPR1/2 compared to GFP or ΔMN cells. Western blotting reveals that FPR1 and FPR2 total protein expression levels are unchanged amongst cell lines, only cells expressing WT L-selectin can increase the surface expression of FPR1 and FPR2 at the plasma membrane (***figure 3.40***). In future, it would be interesting to explore if L-selectin and FPR1/2 form a functional complex with one another. One hypothetical view could be that the

Deleted: although FRR1/2

Deleted: is equal

Deleted: /2

Deleted:

FPR1/2 at the plasma membrane is associated with L-selectin, and can simultaneously respond to fMLP. This initial response to fMLP could lead to serine modification of the L-selectin tail and subsequent shedding, leading to the polarised distribution of FPR1/2 at the leading edge, which would allow chemotaxis to ensue. This could explain why the chemotaxis of ΔMN cells towards fMLP gradients is significantly impaired. If serine phosphorylation of the L-selectin tails is different between WT and ΔMN cells, this could profoundly impact the association between FPR1/2 and L-selectin and FPR1/2 expression at the plasma membrane. Future experiments will include flow cytometric analysis of FPR1/2 expression levels in ΔMN SSAA and ΔMN SSDD cells. Clearly more work is required to determine the precise mechanism, and using mice expressing sheddase-resistant L-selectin could be a useful tool to further investigate the relationship between FRP1/2 and L-selectin shedding *in vivo* and *in vitro*.

Deleted: to

Recently, a study conducted in HL-60 cells demonstrated that in conditions where fMLP concentration is low (i.e. <500nM), p38 MAPK phosphorylates S342 of the cytoplasmic tail of FPR1, which prevents G-protein coupled receptor kinase 2 (GRK2) binding (365) (***figure 6.4***). L-selectin clustering has been demonstrated to phosphorylate p38 MAPK (286). GRK2 is required for FPR1 receptor internalisation through phosphorylation of an intracellular residue (366). Interestingly, extracellular signal regulated kinase (ERK) opposes p38 MAPK function, enhancing the effects of GRK2. It would be important to understand if L-selectin shedding mediates p38 MAPK phosphorylation and conversely if blocking L-selectin shedding in fMLP stimulated cells induce ERK activation. This could be achieved through Western blots probing for phospho-ERK and phospho-p38 MAPK in WT and ΔMN cells, and through the use of micropipette assays releasing fMLP: where WT and ΔMN cells have been pre-treated with specific ERK/p38 MAPK inhibitors. Additionally, genetically engineering a fluorescent protein tag on to FPR1 would allow real time tracking of the receptor, which would be beneficial for the above experiment. The hypothetical model depicted in ***figure 6.4*** could also contribute to the differences observed in surface expression of FPR1 in the WT and ΔMN cells.

Deleted: s

Together the work conducted in this thesis and from previous reports demonstrates a relationship between the fMLP receptor, L-selectin and p38 MAPK.

Deleted: work conducted in this thesis and from previous reports demonstrate

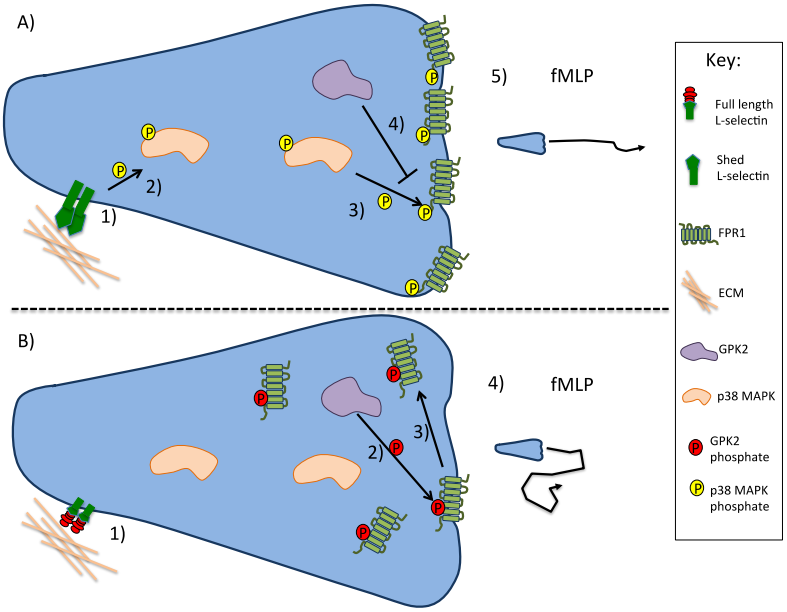

Figure 6.4: Schematic model representing L-selectin dependent FPR1 regulation
This model was produced based on findings from HL-60 cells and currently available literature(286)(365)(366). A) *In cells where L-selectin shedding is not inhibited.* 1) During TEM L-selectin bind to ligands within the ECM, L-selectin clustering occurs. 2) L-selectin clustering activates p38 MAPK. 3) P-p38 MAPK phosphorylates FPR1. 4) GPK2 interaction with FPR1 is prevented through p38 MAPK phosphorylation of FPR1. 5) Successful chemotaxis towards fMLP. B) *In cells where L-selectin shedding is inhibited*. 1) Potentially L-selectin is unsuccessful at indirect activation of p38 MAPK. 2) GPK2 phosphorylates FPR1. 3) Phosphorylated FPR1 is an internalisation signal; less FPR1 is expressed on the cell surface. 4) Unsuccessful chemotaxis towards fMLP.

Deleted: .

6.4 What is the impact of blocking L-selectin shedding on neutrophil effector function?

Neutrophils respond robustly to fMLP, which is derived from both gram-negative bacteria and mitochondria. In fact, and more pertinent to this study, a recent report has shown that fMLP isolated from human mitochondria is a robust driver of L-selectin shedding and p38 MAPK activation (367). Numerous reports have

built confidence in the notion that neutrophils home to sources of fMLP, where, upon arrival, undergo numerous effector functions, such as degranulation, phagocytosis and NETosis. As blocking L-selectin shedding impacts neutrophil polarity and chemotaxis towards fMLP, it would be of great importance to understand if blocking shedding also alters neutrophil effector function: NETosis, degranulation and phagocytosis, for a detailed description see ***section 1.5***. Below the contribution of L-selectin will be discussed for each effector function separately, and future experiments outlined to investigate whether L-selectin shedding is the "green light" for neutrophil effector function.

NETosis

The oral cavity creates a large exposure to external bacterial flora, and so the body must protect itself through appropriate antimicrobial secretions in the saliva. Neutrophils that enter the buccal cavity provide one such example of the defence weaponry. It was found that the L-selectin ligand, sialyl Lewis x (sLe^x), is presented on salival mucins(294). Salival sLe^x promotes L-selectin clustering that culminates in NETosis. The specificity of this response was demonstrated with function-blocking antibodies that target the L-selectin/sLe^x interaction – leading to dramatically decreased NETosis (294). NETs formation is classically defined through two mechanisms. The first mechanism can be induced through NADPH oxidase and elastase activity or candida albicans (368)(369)(370). The second mechanism relies on bacteria stimulation of toll like receptors and is integrin dependent (371)(372). However, these oral NETs form through a unique mechanism that does not fall in either category. Using TAPI-0 in such studies could potentially address the role of L-selectin shedding in NETs formation. Additionally, NETs formation *in vivo* could be observed using mice expressing sheddase-resistant L-selectin (see ***section 6.1***). NETs could be identified through staining the extracellular DNA with Sytox® (a stain that increases fluorescence intensity ~500 fold upon nucleic acid binding and is cell impermeable), or through immunofluorescence approaches that target markers of NETosis: citrullinated histone H3, neutrophil elastase and myeloperoxidase.

Degranulation

Degranulation involves the release of granules containing antimicrobial factors(3). As mentioned previously, ligation and cross-linking of L-selectin in neutrophils enhances the activation of β_2 integrins (see ***section 1.11.1***), β_2 integrin activation has been shown to be responsible for degranulation of eosinophils (373). L-selectin has also be shown to be responsible for directly encouraging degranulation: clustering (or cross-linking) L-selectin with monoclonal antibodies, DREG55 and DREG200, sensitises neutrophils to degranulation when challenged with IL-8 (286).Here, cross-linking potentiates the release of secondary and tertiary granules, and blocking p38 MAPK reverses the release of such granules (286).One method to address the contribution L-selectin shedding in the release of secondary and tertiary granules could be to incubate neutrophils with TAPI-0 or a DMSO carrier (in control conditions), followed by cross-linking L-selectin and stimulate with IL-8. The assay would be carried out in suspension, cell free supernatants would then be collected and assayed for the specific granular markers including lactoferrin and gelatinase correlating to the release of secondary and tertiary granules. Lactoferrin could be assayed using ELISA (anti-lactoferrin antibody), while gelatinase activity could be assessed by zymography. There is also evidence that L-selectin cross-linking enhanced both an fMLP or TNF-α induced "oxidative burst(374)(296)". Here, L-selectin cross-linking mediated an intracellular rise in calcium and stimulates the cellular release of the superoxide radicals and hydrogen peroxide (374)(296). To clarify, if L-selectin shedding contributes to the oxidative burst, then specific probes (such as 2', 7'-dichlorofluorescein diacetate) could be used to detect superoxide formation again in neutrophils with/without TAPI-0. Again, using the knock-in mice that express sheddase-resistant L-selectin mice (and their WT littermates) could eloquently address this issue.

Deleted: linking mediated

Phagocytosis

There is currently no literature that links L-selectin to the induction of phagocytosis. However, from the studies carried out in this thesis blocking L-selectin shedding produces clear defects in polarity. Given that phagocytosis involves the re-organisation of the actin cytoskeleton, it seems likely that phagocytosis and polarity are tightly linked. Proteins crucial for polarity; Rho A,

ROCK, mDia1 have all been implicated in phagocytosis(375) (376). To assess the effect L-selectin shedding in phagocytosis, primary neutrophils could in incubated with an array of fluorescent stimuli e.g. opinisised latex beads, zymosan, bacteria, or apoptotic cells with and without the presence of TAPI-0. Phagocytosis could be assessed in high throughput through flow cytometry or through fluorescence microscopy.

It is important to note that L-selectin cross-linking also drives ectodomain shedding of itself (342)(340). Does clustering of L-selectin therefore become a self-limiting signal? As many of these cross-linking studies have been performed *in vitro* using suspension cells, it raises the question of whether they are physiologically relevant or whether they are just *in vitro* artefacts. Nonetheless, a fundamental question has not yet been addressed: does L-selectin shedding give the "green light" for neutrophils to undergo effector functions – degranulation, NETosis and phagocytosis?

Formatted: Font: Italic

Deleted: and

Formatted: Font: Italic

6.5 Blocking L-selectin shedding – a possible therapy for myocardial infarction?

Following the rupture of an unstable atherosclerotic plaque, the rapid formation of a thrombotic lesion in the coronary artery will rapidly lead to restricted oxygen and nutrient supply downstream of the blocked artery(377). This, in essence, is the first step in myocardial infarction (MI). Within minutes to hours, based on the nature of their high-energy demand, differentiated adult cardiomyocytes will undergo necrosis. This is a critical event – adult cardiomyocytes are terminally differentiated and cannot self-regenerate. This region is known as the "infarct zone", which begins to expand over a number of hours. Neutrophils are known to contribute to the expansion of the infarct zone. They are initially attracted because of the large numbers of necrotic cardiomyocytes, which are packed with mitochondria and are releasing fMLP (***figure 6.5 A***). As demonstrated in a recent study (2015) N-formylated peptides from mitochondria produced severe hypotension, vascular leakage, hyperthermia all signs classically associated in systematic inflammatory response system (SIRS) (378). Upon arrival, neutrophils

exhibit their effector responses: degranulation and phagocytosis. Neutrophil effector function plays a large contribution to the remodelling of the myocardium, post-MI (***figure 6.5 B***). Matrix metalloproteinases derived from the neutrophil, and the stimulation of collagen production by fibroblasts resident in the myocardium, can lead to dramatically altered structure of the left ventricle (LV)(379). The LV is particularly important as many of the coronary arteries feed oxygen to this chamber of the heart, and it is typically the LV that incurs an infarct following MI. The LV is the chamber with the largest muscle mass, as it needs to pump oxygenated blood to the aorta - the largest artery in the body. Failure to effectively pump oxygenated blood to meet the body's demand will result in heart failure(380).

A number of studies have shown that reducing neutrophil effector function post-MI is therapeutically beneficial. DNAse I treatment has been shown to reduce the infarct zone, suggesting that NETs could be a significant driver of myocardial infarction (381). In a pig study, treatment with the drug BW775C (composed of cyclooxygenase and lipoxygenase) significantly reduced infarct size. Immunohistochemical staining showed ~35% decrease in infarct size compared to the control animal group (382). BW775C was shown to reduce neutrophil degranulation by ~46%, and superoxide generation was down by ~74%, although chemotaxis was not inhibited. Reducing neutrophil recruitment has additionally been shown to impact infarct size, infusion of GDF-15 (an endogenous inhibitor of β2 integrin function) inhibited neutrophil arrest and ultimately TEM, leading to a reduction in infract size (383).

In the context of this study, blocking of L-selectin shedding could potentially offer prevention of both fMLP directed migration to the infarct zone and effector function once within the infarct zone (***figure 6.5. C***). In theory, this "double strike" could provide a better patient outcome. Thinking therapeutically, the manufacture of a biopharmaceutical (e.g. monoclonal antibody, or nanobody) to target the cleavage site of L-selectin and render the site unrecognisable to ADAM-17 could result in something that mimics ΔMN L-selectin. In the case of MI, the biopharmaceutical could be administered intravenously to patients by a

paramedic within the first hours of contact post-MI (***figure 6.5. C***). Continued administration of the biopharmaceutical over 3 days post-MI, when neutrophil activity is most aggressive within the infarct zone, could lead to improved patient outcome. Although blocking L-selectin shedding during this period may immunosuppress the individual, the benefit of the 3-day therapy is likely to outweigh the risk of infection. Indeed, other measures, such as antibiotics, could be put in place to decrease chances of infection during this period. Again, using the mice that express a sheddase-resistant form of L-selectin could be used in models of MI to address the therapeutic advantage of blocking L-selectin shedding in this pathology.

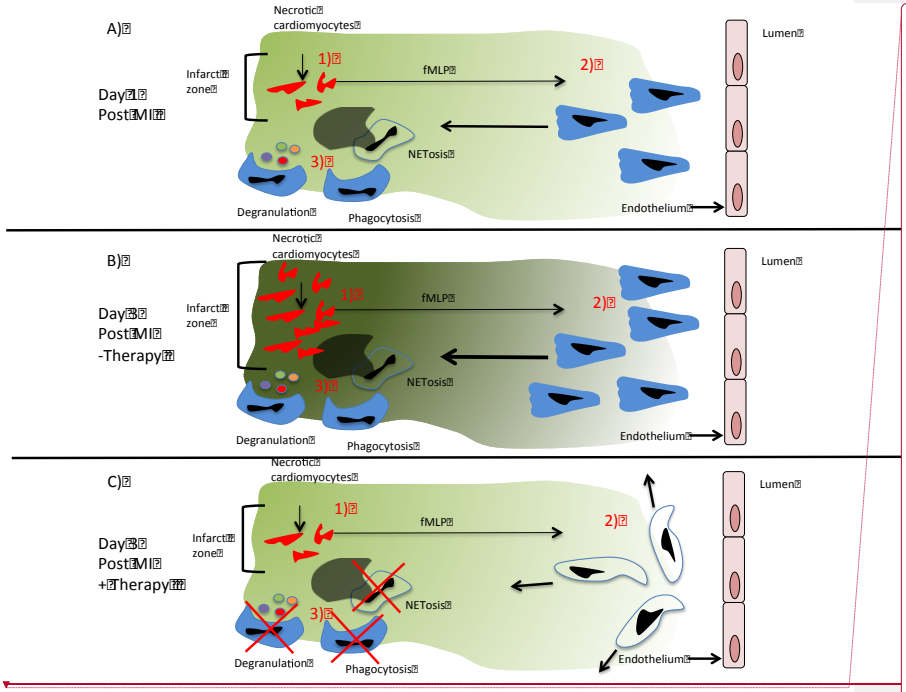

Figure 6.5: A possible therapy for myocardial infarction
This model was produced based on currently available literature and findings from this thesis (173)(377). *A) Day 1 post myocardial infarction.* 1) The anoxia environment (infarct zone) results in cardimyocyte death, destruction of mitochondria releases fMLP. 2) fMLP alongside other inflammatory factors encouraged neutrophil infiltration into the infarct zone. 3) Neutrophils undergo one of three effector functions. B) *Day 3 post myocardial infarction – no therapy* 1) Neutrophil presence and activity is responsible for increased cardiomyocyte death leading to more fMLP released. 2) More neutrophil infiltration. 3) More neutrophil activity at the infarct zone- the infarct zone is increased. C) *Day 3 post myocardial infarction – therapy is present.* 1) fMLP is released from necrotic cells. 2) The blockage of shedding L-selectin therapy prevents

Deleted:
Deleted: ¶

neutrophils effectively chemotaxing to the infarct zone. 3) The blockage of shedding L-selectin therapy prevents fMLP driven neutrophil activation reducing effector functions. Here, both stages 2&3 contribute to the decrease in infarct size.

6.6 Concluding remark

Although this study has set out to tackle some basic biological questions relating to L-selectin shedding and neutrophil chemotaxis, it has exposed some interesting avenues for potential translation into patient benefit.

Deleted: ¶
¶
¶
¶
¶

References

1. Scott A, Khan KM, Cook JL, Duronio V. What is inflammation& are we ready to move beyond Celsus? Br J Sports Med. BMJ Group; 2004 Jun;38(3):248–9.
2. Bagaitkar J, Newson J, Stables M, Karra E, Fullerton J, O'Brien A, et al. Cellular dynamics of resolving inflammation. Blood. American Society of Hematology; 2014 Sep;124(11):1701–3.
3. Charles A Janeway J, Travers P, Walport M, Shlomchik MJ. The front line of host defense. Garland Science; 2001;
4. Fierro IM, Serhan CN. Mechanisms in anti-inflammation and resolution: the role of lipoxins and aspirin-triggered lipoxins. Brazilian J Med Biol Res = Rev Bras Pesqui médicas e biológicas / Soc Bras Biofísica . [et al]. 2001 May;34(5):555–66.
5. Chandrasekharan JA, Sharma-Walia N. Lipoxins: nature's way to resolve inflammation. J Inflamm Res. Dove Press; 2015;8:181–92.
6. Wu Y, Antony S, Meitzler JL, Doroshow JH. Molecular mechanisms underlying chronic inflammation-associated cancers. Cancer Lett. NIH Public Access; 2014 Apr;345(2):164–73.
7. Landskron G, De la Fuente M, Thuwajit P, Thuwajit C, Hermoso MA. Chronic inflammation and cytokines in the tumor microenvironment. J Immunol Res. Hindawi Publishing Corporation; 2014;2014:149185.
8. Ewald N, Hardt PD. Diagnosis and treatment of diabetes mellitus in chronic pancreatitis. World J Gastroenterol. Baishideng Publishing Group Inc; 2013 Nov;19(42):7276–81.
9. Libby P, Ridker PM, Maseri A. Inflammation and atherosclerosis. Circulation. American Heart Association Journals; 2002 Mar;105(9):1135–43.
10. Tuttolomondo A, Di Raimondo D, Pecoraro R, Arnao V, Pinto A, Licata G. Atherosclerosis as an inflammatory disease. Curr Pharm Des. 2012;18(28):4266–88.
11. Ley K, Laudanna C, Cybulsky MI, Nourshargh S. Getting to the site of inflammation: the leukocyte adhesion cascade updated. Nat Rev Immunol. 2007 Sep;7(9):678–89.
12. Kiskin NI, Hellen N, Babich V, Hewlett L, Knipe L, Hannah MJ, et al. Protein

Deleted: &quot

Formatted: Justified

Deleted: ;

Deleted: quot;?

Deleted: A

mobilities and P-selectin storage in Weibel-Palade bodies. J Cell Sci. 2010 Sep;123(Pt 17):2964–75.

13. Schmid-Schönbein GW, Usami S, Skalak R, Chien S. The interaction of leukocytes and erythrocytes in capillary and postcapillary vessels. Microvasc Res. 1980 Jan;19(1):45–70.
14. Sun C, Migliorini C, Munn LL. Red blood cells initiate leukocyte rolling in postcapillary expansions: a lattice Boltzmann analysis. Biophys J. 2003 Jul;85(1):208–22.
15. Pospieszalska MK, Ley K. Dynamics of Microvillus Extension and Tether Formation in Rolling Leukocytes. Cell Mol Bioeng. NIH Public Access; 2009;2(2):207–17.
16. Zhao Y, Chien S, Weinbaum S. Dynamic Contact Forces on Leukocyte Microvilli and Their Penetration of the Endothelial Glycocalyx. Biophys J. 2001;80(3):1124–40.
17. Bruehl RE, Springer TA, Bainton DF. Quantitation of L-selectin distribution on human leukocyte microvilli by immunogold labeling and electron microscopy. J Histochem Cytochem. 1996 Aug;44(8):835–44.
18. Spertini O, Cordey AS, Monai N, Giuffrè L, Schapira M. P-selectin glycoprotein ligand 1 is a ligand for L-selectin on neutrophils, monocytes, and CD34+ hematopoietic progenitor cells. J Cell Biol. 1996 Oct;135(2):523–31.
19. Rosen SD. Ligands for L-Selectin: Homing, Inflammation, and Beyond. Annu Rev Immunol. Annual Reviews ; 2004 Apr;22(1):129–56.
20. Arbonés ML, Ord DC, Ley K, Ratech H, Maynard-Curry C, Otten G, et al. Lymphocyte homing and leukocyte rolling and migration are impaired in L-selectin-deficient mice. Immunity. 1994 Jul;1(4):247–60.
21. Brady HR, Spertini O, Jimenez W, Brenner BM, Marsden PA, Tedder TF. Neutrophils, monocytes, and lymphocytes bind to cytokine-activated kidney glomerular endothelial cells through L-selectin (LAM-1) in vitro. J Immunol. 1992 Oct;149(7):2437–44.
22. Spertini O, Luscinskas FW, Gimbrone MA, Tedder TF. Monocyte attachment to activated human vascular endothelium in vitro is mediated by leukocyte adhesion molecule-1 (L-selectin) under nonstatic conditions. J Exp Med.

The Rockefeller University Press; 1992 Jun;175(6):1789–92.

23. Alon R, Kassner PD, Carr MW, Finger EB, Hemler ME, Springer TA. The Integrin VLA-4 Supports Tethering and Rolling in Flow on VCAM-1.
24. Stein J V, Cheng G, Stockton BM, Fors BP, Butcher EC, von Andrian UH. L-selectin-mediated leukocyte adhesion in vivo: microvillous distribution determines tethering efficiency, but not rolling velocity. J Exp Med. 1999 Jan;189(1):37–50.
25. Eriksson EE, Xie X, Werr J, Thoren P, Lindbom L. Importance of primary capture and L-selectin-dependent secondary capture in leukocyte accumulation in inflammation and atherosclerosis in vivo. J Exp Med. The Rockefeller University Press; 2001 Jul;194(2):205–18.
26. Alon R, Fuhlbrigge RC, Finger EB, Springer TA. Interactions through L-selectin between leukocytes and adherent leukocytes nucleate rolling adhesions on selectins and VCAM-1 in shear flow. J Cell Biol. 1996 Nov;135(3):849–65.
27. Paschall CD, Lawrence MB. L-selectin shear thresholding modulates leukocyte secondary capture. Ann Biomed Eng. 2008 Apr;36(4):622–31.
28. Kadash KE, Lawrence MB, Diamond SL. Neutrophil string formation: hydrodynamic thresholding and cellular deformation during cell collisions. Biophys J. The Biophysical Society; 2004 Jun;86(6):4030–9.
29. Kunkel EJ, Chomas JE, Ley K. Role of Primary and Secondary Capture for Leukocyte Accumulation In Vivo. Circ Res. Lippincott Williams & Wilkins; 1998 Jan;82(1):30–8.
30. Bullard DC, Kunkel EJ, Kubo H, Hicks MJ, Lorenzo I, Doyle NA, et al. Infectious susceptibility and severe deficiency of leukocyte rolling and recruitment in E-selectin and P-selectin double mutant mice. J Exp Med. The Rockefeller University Press; 1996 May;183(5):2329–36.
31. Jung U, Ley K. Mice lacking two or all three selectins demonstrate overlapping and distinct functions for each selectin. J Immunol. 1999 Jun;162(11):6755–62.
32. Jung U, Bullard DC, Tedder TF, Ley K. Velocity differences between L- and P-selectin-dependent neutrophil rolling in venules of mouse cremaster muscle in vivo. Am J Physiol. 1996 Dec;271(6 Pt 2):H2740-7.

33. Kunkel EJ, Ley K. Distinct phenotype of E-selectin-deficient mice. E-selectin is required for slow leukocyte rolling in vivo. Circ Res. 1996 Dec;79(6):1196–204.
34. Dwir O, Kansas GS, Alon R. Cytoplasmic anchorage of L-selectin controls leukocyte capture and rolling by increasing the mechanical stability of the selectin tether. J Cell Biol. 2001 Oct;155(1):145–56.
35. Ley K, Tedder TF, Kansas GS. L-selectin can mediate leukocyte rolling in untreated mesenteric venules in vivo independent of E- or P-selectin. Blood. 1993 Sep;82(5):1632–8.
36. McEver RP, Cummings RD. Perspectives series: cell adhesion in vascular biology. Role of PSGL-1 binding to selectins in leukocyte recruitment. J Clin Invest. American Society for Clinical Investigation; 1997 Aug;100(3):485–91.
37. Kansas GS. Selectins and their ligands: current concepts and controversies. Blood. 1996 Nov;88(9):3259–87.
38. Hidalgo A, Peired AJ, Wild MK, Vestweber D, Frenette PS. Complete identification of E-selectin ligands on neutrophils reveals distinct functions of PSGL-1, ESL-1, and CD44. Immunity. 2007 Apr;26(4):477–89.
39. Sokurenko E V, Vogel V, Thomas WE. Catch-bond mechanism of force-enhanced adhesion: counterintuitive, elusive, but ... widespread? Cell Host Microbe. 2008 Oct;4(4):314–23.
40. Lawrence MB, Kansas GS, Kunkel EJ, Ley K. Threshold levels of fluid shear promote leukocyte adhesion through selectins (CD62L,P,E). J Cell Biol. 1997 Feb;136(3):717–27.
41. Alon R, Chen S, Puri KD, Finger EB, Springer TA. The kinetics of L-selectin tethers and the mechanics of selectin-mediated rolling. J Cell Biol. 1997 Sep;138(5):1169–80.
42. Campbell ID, Humphries MJ. Integrin structure, activation, and interactions. Cold Spring Harb Perspect Biol [Internet]. Cold Spring Harbor Laboratory Press; 2011 Mar 1 [cited 2016 Dec 31];3(3):a004994. Available from: http://www.ncbi.nlm.nih.gov/pubmed/21421922
43. Canalli AA, Proença RF, Franco-Penteado CF, Traina F, Sakamoto TM, Saad STO, et al. Participation of Mac-1, LFA-1 and VLA-4 integrins in the in vitro

adhesion of sickle cell disease neutrophils to endothelial layers, and reversal of adhesion by simvastatin. Haematologica. 2011;96(4).

44. Conran N, Gambero A, Ferreira HHA, Antunes E, de Nucci G. Nitric oxide has a role in regulating VLA-4-integrin expression on the human neutrophil cell surface. Biochem Pharmacol. 2003;66(1):43–50.

45. Wang J. Pull and push: Talin activation for integrin signaling. Cell Res. Nature Publishing Group; 2012 Nov;22(11):1512–4.

46. Zarbock A, Lowell CA, Ley K. Syk signaling is necessary for E-selectin-induced LFA-1-ICAM-1 association and rolling but not arrest. Immunity. NIH Public Access; 2007;26(6):773.

47. Giagulli C, Ottoboni L, Caveggion E, Rossi B, Lowell C, Constantin G, et al. The Src Family Kinases Hck and Fgr Are Dispensable for Inside-Out, Chemoattractant-Induced Signaling Regulating 2 Integrin Affinity and Valency in Neutrophils, but Are Required for 2 Integrin-Mediated Outside-In Signaling Involved in Sustained Adhesion. J Immunol. American Association of Immunologists; 2006 Jul;177(1):604–11.

48. Hyduk SJ, Cybulsky MI. Role of alpha4beta1 integrins in chemokine-induced monocyte arrest under conditions of shear stress. Microcirculation. 2009 Jan;16(1):17–30.

49. Totani L, Evangelista V. Platelet-leukocyte interactions in cardiovascular disease and beyond. Arterioscler Thromb Vasc Biol. 2010 Dec;30(12):2357–61.

50. Bunting M, Harris ES, McIntyre TM, Prescott SM, Zimmerman GA. Leukocyte adhesion deficiency syndromes: adhesion and tethering defects involving beta 2 integrins and selectin ligands. Curr Opin Hematol. 2002 Jan;9(1):30–5.

51. Valignat M-P, Theodoly O, Gucciardi A, Hogg N, Lellouch AC. T lymphocytes orient against the direction of fluid flow during LFA-1-mediated migration. Biophys J [Internet]. The Biophysical Society; 2013 Jan 22 [cited 2016 Dec 31];104(2):322–31.

52. Dunne JL, Collins RG, Beaudet AL, Ballantyne CM, Ley K. Mac-1, but not LFA-1, uses intercellular adhesion molecule-1 to mediate slow leukocyte rolling in TNF-alpha-induced inflammation. J Immunol. 2003 Dec;171(11):6105–

Deleted: Available from: http://www.ncbi.nlm.nih.gov/pubmed/23442854

11.

53. Phillipson M, Heit B, Colarusso P, Liu L, Ballantyne CM, Kubes P. Intraluminal crawling of neutrophils to emigration sites: a molecularly distinct process from adhesion in the recruitment cascade. J Exp Med. 2006 Nov;203(12):2569–75.
54. Carman C V. Mechanisms for transcellular diapedesis: probing and pathfinding by "invadosome-like protrusions". J Cell Sci. The Company of Biologists Ltd; 2009 Sep;122(Pt 17):3025–35.
55. Carman C V, Springer TA. A transmigratory cup in leukocyte diapedesis both through individual vascular endothelial cells and between them. J Cell Biol. 2004 Oct;167(2):377–88.
56. Carman C V, Jun C-D, Salas A, Springer TA. Endothelial cells proactively form microvilli-like membrane projections upon intercellular adhesion molecule 1 engagement of leukocyte LFA-1. J Immunol. 2003 Dec;171(11):6135–44.
57. Barreiro O, Yáñez-Mó M, Sala-Valdés M, Gutiérrez-López MD, Ovalle S, Higginbottom A, et al. Endothelial tetraspanin microdomains regulate leukocyte firm adhesion during extravasation. Blood. 2005 Apr;105(7):2852–61.
58. Barreiro O, Zamai M, Yáñez-Mó M, Tejera E, López-Romero P, Monk PN, et al. Endothelial adhesion receptors are recruited to adherent leukocytes by inclusion in preformed tetraspanin nanoplatforms. J Cell Biol. Rockefeller University Press; 2008 Nov;183(3):527–42.
59. Yang L, Froio RM, Sciuto TE, Dvorak AM, Alon R, Luscinskas FW. ICAM-1 regulates neutrophil adhesion and transcellular migration of TNF-alpha-activated vascular endothelium under flow. Blood. 2005 Jul;106(2):584–92.
60. Ellerbroek SM, Wennerberg K, Arthur WT, Dunty JM, Bowman DR, DeMali KA, et al. SGEF, a RhoG guanine nucleotide exchange factor that stimulates macropinocytosis. Mol Biol Cell. American Society for Cell Biology; 2004 Jul;15(7):3309–19.
61. van Buul JD, Allingham MJ, Samson T, Meller J, Boulter E, García-Mata R, et al. RhoG regulates endothelial apical cup assembly downstream from ICAM1 engagement and is involved in leukocyte trans-endothelial

migration. J Cell Biol. 2007 Sep;178(7):1279–93.

62. Ley K, Zhang H. Dances with leukocytes: how tetraspanin-enriched microdomains assemble to form endothelial adhesive platforms. J Cell Biol. The Rockefeller University Press; 2008 Nov;183(3):375–6.

63. Phillipson M, Kaur J, Colarusso P, Ballantyne CM, Kubes P. Endothelial domes encapsulate adherent neutrophils and minimize increases in vascular permeability in paracellular and transcellular emigration. PLoS One. 2008;3(2):e1649.

64. Heemskerk N, Schimmel L, Oort C, van Rijssel J, Yin T, Ma B, et al. F-actin-rich contractile endothelial pores prevent vascular leakage during leukocyte diapedesis through local RhoA signalling. Nat Commun. Nature Publishing Group; 2016 Jan;7:10493.

65. Petri B, Kaur J, Long EM, Li H, Parsons SA, Butz S, et al. Endothelial LSP1 is involved in endothelial dome formation, minimizing vascular permeability changes during neutrophil transmigration in vivo. Blood. 2011 Jan;117(3):942–52.

66. Carman C V, Sage PT, Sciuto TE, de la Fuente MA, Geha RS, Ochs HD, et al. Transcellular diapedesis is initiated by invasive podosomes. Immunity. 2007 Jun;26(6):784–97.

67. Mamdouh Z, Mikhailov A, Muller WA. Transcellular migration of leukocytes is mediated by the endothelial lateral border recycling compartment. J Exp Med. 2009 Nov;206(12):2795–808.

68. von Wedel-Parlow M, Schrot S, Lemmen J, Treeratanapiboon L, Wegener J, Galla H-J. Neutrophils cross the BBB primarily on transcellular pathways: an in vitro study. Brain Res. 2011 Jan;1367:62–76.

69. Wewer C, Seibt A, Wolburg H, Greune L, Schmidt MA, Berger J, et al. Transcellular migration of neutrophil granulocytes through the blood-cerebrospinal fluid barrier after infection with Streptococcus suis. J Neuroinflammation. BioMed Central; 2011;8(1):51.

70. Takeshita Y, Ransohoff RM. Inflammatory cell trafficking across the blood-brain barrier: chemokine regulation and in vitro models. Immunol Rev. NIH Public Access; 2012 Jul;248(1):228–39.

71. Muller WA. Mechanisms of Transendothelial Migration of Leukocytes. Circ

Res. Lippincott Williams & Wilkins; 2009 Jul;105(3):223–30.

72. Stroka KM, Aranda-Espinoza H. Endothelial cell substrate stiffness influences neutrophil transmigration via myosin light chain kinase-dependent cell contraction. Blood. American Society of Hematology; 2011 Aug;118(6):1632–40.
73. Vestweber D. ATVB In Focus Vascular Adhesion Molecules VE-Cadherin The Major Endothelial Adhesion Molecule Controlling Cellular Junctions and Blood Vessel Formation. Arter Thromb Vasc Biol Arter Thromb Vasc Biol @BULLET Galkina E Arter Thromb Vasc Biol @BULLET Jalkanen S Arter Thromb Vasc Biol. 2007;27272728.
74. Dejana E, Orsenigo F, Lampugnani MG. The role of adherens junctions and VE-cadherin in the control of vascular permeability. J Cell Sci. The Company of Biologists Ltd; 2008 Jul;121(Pt 13):2115–22.
75. Potter MD, Barbero S, Cheresh DA. Tyrosine phosphorylation of VE-cadherin prevents binding of p120- and beta-catenin and maintains the cellular mesenchymal state. J Biol Chem. 2005 Sep;280(36):31906–12.
76. Hatanaka K, Simons M, Murakami M. Phosphorylation of VE-cadherin controls endothelial phenotypes via p120-catenin coupling and Rac1 activation. Am J Physiol Heart Circ Physiol. American Physiological Society; 2011 Jan;300(1):H162-72.
77. Alcaide P, Newton G, Auerbach S, Sehrawat S, Mayadas TN, Golan DE, et al. p120-Catenin regulates leukocyte transmigration through an effect on VE-cadherin phosphorylation. Blood. 2008 Oct;112(7):2770–9.
78. Mamdouh Z, Chen X, Pierini LM, Maxfield FR, Muller WA. Targeted recycling of PECAM from endothelial surface-connected compartments during diapedesis. Nature. 2003 Feb;421(6924):748–53.
79. Dasgupta B, Dufour E, Mamdouh Z, Muller WA. A novel and critical role for tyrosine 663 in platelet endothelial cell adhesion molecule-1 trafficking and transendothelial migration. J Immunol. NIH Public Access; 2009 Apr;182(8):5041–51.
80. Gonzalez AM, Cyrus B, Muller WA. VE-cadherin “gap” formation during transendothelial migration is regulated by a novel mechansim involving the lateral border recycling compartment. FASEB J. Federation of American

Societies for Experimental Biology; 2013;27(1 Supplement):57.11-57.11.

81. Dasgupta B, Muller WA. Endothelial Src kinase regulates membrane recycling from the lateral border recycling compartment during leukocyte transendothelial migration. Eur J Immunol. 2008 Dec;38(12):3499–507.

82. Winger RC, Koblinski JE, Kanda T, Ransohoff RM, Muller WA. Rapid remodeling of tight junctions during paracellular diapedesis in a human model of the blood-brain barrier. J Immunol [Internet]. NIH Public Access; 2014 Sep 1 [cited 2016 Dec 31];193(5):2427–37.

83. Schenkel AR, Mamdouh Z, Chen X, Liebman RM, Muller WA. CD99 plays a major role in the migration of monocytes through endothelial junctions. Nat Immunol. 2002 Feb;3(2):143–50.

84. Schenkel AR, Mamdouh Z, Muller WA. Locomotion of monocytes on endothelium is a critical step during extravasation. Nat Immunol. Nature Publishing Group; 2004 Apr;5(4):393–400.

85. Lou O, Alcaide P, Luscinskas FW, Muller WA. CD99 is a key mediator of the transendothelial migration of neutrophils. J Immunol. 2007 Jan;178(2):1136–43.

86. Woodfin A, Voisin M-B, Imhof BA, Dejana E, Engelhardt B, Nourshargh S. Endothelial cell activation leads to neutrophil transmigration as supported by the sequential roles of ICAM-2, JAM-A, and PECAM-1. Blood. 2009 Jun;113(24):6246–57.

87. Bixel MG, Li H, Petri B, Khandoga AG, Khandoga A, Zarbock A, et al. CD99 and CD99L2 act at the same site as, but independently of, PECAM-1 during leukocyte diapedesis. Blood. 2010 Aug;116(7):1172–84.

88. Feng D, Nagy JA, Pyne K, Dvorak HF, Dvorak AM. Neutrophils emigrate from venules by a transendothelial cell pathway in response to FMLP. J Exp Med. The Rockefeller University Press; 1998 Mar;187(6):903–15.

89. Lossinsky AS, Shivers RR. Structural pathways for macromolecular and cellular transport across the blood-brain barrier during inflammatory conditions. Review. Histol Histopathol. 2004 Apr;19(2):535–64.

90. Millán J, Hewlett L, Glyn M, Toomre D, Clark P, Ridley AJ. Lymphocyte transcellular migration occurs through recruitment of endothelial ICAM-1 to caveola- and F-actin-rich domains. Nat Cell Biol. Nature Publishing

Deleted: Available from: http://www.ncbi.nlm.nih.gov/pubmed/25063869

Group; 2006 Feb;8(2):113–23.

91. Marmon S, Hinchey J, Oh P, Cammer M, de Almeida CJ, Gunther L, et al. Caveolin-1 expression determines the route of neutrophil extravasation through skin microvasculature. Am J Pathol. American Society for Investigative Pathology; 2009 Feb;174(2):684–92.
92. Starnes TW, Huttenlocher A, Starnes TW, Huttenlocher A. Neutrophil Reverse Migration Becomes Transparent with Zebrafish. Adv Hematol. Hindawi Publishing Corporation; 2012;2012:1–11.
93. Raffaghello L, Pistoia V. Editorial: In-and-out blood vessels: new insights into T cell reverse transmigration. J Leukoc Biol. Society for Leukocyte Biology; 2009 Dec;86(6):1271–3.
94. Woodfin A, Voisin M-B, Beyrau M, Colom B, Caille D, Diapouli F-M, et al. The junctional adhesion molecule JAM-C regulates polarized transendothelial migration of neutrophils in vivo. Nat Immunol. Nature Research; 2011 Jun;12(8):761–9.
95. Colom B, Bodkin J V, Beyrau M, Woodfin A, Ody C, Rourke C, et al. Leukotriene B4-Neutrophil Elastase Axis Drives Neutrophil Reverse Transendothelial Cell Migration In Vivo. Immunity. 2015 Jun;42(6):1075–86.
96. Santoso S, Sachs UJH, Kroll H, Linder M, Ruf A, Preissner KT, et al. The junctional adhesion molecule 3 (JAM-3) on human platelets is a counterreceptor for the leukocyte integrin Mac-1. J Exp Med. 2002 Sep;196(5):679–91.
97. Yoo SK, Huttenlocher A. Spatiotemporal photolabeling of neutrophil trafficking during inflammation in live zebrafish. J Leukoc Biol. 2011 May;89(5):661–7.
98. Mathias JR, Perrin BJ, Liu T-X, Kanki J, Look AT, Huttenlocher A. Resolution of inflammation by retrograde chemotaxis of neutrophils in transgenic zebrafish. J Leukoc Biol. 2006 Aug;80(6):1281–8.
99. de Oliveira S, Rosowski EE, Huttenlocher A. Neutrophil migration in infection and wound repair: going forward in reverse. Nat Rev Immunol. Nature Research; 2016 May;16(6):378–91.
100. Paquet-Fifield S, Schlüter H, Li A, Aitken T, Gangatirkar P, Blashki D, et al. A

role for pericytes as microenvironmental regulators of human skin tissue regeneration. J Clin Invest. American Society for Clinical Investigation; 2009 Aug;119(9):7–25.

101. Hill J, Rom S, Ramirez SH, Persidsky Y. Emerging roles of pericytes in the regulation of the neurovascular unit in health and disease. J Neuroimmune Pharmacol. 2014 Dec;9(5):591–605.
102. Stark K, Eckart A, Haidari S, Tirniceriu A, Lorenz M, von Brühl M-L, et al. Capillary and arteriolar pericytes attract innate leukocytes exiting through venules and "instruct" them with pattern-recognition and motility programs. Nat Immunol. Nature Research; 2012 Nov;14(1):41–51.
103. Proebstl D, Voisin M-B, Woodfin A, Whiteford J, D'Acquisto F, Jones GE, et al. Pericytes support neutrophil subendothelial cell crawling and breaching of venular walls in vivo. J Exp Med. 2012 Jun;209(6):1219–34.
104. Wang S, Cao C, Chen Z, Bankaitis V, Tzima E, Sheibani N, et al. Pericytes Regulate Vascular Basement Membrane Remodeling and Govern Neutrophil Extravasation during Inflammation. Plow EF, editor. PLoS One. Public Library of Science; 2012 Sep;7(9):e45499.
105. Wiener J, Lattes RG, Spiro D. An electron microscopic study of leukocyte emigration and vascular permeability in tuberculin sensitivity. Am J Pathol. American Society for Investigative Pathology; 1967 Mar;50(3):485–521.
106. Wang S, Voisin M-B, Larbi KY, Dangerfield J, Scheiermann C, Tran M, et al. Venular basement membranes contain specific matrix protein low expression regions that act as exit points for emigrating neutrophils. J Exp Med. 2006 Jun;203(6):1519–32.
107. Carman C V, Springer TA. Trans-cellular migration: cell-cell contacts get intimate. Curr Opin Cell Biol. 2008 Oct;20(5):533–40.
108. Huttenlocher A, Horwitz AR. Integrins in Cell Migration. Cold Spring Harb Perspect Biol. Cold Spring Harbor Laboratory Press; 2011 Sep;3(9):a005074–a005074.
109. Lämmermann T, Germain RN. The multiple faces of leukocyte interstitial migration. Semin Immunopathol. NIH Public Access; 2014 Mar;36(2):227–51.
110. Lorentzen A, Bamber J, Sadok A, Elson-Schwab I, Marshall CJ. An ezrin-rich,

rigid uropod-like structure directs movement of amoeboid blebbing cells. J Cell Sci. 2011;124(8).

111. Thelen M, Stein J V. How chemokines invite leukocytes to dance. Nat Immunol [Internet]. Nature Publishing Group; 2008 Sep [cited 2016 Dec 31];9(9):953–9.

112. Baggiolini M. Chemokines and leukocyte traffic. Nature [Internet]. Nature Publishing Group; 1998 Apr 9;392(6676):565–8.

113. Altschuler SJ, Angenent SB, Wang Y, Wu LF. On the spontaneous emergence of cell polarity. Nature. Nature Publishing Group; 2008 Aug;454(7206):886–9.

114. Wedlich-Soldner R, Li R. Spontaneous cell polarization: undermining determinism. Nat Cell Biol. Nature Publishing Group; 2003 Apr;5(4):267–70.

115. Friedl P, Weigelin B. Interstitial leukocyte migration and immune function. Nat Immunol. 2008 Sep;9(9):960–9.

116. Marone R, Cmiljanovic V, Giese B, Wymann MP. Targeting phosphoinositide 3-kinase: moving towards therapy. Biochim Biophys Acta. 2008 Jan;1784(1):159–85.

117. Innocenti M, Frittoli E, Ponzanelli I, Falck JR, Brachmann SM, Paolo P, et al. Phosphoinositide 3-kinase activates Rac by entering in a complex with Eps8, Abi1, and Sos-1. J Cell Biol JCB J Cell Biol. Rockefeller University Press; 2003;1177(1):21–9525.

118. Heit B, Tavener S, Raharjo E, Kubes P. An intracellular signaling hierarchy determines direction of migration in opposing chemotactic gradients. J Cell Biol. 2002 Oct;159(1):91–102.

119. Germena G, Hirsch E. PI3Ks and small GTPases in neutrophil migration: two sides of the same coin. Mol Immunol. 2013 Aug;55(1):83–6.

120. Lämmermann T, Bader BL, Monkley SJ, Worbs T, Wedlich-Söldner R, Hirsch K, et al. Rapid leukocyte migration by integrin-independent flowing and squeezing. Nature. 2008 May;453(7191):51–5.

121. Li Z, Dong X, Dong X, Wang Z, Liu W, Deng N, et al. Regulation of PTEN by Rho small GTPases. Nat Cell Biol. 2005 Apr;7(4):399–404.

122. Heit B, Robbins SM, Downey CM, Guan Z, Colarusso P, Miller BJ, et al. PTEN

Deleted: Available from: http://www.nature.com/doifinder/10.1038/ni.f.207

Deleted: [cited 2016 Dec 31]

Deleted: ;

Deleted: Available from: http://www.nature.com/doifinder/10.1038/33340

functions to “prioritize” chemotactic cues and prevent “distraction” in migrating neutrophils. Nat Immunol. Nature Publishing Group; 2008 Jul;9(7):743–52.

123. Petrie RJ, Koo H, Yamada KM. Generation of compartmentalized pressure by a nuclear piston governs cell motility in a 3D matrix. Science (80-). 2014 Aug;345(6200):1062–5.
124. Worthylake RA, Burridge K. RhoA and ROCK promote migration by limiting membrane protrusions. J Biol Chem. 2003 Apr;278(15):13578–84.
125. Heasman SJ, Carlin LM, Cox S, Ng T, Ridley AJ. Coordinated RhoA signaling at the leading edge and uropod is required for T cell transendothelial migration. J Cell Biol. 2010 Aug;190(4):553–63.
126. Sánchez-Madrid F, Serrador JM. Bringing up the rear: defining the roles of the uropod. Nat Rev Mol Cell Biol. Nature Publishing Group; 2009 May;10(5):353–9.
127. Chen E, Shaffer M, Niggli V, Burkhardt J. Flotillins and ERM proteins function to promote uropod formation in T cells (44.10). J Immunol. American Association of Immunologists; 2010;184(1 Supplement):44.10-44.10.
128. Baumann T, Affentranger S, Niggli V. Analysis of close associations of uropod-associated proteins in human T-cells using the proximity ligation assay. PeerJ. 2013;1:e186.
129. Wenceslau CF, McCarthy CG, Goulopoulou S, Szasz T, NeSmith EG, Webb RC. Mitochondrial-derived N-formyl peptides: Novel links between trauma, vascular collapse and sepsis. Med Hypotheses [Internet]. 2013 Oct [cited 2016 Dec 31];81(4):532–5.
130. Campbell JJ, Foxman EF, Butcher EC. Chemoattractant receptor cross talk as a regulatory mechanism in leukocyte adhesion and migration. Eur J Immunol. 1997 Oct;27(10):2571–8.
131. Foxman EF, Campbell JJ, Butcher EC. Multistep navigation and the combinatorial control of leukocyte chemotaxis. J Cell Biol. 1997 Dec;139(5):1349–60.
132. Shen W, Li B, Wetzel MA, Rogers TJ, Henderson EE, Su SB, et al. Down-regulation of the chemokine receptor CCR5 by activation of chemotactic

Deleted: Available from: http://www.ncbi.nlm.nih.gov/pubmed/23890799

formyl peptide receptor in human monocytes. Blood. 2000 Oct;96(8):2887–94.

133. Heit B, Colarusso P, Kubes P. Fundamentally different roles for LFA-1, Mac-1 and alpha4-integrin in neutrophil chemotaxis. J Cell Sci. 2005 Nov;118(Pt 22):5205–20.
134. Ali H, Richardson RM, Haribabu B, Snyderman R. Chemoattractant Receptor Cross-desensitization. J Biol Chem. American Society for Biochemistry and Molecular Biology; 1999 Mar;274(10):6027–30.
135. Ali H, Ali H, Tomhave ED, Haribabu B, Snyderman R. Cross-desensitization of Chemoattractant Receptors Occurs at Multiple Levels. J Biol Chem. American Society for Biochemistry and Molecular Biology; 1995 Nov;270(46):27829–33.
136. Bohn LM, Lefkowitz RJ, Gainetdinov RR, Peppel K, Caron MG, Lin FT. Enhanced morphine analgesia in mice lacking beta-arrestin 2. Science. 1999 Dec;286(5449):2495–8.
137. Luttrell LM, Lefkowitz RJ. The role of beta-arrestins in the termination and transduction of G-protein-coupled receptor signals. J Cell Sci. 2002 Feb;115(Pt 3):455–65.
138. Reiter E, Lefkowitz RJ, Takeda S, al. et, Pierce KL, al. et, et al. GRKs and β-arrestins: roles in receptor silencing, trafficking and signaling. Trends Endocrinol Metab. Elsevier; 2006 May;17(4):159–65.
139. Barak LS, Oakley RH, Laporte SA, Caron MG. Constitutive arrestin-mediated desensitization of a human vasopressin receptor mutant associated with nephrogenic diabetes insipidus. Proc Natl Acad Sci U S A. 2001 Jan;98(1):93–8.
140. Davis GE, Senger DR. Endothelial Extracellular Matrix: Biosynthesis, Remodeling, and Functions During Vascular Morphogenesis and Neovessel Stabilization. Circ Res. Lippincott Williams & Wilkins; 2005 Nov;97(11):1093–107.
141. Sava P, Cook IO, Mahal RS, Gonzalez AL. Human microvascular pericyte basement membrane remodeling regulates neutrophil recruitment. Microcirculation. 2015 Jan;22(1):54–67.
142. Collins C, Osborne LD, Guilluy C, Chen Z, O'Brien ET, Reader JS, et al.

Haemodynamic and extracellular matrix cues regulate the mechanical phenotype and stiffness of aortic endothelial cells. Nat Commun. NIH Public Access; 2014;5:3984.

143. Adair-Kirk TL, Senior RM. Fragments of extracellular matrix as mediators of inflammation. Int J Biochem Cell Biol [Internet]. NIH Public Access; 2008 [cited 2016 Dec 31];40(6–7):1101–10. Available from: http://www.ncbi.nlm.nih.gov/pubmed/18243041
144. Weathington NM, van Houwelingen AH, Noerager BD, Jackson PL, Kraneveld AD, Galin FS, et al. A novel peptide CXCR ligand derived from extracellular matrix degradation during airway inflammation. Nat Med. 2006 Mar;12(3):317–23.
145. Handel TM, Johnson Z, Crown SE, Lau EK, Proudfoot AE. Regulation of protein function by glycosaminoglycans--as exemplified by chemokines. Annu Rev Biochem. 2005;74:385–410.
146. Kumar A V, Katakam SK, Urbanowitz A-K, Gotte M. Heparan sulphate as a regulator of leukocyte recruitment in inflammation. Curr Protein Pept Sci. 2015;16(1):77–86.
147. Kolaczkowska E, Kubes P. Neutrophil recruitment and function in health and inflammation. Nat Rev Immunol. 2013 Mar;13(3):159–75.
148. García-García E, Rosales C. Signal transduction during Fc receptor-mediated phagocytosis. J Leukoc Biol. 2002 Dec;72(6):1092–108.
149. Freeman SA, Grinstein S. Phagocytosis: receptors, signal integration, and the cytoskeleton. Immunol Rev. 2014 Nov;262(1):193–215.
150. Smirnov A, Daily KP, Criss AK. Assembly of NADPH oxidase in human neutrophils is modulated by the opacity-associated protein expression State of Neisseria gonorrhoeae. Infect Immun. American Society for Microbiology (ASM); 2014 Mar;82(3):1036–44.
151. Hawes MC, Curlango-Rivera G, Wen F, White GJ, Vanetten HD, Xiong Z. Extracellular DNA: the tip of root defenses? Plant Sci. 2011 Jun;180(6):741–5.
152. von Köckritz-Blickwede M, Goldmann O, Thulin P, Heinemann K, Norrby-Teglund A, Rohde M, et al. Phagocytosis-independent antimicrobial activity of mast cells by means of extracellular trap formation. Blood. 2008

Mar;111(6):3070–80.

153. Chow OA, von Köckritz-Blickwede M, Bright AT, Hensler ME, Zinkernagel AS, Cogen AL, et al. Statins enhance formation of phagocyte extracellular traps. Cell Host Microbe. 2010 Nov;8(5):445–54.
154. Aulik NA, Hellenbrand KM, Klos H, Czuprynski CJ. Mannheimia haemolytica and its leukotoxin cause neutrophil extracellular trap formation by bovine neutrophils. Infect Immun. American Society for Microbiology (ASM); 2010 Nov;78(11):4454–66.
155. Menegazzi R, Decleva E, Dri P. Killing by neutrophil extracellular traps: fact or folklore? 2012;119(5):1214–6.
156. Saitoh T, Komano J, Saitoh Y, Misawa T, Takahama M, Kozaki T, et al. Neutrophil extracellular traps mediate a host defense response to human immunodeficiency virus-1. Cell Host Microbe. 2012 Jul;12(1):109–16.
157. Megens RTA, Vijayan S, Lievens D, Döring Y, van Zandvoort MAMJ, Grommes J, et al. Presence of luminal neutrophil extracellular traps in atherosclerosis. Thromb Haemost. 2012 Mar;107(3):597–8.
158. Metzler KD, Fuchs TA, Nauseef WM, Reumaux D, Roesler J, Schulze I, et al. Myeloperoxidase is required for neutrophil extracellular trap formation: implications for innate immunity. Blood. 2011 Jan;117(3):953–9.
159. Branzk N, Lubojemska A, Hardison SE, Wang Q, Gutierrez MG, Brown GD, et al. Neutrophils sense microbe size and selectively release neutrophil extracellular traps in response to large pathogens. Nat Immunol. Nature Research; 2014 Sep;15(11):1017–25.
160. Craig A, Mai J, Cai S, Jeyaseelan S. Neutrophil Recruitment to the Lungs during Bacterial Pneumonia. Infect Immun. American Society for Microbiology; 2009 Feb;77(2):568–75.
161. Davey MS, Lin C-Y, Roberts GW, Heuston S, Brown AC, Chess JA, et al. Human Neutrophil Clearance of Bacterial Pathogens Triggers Anti-Microbial γδ T Cell Responses in Early Infection. Wherry EJ, editor. PLoS Pathog. Public Library of Science; 2011 May;7(5):e1002040.
162. Segal AW. How Neutrophils Kill Microbes. Annu Rev Immunol. Europe PMC Funders; 2005;23:197.
163. DevelopingCountries I of M (US) C on P the GE of CDM the C in, Fuster V,

Kelly BB. Epidemiology of Cardiovascular Disease. National Academies Press (US); 2010;

164. Rotzius P, Thams S, Soehnlein O, Kenne E, Tseng C-N, Björkström NK, et al. Distinct infiltration of neutrophils in lesion shoulders in ApoE-/- mice. Am J Pathol. American Society for Investigative Pathology; 2010 Jul;177(1):493–500.
165. Hosokawa T, Kumon Y, Kobayashi T, Enzan H, Nishioka Y, Yuri K, et al. Neutrophil infiltration and oxidant-production in human atherosclerotic carotid plaques. Histol Histopathol. 2011 Jan;26(1):1–11.
166. Barnathan ES, Raghunath PN, Tomaszewski JE, Ganz T, Cines DB, Higazi A al-R. Immunohistochemical localization of defensin in human coronary vessels. Am J Pathol. 1997 Mar;150(3):1009–20.
167. Boisvert WA, Rose DM, Johnson KA, Fuentes ME, Lira SA, Curtiss LK, et al. Up-regulated expression of the CXCR2 ligand KC/GRO-alpha in atherosclerotic lesions plays a central role in macrophage accumulation and lesion progression. Am J Pathol. American Society for Investigative Pathology; 2006 Apr;168(4):1385–95.
168. Warnatsch A, Ioannou M, Wang Q, Papayannopoulos V. Inflammation. Neutrophil extracellular traps license macrophages for cytokine production in atherosclerosis. Science. Europe PMC Funders; 2015 Jul;349(6245):316–20.
169. Oyama J, Blais C, Liu X, Pu M, Kobzik L, Kelly RA, et al. Reduced myocardial ischemia-reperfusion injury in toll-like receptor 4-deficient mice. Circulation. 2004 Feb;109(6):784–9.
170. Oka T, Hikoso S, Yamaguchi O, Taneike M, Takeda T, Tamai T, et al. Mitochondrial DNA that escapes from autophagy causes inflammation and heart failure. Nature. Nature Research; 2012 Apr;485(7397):251–5.
171. Jolly SR, Kane WJ, Hook BG, Abrams GD, Kunkel SL, Lucchesi BR. Reduction of myocardial infarct size by neutrophil depletion: effect of duration of occlusion. Am Heart J. 1986 Oct;112(4):682–90.
172. Romson JL, Hook BG, Kunkel SL, Abrams GD, Schork MA, Lucchesi BR. Reduction of the extent of ischemic myocardial injury by neutrophil depletion in the dog. Circulation. 1983 May;67(5):1016–23.

173. Epelman S, Liu PP, Mann DL. Role of innate and adaptive immune mechanisms in cardiac injury and repair. Nat Rev Immunol. Nature Research; 2015 Jan;15(2):117–29.
174. Isenberg WM, McEver RP, Shuman MA, Bainton DF. Topographic distribution of a granule membrane protein (GMP-140) that is expressed on the platelet surface after activation: an immunogold-surface replica study. Blood Cells. 1986;12(1):191–204.
175. Berman CL, Yeo EL, Wencel-Drake JD, Furie BC, Ginsberg MH, Furie B. A platelet alpha granule membrane protein that is associated with the plasma membrane after activation. Characterization and subcellular localization of platelet activation-dependent granule-external membrane protein. J Clin Invest. 1986 Jul;78(1):130–7.
176. Gallatin WM, Weissman IL, Butcher EC. A cell-surface molecule involved in organ-specific homing of lymphocytes. Nature. 304(5921):30–4.
177. Bonfanti R, Furie BC, Furie B, Wagner DD. PADGEM (GMP140) is a component of Weibel-Palade bodies of human endothelial cells. Blood. 1989 Apr;73(5):1109–12.
178. Hickey MJ, Kanwar S, McCafferty DM, Granger DN, Eppihimer MJ, Kubes P. Varying roles of E-selectin and P-selectin in different microvascular beds in response to antigen. J Immunol. 1999 Jan;162(2):1137–43.
179. Chapman PT, Jamar F, Keelan ETM, Peters AM, Haskard DO. Use of a radiolabeled monoclonal antibody against e-selectin for imaging of endothelial activation in rheumatoid arthritis. Arthritis Rheum. 1996 Aug;39(8):1371–5.
180. Huang RB, Eniola-Adefeso O, Coussens L, Werb Z, Davies P, Shi C, et al. Shear Stress Modulation of IL-1β-Induced E-Selectin Expression in Human Endothelial Cells. Chan C, editor. PLoS One. Public Library of Science; 2012 Feb;7(2):e31874.
181. Geng JG, Moore KL, Johnson AE, McEver RP. Neutrophil recognition requires a Ca(2+)-induced conformational change in the lectin domain of GMP-140. J Biol Chem. 1991 Nov;266(33):22313–8.
182. O'Connell D, Koenig A, Jennings S, Hicke B, Han HL, Fitzwater T, et al. Calcium-dependent oligonucleotide antagonists specific for L-selectin. Proc

Natl Acad Sci U S A. National Academy of Sciences; 1996 Jun;93(12):5883–7.

183. Somers WS, Tang J, Shaw GD, Camphausen RT. Insights into the molecular basis of leukocyte tethering and rolling revealed by structures of P- and E-selectin bound to SLe(X) and PSGL-1. Cell. 2000 Oct;103(3):467–79.
184. Zhao L, Shey M, Farnsworth M, Dailey MO. Regulation of membrane metalloproteolytic cleavage of L-selectin (CD62l) by the epidermal growth factor domain. J Biol Chem. 2001 Aug;276(33):30631–40.
185. Phan UT, Waldron TT, Springer TA. Remodeling of the lectin-EGF-like domain interface in P- and L-selectin increases adhesiveness and shear resistance under hydrodynamic force. Nat Immunol. 2006 Aug;7(8):883–9.
186. Lou J, Yago T, Klopocki AG, Mehta P, Chen W, Zarnitsyna VI, et al. Flow-enhanced adhesion regulated by a selectin interdomain hinge. J Cell Biol. Rockefeller University Press; 2006 Sep;174(7):1107–17.
187. McEver RP, Beckstead JH, Moore KL, Marshall-Carlson L, Bainton DF. GMP-140, a platelet alpha-granule membrane protein, is also synthesized by vascular endothelial cells and is localized in Weibel-Palade bodies. J Clin Invest. American Society for Clinical Investigation; 1989 Jul;84(1):92–9.
188. Tedder TF, Isaacs CM, Ernst TJ, Demetri GD, Adler DA, Disteche CM. Isolation and chromosomal localization of cDNAs encoding a novel human lymphocyte cell surface molecule, LAM-1. Homology with the mouse lymphocyte homing receptor and other human adhesion proteins. J Exp Med. 1989 Jul;170(1):123–33.
189. Kansas GS, Saunders KB, Ley K, Zakrzewicz A, Gibson RM, Furie BC, et al. A role for the epidermal growth factor-like domain of P-selectin in ligand recognition and cell adhesion. J Cell Biol. 1994 Feb;124(4):609–18.
190. Barkalow FJ, Barkalow KL, Mayadas TN. Dimerization of P-selectin in platelets and endothelial cells. Blood. 2000 Nov;96(9):3070–7.
191. Lemmon MA, Treutlein HR, Adams PD, Brünger AT, Engelman DM. A dimerization motif for transmembrane α–helices. Nat Struct Biol. Nature Publishing Group; 1994 Mar;1(3):157–63.
192. Ushiyama S, Laue TM, Moore KL, Erickson HP, McEver RP. Structural and functional characterization of monomeric soluble P-selectin and

comparison with membrane P-selectin. J Biol Chem. 1993 Jul;268(20):15229–37.

193. Ramachandran V, Yago T, Epperson TK, Kobzdej MMA, Nollert MU, Cummings RD, et al. Dimerization of a selectin and its ligand stabilizes cell rolling and enhances tether strength in shear flow. Proc Natl Acad Sci. 2001 Aug;98(18):10166–71.
194. Buscher K, Riese SB, Shakibaei M, Reich C, Dernedde J, Tauber R, et al. The transmembrane domains of L-selectin and CD44 regulate receptor cell surface positioning and leukocyte adhesion under flow. J Biol Chem. 2010 Apr;285(18):13490–7.
195. Yoshida M, Westlin WF, Wang N, Ingber DE, Rosenzweig A, Resnick N, et al. Leukocyte adhesion to vascular endothelium induces E-selectin linkage to the actin cytoskeleton. J Cell Biol. 1996 Apr;133(2):445–55.
196. Gimbrone MA, Masayuki Yoshida J, Szente BE, Kiely J-M, Yoshida M, Rosenzweig A. Leukocyte-Endothelial Adhesion E-Selectin Is Regulated During Phosphorylation of the Cytoplasmic Domain of Phosphorylation of the Cytoplasmic Domain of E-Selectin Is Regulated During Leukocyte-Endothelial Adhesion. J Immunol Ref. 1998;161:933–41.
197. Yoshida M, Szente BE, Kiely JM, Rosenzweig A, Gimbrone MA. Phosphorylation of the cytoplasmic domain of E-selectin is regulated during leukocyte-endothelial adhesion. J Immunol. American Association of Immunologists; 1998 Jul;161(2):933–41.
198. Hartwell DW, Mayadas TN, Berger G, Frenette PS, Rayburn H, Hynes RO, et al. Role of P-Selectin Cytoplasmic Domain in Granular Targeting In Vivo and in Early Inflammatory Responses. J Cell Biol. 1998;143(4):1129–41.
199. Ivetic A, Ridley AJ. The telling tail of L-selectin. Biochem Soc Trans. 2004 Dec;32(Pt 6):1118–21.
200. Pavalko FM, Walker DM, Graham L, Goheen M, Doerschuk CM, Kansas GS. The cytoplasmic domain of L-selectin interacts with cytoskeletal proteins via alpha-actinin: receptor positioning in microvilli does not require interaction with alpha-actinin. J Cell Biol. 1995 May;129(4):1155–64.
201. Pearson MA, Reczek D, Bretscher A, Karplus PA. Structure of the ERM Protein Moesin Reveals the FERM Domain Fold Masked by an Extended

Actin Binding Tail Domain. Cell. 2000;101(3):259–70.

202. Fehon RG, McClatchey AI, Bretscher A. Organizing the cell cortex: the role of ERM proteins. Nat Rev Mol Cell Biol. Nature Publishing Group; 2010 Apr;11(4):276–87.

203. Hirao M, Sato N, Kondo T, Yonemura S, Monden M, Sasaki T, et al. Regulation mechanism of ERM (ezrin/radixin/moesin) protein/plasma membrane association: possible involvement of phosphatidylinositol turnover and Rho-dependent signaling pathway. J Cell Biol. 1996 Oct;135(1):37–51.

204. Baumgartner M, Sillman AL, Blackwood EM, Srivastava J, Madson N, Schilling JW, et al. The Nck-interacting kinase phosphorylates ERM proteins for formation of lamellipodium by growth factors. Proc Natl Acad Sci U S A. 2006 Sep;103(36):13391–6.

205. Nakamura N, Oshiro N, Fukata Y, Amano M, Fukata M, Kuroda S, et al. Phosphorylation of ERM proteins at ®lopodia induced by Cdc42.

206. Ng T, Parsons M, Hughes WE, Monypenny J, Zicha D, Gautreau A, et al. Ezrin is a downstream effector of trafficking PKC-integrin complexes involved in the control of cell motility. EMBO J. European Molecular Biology Organization; 2001 Jun;20(11):2723–41.

207. Ivetic A, Ridley AJ. Ezrin/radixin/moesin proteins and Rho GTPase signalling in leucocytes. Immunology. Wiley-Blackwell; 2004 Jun;112(2):165–76.

208. Sit S-T, Manser E, Albiges-Rizo C, Destaing O, Fourcade B, Planus E, et al. Rho GTPases and their role in organizing the actin cytoskeleton. J Cell Sci. The Company of Biologists Ltd; 2011 Mar;124(Pt 5):679–83.

209. Killock DJ, Ivetić A. The cytoplasmic domains of TNFalpha-converting enzyme (TACE/ADAM17) and L-selectin are regulated differently by p38 MAPK and PKC to promote ectodomain shedding. Biochem J. 2010 Jun;428(2):293–304.

210. Ivetic A, Florey O, Deka J, Haskard DO, Ager A, Ridley AJ. Mutagenesis of the Ezrin-Radixin-Moesin Binding Domain of L-selectin Tail Affects Shedding, Microvillar Positioning, and Leukocyte Tethering. J Biol Chem. American Society for Biochemistry and Molecular Biology; 2004 Aug;279(32):33263–

72.

211. Kahn J, Walcheck B, Migaki GI, Jutila MA, Kishimoto TK. Calmodulin Regulates L-Selectin Adhesion Molecule Expression and Function through a Protease-Dependent Mechanism. Cell. 1998;92(6):809–18.
212. Rzeniewicz K, Newe A, Rey Gallardo A, Davies J, Holt MR, Patel A, et al. L-selectin shedding is activated specifically within transmigrating pseudopods of monocytes to regulate cell polarity in vitro. Proc Natl Acad Sci. National Academy of Sciences; 2015 Mar;112(12):201417100.
213. Gifford JL, Ishida H, Vogel HJ. Structural insights into calmodulin-regulated L-selectin ectodomain shedding. J Biol Chem. American Society for Biochemistry and Molecular Biology; 2012 Aug;287(32):26513–27.
214. Giblin PA, Hwang ST, Katsumoto TR, Rosen SD. Ligation of L-selectin on T lymphocytes activates beta1 integrins and promotes adhesion to fibronectin. J Immunol. 1997 Oct;159(7):3498–507.
215. Hwang ST, Singer MS, Giblin PA, Yednock TA, Bacon KB, Simon SI, et al. GlyCAM-1, a physiologic ligand for L-selectin, activates beta 2 integrins on naive peripheral lymphocytes. J Exp Med. 1996 Oct;184(4):1343–8.
216. Killock DJ, Parsons M, Zarrouk M, Ameer-Beg SM, Ridley AJ, Haskard DO, et al. In Vitro and in Vivo Characterization of Molecular Interactions between Calmodulin, Ezrin/Radixin/Moesin, and L-selectin. J Biol Chem. 2009 Mar;284(13):8833–45.
217. Deng W, Putkey JA, Li R, Schlondorff J, Blobel C, Mechtersheimer S, et al. Calmodulin Adopts an Extended Conformation when Interacting with L-Selectin in Membranes. Hong W, editor. PLoS One. Public Library of Science; 2013 May;8(5):e62861.
218. Deng W, Cho S, Li R. FERM Domain of Moesin Desorbs the Basic-Rich Cytoplasmic Domain of l-Selectin from the Anionic Membrane Surface. J Mol Biol. 2013 Sep;425(18):3549–62.
219. Brenner B, Gulbins E, Schlottmann K, Koppenhoefer U, Busch GL, Walzog B, et al. L-selectin activates the Ras pathway via the tyrosine kinase p56lck. Proc Natl Acad Sci U S A. National Academy of Sciences; 1996 Dec;93(26):15376–81.
220. Sperka T, Geissler KJ, Merkel U, Scholl I, Rubio I, Herrlich P, et al. Activation

of Ras requires the ERM-dependent link of actin to the plasma membrane. PLoS One. 2011;6(11):e27511.

221. Villalonga P, López-Alcalá C, Bosch M, Chiloeches A, Rocamora N, Gil J, et al. Calmodulin binds to K-Ras, but not to H- or N-Ras, and modulates its downstream signaling. Mol Cell Biol. 2001 Nov;21(21):7345–54.
222. Castellano E, Downward J. RAS Interaction with PI3K: More Than Just Another Effector Pathway. Genes Cancer. Impact Journals, LLC; 2011 Mar;2(3):261–74.
223. Chang F, Steelman LS, Lee JT, Shelton JG, Navolanic PM, Blalock WL, et al. Signal transduction mediated by the Ras/Raf/MEK/ERK pathway from cytokine receptors to transcription factors: potential targeting for therapeutic intervention. Leukemia. Nature Publishing Group; 2003 Jul;17(7):1263–93.
224. Castellano E, Molina-Arcas M, Krygowska AA, East P, Warne P, Nicol A, et al. RAS signalling through PI3-Kinase controls cell migration via modulation of Reelin expression. Nat Commun. Nature Publishing Group; 2016 Apr;7:11245.
225. Secko DM, Siu C-H, Spiegelman GB, Weeks G. An activated Ras protein alters cell adhesion by dephosphorylating Dictyostelium DdCAD-1. Microbiology. 2006 May;152(Pt 5):1497–505.
226. Kilian K, Dernedde J, Mueller E-C, Bahr I, Tauber R. The interaction of protein kinase C isozymes alpha, iota, and theta with the cytoplasmic domain of L-selectin is modulated by phosphorylation of the receptor. J Biol Chem. 2004 Aug;279(33):34472–80.
227. Fuhlbrigge RC, Alon R, Puri KD, Lowe JB, Springer TA. Sialylated, fucosylated ligands for L-selectin expressed on leukocytes mediate tethering and rolling adhesions in physiologic flow conditions. J Cell Biol [Internet]. The Rockefeller University Press; 1996 Nov [cited 2016 Dec 31];135(3):837–48.
228. Imai Y, Singer MS, Fennie C, Lasky LA, Rosen SD. Identification of a carbohydrate-based endothelial ligand for a lymphocyte homing receptor. J Cell Biol. 1991 Jun;113(5):1213–21.
229. Alon R, Rosen S. Rolling on N-linked glycans: a new way to present L-

Deleted: Available from: http://www.ncbi.nlm.nih.gov/pubmed/8909555

selectin binding sites. Nat Immunol. 2007 Apr;8(4):339–41.

230. Rodgers SD, Camphausen RT, Hammer DA. Tyrosine Sulfation Enhances but Is Not Required for PSGL-1 Rolling Adhesion on P-Selectin. Repr from Biophys J. 2001;81(4):2001–9.
231. Martinez M, Joffraud M, Giraud S, Baisse B, Bernimoulin MP, Schapira M, et al. Regulation of PSGL-1 Interactions with L-selectin, P-selectin, and E-selectin: ROLE OF HUMAN FUCOSYLTRANSFERASE-IV AND -VII. J Biol Chem. American Society for Biochemistry and Molecular Biology; 2005 Feb;280(7):5378–90.
232. Umemoto E, Tanaka T, Kanda H, Jin S, Tohya K, Otani K, et al. Nepmucin, a novel HEV sialomucin, mediates L-selectin-dependent lymphocyte rolling and promotes lymphocyte adhesion under flow. J Exp Med. The Rockefeller University Press; 2006 Jun;203(6):1603–14.
233. Puri KD, Finger EB, Gaudernack G, Springer TA. Sialomucin CD34 is the major L-selectin ligand in human tonsil high endothelial venules. J Cell Biol. 1995 Oct;131(1):261–70.
234. Joseph A, Hossain P, Jham S, Jones RE, Tighe P, McIntosh RS, et al. Expression of CD34 and L-selectin on human corneal keratocytes. Invest Ophthalmol Vis Sci. 2003 Nov;44(11):4689–92.
235. Baumheter S, Singer M, Henzel W, Hemmerich S, Renz M, Rosen S, et al. Binding of L-selectin to the vascular sialomucin CD34. Science (80-). 1993 Oct;262(5132):436–8.
236. Rosen SD, Tsay D, Singer MS, Hemmerich S, Abraham WM. Therapeutic targeting of endothelial ligands for L-selectin (PNAd) in a sheep model of asthma. Am J Pathol. 2005 Mar;166(3):935–44.
237. Thomas SN, Schnaar RL, Konstantopoulos K. Podocalyxin-like protein is an E-/L-selectin ligand on colon carcinoma cells: comparative biochemical properties of selectin ligands in host and tumor cells. Am J Physiol Cell Physiol. American Physiological Society; 2009 Mar;296(3):C505-13.
238. Berg EL, McEvoy LM, Berlin C, Bargatze RF, Butcher EC. L-selectin-mediated lymphocyte rolling on MAdCAM-1. Nature. Nature Publishing Group; 1993 Dec;366(6456):695–8.
239. Kawashima H, Hirose M, Hirose J, Nagakubo D, Plaas AH, Miyasaka M.

Binding of a large chondroitin sulfate/dermatan sulfate proteoglycan, versican, to L-selectin, P-selectin, and CD44. J Biol Chem. 2000 Nov;275(45):35448–56.

240. Kawashima H, Li YF, Watanabe N, Hirose J, Hirose M, Miyasaka M. Identification and characterization of ligands for L-selectin in the kidney. I. Versican, a large chondroitin sulfate proteoglycan, is a ligand for L-selectin. Int Immunol. 1999 Mar;11(3):393–405.
241. Kitaya K, Yasuo T. Dermatan sulfate proteoglycan biglycan as a potential selectin L/CD44 ligand involved in selective recruitment of peripheral blood CD16(-) natural killer cells into human endometrium. J Leukoc Biol. 2009 Mar;85(3):391–400.
242. Kawashima H, Watanabe N, Hirose M, Sun X, Atarashi K, Kimura T, et al. Collagen XVIII, a basement membrane heparan sulfate proteoglycan, interacts with L-selectin and monocyte chemoattractant protein-1. J Biol Chem. 2003 Apr;278(15):13069–76.
243. Azadeh Z, Ditmer TT, Saleh Y, Johanna WAMC, Mari A, Ritva H, et al. Collagen XVIII interacts with L-selectin and MCP-1 via its N-terminal HS side chains. 2014;
244. Stoolman Mark A Jutila LM, Kurk S, Jackiw L, Lymphoblasts T, Jutila MA, Knibbs RN, et al. Cultured Human T Lymphoblasts L-Selectin Serves as an E-Selectin Ligand on L-Selectin Serves as an E-Selectin Ligand on Cultured Human. J Immunol Ref. 2002;169(4):1768–73.
245. Ord DC, Ernst TJ, Zhou LJ, Rambaldi A, Spertini O, Griffin J, et al. Structure of the gene encoding the human leukocyte adhesion molecule-1 (TQ1, Leu-8) of lymphocytes and neutrophils. J Biol Chem. 1990 May;265(14):7760–7.
246. Hirata T, Usui T, Kobayashi S, Mimori T. A novel splice variant of human L-selectin encodes a soluble molecule that is elevated in serum of patients with rheumatic diseases. Biochem Biophys Res Commun. 2015 Jul;462(4):371–7.
247. Dang X, Raffler NA, Ley K. Transcriptional regulation of mouse L-selectin. BBA - Gene Regul Mech. 2008;1789:146–52.
248. Arlian LG, Fall N, Morgan MS. In vivo evidence that Sarcoptes scabiei (Acari: Sarcoptidae) is the source of molecules that modulate splenic gene

expression. J Med Entomol. 2007 Nov;44(6):1054–63.

249. Tedder TF, Matsuyama T, Rothstein D, Schlossman SF, Morimoto C. Human antigen-specific memory T cells express the homing receptor (LAM-1) necessary for lymphocyte recirculation. Eur J Immunol. 1990 Jun;20(6):1351–5.

250. Zöllner O, Lenter MC, Blanks JE, Borges E, Steegmaier M, Zerwes HG, et al. L-selectin from human, but not from mouse neutrophils binds directly to E-selectin. J Cell Biol. The Rockefeller University Press; 1997 Feb;136(3):707–16.

251. Kahn J, Ingraham RH, Shirley F, Migaki GI, Kishimoto TK. Membrane proximal cleavage of L-selectin: identification of the cleavage site and a 6-kD transmembrane peptide fragment of L-selectin. J Cell Biol. 1994 Apr;125(2):461–70.

252. Le Gall SM, Bobé P, Reiss K, Horiuchi K, Niu X-D, Lundell D, et al. ADAMs 10 and 17 represent differentially regulated components of a general shedding machinery for membrane proteins such as transforming growth factor alpha, L-selectin, and tumor necrosis factor alpha. Mol Biol Cell. American Society for Cell Biology; 2009 Mar;20(6):1785–94.

253. Gómez-Gaviro M, Domínguez-Luis M, Canchado J, Calafat J, Janssen H, Lara-Pezzi E, et al. Expression and regulation of the metalloproteinase ADAM-8 during human neutrophil pathophysiological activation and its catalytic activity on L-selectin shedding. J Immunol. 2007 Jun;178(12):8053–63.

254. Chen A, Engel P, Tedder TF. Structural requirements regulate endoproteolytic release of the L-selectin (CD62L) adhesion receptor from the cell surface of leukocytes. J Exp Med. 1995 Aug;182(2):519–30.

255. Li Y, Brazzell J, Herrera A, Walcheck B. ADAM17 deficiency by mature neutrophils has differential effects on L-selectin shedding. Blood. American Society of Hematology; 2006 Oct;108(7):2275–9.

256. Walcheck B, Alexander SR, Hill CAS, Matala E. ADAM-17-independent shedding of L-selectin.

257. Walcheck B, Alexander SR, St Hill CA, Matala E. ADAM-17-independent shedding of L-selectin. J Leukoc Biol. 2003 Sep;74(3):389–94.

258. Schleiffenbaum B, Spertini O, Tedder TF. Soluble L-selectin is present in

human plasma at high levels and retains functional activity. J Cell Biol. 1992 Oct;119(1):229–38.

259. Spertini O, Schleiffenbaum B, White-Owen C, Ruiz P, Tedder TF. ELISA for quantitation of l-selectin shed from leukocytes in vivo. J Immunol Methods. Elsevier; 1992 Nov;156(1):115–23.
260. Schleiffenbaum B, Spertini O, Tedder TE. Soluble L-selectin Is Present in Human Plasma at High Levels and Retains Functional Activity.
261. Font J, Pizcueta P, Ramos-Casals M, Cervera R, García-Carrasco M, Navarro M, et al. Increased serum levels of soluble L-selectin (CD62L) in patients with active systemic lupus erythematosus (SLE). Clin Exp Immunol. 2000 Jan;119(1):169–74.
262. Russell AI, Cunninghame Graham DS, Chadha S, Roberton C, Fernandez-Hart T, Griffiths B, et al. No association between E- and L-selectin genes and SLE: soluble L-selectin levels do correlate with genotype and a subset in SLE. Genes Immun. 2005 Aug;6(5):422–9.
263. Kretowski A, Gillespie KM, Bingley PJ, Kinalska I. Soluble L-selectin levels in type I diabetes mellitus: a surrogate marker for disease activity? Immunology. 2000 Feb;99(2):320–5.
264. Venturi GM, Tu L, Kadono T, Khan AI, Fujimoto Y, Oshel P, et al. Leukocyte migration is regulated by L-selectin endoproteolytic release. Immunity. 2003 Nov;19(5):713–24.
265. Schaff U, Mattila PE, Simon SI, Walcheck B. Neutrophil adhesion to E-selectin under shear promotes the redistribution and co-clustering of ADAM17 and its proteolytic substrate L-selectin. J Leukoc Biol. 2008 Jan;83(1):99–105.
266. Haribabu B, Steeber DA, Ali H, Richardson RM, Snyderman R, Tedder TF. Chemoattractant receptor-induced phosphorylation of L-selectin. J Biol Chem. 1997 May;272(21):13961–5.
267. Stoddart JH, Jasuja RR, Sikorski MA, von Andrian UH, Mier JW. Protease-resistant L-selectin mutants. Down-modulation by cross-linking but not cellular activation. J Immunol. 1996 Dec;157(12):5653–9.
268. Lee D, Schultz JB, Knauf PA, King MR. Mechanical shedding of L-selectin from the neutrophil surface during rolling on sialyl Lewis x under flow. J

Biol Chem. 2007 Feb;282(7):4812–20.

269. Dailey MO, Gallatin WM, Weissman IL. The in vivo behavior of T cell clones: altered migration due to loss of the lymphocyte surface homing receptor. J Mol Cell Immunol. 1985;2(1):27–36.
270. Reichert RA, Gallatin WM, Weissman IL, Butcher EC. Germinal center B cells lack homing receptors necessary for normal lymphocyte recirculation. J Exp Med. 1983 Mar;157(3):813–27.
271. Chao CC, Jensen R, Dailey MO. Mechanisms of L-selectin regulation by activated T cells. J Immunol. 1997 Aug;159(4):1686–94.
272. Tedder TF, Steeber DA, Pizcueta P. L-selectin-deficient mice have impaired leukocyte recruitment into inflammatory sites. J Exp Med. The Rockefeller University Press; 1995 Jun;181(6):2259–64.
273. Chen S, Alon R, Fuhlbrigge RC, Springer TA. Rolling and transient tethering of leukocytes on antibodies reveal specializations of selectins. Proc Natl Acad Sci U S A. National Academy of Sciences; 1997 Apr;94(7):3172–7.
274. Yago T, Wu J, Wey CD, Klopocki AG, Zhu C, McEver RP. Catch bonds govern adhesion through L-selectin at threshold shear. J Cell Biol. 2004 Sep;166(6):913–23.
275. Ley K, Gaehtgens P, Fennie C, Singer MS, Lasky LA, Rosen SD. Lectin-Like Cell Adhesion Molecule 1 Mediates Leukocyte Rolling in Mesenteric Venules In Vivo.
276. Ley K, Bullard DC, Arbonés ML, Bosse R, Vestweber D, Tedder TF, et al. Sequential contribution of L- and P-selectin to leukocyte rolling in vivo. J Exp Med. The Rockefeller University Press; 1995 Feb;181(2):669–75.
277. Luscinskas FW, Kansas GS, Ding H, Pizcueta P, Schleiffenbaum BE, Tedder TF, et al. Monocyte rolling, arrest and spreading on IL-4-activated vascular endothelium under flow is mediated via sequential action of L-selectin, beta 1-integrins, and beta 2-integrins. J Cell Biol. 1994 Jun;125(6):1417–27.
278. Mitchell DJ, Li P, Reinhardt PH, Kubes P, Lawrence M, Springer T, et al. Importance of L-selectin-dependent leukocyte-leukocyte interactions in human whole blood. Blood. American Society of Hematology; 2000 May;95(9):2954–9.
279. Diacovo TG, Catalina MD, Siegelman MH, von Andrian UH. Circulating

activated platelets reconstitute lymphocyte homing and immunity in L-selectin-deficient mice. J Exp Med. The Rockefeller University Press; 1998 Jan;187(2):197–204.

280. Doyle NA, Bhagwan SD, Meek BB, Kutkoski GJ, Steeber DA, Tedder TF, et al. Neutrophil margination, sequestration, and emigration in the lungs of L-selectin-deficient mice. J Clin Invest. American Society for Clinical Investigation; 1997 Feb;99(3):526–33.
281. Mohammed RN, Watson HA, Vigar M, Ohme J, Thomson A, Humphreys IR, et al. L-selectin Is Essential for Delivery of Activated CD8(+) T Cells to Virus-Infected Organs for Protective Immunity. Cell Rep. Elsevier; 2016 Feb;14(4):760–71.
282. Inaoki M, Sato S, Shimada Y, Kawara S, Steeber DA, Tedder TF. Decreased expression levels of L-selectin on subsets of leucocytes and increased serum L-selectin in severe psoriasis. Clin Exp Immunol. 2000 Dec;122(3):484–92.
283. Venturi GM, Conway RM, Steeber DA, Tedder TF. CD25+CD4+ Regulatory T Cell Migration Requires L-Selectin Expression: L-Selectin Transcriptional Regulation Balances Constitutive Receptor Turnover. J Immunol. American Association of Immunologists; 2007 Jan;178(1):291–300.
284. Hickey MJ, Forster M, Mitchell D, Kaur J, De Caigny C, Kubes P. L-selectin facilitates emigration and extravascular locomotion of leukocytes during acute inflammatory responses in vivo. J Immunol. 2000 Dec;165(12):7164–70.
285. Galkina E, Tanousis K, Preece G, Tolaini M, Kioussis D, Florey O, et al. L-selectin shedding does not regulate constitutive T cell trafficking but controls the migration pathways of antigen-activated T lymphocytes. J Exp Med. The Rockefeller University Press; 2003 Nov;198(9):1323–35.
286. Stadtmann A, Germena G, Block H, Boras M, Rossaint J, Sundd P, et al. The PSGL-1–L-selectin signaling complex regulates neutrophil adhesion under flow. J Exp Med. Rockefeller University Press; 2013 Oct;210(11):2171–80.
287. Zarbock A, Ley K, McEver RP, Hidalgo A, Vestweber D, Blanks J, et al. Leukocyte ligands for endothelial selectins: specialized glycoconjugates that mediate rolling and signaling under flow. Blood. American Society of

Hematology; 2011 Dec;118(26):6743–51.

288. Smolen JE, Petersen TK, Koch C, O'Keefe SJ, Hanlon WA, Seo S, et al. L-Selectin Signaling of Neutrophil Adhesion and Degranulation Involves p38 Mitogen-activated Protein Kinase. J Biol Chem. American Society for Biochemistry and Molecular Biology; 2000 May;275(21):15876–84.
289. Simon SI, Cherapanov V, Nadra I, Waddell TK, Seo SM, Wang Q, et al. Signaling functions of L-selectin in neutrophils: alterations in the cytoskeleton and colocalization with CD18. J Immunol. American Association of Immunologists; 1999 Sep;163(5):2891–901.
290. Ding Z, Issekutz TB, Downey GP, Waddell TK. L-selectin stimulation enhances functional expression of surface CXCR4 in lymphocytes: implications for cellular activation during adhesion and migration. Blood. 2003 Jun;101(11):4245–52.
291. Duchesneau P, Gallagher E, Walcheck B, Waddell TK. Up-regulation of leukocyte CXCR4 expression by sulfatide: an L-selectin-dependent pathway on CD4+ T cells. Eur J Immunol. 2007 Oct;37(10):2949–60.
292. Subramanian H, Grailer JJ, Ohlrich KC, Rymaszewski AL, Loppnow JJ, Kodera M, et al. Signaling through L-Selectin Mediates Enhanced Chemotaxis of Lymphocyte Subsets to Secondary Lymphoid Tissue Chemokine. J Immunol. American Association of Immunologists; 2012 Apr;188(7):3223–36.
293. Tang J, Zarbock A, Gomez I, Wilson CL, Lefort CT, Stadtmann A, et al. Adam17-dependent shedding limits early neutrophil influx but does not alter early monocyte recruitment to inflammatory sites. Blood. 2011 Jul;118(3):786–94.
294. Mohanty T, Sjögren J, Kahn F, Abu-Humaidan AHA, Fisker N, Assing K, et al. A novel mechanism for NETosis provides antimicrobial defense at the oral mucosa. Blood. 2015 Oct;126(18):2128–37.
295. Etulain J, Martinod K, Wong SL, Cifuni SM, Schattner M, Wagner DD. P-selectin promotes neutrophil extracellular trap formation in mice. Blood. 2015 Jul;126(2):242–6.
296. Waddell TK, Fialkow L, Chan CK, Kishimoto TK, Downey GP. Potentiation of the oxidative burst of human neutrophils. A signaling role for L-selectin. J Biol Chem. 1994 Jul;269(28):18485–91.

297. Eriksson EE. Intravital microscopy on atherosclerosis in apolipoprotein e-deficient mice establishes microvessels as major entry pathways for leukocytes to advanced lesions. Circulation. 2011 Nov;124(19):2129–38.
298. Rozenberg I, Sluka SHM, Mocharla P, Hallenberg A, Rotzius P, Borén J, et al. Deletion of L-Selectin Increases Atherosclerosis Development in ApoE−/− Mice. Reitsma PH, editor. PLoS One. Public Library of Science; 2011 Jul;6(7):e21675.
299. Steinman L. Blocking adhesion molecules as therapy for multiple sclerosis: natalizumab. Nat Rev Drug Discov [Internet]. Nature Publishing Group; 2005 Jun [cited 2016 Dec 31];4(6):510–8. Available from: http://www.nature.com/doifinder/10.1038/nrd1752
300. Stengel D, Bauwens K, Keh D, Gerlach H, Ekkernkamp A, Tauber R, et al. Prognostic Value of an Early Soluble L-Selectin (sCD62L) Assay for Risk Assessment in Blunt Multiple Trauma: A Metaanalysis. Clin Chem. 2004;51(1).
301. Seekamp A, van Griensven M, Dhondt E, Diefenbeck M, Demeyer I, Vundelinckx G, et al. The effect of anti-L-selectin (aselizumab) in multiple traumatized patients--results of a phase II clinical trial. Crit Care Med. 2004 Oct;32(10):2021–8.
302. Schön MP. Inhibitors of selectin functions in the treatment of inflammatory skin disorders. Ther Clin Risk Manag. Dove Press; 2005 Sep;1(3):201–8.
303. Gaber AO, Mulgaonkar S, Kahan BD, Woodle ES, Alloway R, Bajjoka I, et al. YSPSL (rPSGL-Ig) for improvement of early renal allograft function: a double-blind, placebo-controlled, multi-center Phase IIa study. Clin Transplant. 25(4):523–33.
304. Bernal A, San Martín N, Fernández M, Covarello D, Molla F, Soldo A, et al. L-selectin and SDF-1 enhance the migration of mouse and human cardiac mesoangioblasts. Cell Death Differ. 2012 Feb;19(2):345–55.
305. James SY, Williams MA, Kelsey SM, Newland AC, Colston KW. Interaction of vitamin D derivatives and granulocyte-macrophage colony-stimulating factor in leukaemic cell differentiation. Leukemia. 1997 Jul;11(7):1017–25.
306. Gorelik R, Gautreau A. Quantitative and unbiased analysis of directional persistence in cell migration. Nat Protoc. Nature Publishing Group;

2014;9(8):1931–43.

307. Brightman AO, Rajwa BP, Sturgis JE, McCallister ME, Robinson JP, Voytik-Harbin SL. Time-lapse confocal reflection microscopy of collagen fibrillogenesis and extracellular matrix assembly in vitro. Biopolymers. 2000 Sep;54(3):222–34.
308. Millius A, Weiner OD. Chemotaxis in neutrophil-like HL-60 cells. Methods Mol Biol. NIH Public Access; 2009;571:167–77.
309. Hauert AB, Martinelli S, Marone C, Niggli V. Differentiated HL-60 cells are a valid model system for the analysis of human neutrophil migration and chemotaxis. Int J Biochem Cell Biol. 2002;34(7):838–54.
310. Allport JR, Ding HT, Ager A, Steeber DA, Tedder TF, Luscinskas FW. L-selectin shedding does not regulate human neutrophil attachment, rolling, or transmigration across human vascular endothelium in vitro. J Immunol. 1997 May;158(9):4365–72.
311. Lämmermann T, Afonso P V, Angermann BR, Wang JM, Kastenmüller W, Parent CA, et al. Neutrophil swarms require LTB4 and integrins at sites of cell death in vivo. Nature. 2013 Jun;498(7454):371–5.
312. Evans BJ, McDowall A, Taylor PC, Hogg N, Haskard DO, Landis RC. Shedding of lymphocyte function-associated antigen-1 (LFA-1) in a human inflammatory response. Blood. American Society of Hematology; 2006 May;107(9):3593–9.
313. Tsubota Y, Frey JM, Tai PWL, Welikson RE, Raines EW. Monocyte ADAM17 promotes diapedesis during transendothelial migration: identification of steps and substrates targeted by metalloproteinases. J Immunol. 2013 Apr;190(8):4236–44.
314. Peschon JJ, Slack JL, Reddy P, Stocking KL, Sunnarborg SW, Lee DC, et al. An essential role for ectodomain shedding in mammalian development. Science. 1998 Nov;282(5392):1281–4.
315. Ivetic A. Signals regulating L-selectin-dependent leucocyte adhesion and transmigration. Int J Biochem Cell Biol. 2013 Mar;45(3):550–5.
316. Granger DN, Senchenkova E. Leukocyte–Endothelial Cell Adhesion. Morgan & Claypool Life Sciences; 2010;
317. Pericytes support neutrophil transmigration via interleukin-8 across a

porcine co-culture model of the blood-brain barrier. - PubMed - NCBI.

318. Smith WB, Gamble JR, Clark-Lewis I, Vadas MA. Interleukin-8 induces neutrophil transendothelial migration. Immunology. Wiley-Blackwell; 1991 Jan;72(1):65–72.
319. Tajima A, Iwase T, Shinji H, Seki K, Mizunoe Y. Inhibition of Endothelial Interleukin-8 Production and Neutrophil Transmigration by Staphylococcus aureus Beta-Hemolysin. Infect Immun. American Society for Microbiology; 2009 Jan;77(1):327–34.
320. Sai J, Walker G, Wikswo J, Richmond A. The IL sequence in the LLKIL motif in CXCR2 is required for full ligand-induced activation of Erk, Akt, and chemotaxis in HL60 cells. J Biol Chem. 2006 Nov;281(47):35931–41.
321. Sai J, Fan G-H, Wang D, Richmond A. The C-terminal domain LLKIL motif of CXCR2 is required for ligand-mediated polarization of early signals during chemotaxis. J Cell Sci. 2004 Nov;117(Pt 23):5489–96.
322. Janetopoulos C, Ma L, Devreotes PN, Iglesias PA. Chemoattractant-induced phosphatidylinositol 3,4,5-trisphosphate accumulation is spatially amplified and adapts, independent of the actin cytoskeleton. Proc Natl Acad Sci U S A. 2004 Jun;101(24):8951–6.
323. Huang YE, Iijima M, Parent CA, Funamoto S, Firtel RA, Devreotes P. Receptor-mediated regulation of PI3Ks confines PI(3,4,5)P3 to the leading edge of chemotaxing cells. Mol Biol Cell. American Society for Cell Biology; 2003 May;14(5):1913–22.
324. Andrew N, Insall RH. Chemotaxis in shallow gradients is mediated independently of PtdIns 3-kinase by biased choices between random protrusions. Nat Cell Biol. 2007 Feb;9(2):193–200.
325. Derry CJ, Faveeuw C, Mordsley KR, Ager A. Novel chondroitin sulfate-modified ligands for L-selectin on lymph node high endothelial venules. Eur J Immunol. 1999 Feb;29(2):419–30.
326. Akiyama SK. Integrins in cell adhesion and signaling. Hum Cell. 1996 Sep;9(3):181–6.
327. Haribabu B, Steeber DA, Ali H, Richardson RM, Snyderman R, Tedder TF. Chemoattractant Receptor-induced Phosphorylation of L-selectin. J Biol Chem. American Society for Biochemistry and Molecular Biology; 1997

May;272(21):13961–5.

328. Hayashida K, Bartlett AH, Chen Y, Pyong A, Park W. Molecular and Cellular Mechanisms of Ectodomain Shedding.
329. Gifford JL, Ishida H, Vogel HJ. Structural Insights into Calmodulin-regulated L-selectin Ectodomain Shedding * □ S. 2012;
330. Krump E, Sanghera JS, Pelech SL, Furuya W, Grinstein S. Chemotactic Peptide N-formyl-Met-Leu-Phe Activation of p38 Mitogen-activated Protein Kinase (MAPK) and MAPK-activated Protein Kinase-2 in Human Neutrophils. J Biol Chem. American Society for Biochemistry and Molecular Biology; 1997 Jan;272(2):937–44.
331. Quehenberger O, Prossnitz ER, Cavanagh SL, Cochrane CG, Ye RD. Multiple domains of the N-formyl peptide receptor are required for high-affinity ligand binding. Construction and analysis of chimeric N-formyl peptide receptors. J Biol Chem. 1993 Aug;268(24):18167–75.
332. Dorward DA, Lucas CD, Chapman GB, Haslett C, Dhaliwal K, Rossi AG. The role of formylated peptides and formyl peptide receptor 1 in governing neutrophil function during acute inflammation. Am J Pathol. American Society for Investigative Pathology; 2015 May;185(5):1172–84.
333. Kobayashi T, Vischer UM, Rosnoblet C, Lebrand C, Lindsay M, Parton RG, et al. The tetraspanin CD63/lamp3 cycles between endocytic and secretory compartments in human endothelial cells. Mol Biol Cell. American Society for Cell Biology; 2000 May;11(5):1829–43.
334. Rubino M, Miaczynska M, Lippé R, Zerial M. Selective membrane recruitment of EEA1 suggests a role in directional transport of clathrin-coated vesicles to early endosomes. J Biol Chem. 2000 Feb;275(6):3745–8.
335. Bastin G, Heximer SP. Rab Family Proteins Regulate the Endosomal Trafficking and Function of RGS4. J Biol Chem. American Society for Biochemistry and Molecular Biology; 2013 Jul;288(30):21836–49.
336. Abbal C, Lambelet M, Bertaggia D, Gerbex C, Martinez M, Arcaro A, et al. Lipid raft adhesion receptors and Syk regulate selectin-dependent rolling under flow conditions. Blood. 2006 Nov;108(10):3352–9.
337. Pike LJ. The challenge of lipid rafts. J Lipid Res. American Society for Biochemistry and Molecular Biology; 2009 Apr;50 Suppl(Suppl):S323-8.

338. Pike LJ, Han X, Chung K-N, Gross RW. Lipid rafts are enriched in arachidonic acid and plasmenylethanolamine and their composition is independent of caveolin-1 expression: a quantitative electrospray ionization/mass spectrometric analysis. Biochemistry. 2002 Feb;41(6):2075–88.
339. Pike LJ, Han X, Gross RW. Epidermal growth factor receptors are localized to lipid rafts that contain a balance of inner and outer leaflet lipids: a shotgun lipidomics study. J Biol Chem. 2005 Jul;280(29):26796–804.
340. Palecanda A, Walcheck B, Bishop DK, Jutila MA. Rapid activation-independent shedding of leukocyte L-selectin induced by cross-linking of the surface antigen. Eur J Immunol. 1992 May;22(5):1279–86.
341. Frey M, Appenheimer MM, Evans SS. Tyrosine kinase-dependent regulation of L-selectin expression through the Leu-13 signal transduction molecule: evidence for a protein kinase C-independent mechanism of L-selectin shedding. J Immunol. 1997 Jun;158(11):5424–34.
342. Jasuja RR, Mier JW. Differential effects of hydroxamate inhibitors on PMA and ligand-induced L-Selectin down-modulation: role of membrane proximal and cytoplasmic domains. Int J Immunopathol Pharmacol. 13(1):1–12.
343. Liu S, Kiick K. Architecture effects on L-selectin shedding induced by polypeptide-based multivalent ligands. Polym Chem. 2011 Jul;2(7):1513–22.
344. Gordon EJ, Strong LE, Kiessling LL. Glycoprotein-inspired materials promote the proteolytic release of cell surface L-selectin. Bioorg Med Chem. 1998 Aug;6(8):1293–9.
345. Saadi W, Rhee SW, Lin F, Vahidi B, Chung BG, Jeon NL. Generation of stable concentration gradients in 2D and 3D environments using a microfluidic ladder chamber. Biomed Microdevices. 2007 Oct;9(5):627–35.
346. Kim BJ, Wu M. Microfluidics for mammalian cell chemotaxis. Ann Biomed Eng. NIH Public Access; 2012 Jun;40(6):1316–27.
347. Wilson K, Lewalle A, Fritzsche M, Thorogate R, Duke T, Charras G, et al. Mechanisms of leading edge protrusion in interstitial migration. Nat Commun. Nature Publishing Group; 2013 Dec;4:445–57.
348. Cain RJ, d'Água BB, Ridley AJ. Quantification of Transendothelial Migration

Using Three-Dimensional Confocal Microscopy. In 2011. p. 167–90.

349. Friedl P, Wolf K, Lammerding J. Nuclear mechanics during cell migration. Curr Opin Cell Biol. NIH Public Access; 2011 Feb;23(1):55–64.

350. Wolf K, Te Lindert M, Krause M, Alexander S, Te Riet J, Willis AL, et al. Physical limits of cell migration: control by ECM space and nuclear deformation and tuning by proteolysis and traction force. J Cell Biol. The Rockefeller University Press; 2013 Jun;201(7):1069–84.

351. Wolf K, te Lindert M, Krause M, Alexander S, te Riet J, Willis AL, et al. Physical limits of cell migration: Control by ECM space and nuclear deformation and tuning by proteolysis and traction force. J Cell Biol. Rockefeller University Press; 2013 Jun;201(7):1069–84.

352. Achilli M, Mantovani D. Tailoring Mechanical Properties of Collagen-Based Scaffolds for Vascular Tissue Engineering: The Effects of pH, Temperature and Ionic Strength on Gelation. Polymers (Basel). Molecular Diversity Preservation International; 2010 Dec;2(4):664–80.

353. Johnson TD, Lin SY, Christman KL. Tailoring material properties of a nanofibrous extracellular matrix derived hydrogel. Nanotechnology. NIH Public Access; 2011 Dec;22(49):494015.

354. Allen SJ, Hamel DJ, Handel TM. A Rapid And Efficient Way To Obtain Modified Chemokines For Functional And Biophysical Studies.

355. Waddell TK, Fialkow L, Chan CK, Kishimoto TK, Downey GP. Signaling Functions of L-selectin: ENHANCEMENT OF TYROSINE PHOSPHORYLATION AND ACTIVATION OF MAP KINASE. J Biol Chem. American Society for Biochemistry and Molecular Biology; 1995 Jun;270(25):15403–11.

356. Gómez-Moutón C, Mañes S. Establishment and maintenance of cell polarity during leukocyte chemotaxis. Cell Adh Migr. Landes Bioscience; 2007;1(2):69–76.

357. Tellier E, Canault M, Rebsomen L, Bonardo B, Juhan-Vague I, Nalbone G, et al. The shedding activity of ADAM17 is sequestered in lipid rafts. Exp Cell Res. 2006 Dec;312(20):3969–80.

358. Tellier E, Canault M, Poggi M, Bonardo B, Nicolay A, Alessi M-C, et al. HDLs activate ADAM17-dependent shedding. J Cell Physiol. 2008

Mar;214(3):687–93.

359. Yip S-C, El-Sibai M, Coniglio SJ, Mouneimne G, Eddy RJ, Drees BE, et al. The distinct roles of Ras and Rac in PI 3-kinase-dependent protrusion during EGF-stimulated cell migration. J Cell Sci. The Company of Biologists Ltd; 2007 Sep;120(Pt 17):3138–46.
360. Jun JE, Yang M, Chen H, Chakraborty AK, Roose JP. Activation of extracellular signal-regulated kinase but not of p38 mitogen-activated protein kinase pathways in lymphocytes requires allosteric activation of SOS. Mol Cell Biol. 2013 Jun;33(12):2470–84.
361. Hyun Y-M, Sumagin R, Sarangi PP, Lomakina E, Overstreet MG, Baker CM, et al. Uropod elongation is a common final step in leukocyte extravasation through inflamed vessels. J Exp Med. 2012;209(7).
362. Yoshinaga-Ohara N, Takahashi A, Uchiyama T, Sasada M. Spatiotemporal Regulation of Moesin Phosphorylation and Rear Release by Rho and Serine/Threonine Phosphatase during Neutrophil Migration. Exp Cell Res. Academic Press; 2002 Aug;278(1):112–22.
363. Liu X, Yang T, Suzuki K, Tsukita S, Ishii M, Zhou S, et al. Moesin and myosin phosphatase confine neutrophil orientation in a chemotactic gradient. J Exp Med. Rockefeller University Press; 2015 Feb;212(2):267–80.
364. Doedens JR, Mahimkar RM, Black RA. TACE/ADAM-17 enzymatic activity is increased in response to cellular stimulation. Biochem Biophys Res Commun [Internet]. 2003 Aug 22 [cited 2016 Dec 31];308(2):331–8. Available from: http://www.ncbi.nlm.nih.gov/pubmed/12901873
365. Liu X, Ma B, Malik AB, Tang H, Yang T, Sun B, et al. Bidirectional regulation of neutrophil migration by mitogen-activated protein kinases. Nat Immunol. Nature Research; 2012 Mar;13(5):457–64.
366. Maaty WS, Lord CI, Gripentrog JM, Riesselman M, Keren-Aviram G, Liu T, et al. Identification of C-terminal Phosphorylation Sites of *N* -Formyl Peptide Receptor-1 (FPR1) in Human Blood Neutrophils. J Biol Chem. American Society for Biochemistry and Molecular Biology; 2013 Sep;288(38):27042–58.
367. Hazeldine J, Hampson P, Opoku FA, Foster M, Lord JM. N-Formyl peptides drive mitochondrial damage associated molecular pattern induced

neutrophil activation through ERK1/2 and P38 MAP kinase signalling pathways. Injury [Internet]. 2015 Jun [cited 2016 Dec 31];46(6):975–84.

368. Fuchs TA, Abed U, Goosmann C, Hurwitz R, Schulze I, Wahn V, et al. Novel cell death program leads to neutrophil extracellular traps. J Cell Biol. 2007 Jan;176(2):231–41.
369. Papayannopoulos V, Metzler KD, Hakkim A, Zychlinsky A. Neutrophil elastase and myeloperoxidase regulate the formation of neutrophil extracellular traps. J Cell Biol. 2010 Nov;191(3):677–91.
370. Schauer C, Janko C, Munoz LE, Zhao Y, Kienhöfer D, Frey B, et al. Aggregated neutrophil extracellular traps limit inflammation by degrading cytokines and chemokines. Nat Med. 2014 May;20(5):511–7.
371. Clark SR, Ma AC, Tavener SA, McDonald B, Goodarzi Z, Kelly MM, et al. Platelet TLR4 activates neutrophil extracellular traps to ensnare bacteria in septic blood. Nat Med. 2007 Apr;13(4):463–9.
372. Yipp BG, Kubes P. NETosis: how vital is it? Blood. 2013 Oct;122(16):2784–94.
373. Kaneko M, Horie S, Kato M, Gleich GJ, Kita H. A crucial role for beta 2 integrin in the activation of eosinophils stimulated by IgG. J Immunol. 1995 Sep;155(5):2631–41.
374. Nagahata H, Higuchi H, Yamashiki N, Yamaguchi M. Analysis of the functional characteristics of L-selectin and its expression on normal and CD18-deficient bovine neutrophils. Immunol Cell Biol. Nature Publishing Group; 2000 Jun;78(3):264–71.
375. Shi Y, Zhang J, Mullin M, Dong B, Alberts AS, Siminovitch KA. The mDial formin is required for neutrophil polarization, migration, and activation of the LARG/RhoA/ROCK signaling axis during chemotaxis. J Immunol. 2009 Mar;182(6):3837–45.
376. Barcia C, Ros CM, Annese V, Carrillo-de Sauvage MA, Ros-Bernal F, Gómez A, et al. ROCK/Cdc42-mediated microglial motility and gliapse formation lead to phagocytosis of degenerating dopaminergic neurons in vivo. Sci Rep. 2012;2:809.
377. Rajendran P, Rengarajan T, Thangavel J, Nishigaki Y, Sakthisekaran D, Sethi G, et al. The vascular endothelium and human diseases. Int J Biol Sci

Deleted: Available from: http://www.ncbi.nlm.nih.gov/pubmed/25817163

[Internet]. Ivyspring International Publisher; 2013 [cited 2016 Dec 31];9(10):1057–69.

378. Wenceslau CF, McCarthy CG, Szasz T, Goulopoulou S, Webb RC. Mitochondrial N-formyl peptides induce cardiovascular collapse and sepsis-like syndrome. Am J Physiol Heart Circ Physiol. 2015 Apr;308(7):H768-77.
379. Sutton MGSJ, Sharpe N. Left Ventricular Remodeling After Myocardial Infarction. Circulation. 2000;101(25).
380. Jessup M, Marwick TH, Ponikowski P, Voors AA, Yancy CW. 2016 ESC and ACC/AHA/HFSA heart failure guideline update - what is new and why is it important? Nat Rev Cardiol. 2016 Sep;13(10):623–8.
381. Savchenko AS, Borissoff JI, Martinod K, De Meyer SF, Gallant M, Erpenbeck L, et al. VWF-mediated leukocyte recruitment with chromatin decondensation by PAD4 increases myocardial ischemia/reperfusion injury in mice. Blood. 2014 Jan;123(1):141–8.
382. Amsterdam EA, Pan HL, Rendig S V, Symons JD, Fletcher MP, Longhurst JC. Limitation of myocardial infarct size in pigs with a dual lipoxygenase-cyclooxygenase blocking agent by inhibition of neutrophil activity without reduction of neutrophil migration. J Am Coll Cardiol. 1993 Nov;22(6):1738–44.
383. Kempf T, Zarbock A, Widera C, Butz S, Stadtmann A, Rossaint J, et al. GDF-15 is an inhibitor of leukocyte integrin activation required for survival after myocardial infarction in mice. Nat Med. Nature Research; 2011 May;17(5):581–8.

Deleted: Available from: http://www.ncbi.nlm.nih.gov/pubmed/24250251